Research Programme of the Research Fund for Coal and Steel

FIre and Seismic performances of Hybrid fire WALLs in case of single-storey industrial and commercial steel buildings (FISHWALL)

Development and Validation of FE numerical models

Christophe Renaud – CTICM

Sara Pasquali, Nicola Tondini, Gabriele Zanon - University of Trento

WP4: Analysis of regulation requirements, fire and seismic actions applied to partition walls and design of tests

Deliverable: D4.2

Grant agreement No: 101034083

Grant agreement No: 101034083

Version	Issue	Purpose	Author	Reviewer	Approved
A	D4.2	first version (10/10/2024)	C. Renaud S.Pasquali N Tondini G. Zanon	ALL	C. Renaud
B	D4.2	Revised version following comments from EU experts (26/09/2025)	C. Renaud S.Pasquali N Tondini G. Zanon	ALL	C. Renaud

TABLE OF CONTENTS

Abstract **1**
1 Introduction **2**
2 Validation work of 3D FE models **3**
2.1 Modelling considerations 3
2.2 Analysis results 12
2.2.1 Fusible link configuration n°1 12
2.2.1.1 Monotonic tension loading 12
2.2.1.2 Monotonic compression loading 15
2.2.1.3 Cyclic loading 19
2.2.2 Fusible link configuration n°2 25
2.2.2.1 Monotonic tension loading 25
2.2.2.2 Monotonic compression loading 28
2.2.2.3 Cyclic loading 33
2.2.3 Fusible link configuration n°3.1 39
2.2.3.1 Monotonic tension loading 39
2.2.3.2 Monotonic compression loading 43
2.2.3.3 Cyclic loading 47
2.2.4 Fusible link configuration n°3.2 52
2.2.4.1 Monotonic tension loading 52
2.2.4.2 Monotonic compression loading 56
2.2.4.3 Cyclic loading 60
2.2.5 Fusible link configuration n°4 67
2.2.5.1 Monotonic tension loading 67
2.2.5.2 Monotonic compression loading 71
2.2.5.3 Cyclic loadings 74
2.2.6 Fusible link configuration n°5 80
2.2.6.1 Monotonic tension loading 80
2.2.6.2 Monotonic compression loading 86
2.2.6.3 Cyclic loading 90
3 Calibration of lumped plasticity models **96**
3.1 Pinching4 Material 96
3.2 Fusible link configuration n°1 96
3.3 Fusible link configuration n°2 99
3.4 Fusible link configuration n°3.1 103
3.5 Fusible link configuration n°3.2 105
3.6 Fusible link configuration n°4 108
3.7 Fusible link configuration n°5 113
4 Conclusions **116**
5 References **118**

ABSTRACT

It is well known that the intrinsic fire resistance of single-storey unprotected steel-framed buildings is largely sufficient to guarantee the evacuation of occupants in the event of fire. In consequence, for this type of building, the main concern of national fire regulations in Europe is how to prevent the spread of fire to the whole building. To achieve this objective, two performances shall be usually satisfied, namely, the appropriateness of constructive systems to ensure that there is no progressive collapse between fire compartments, and the efficiency of fire walls to stop the fire inside the initial compartment regardless of the state of structures exposed to fire. In practice, many constructional solutions can be implemented to preserve the integrity of the fire walls, while accepting that the fire exposed part of the structure may collapse. One of the most common solutions is to place a non-load-bearing wall between two independent steel structures and to connect it to them by means of "fusible" links. In fire situation, these fusible links must allow the wall to be disconnected from the structure affected by fire without endangering the separating function of the wall, which shall remain fixed to the steel structure on the other side of the wall and therefore not exposed to fire. However, due to the lack of corresponding scientific evidence, questions are being very often raised about the real efficiency of such systems in fire situation, which, in certain cases, have also to provide an adequate seismic resistance, if they are used in seismic areas.

Today, concrete or masonry wall solutions are frequently used for the compartmentation of buildings, predominately for low-rise commercial and industrial steel buildings. However, as an alternative, lightweight sandwich panels (comprising two thin flat metal faces and an insulated core) could become an appropriate steel fire wall solution, offering numerous benefits in comparison to other solutions, including fire resistance, durability, flexibility, easy dismounting and fast construction times. But there is an evident lack of technical information about the adequate fire performance of such type of wall solutions when they are implemented in single-storey buildings with unprotected steel structure, which constitutes a major obstacle for their large use.

In this context, the overall goal of the FISHWALL project is to develop a design guidance and recommendations for an innovative hybrid fire wall solution based on lightweight steel-faced sandwich panels associated with unprotected steel structure under both fire and seismic actions, but considered individually. This will be achieved through the following specific tasks: i) Establishing of a full range of experimental evidence about the fire and seismic behaviour of the investigated hybrid fire wall solution by carrying out a number of tests; ii) Investigating intensively the fire and seismic performances of the above hybrid fire wall solution in combination with unprotected single-storey steel structures through a variety of parametric numerical studies by means of validated FE numerical models; iii) Developing both cost-effective and innovative "fusible" connection systems for fire walls to be used in combination with unprotected steel structures of single-storey buildings; and iv) Developing a design guidance and practical recommendations for the studied hybrid fire wall and fusible links solutions, on the basis of above studies, from which engineers can carry out very efficient design.

The present report aims to report on the comparison study conducted between the results of monotonic and cyclic tests carried out at University of Trento on 6 different fusible link configurations at the University of Trento (detailed in Deliverable 4.1) and the results of FE models developed in the scope of the project to analyse in detail the structural behaviour of the studied fusible links under cyclic loading. Simplified hysteretic numerical models developed to reproduce in the best possible way the actual behaviour of the investigated "fusible" connection systems are also described.

1 INTRODUCTION

The aim of the project FISHWALL is to provide a hybrid steel-based fire wall solution using sandwich panels for single-storey buildings with unprotected steel structure. This fire wall is placed between two independent building structures and connected to them by means of "fusible" systems. In case of fire event, the fusible systems will break and will allow the wall to be disconnected from the structure affected by the fire, without endangering the separating function of the wall, which remains fixed to the steel structure on the other side of the wall and therefore not exposed to the fire.

To investigate the seismic behaviour of studied fusible solutions, a set of cyclic tests were conducted on 6 different fusible link configurations at the University of Trento. The results from the tests, presented in Deliverable D4.1 [1], were used to check the capability of the 3D FE models developed under ANSYS [2]and Ls-dyna [3] in a pre-modelling work to simulate safely the structural behaviour of the studied fusible links, at least to predict satisfactory their maximum load bearing capacities. This deliverable aims to report on the comparison results and the developed FE models It is worth pointing out that the fusible links are not conceived to dissipate energy in case of a seismic event and the aluminium bolts are not adequate for this task given their brittle nature. Thus, the main aim of the model validation is to reproduce the failure mechanism and the maximum capacity of the fusible link details to assess their possible damage during a low-to-moderate intensity earthquake.

This deliverable aims also at reporting on the development and calibration for each tested fusible link configuration of a lumped plasticity model by means of OpenSees software [4], where the fusible links were modelled as ZeroLength Element [5]. It is important to highlight that the calibration was performed on the whole detail. Due to the limited hysteretic behaviour of the investigated details, the Pinching4 Material was chosen to represent the details behaviour observed during the cyclic tests. For each detail, the same displacement history, in accordance with the testing protocol, was applied in the numerical model and the parameters of the abovementioned material were calibrated based on the experimental campaign results. In detail, each model was calibrated considering the cyclic tests and then validated against the monotonic tests. The calibrated models will then be used in nonlinear time-history analyses applied to global models representing the case studies. Considering the brittle nature of the details, the calibration procedure was conducted in terms of the maximum force capacity of the fusible links. Indeed, the global seismic analyses performed after calibration will aim at assessing possible failure of the fusible link details.

2 VALIDATION WORK OF 3D FE MODELS

2.1 Modelling considerations

The detailed numerical modelling of fusible links has been made with two general computer codes, that is ANSYS and Ls-dyna. A static-dynamic procedure was used to run the monotonic and cyclic analyses in order to simulate the progressive failure mechanism of the studied specimens.

Several simplifications in the modelling were considered to reach an adequate compromise between the FE model accuracy and its computational cost. The main assumptions finally adopted in modelling are the following:

- Only a part of the test specimens is meshed. Because of the symmetry of geometry and loading, only 1/4 or 1/2 of real tested specimens were modelled when possible;
- All the modelled components are meshed with 20-nodes brick FEs in order to have a suitable accuracy with a limited number of meshes. Several mesh densities were tried, and a structured mesh was employed with varying mesh density in the different parts of models. A minimum of three elements is used for modelling correctly the thickness in steel profiles. The meshing details of the FE modelling are outlined in Figure 2.4 to Figure 2.9;
- Bolts and steel rods are modelled as detailed as possible. Nevertheless, some features of the geometry that are assumed to have negligible effects on the response of the fusible links are ignored. First, since the stripping of the nuts threads was not observed in tests, threaded parts of the bolts, rods and nuts are omitted and the bolt–nut assembly is modelled as a simple component, assuming that relative motion between bolts and nuts, or loosening, does not take place during loading. Secondly, no washers are modelled. Aluminium bolts were modelled by considering an effective diameter instead of the nominal diameter. The effective diameter of aluminium bolts was estimated from the shear test results reported in the project deliverable D3.1 [7], which leads to an even lower diameter of the bolt shank;
- Bolt-hole clearances are either taken into account (bolt holes are 1 or 2mm larger in diameter than the bolts) or neglected in the analyses;
- Surface-to-surface contact with finite sliding was assumed for all contact surfaces. This includes the contact between the steel profiles, between the bolts (heads and shanks) and the steel profiles (upper surface and holes). To model the contact and frictional sliding in ANSYS, 3D height-node surface-to-surface contact elements (CONTA174) were used, which are paired with target elements (TARGE170). A single coefficient of friction equal to 0.3 was assigned for all the contact elements, which lies within the values of 0.2-0.33 recommended in the literature for steel, stainless steel and aluminium connections. Aluminium bolts are less resistant and rigid than steel members. Hence, they are denoted as the master surfaces in contact parts and meshed coarser than the slave surfaces to increase the contact convergence rate. Penalty function was chosen as the contact algorithm. Automatic surface to surface contacts are used in Ls-dyna. Default values were adopted for most of the contact-related parameters;
- Supporting conditions coming from the non-modelled parts of the test specimen are considered by introducing appropriate boundary conditions into the models, restraining the relevant degrees of freedom (displacements and rotations). These conditions are assumed to be unchanged during the loading;
- Fixed boundary condition was applied at the bottom end of the meshed parts of considered test specimens. The loaded end was coupled to a reference point and all degrees of freedom were restrained, with the exception that vertical displacement was allowed for the application of loading.
- In each analysis, the considered specimen is subjected to a monotonically increasing vertical displacement, either tensile or compressive. The prescribed displacements were applied gradually until failure to ensure that dynamic effects were negligible (i.e., to ensure quasi-static loading conditions) and slowly to improve convergence. Regarding cyclic loading, the loading sequence follows the ECCS procedure. It comprises one cycle at a displacement amplitude of 0.25Dy, 0.5Dy, 0.75Dy, and 1.0 Dy, followed by three cycles of 2Dy, 4Dy, 6Dy, 8Dy, etc., as shown in Figure 2.1. All specimens were first loaded in tension and then in compression. The governing parameters are the tensile yield displacement, denoted Dy^+, and the compression yield displacement, denoted Dy^-, which are evaluated from the force-displacement curves obtained from the monotonic tension and compression analyses previously performed for the test specimens. Each yield displacement is determined according to the ECCS recommendations as illustrated in Figure 2.2. It is defined by the intersection of the initial elastic stiffness and the tangent stiffness as 1/10 of the initial one.

The initial elastic stiffness is defined as the slope of the line connecting the 10% peak load point and the 40% peak load point;

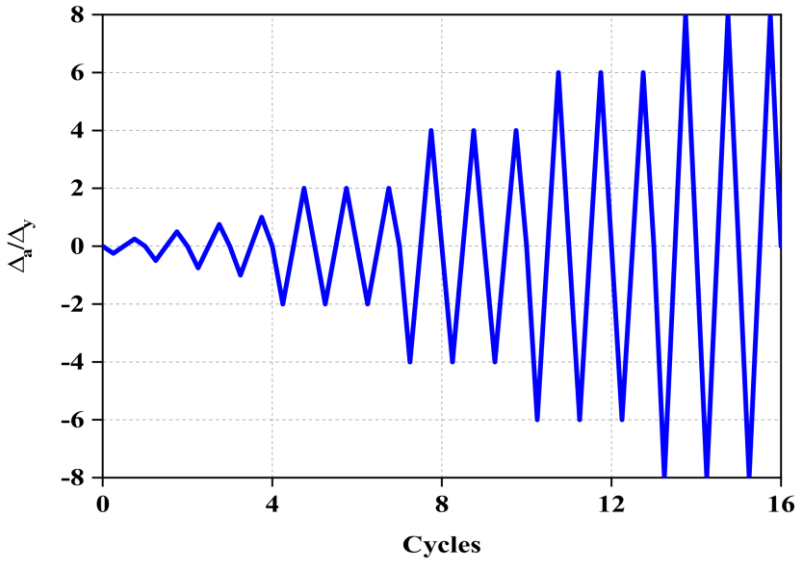

Figure 2.1: ECCS loading sequence adopted in cyclic analyses

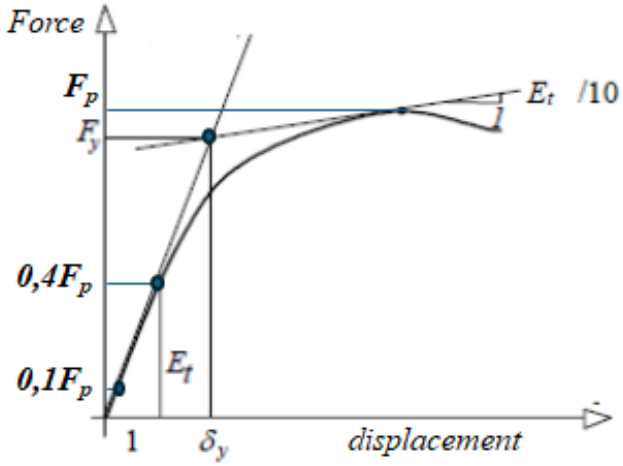

Figure 2.2*:* Definition of the yielding displacement

- No pretension in the bolts and rods caused by the tightening of each bolt and rod was considered in the analyses;
- The behaviour of structural steel is represented by a linear hardening plastic material model, defined by the means of a quadri-linear relationship as illustrated in Figure 2.3(a). Based on test results given in the project deliverable D3.1 [7], a trilinear stress-strain relationship is assigned to aluminium bolts (see Figure 2.3(b)). A tri-linear model is also used for the steel of all bolts and rods;
- The material characteristics (Young's modulus, yield strength, and ultimate strength) considered at ambient temperature are reported in Table 1. Mechanical properties of aluminium bolts are taken in accordance with the material test results, while those of steel profiles are derived from the mechanical properties reported on the mill test certificates provided by the suppliers. With regards to both steel bolts and rods, as there is no data, nominal values of steel yield strength and ultimate strength are considered;
- The use of plasticity material models with isotropic type hardening is generally not recommended to investigate the mechanical behaviour of steel members under cyclic loading conditions. So, all components are modelled using a kinematic hardening constitutive model, considering the Von Mises yield criterion and related flow rules;

- As observed in the experimental tests, a major part of specimens failed due to the shear fracture of aluminium bolts. The use of explicit finite element software like Ls-dyna allows for modelling of sequential failures, including fracture. Fracture can be simulated using element erosion, in which elements are removed from the analysis when specified failure criteria are satisfied. However, the basis for determining and implementing accurate material failure criteria for aluminium is missing in the literature. Moreover, the progressive deletion of finite elements should require updating contact surfaces accordingly, which is very computational time consuming. Consequently, the fracture of bolts was not explicitly simulated in the analyses. A simplified approach was followed, according to which fracture of the bolts is indirectly defined from a failure strain criterion not to be exceeded. Hence, the aluminium bolts are considered to have fractured in analyses when the Von Mises total mechanical strain obtained from the analysis exceeded 5%. In some cases, the fracture of bolts was simulated by introducing a descending branch in the stress–strain curve affected to aluminium bolts.

Table 1: Materials properties of steel components and aluminium bolts

Properties	Steel profile*	Steel bolts and rods	Aluminium bolts
Young's modulus E (N/mm^2)	210000	210000	70000
Yield strength f_y (N/mm^2)	298 – 424	640	400
ultimate strength f_u (N/mm^2)	443 - 525	800	505
* According to the steel profile sizes			

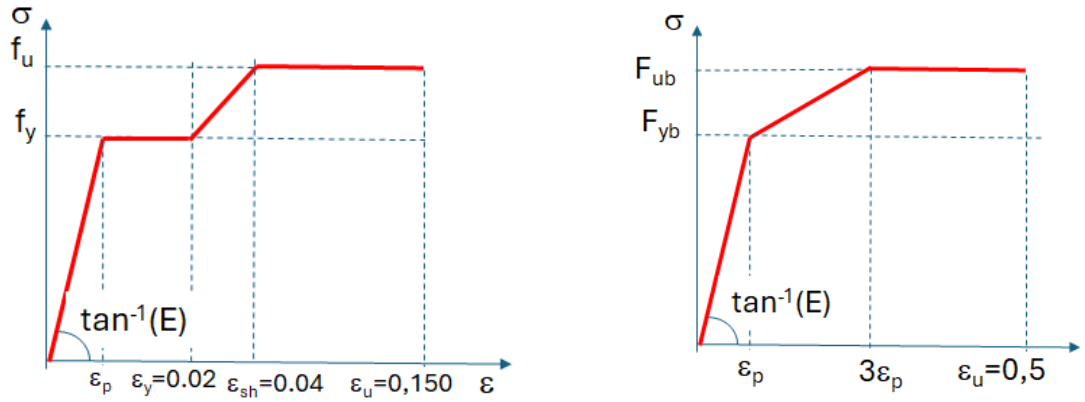

a) Steel profiles

b) bolts and rods

Figure 2.3: Idealised stress-strain models for materials adopted in modelling

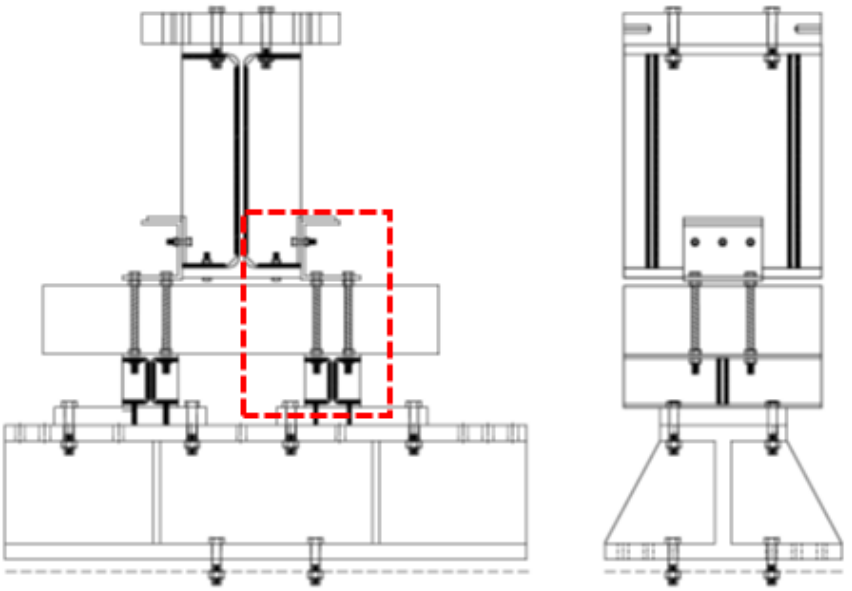

a) Experimental set-up

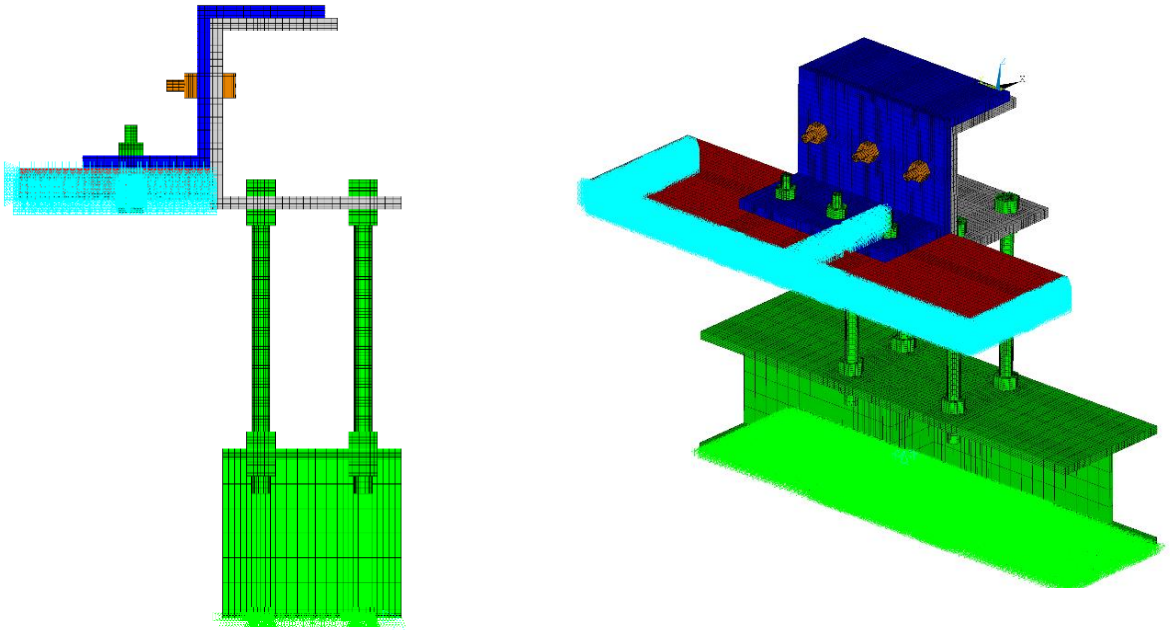

Side view Isoparametric view

b) Corresponding modelling

Figure 2.4: 3D FE model developed for the fusible link configuration n°1

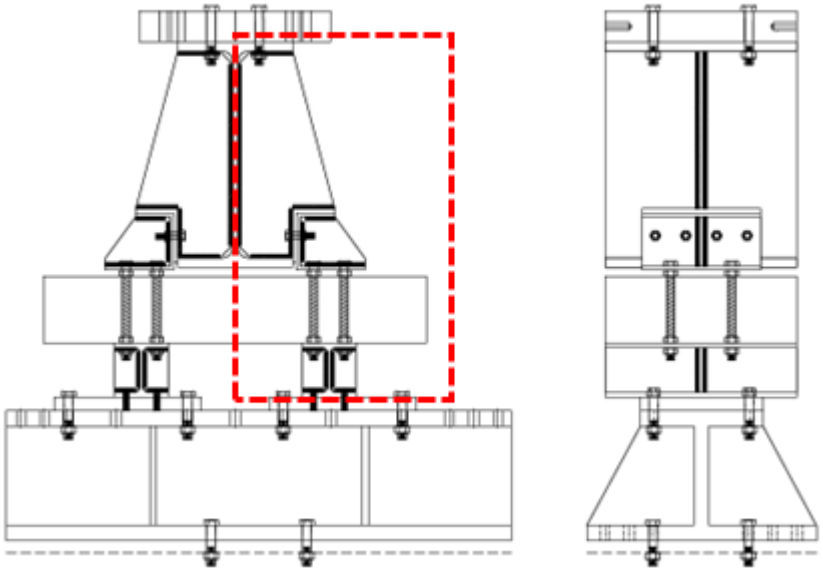

a) Experimental set-up

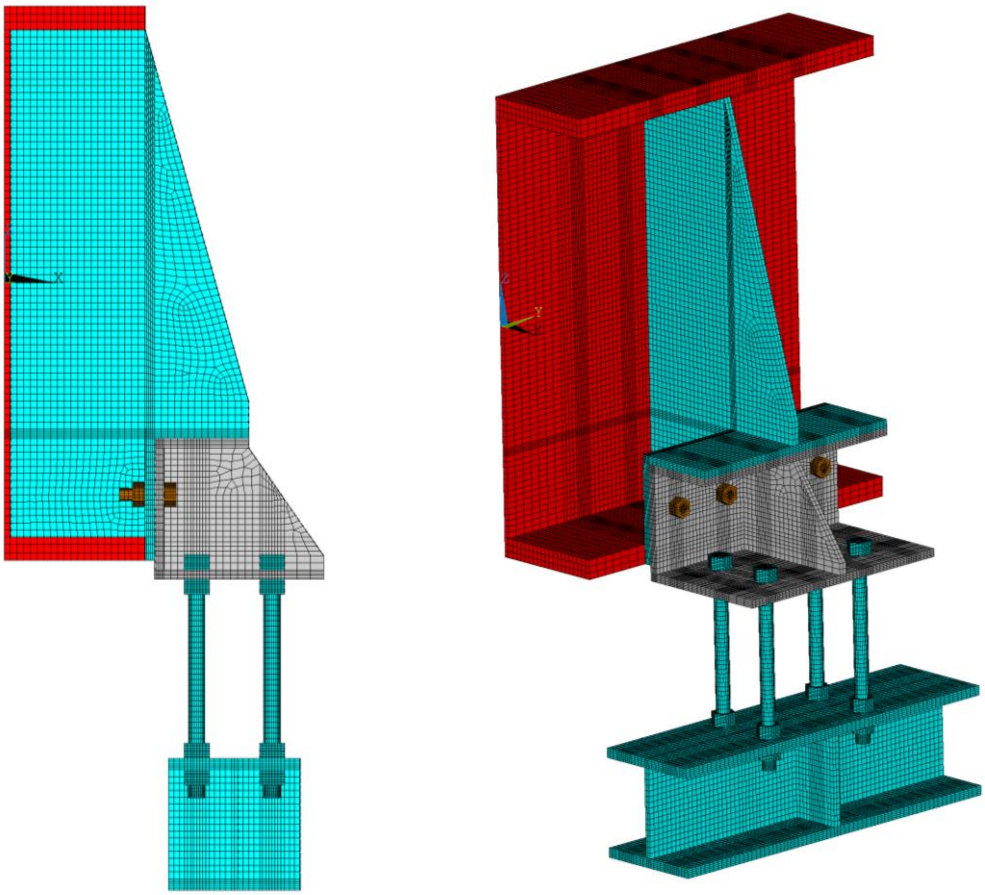

Side view Isoparametric view

b) Corresponding modelling

Figure 2.5: 3D FE model developed for the fusible link configuration n°2

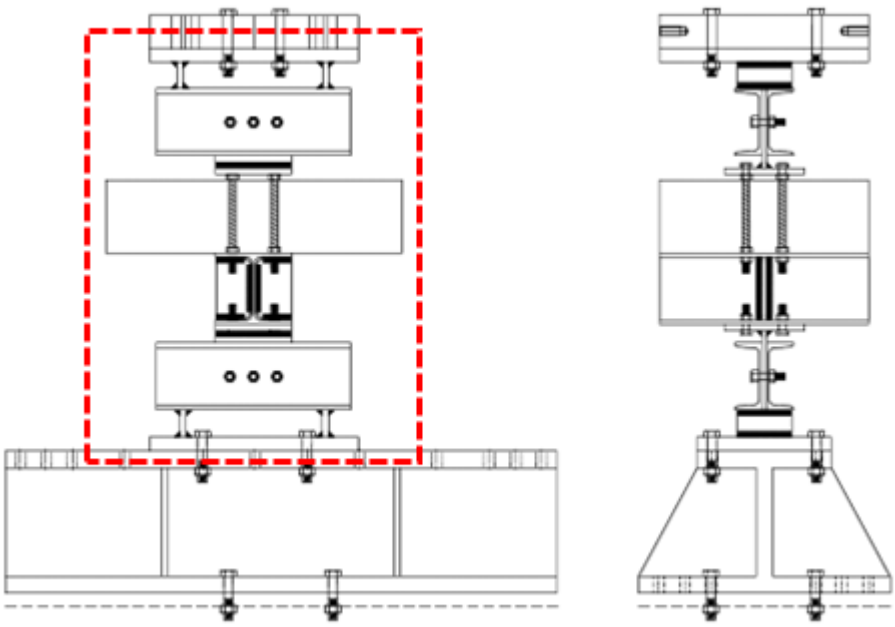

a) Experimental set-up

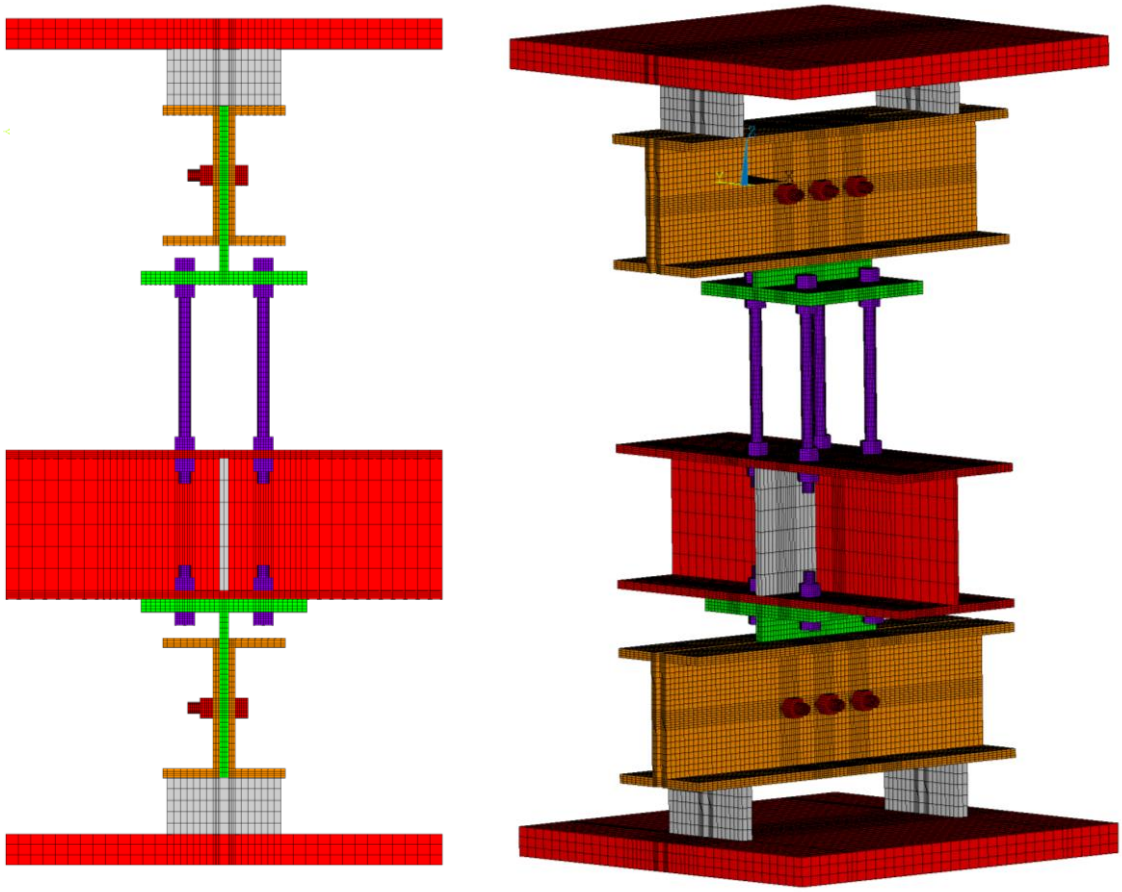

Side view Isoparametric view

b) Corresponding modelling

Figure 2.6: 3D FE model developed for the fusible link configuration n°3.1

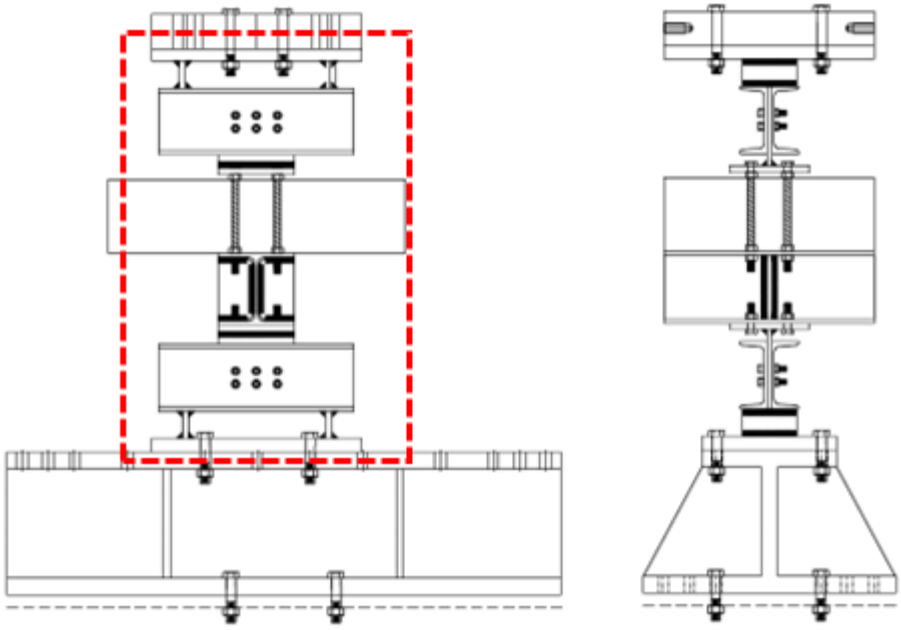

a) Experimental set-up

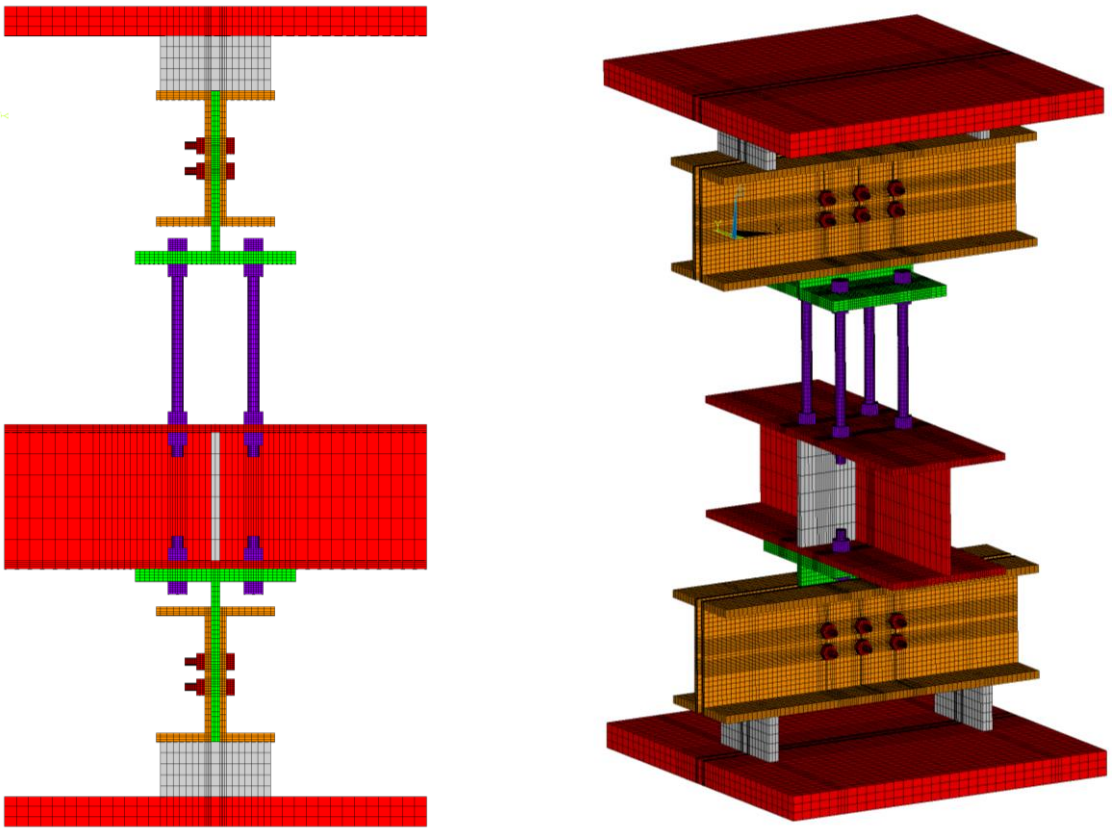

Side view Isoparametric view

b) Corresponding modelling

Figure 2.7: 3D FE model developed for the fusible link configuration n°3.2

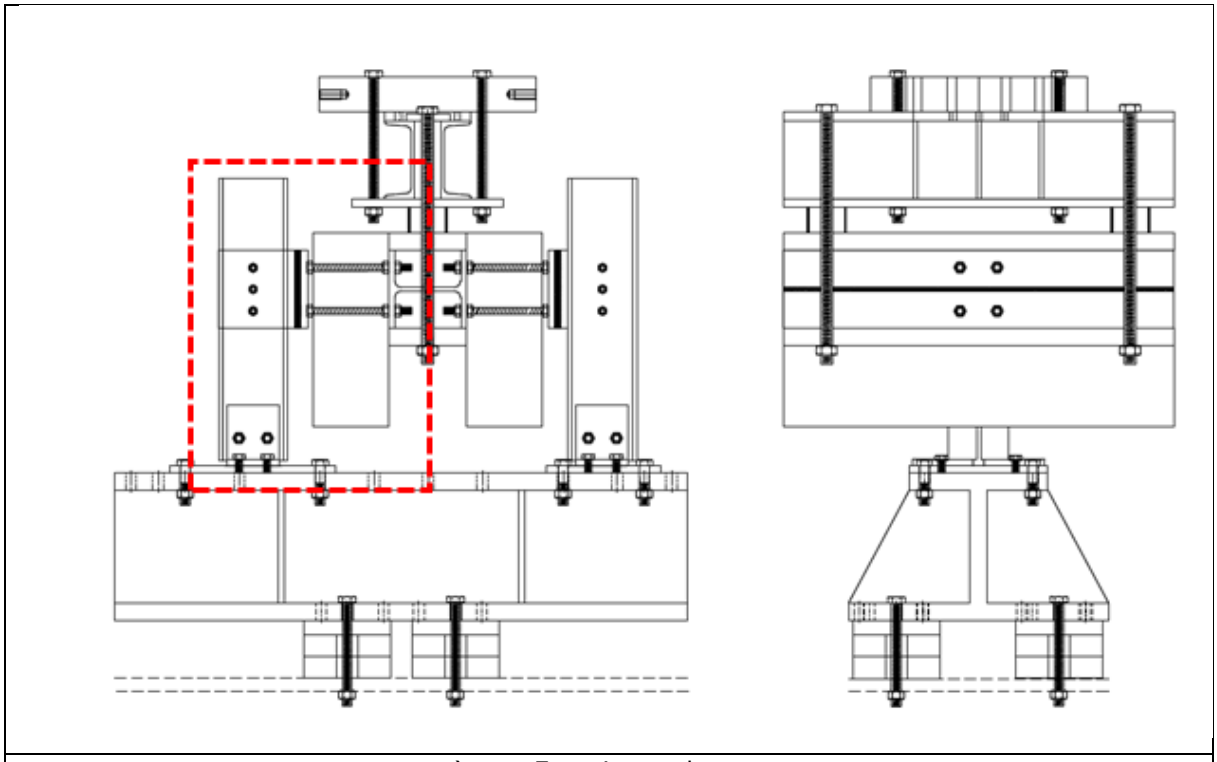

a) Experimental set-up

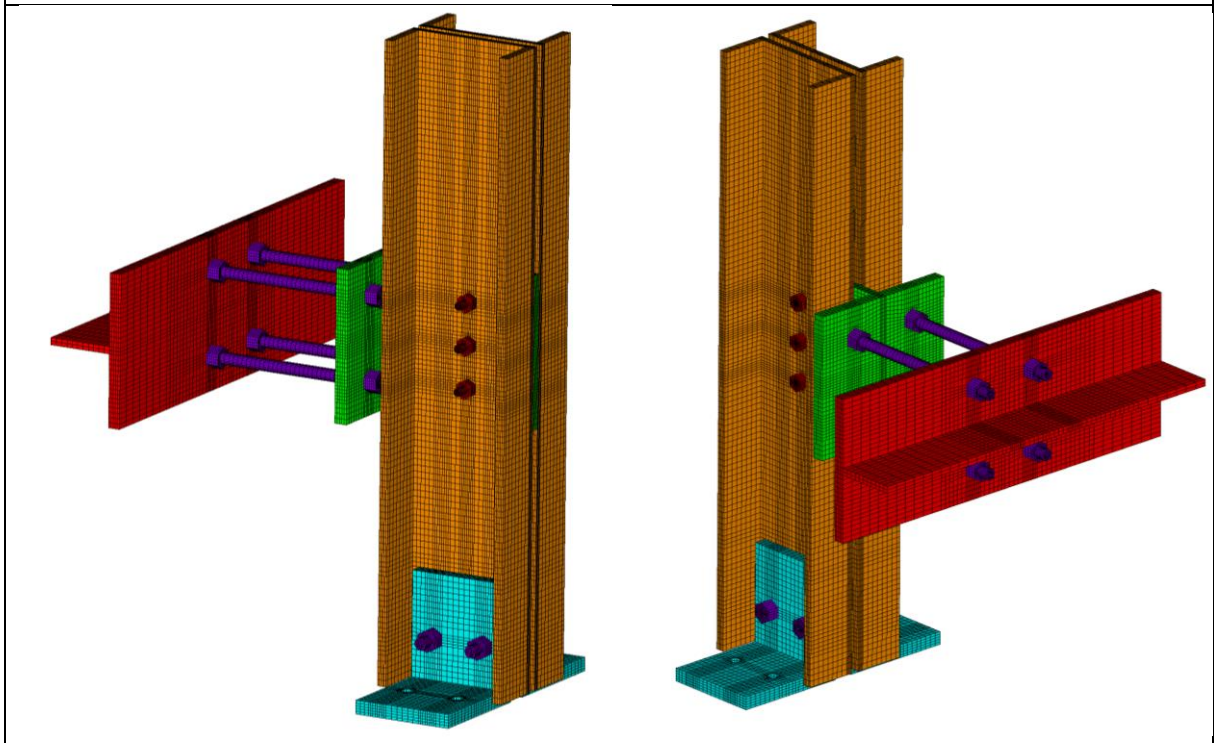

Side view Isoparametric view

b) Corresponding modelling

Figure 2.8: 3D FE model developed for the fusible link configuration n°4

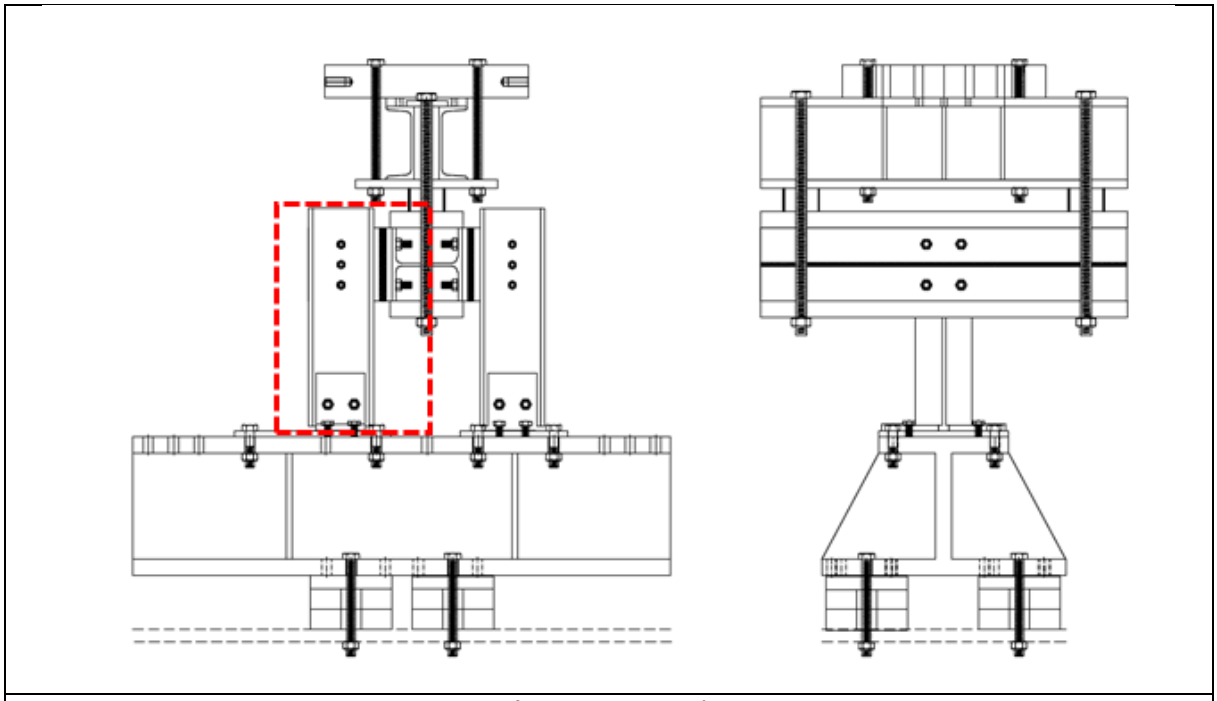

a) Experimental set-up

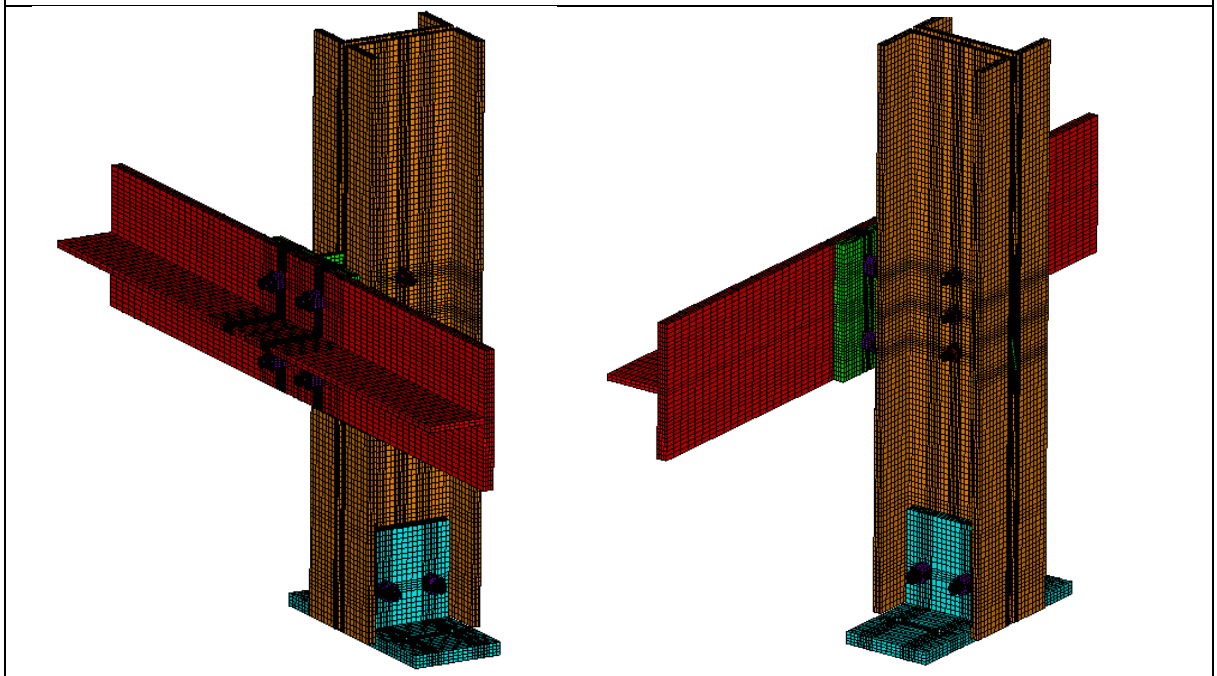

Side view Isoparametric view

b) Corresponding modelling

Figure 2.9: 3D FE model developed for the fusible link configuration n°5

2.2 Analysis results

The main results of mechanical analyses are presented hereafter and compared to test results. The results from numerical analyses are shown in terms of force-displacement curves, Von Mises strain distribution and failure modes predicted for the studied test specimens. An illustration of the failure mode observed during some tests is also shown.

2.2.1 Fusible link configuration n°1

For the first studied configuration, numerical analyses were performed with or without bolt-hole clearances. An additional analysis was also carried out under ANSYS by modelling the sandwich panel to investigate its effect on the load-bearing capacity of the link under monotonic compressive force. Due to a lack of accurate data, the insulating core was assumed to be isotropic as a first approximation. A simple bi-linear elasto-plastic model was used, assuming the following core properties (consistent with the material properties given by the manufacturer) in the model:

- Compressive strength fc= 0.095 N/mm², and
- Young's modulus E= 5000 N/mm²

2.2.1.1 Monotonic tension loading

Figure 2.10 compares the predicted link response in terms of force-displacement to the experimental ones (denoted by "CH6" and "CH7" in the figure). Each predicted curve is a resulting plot of the total vertical force calculated by summing the reaction forces of all nodes at the fixed end of models against the prescribed vertical displacement. Through the figure, it can be noted that the experimental force–displacement curves exhibit a first stage that appears linear (or lightly nonlinear), followed by a brittle failure stage evidenced by a sudden drop in force. When bolt-hole clearances are not considered, the predicted force–displacement curves experience also a linear stage, up to a vertical displacement Dy^+=2.8 mm corresponding to a maximum force value F=125 kN, followed by a plateau stage corresponding to the shear yielding of the cross-sectional area of all aluminium bolts. Accounting for bolt-hole clearances leads to a delay in the force increase, which starts when bolts come into bearing within the holes, as well as an increase of the yield displacement Dy^+, which can be estimated to 5.6mm (by including bolts slipping). On the other hand, bolt-hole clearances have no significant effect on the predicted failure load value. As expected, the models predict the failure of the studied link by shearing of the aluminium bolts row. The load-bearing capacity predicted is very close to the one observed during the test, namely 128.8 KN (which corresponds to an error of 3% between the predicted and measured values). However, it can also be seen that there is a discrepancy in the prediction of the initial stiffness of the studied link in comparison to the experimental stiffness, which appears significantly lower than the numerically predicted one. Usually, because the bolt diameter is smaller than the hole diameter, bolt slippage occurs when a bolted steel connection is subjected to a certain amount of load. Thus, when the applied load exceeds the sliding load of the bolt (equal to the sum of the static friction force between the contact surfaces of the link, increased by any bolt preload), relative sliding will occur between the bolts and the steel profiles, resulting in a plateau in the load-displacement curve that characterises the behaviour of the bolted steel connection. However, no plateau was observed in the experimental curves. As no preload force (or only a minimal amount) was applied to the aluminium bolts during installation, it was believed that the initial stiffness had been overestimated mainly due to the clearances and corresponding slippage between the steel profiles and bolting, which are difficult to simulate accurately. Clearances in the bolt holes allow some movement in the link, which can lead to increased bolt rotation and decreased bolt-hole contact areas, thereby decreasing the link stiffness. . The stiffness discrepancy could also be due to phenomena which are not accounted in FE models, like possible slipping between the screw and nut thread or progressive crushing of the bearing flank of the thread (that supports shearing forces) of aluminium bolts with the bearing stresses. Moreover, it is worth noting that the final part of the experimental curves is not accurately captured and that the specimen deformations, and hence the specimen ductility, are over-estimated if the bolts fracture is not explicitly considered. On the other hand, a sharply force decrease can been observed if the fracture of bolts is considered in modelling by adding a descending branch in the bolt material law (curve denoted "MLWDB" in Figure 2.10), because the link suddenly lost bearing capacity. At last, it can be also underlined the satisfactory agreement between the two models developed under ANSYS and Ls-dyna, even if some discrepancies can be noted which are mainly attributed to the different contact types used in both models.

The failure modes of the specimen are recognized by checking/analysing the strain level reached in the different components constituting the studied fusible link. For illustrative purpose, Figure 2.12 shows the distribution of the Von mises total mechanical strain predicted in aluminium bolts from the ANSYS model without bolt-hole clearances. The strain distribution is given for different levels of imposed displacement (so different force levels), by showing strain values exceeding 5% only. It

clearly shows a yielding line progressively propagating in the cross-sectional area of bolts, in the shear plane at the junction between the U and Z shaped steel profiles. Figure 2.13 displays the distribution of the Von mises total mechanical strain predicted in other components of the link with the ANSYS model without bolt-hole clearances, at the simulation end. It can be noted that the strain level exceeds locally the 0.2% yield strain, around the holes of aluminium bolts only, highlighting that some bearing occurs in steel plates, with limited holes elongation. Steel bolts and steel rods have only slight deformation, and no damage occurs in analyses.

For information, Figure 2.14 summarises the main results obtained at failure time of aluminium bolts from modelling developed under Ls-dyna without bolt-hole clearances. The results are in good agreement with the ones reported for the ANSYS model.

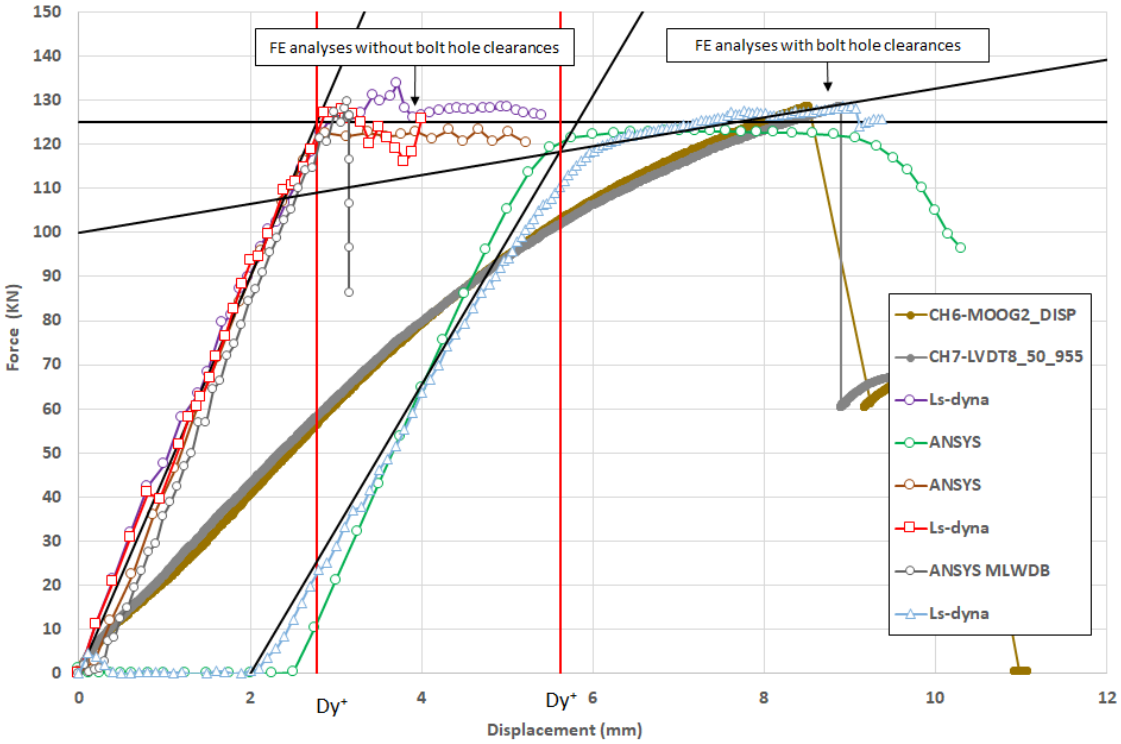

Figure 2.10: Force-displacement curves obtained from FE analyses and experiment for the fusible link configuration n°1 under tensile action

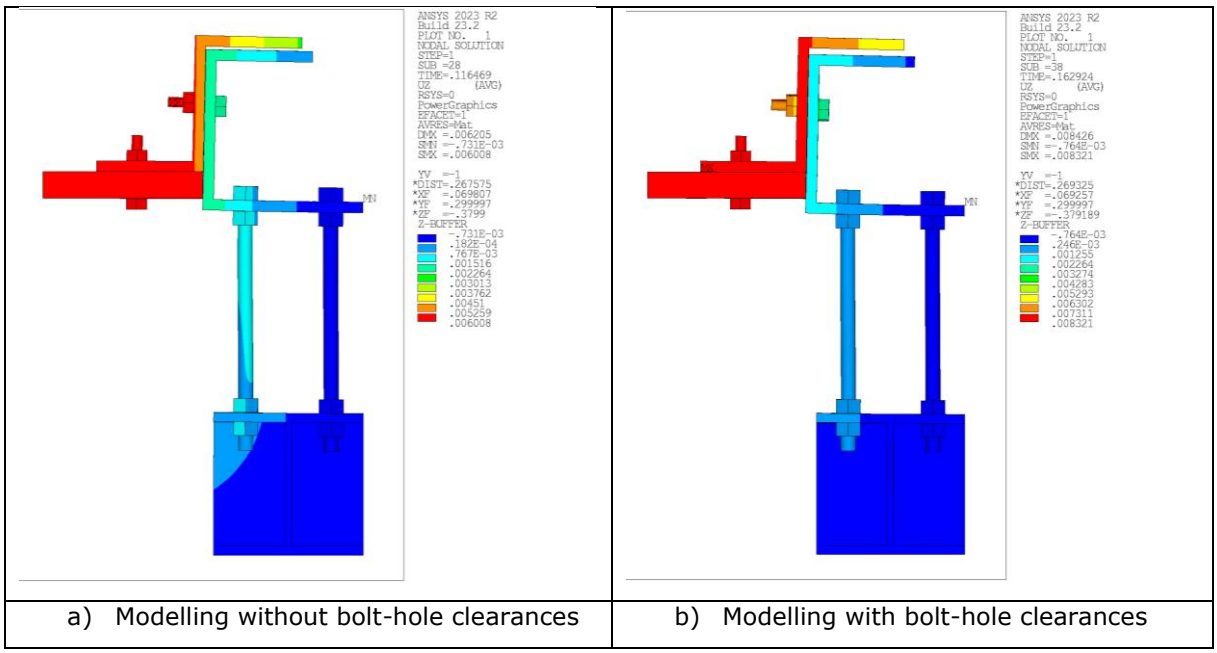

a) Modelling without bolt-hole clearances

b) Modelling with bolt-hole clearances

Figure 2.11: Deformed shape of the fusible link configuration n°1 predicted with the ANSYS models at simulation ends

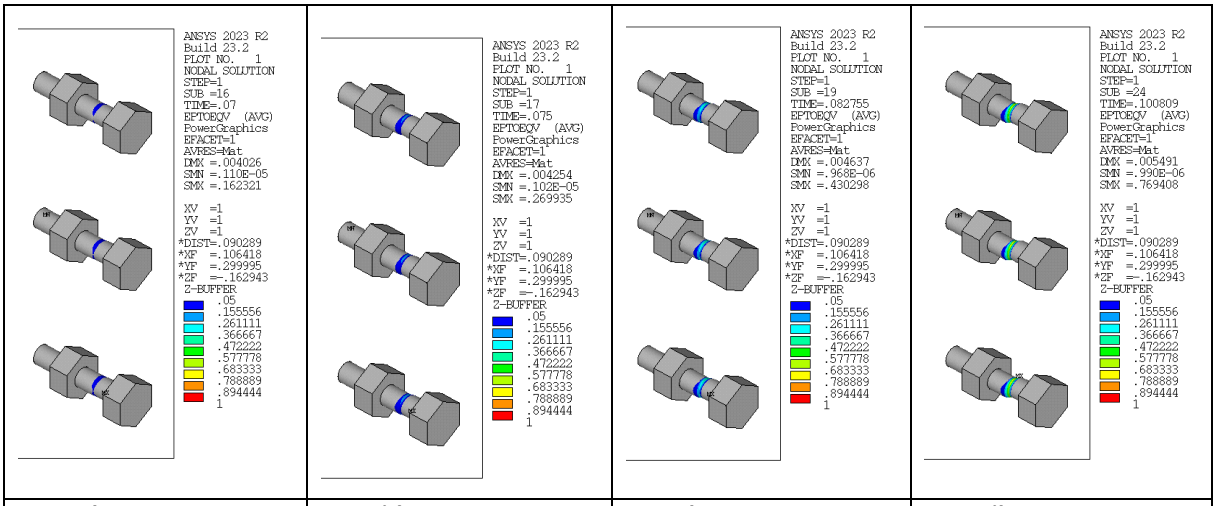

a) U=1.1Dy⁺ (T=122 kN)	b) U=1.2Dy⁺ (T=122 kN)	c) U=1.35Dy⁺ (T=122.2)	d) U=1.8Dy⁺ (T=123.0)

Figure 2.12: Von mises total mechanical strain in aluminium bolts of the fusible link configuration n°1 predicted for different values of imposed displacement with the ANSYS model without bolt-hole clearances

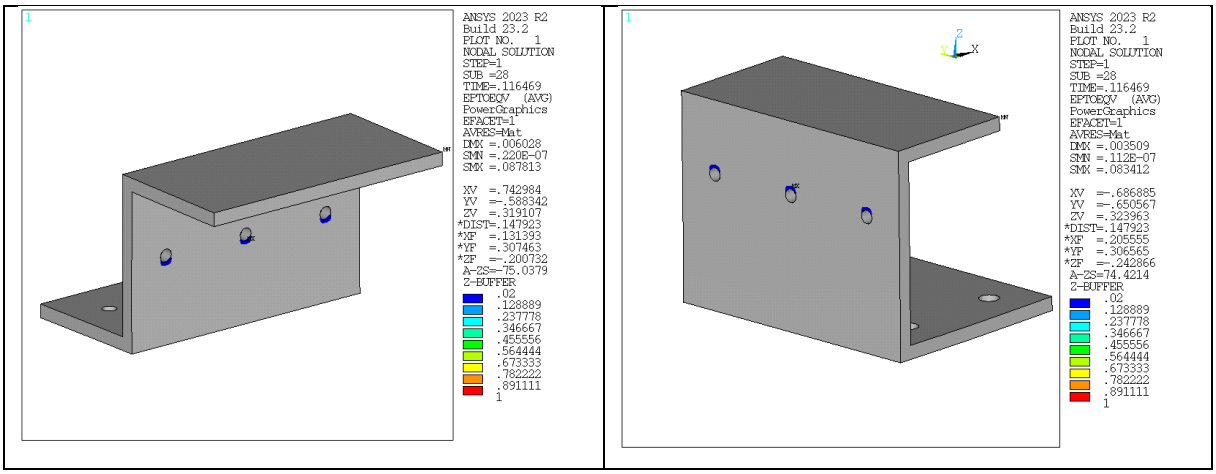

Figure 2.13: Von mises total mechanical strain in steel profiles of the fusible link configuration n°1 predicted with the ANSYS model without bolt-hole clearances, at simulation end

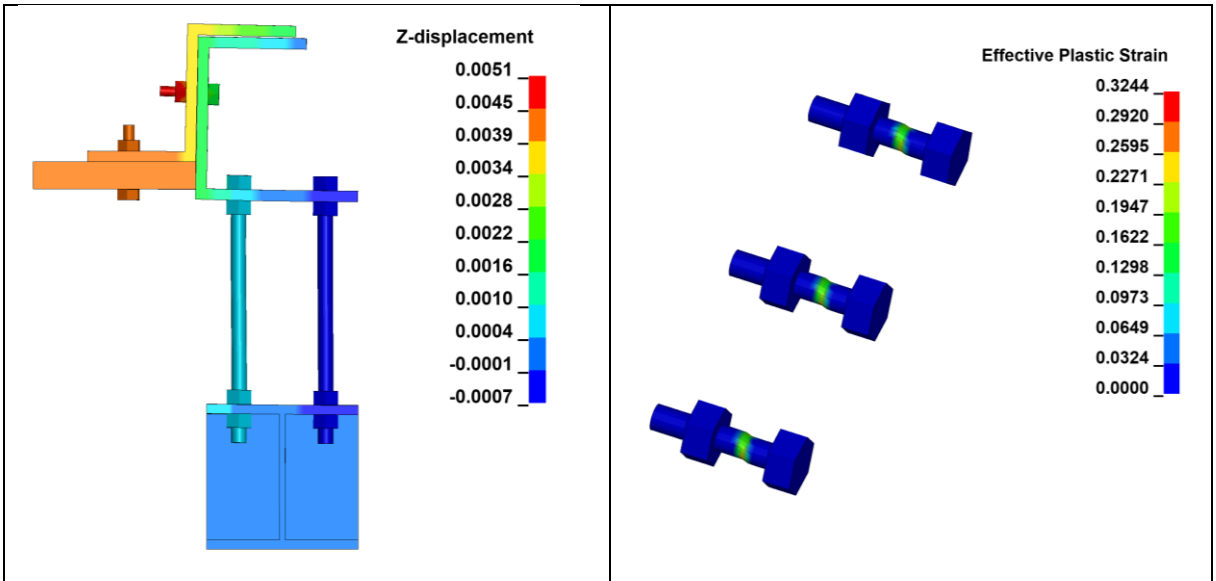

a) Deformed shape	b) Effective plastic strain in aluminium bolts

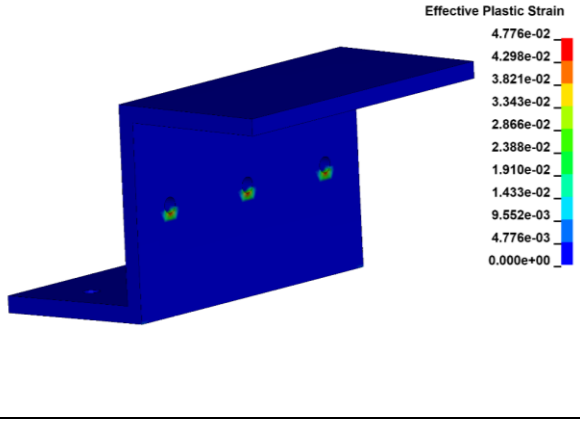

c) Effective plastic strain in the Z-shaped profile

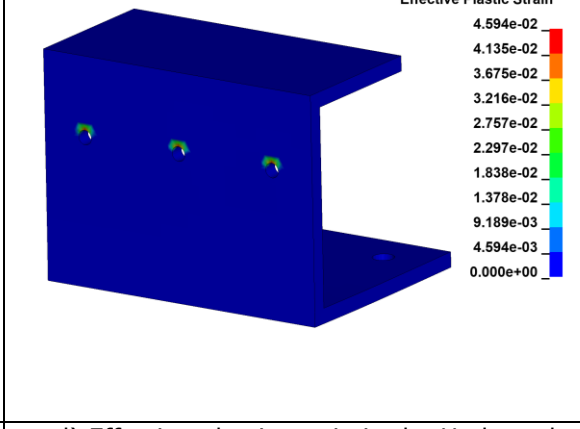

d) Effective plastic strain in the U-shaped profile

Figure 2.14: Main results obtained at failure time of bolts from modelling without bolt-hole clearances developed under Ls-dyna

2.2.1.2 Monotonic compression loading

Figure 2.15 compares the predicted force-displacement curves to the experimental ones (denoted "CH4" and "CH6" in the figure). The predicted curves are a resulting plot of the vertical force calculated by summing the vertical reaction forces of all nodes at the fixed end against the vertical displacement imposed to the specimen. In contrast to the monotonic tension loading, the test specimen exhibits a ductile behaviour rather than a brittle one, by undergoing large plastic deformations. For increasing value of imposed displacements, the experimental curves mainly consist of four different stages: (i) a first linear stage at which corresponds an initial elastic stiffness, (ii) a stiffness degradation stage highlighting the nonlinear behaviour of the fusible link, in which the load-bearing capacity reaches a peak value, (iii) a yield plateau stage in which the bearing capacity is maintained at the same or at a slightly lower level, and then (iv) a failure stage, in which the specimen fails. The predicted force–displacement curves have the same overall shape as the experimental ones, even if there is a large initial slip stage happening in the predicted curves when bolt-hole clearances are considered in modelling. Through the figure, it can be also noted that the bolt clearances seem to have an unfavourable effect on the load-bearing capacity of the studied link, at least where the sandwich panel is not modelled, the latter noticeably decreasing in comparison to that achieved without bolt-hole clearances. On the other hand, a lightly higher load-bearing capacity is reached if the sandwich panel is modelled, despite the hole clearances. Lastly, as for the previous case, the test specimen still exhibits a stiffness lower than the one predicted by the models during the initial loading stage. According to the ECCS procedure, the yielding displacement derived from the numerical force-displacement curves is estimated to Dy^{-}= 4.4 mm, whether bolt-hole clearances are considered.

The failure modes of the studied fusible link are assessed by monitoring the strain states of different components constituting the link. For illustrative purpose, Figure 2.17 illustrates the distribution of the Von mises total mechanical strain predicted in all components of the fusible link from the ANSYS model without bolt-hole clearances, at simulation end. Strain values exceeding 2% in steel members and 5% in bolts and rods respectively are highlighted. The strain distribution in components shows clearly the yield-line patterns arising in the steel plates, along the bolt row and along the rod row closest to the flange of the U-shaped steel-profile. It can also be noted that the maximum strain in bolts and rods does not exceed the maximum admissible material elongation at break.

The fusible link behaviour in terms of displacements, deformations and failure modes predicted by the two models are very close. The models predict the same failure modes that those observed during the test (see Figure 2.19), corresponding to the bending failures of flanges and webs of the steel profiles forming the fusible link. Steel rods suffer also important bending caused by the deformation of steel profiles. As expected, the aluminium bolts are not damaged, the load-bearing capacity being provided mainly by the steel profiles forming the fusible link.

The load-bearing capacity predicted by the models ranges from 90 to 105 kN, depending on whether bolt clearances are considered in modelling. It is lower than the experimental failure load, which is around 116 kN. In the present case, differences are believed to be due partly to uncertainties concerning the actual values of the steel strengths of profiles and bolting as well as actual bolt-hole clearances. This could be also due to the presence of the sandwich panel, which is not accurately

modelled or not considered. The sandwich panel has beyond any doubt a favourable effect on the load-bearing capacity of the link, on one hand by limiting both the steel profiles and rods deformations, and on the other hand by contributing to the overall load-bearing capacity of the link.

For information, Figure 2.18 summarises the main results obtained at failure time of bolts from modelling developed under Ls-dyna without bolt-hole clearances. The results are in good agreement with the ones reported for the ANSYS model.

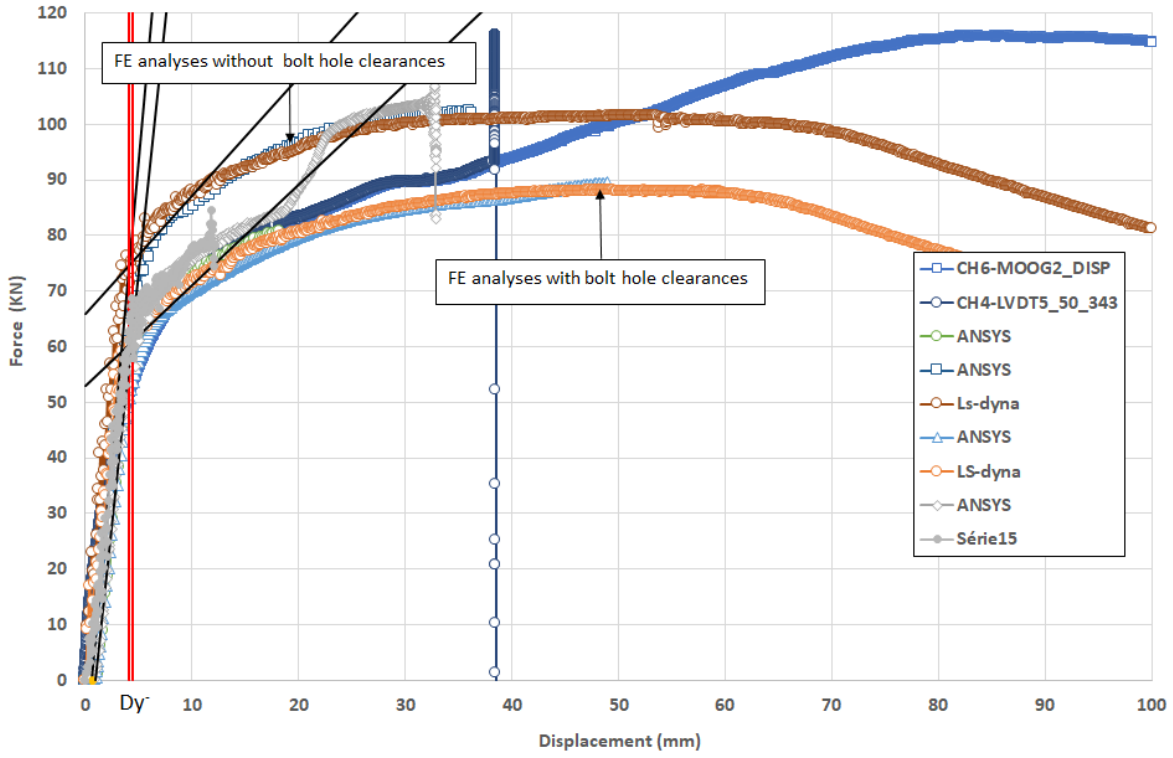

Figure 2.15: Force-displacement curves obtained from FE analyses and experiment for the fusible link configuration n°1 under compressive action

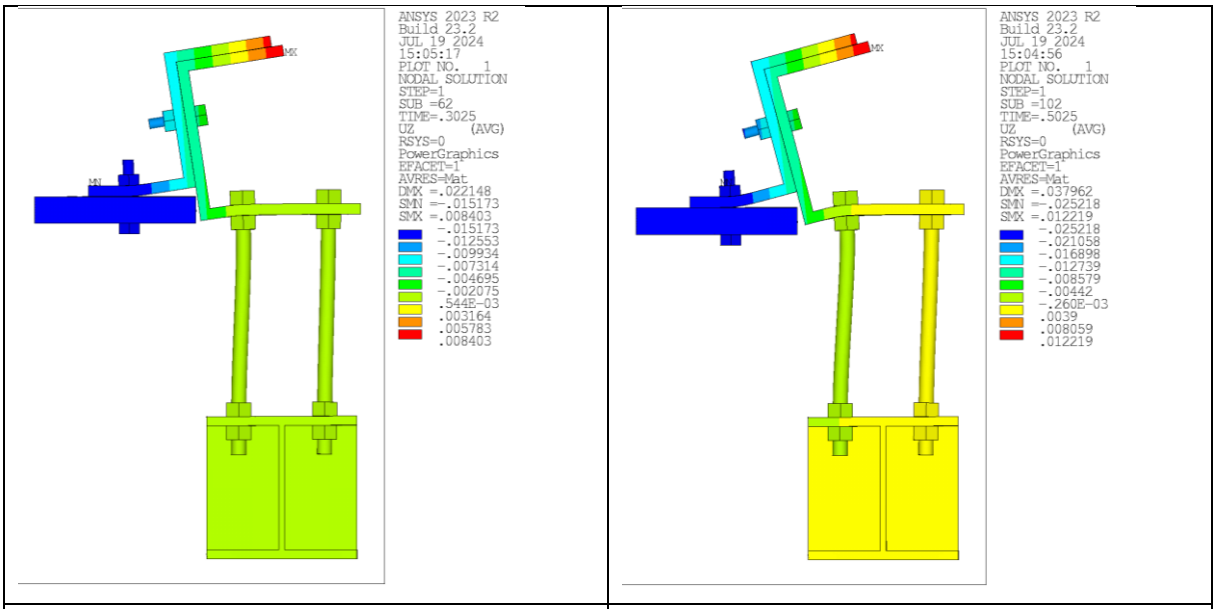

a) U=3.4Dy⁻ (T=92 kN)	a) U=5.8Dy⁻ (T=100 kN)

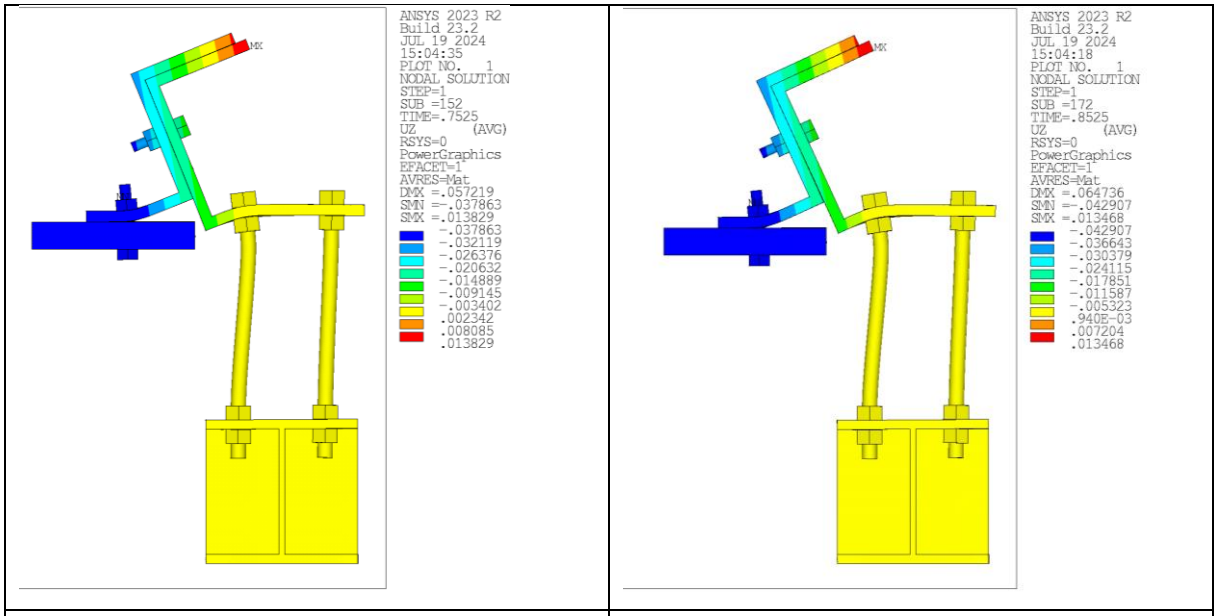

a) U=8.5Dy⁻ (T=102 kN)	a) U=10Dy⁺ (T=103 kN)

Figure 2.16: Deformed shape of the fusible link configuration n°1 predicted with the ANSYS model without bolt-hole clearances

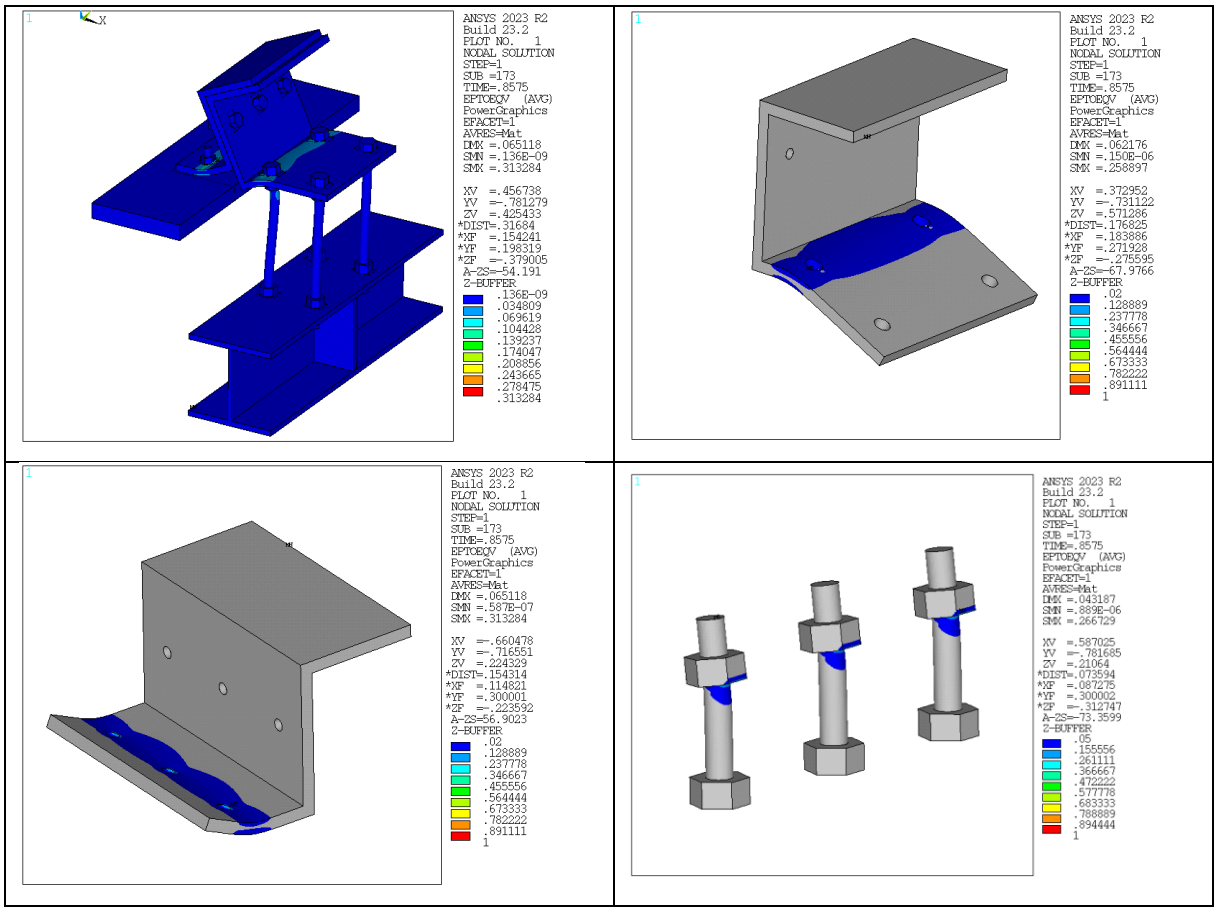

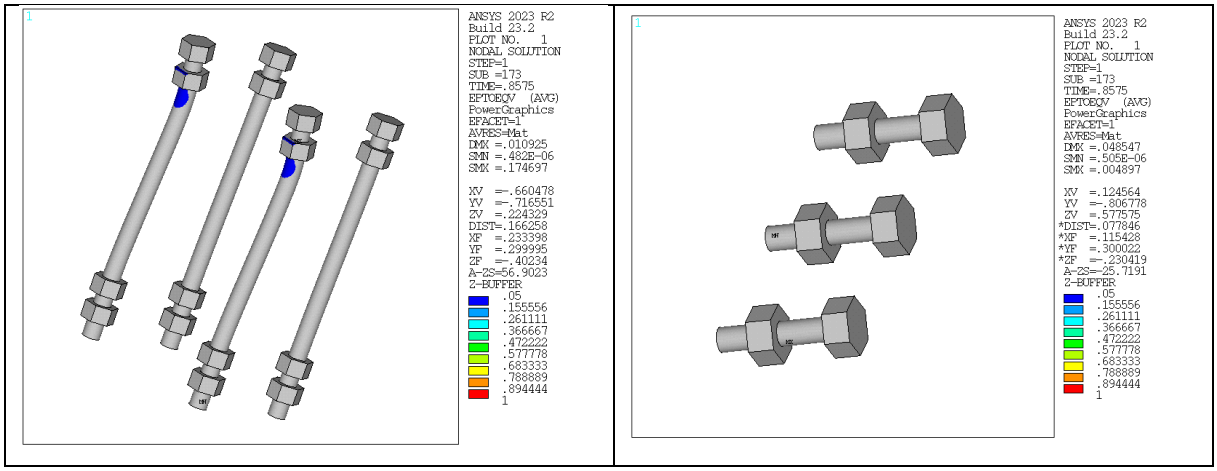

Figure 2.17: Von mises total mechanical strain in all components of the fusible link configuration n°1 predicted with the ANSYS model without bolt-hole clearances, at simulation end

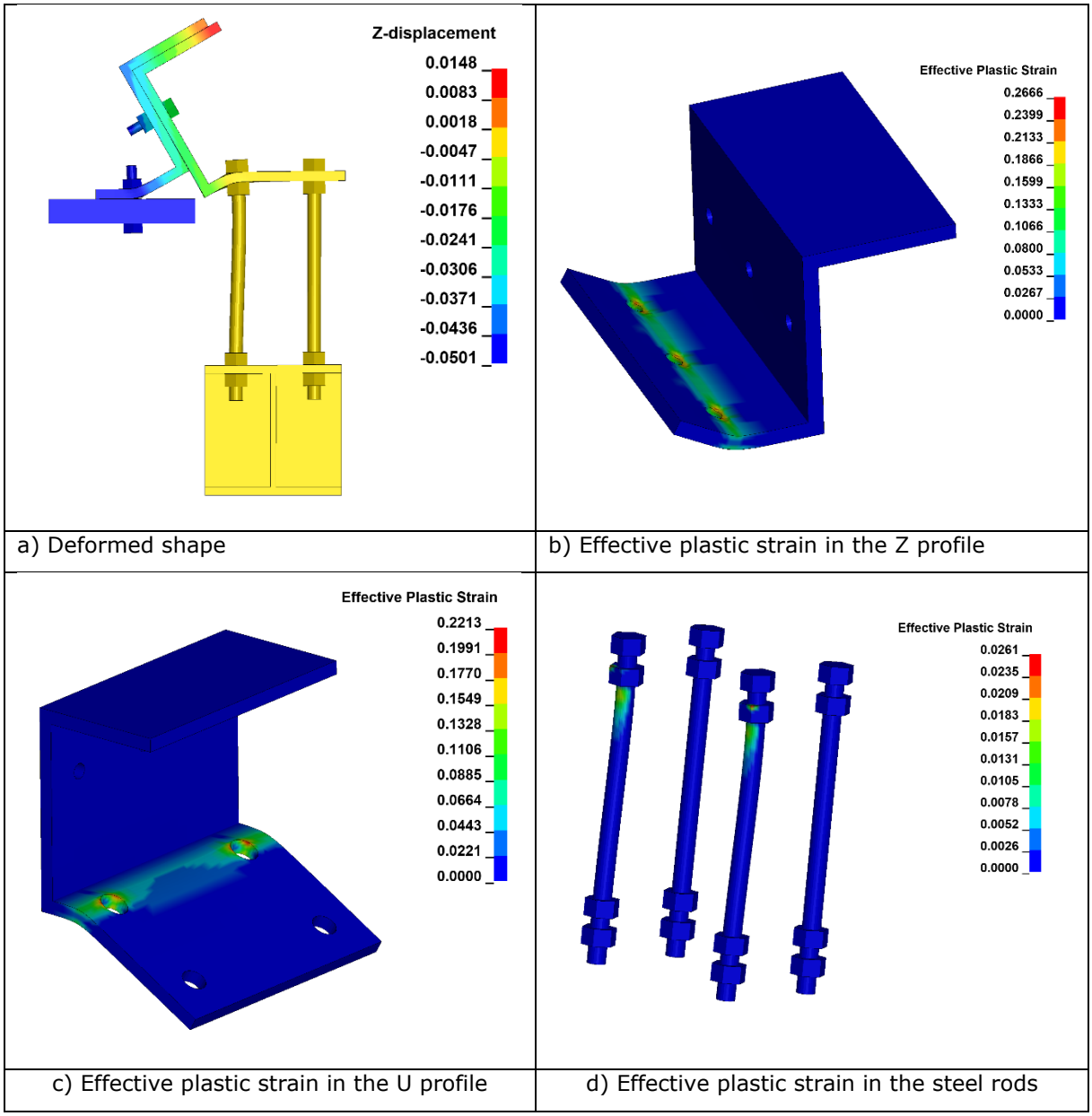

a) Deformed shape

b) Effective plastic strain in the Z profile

c) Effective plastic strain in the U profile

d) Effective plastic strain in the steel rods

Figure 2.18: Main results obtained at simulation end from modelling without bolt-hole clearances developed under Ls-dyna

Figure 2.19: Photos of the test specimen after the test.

2.2.1.3 Cyclic loading

The displacement-time curve prescribed for the numerical cyclic analyses, carried out without bolt-hole clearances, is given in Figure 2.20 while the yield displacements obtained from monotonic analyses are reported in Table 2.

Table 2: Yield displacements determined from monotonic analyses of the fusible link detail n°1

	without bolt-hole clearances	with bolt-hole clearances
Dy^+	2.8 mm	5.6 mm
Dy^-	4.4 mm	4.4 mm

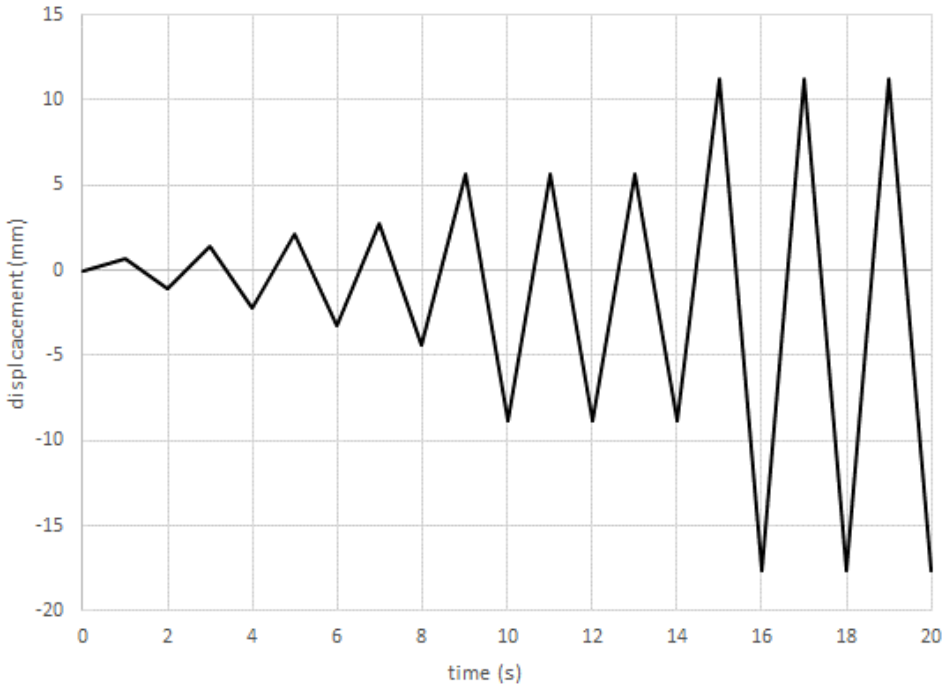

Figure 2.20: Vertical displacement-time curve used in numerical analyses carried out without bolt-hole clearances for the fusible link detail n°1

Figure 2.21 and Figure 2.22 depict the comparison between the FE predicted hysteresis axial force-displacement responses and the test results. In these figures, the negative values mean that the components are under compression, and positive values are for tension. Through the predicted hysteresis curves, it can be noted that in the early stage of loading the specimen remains in the elastic stage and the predicted force–displacement curves are predominantly linear for non-zero forces. The area of the hysteresis loops is very small, and there is no residual deformation. Then, with the increase of loading displacement, the hysteresis loops are still linear in tension, while the hysteresis loops in compression are progressively bow-shaped, indicating that the studied specimen enters the yielding stage. For illustrative purpose, the strain distribution reported in Figure 2.25 illustrates clearly the yield-line patterns which arise in the steel plates, along the bolt row and along the rod row closest to the flange of the U-shaped steel-profile. By comparing the models, it can be noticed that the hysteresis loops are lightly wider with the Ls-dyna model than that of the ANSYS model, probably because of a little larger plasticisation and then a more energy dissipation. Accounting for bolt-hole clearance in modelling only leads to a delay in the force increase, which starts when bolts come into bearing within the holes. In this case, the force remains small during the first cycles, until the prescribed displacement peaks exceed the maximum value of displacement that the bolts can undergo inside holes. It can be also noted that the predicted cyclic response displays a dissymmetric behaviour in tension and compression, as observed experimentally. It coincides well with the monotonic responses obtained in tension or compression loading.

The failure predicted for the studied specimen occurred on the reloading stage at the first cycle to $2Dy^{+}$ because of the shearing of all aluminium bolts. For illustrative purposes, Figure 2.24 shows the distribution of the Von mises total mechanical strain predicted in aluminium bolts from the ANSYS model without bolt-hole clearances. The strain distribution is given here for different levels of imposed displacement, by showing strain values exceeding 5% only. It clearly shows a yielding line progressively propagating in the cross-sectional area of bolts, at the junction between the U and Z shaped steel profiles. Figure 2.25 displays the distribution of the Von mises total mechanical strain predicted in other link components with the ANSYS model without bolt-hole clearances, at the simulation end. It can be noted that the strain level exceeds locally the 0.2% yield strain, around the holes of aluminium bolts only, highlighting that some bearing occurs in steel plates, with limited holes elongation. Steel bolts and steel rods have only slight deformation, and no damage occurred in analyses.

It should be noted that there is a noticeable discrepancy in the cyclic response of the studied link, between the experiment and the FE modelling. Firstly, like monotonic loading cases, there is a difference in the prediction of the initial stiffness of the specimen, as the experimental stiffness is lower than the numerically predicted one. Secondly, on the experimental curves, unloading and reloading take place from the first cycle along a different path from that of the first loading stage.

The unloading path includes two parts, an elastic unloading phase along a path that seems parallel to the loading path followed in the force-displacement curves predicted by models and a pinched unloading phase until the loading in the opposite direction happens. When unloaded to a 0 kN load in compression, the residual displacement remains small, indicating that the link is still in an elastic stage (or a very partially plastic stage), while when unloaded in tension there is a larger non-zero displacement than numerically predicted which increases progressively with the repeated unloading-reloading cycles. However, the load-bearing capacity predicted for the fusible link is close to the one observed during the tests, namely 124.7 and 127.8 KN respectively. The dissimilarities between the experimental and FE results are believed mainly to be due to clearances and slipping in all hole bolting. Bolt-hole clearances allow some movement in the link and can lead to increased bolt rotation, decreased bolt-hole contact area and then decreased link stiffness. Moreover, the misalignment of bolt and hole, the misalignment of profile or holes of varying sizes can lead to some bolts to remain unstressed from the start of loading. All these phenomena are difficult to be considered accurately in models. This could be also due to phenomena which are not accounted in FE models, like possible slipping between the screw and nut thread or progressive crushing of the bearing flank of the thread (that supports shearing forces) of aluminium bolts with the bearing stresses.

It should be underlined that the cyclic loading does not affect greatly the load-bearing capacity predicted for the studied fusible link. Indeed, the difference between the monotonic and cyclic maximum resistance does not exceed 5 %.

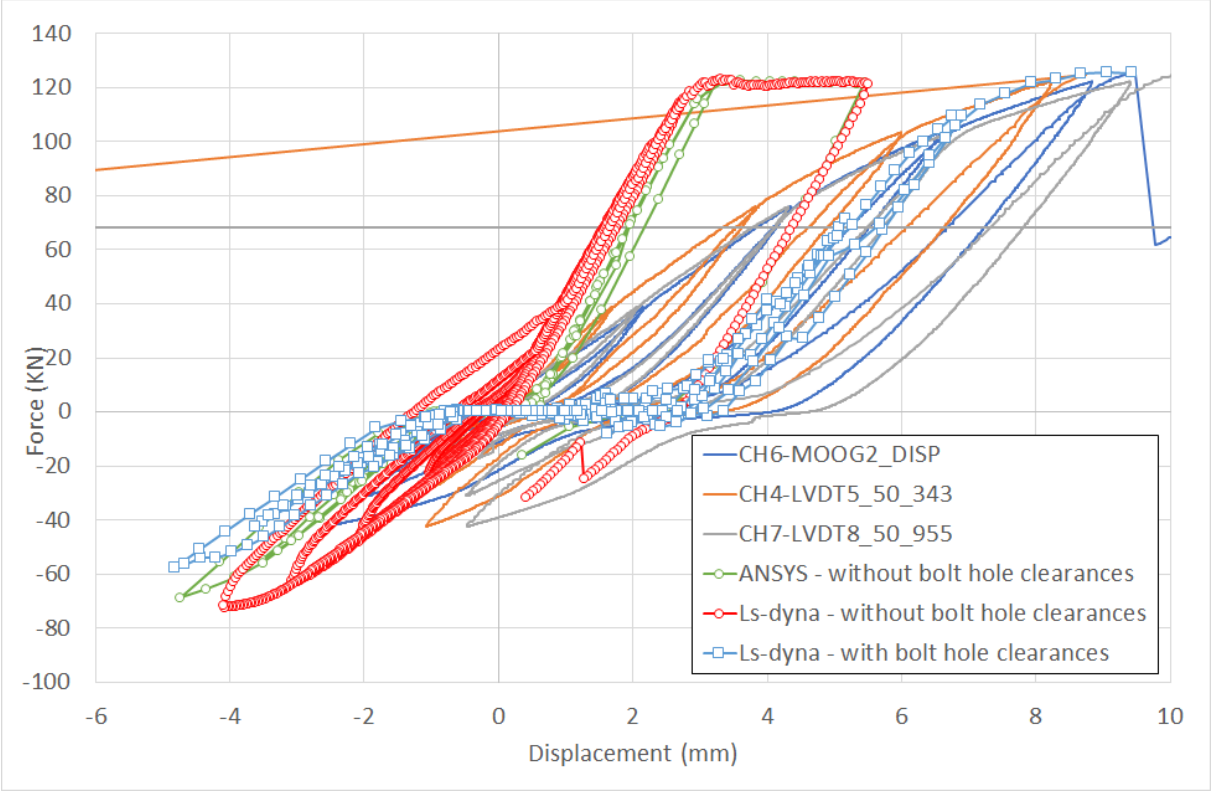

Figure 2.21: Force-displacement curves obtained from FE analyses and experiment (cyclic test n°1) for the fusible link configuration n°1 under cyclic action

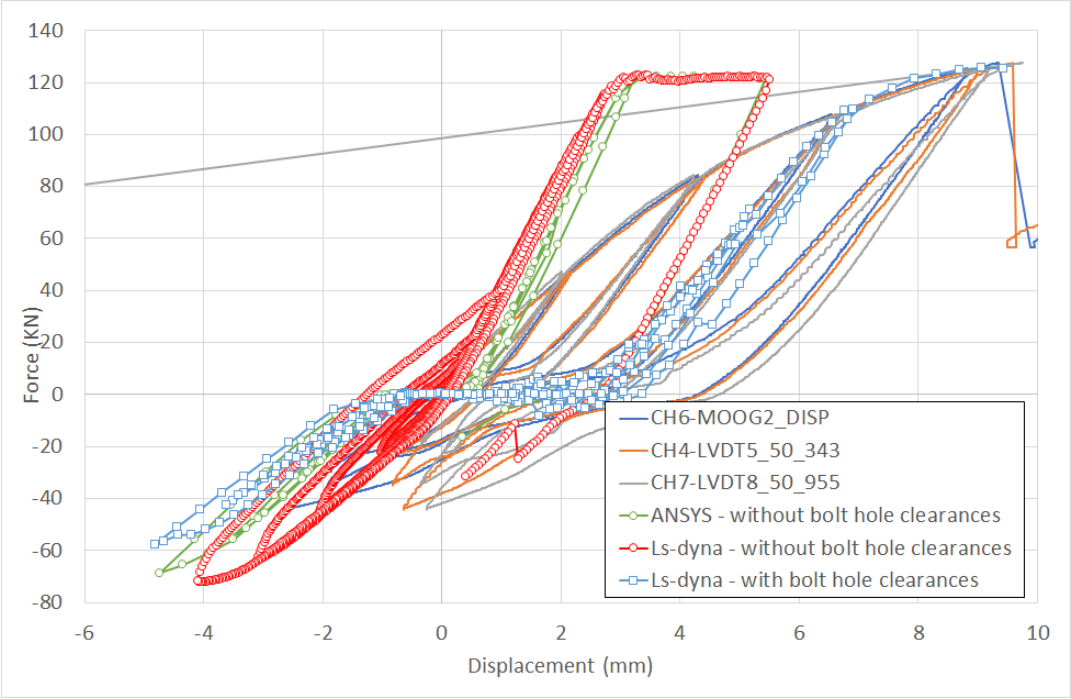

Figure 2.22: Force-displacement curves obtained from FE analyses and experiment (cyclic test n°2) for the fusible link configuration n°1 under cyclic action

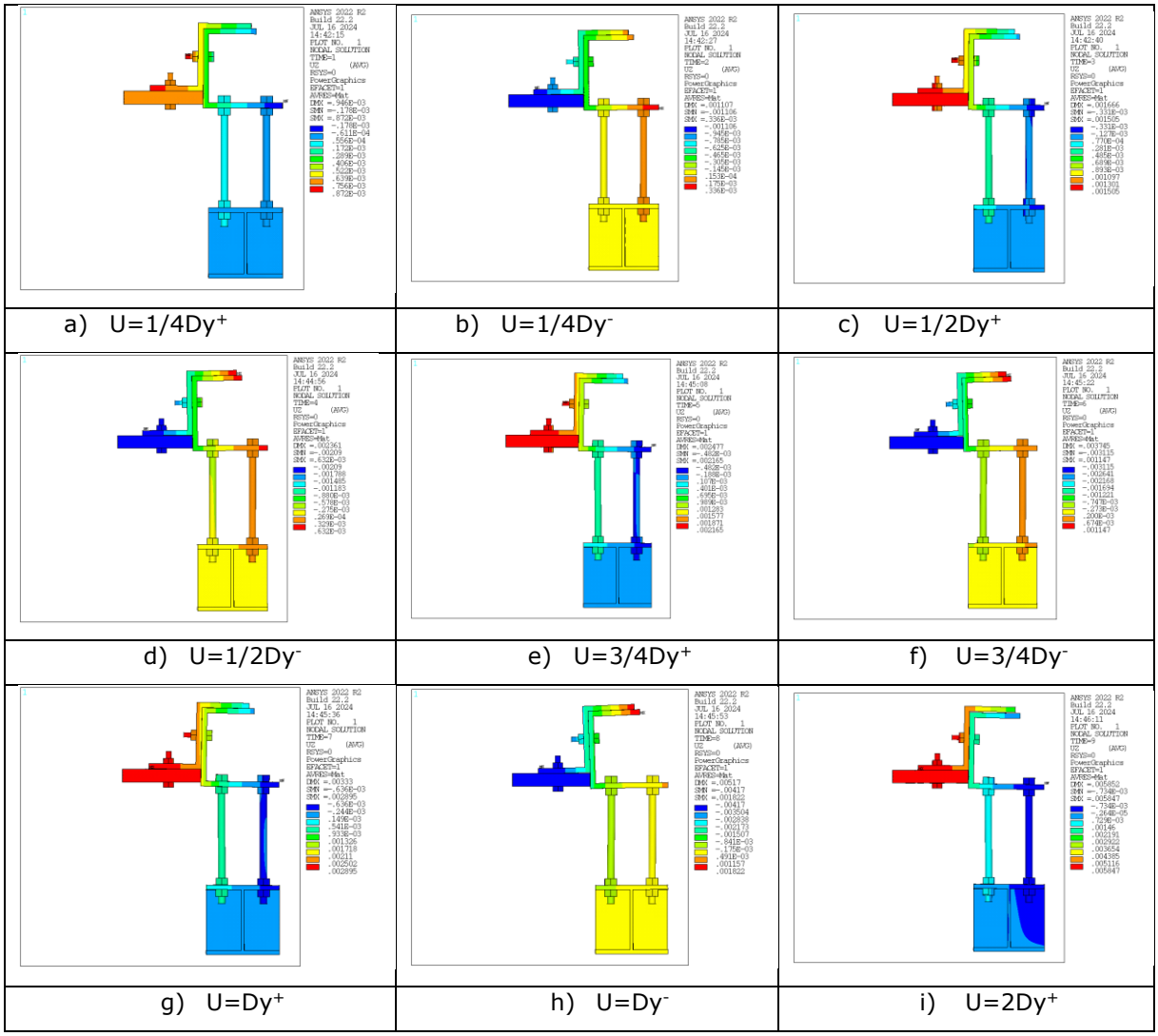

Figure 2.23: Deformed shape of the fusible link configuration n°1 according to imposed displacement values predicted with the ANSYS model without bolt-hole clearances

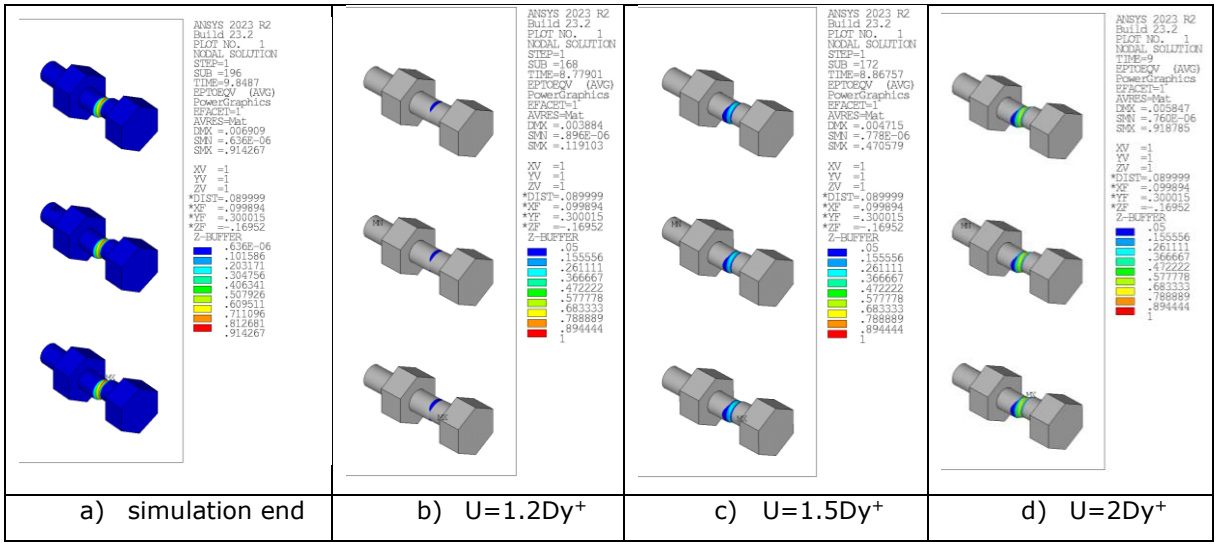

a) simulation end	b) U=1.2Dy⁺	c) U=1.5Dy⁺	d) U=2Dy⁺

Figure 2.24: Von mises total mechanical strain in aluminium bolts of the fusible link configuration n°1 predicted for different values of imposed displacement with the ANSYS model without bolt-hole clearances

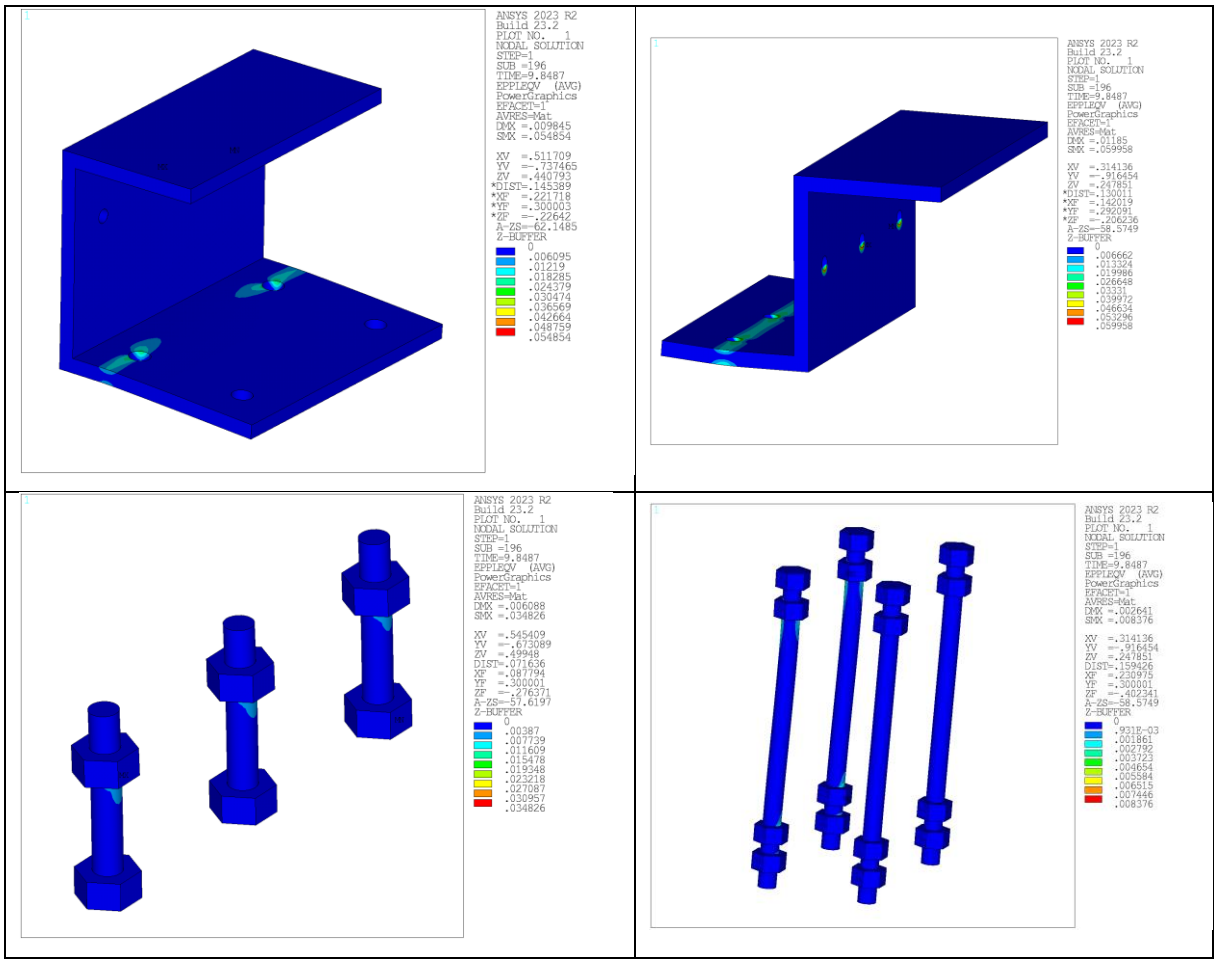

Figure 2.25: Von mises total mechanical strain in components of the fusible link configuration n°1 predicted with the ANSYS model without bolt-hole clearances, at simulation end

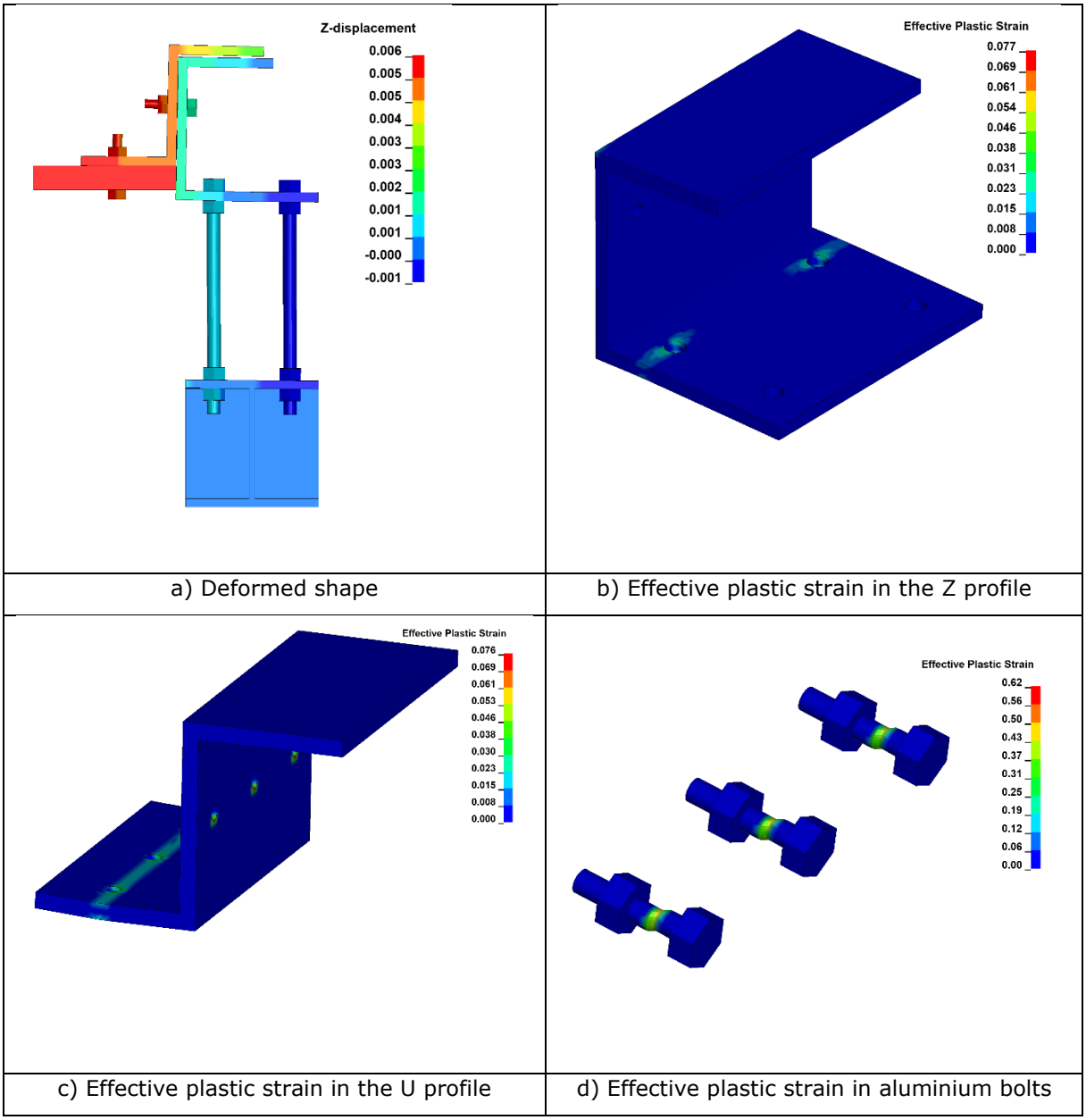

a) Deformed shape

b) Effective plastic strain in the Z profile

c) Effective plastic strain in the U profile

d) Effective plastic strain in aluminium bolts

Figure 2.26: Main results of the modelling of the fusible link n°1 under Ls-dyna without bolt-hole clearances

a) Cyclic test n°1

b) Cyclic test n°2

Figure 2.27: Photos of aluminium bolts after the cyclic tests.

2.2.2 Fusible link configuration n°2

For the detail 2, monotonic analyses were performed with or without bolt-hole clearances.

2.2.2.1 Monotonic tension loading

Figure 2.28 compares the predicted link response in terms of force-displacement to the experimental ones (denoted by "CH5" and "CH6" in the figure). Each predicted curve is a resulting plot of the total vertical force calculated by summing the reaction forces of all nodes at the fixed end of the specimen against the prescribed vertical displacement. Through the figure, it can be noted that the experimental force–displacement curves consist mainly of a slightly non-linear stage, followed a brittle failure stage. When bolt-hole clearances are not considered, the predicted force–displacement curves experience a linear stage up to a vertical displacement Dy^{+}=2.7 mm, followed by a short non-linear stage and then by a plateau stage corresponding approximately to a vertical force F=315 kN, because of the shear yielding of the cross-sectional area of all aluminium bolts. Accounting for bolt-hole clearances leads to a delay in the force increase, which starts when bolts come into bearing within the holes, as well as an increase of the yield displacement Dy^{+}, which can be estimated to 4.6mm (by including bolts slipping). In the other hand, bolt-hole clearances have no significant effect on the failure load value. As expected, the models predict the failure of the test specimen by shearing of aluminium bolts. The predicted load-bearing capacity is slightly underestimated in comparison to experiment, which was estimated to 325.8 KN (which corresponds to an error of 4% between the predicted and measured values). However, as for the first test specimen, there is still a discrepancy in the prediction of the initial stiffness of the specimen, as the experimental stiffness appears noticeably lower than the numerically predicted one. As previously mentioned, this could be attributed to clearances and slipping between the steel profiles and all bolting, which are difficult to accurately consider in models. This could also be due to phenomena which are not accounted in FE models, like possible slipping between the screw and nut thread or progressive crushing of the bearing flank of the thread (that supports shearing forces) of aluminium bolts with the bearing stresses. Moreover, it is worth noting that the final part of the experimental curves is not captured accurately, since not considering bolt fracture leads to an overestimation of the deformations that the specimens can reach and hence the specimen ductility in tension. The predicted curves also coincide quite well with each other, highlighting the satisfactory agreement between the two models developed, even if some discrepancies can be noted which are mainly attributed to the different contact types used in the ANSYS and Ls-dyna models. It should be noted that the predicted curves may be non-smooth in certain loading stages. The developed numerical models take contact interactions between the different parts of the studied fusible links into account. A dynamic solver (either implicit or explicit) was used for the finite element (FE) analyses, depending on the FE codes used. The rough shape observed in the numerical curves is attributed to dynamic effects (due to the speed of load application and the resulting inertia forces), which can cause oscillations at the contact surfaces and interpenetration issues. These phenomena are accentuated when the contacts involve materials with different stiffnesses (e.g. aluminium bolts and steel profiles) and when elements can move relative to each other (sliding). To reduce computing time, the speed of displacement application was minimised while remaining sufficiently high to prevent contact loss between the link components. Dynamic effects were limited as far as possible by changing the meshing, some contact parameters, or by using damping.

The failure modes of the specimen can be recognized by checking/analysing the strain level reached in the different components constituting the studied fusible link. For illustrative purpose, Figure 2.30 shows the distribution of the Von Mises total mechanical strain predicted in aluminium bolts from the ANSYS model without bolt-hole clearances. The strain distribution is given here for different levels of imposed displacement (so different load levels), by showing strain values exceeding 5% only. As it can be clearly recognized, a yielding line progressively propagates in the cross-sectional area of bolts in the shear plane at the junction between the L and U-shaped steel profiles. Figure 2.31 shows the distribution of the Von mises total mechanical strain predicted in the other components of the fusible link with the ANSYS model without bolt-hole clearances, at the simulation end. It can be noted that the strain level exceeds locally the 0.2% yield strain in steel profiles, around the holes of aluminium bolts, highlighting that some bearing occurs in steel plates, with limited holes elongation. Steel rods have only slight deformation and don't suffer any damage in analyses.

For information, Figure 2.32 summarises the main results obtained at failure time of bolts from modelling developed under Ls-dyna without bolt-hole clearances. The results are in good agreement with the ones reported for the ANSYS model.

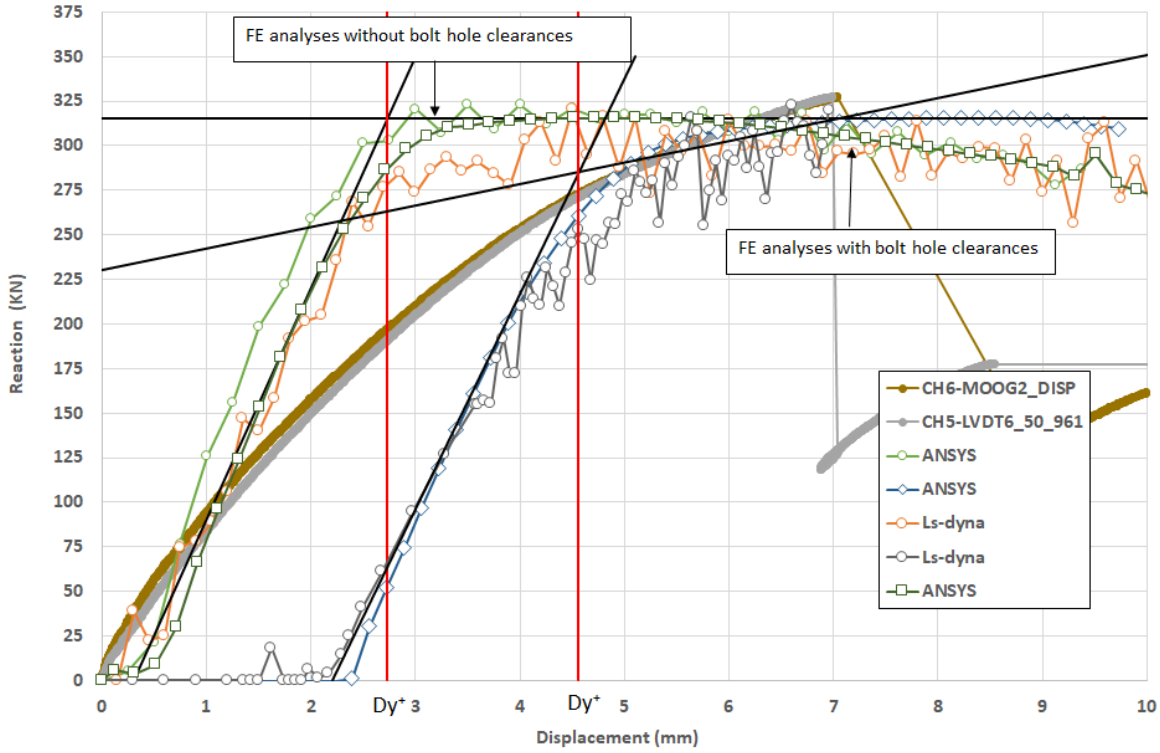

Figure 2.28: Force-displacement curves obtained from FE analyses and experiment for the fusible link configuration n°2 under tensile action

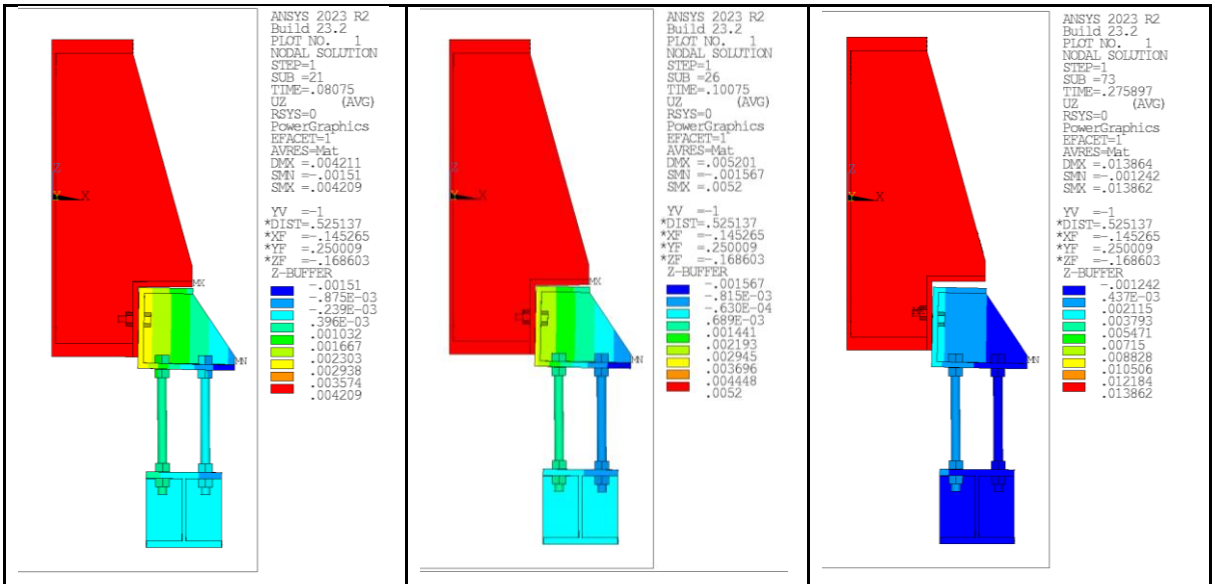

a) U=1.4Dy⁺ (T=313 kN)	b) U=1.8Dy⁺ (T=315 kN)	c) U=5 Dy⁺ (T=191 kN)

Figure 2.29: Deformed shape of the fusible link configuration n°2 predicted with the ANSYS model without bolt-hole clearances

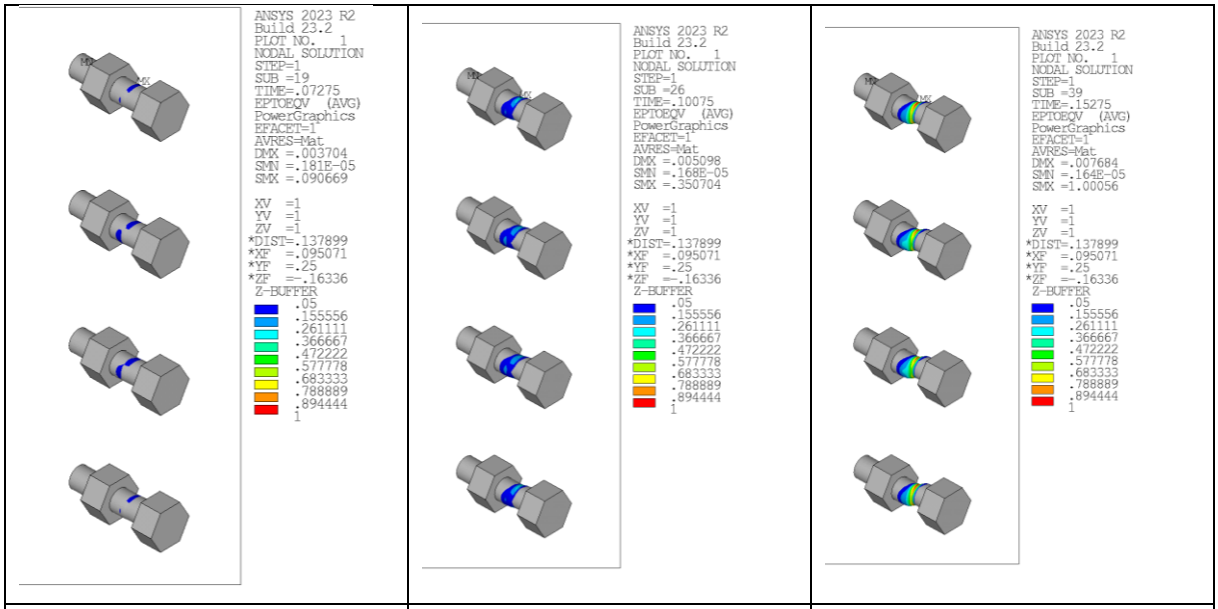

a) U=1.3Dy⁺ (T=315 kN)	b) U=1.8Dy⁺ (T=315 kN)	c) U=2.7Dy⁺ (T=301 kN)

Figure 2.30: Von mises total mechanical strain in aluminium bolts of the fusible link configuration n°2 predicted for different values of imposed displacement with the ANSYS model without bolt-hole clearances

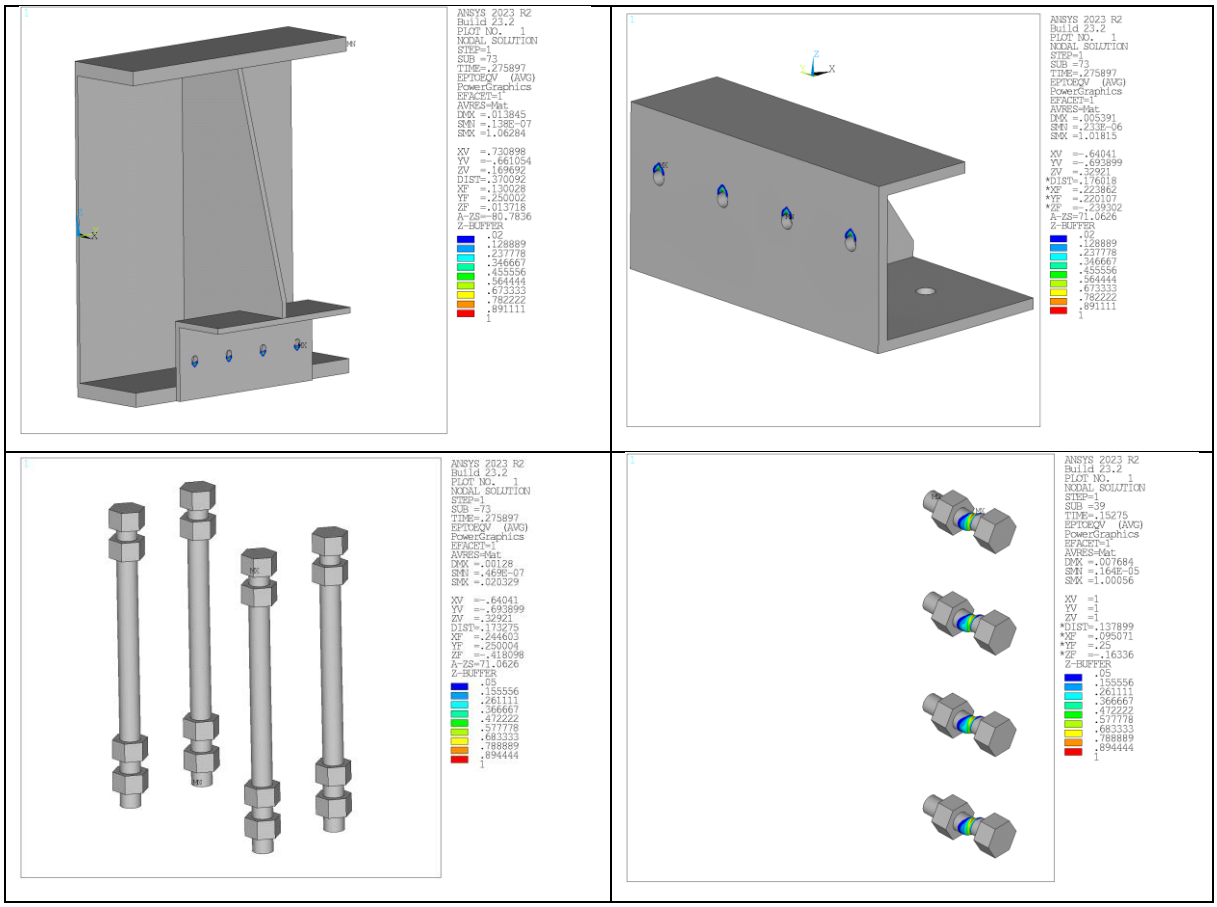

Figure 2.31: Von mises total mechanical strain in components of the fusible link configuration n°2 predicted with the ANSYS model without bolt-hole clearances, at simulation end

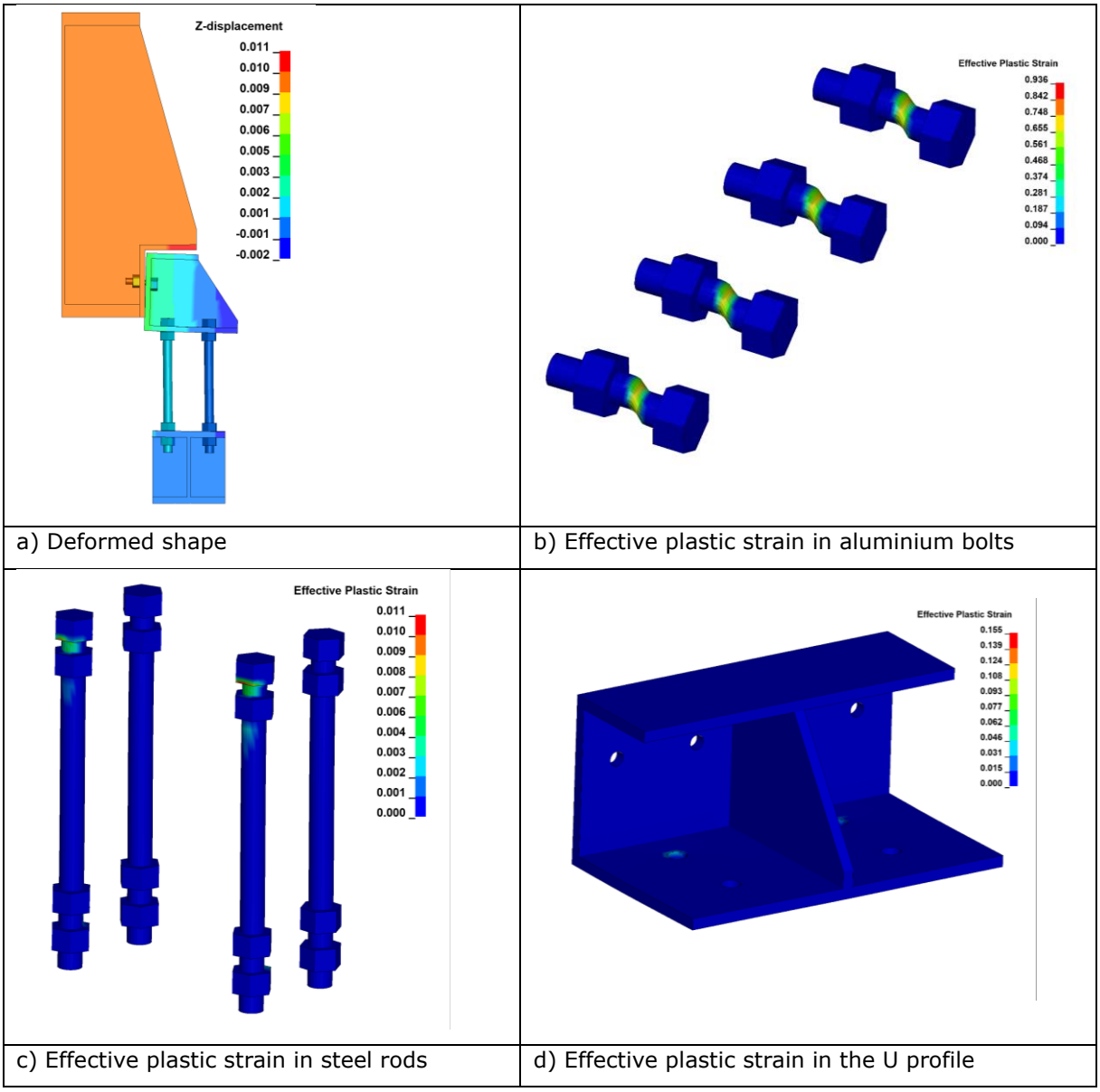

a) Deformed shape

b) Effective plastic strain in aluminium bolts

c) Effective plastic strain in steel rods

d) Effective plastic strain in the U profile

Figure 2.32: Main results of the modelling under Ls-dyna without bolt-hole clearances

2.2.2.2 Monotonic compression loading

Figure 2.33 compares the predicted force-displacement curves to the experimental ones (denoted "CH5" and "CH6" in the figure). The predicted curve is a resulting plot of the vertical force calculated by summing the vertical reaction forces of all nodes at the fixed end against the imposed vertical displacement. In contrast to the tension test, the test specimen under compression force exhibits a ductile behaviour rather than a brittle one, by undergoing large plastic deformations. For increasing value of imposed displacements, the experimental curves mainly consist of four different stages: (i) a first linear stage at which correspond an initial elastic stiffness, (ii) a stiffness degradation stage highlighting the nonlinear behaviour of the fusible link, in which the load-bearing capacity reaches a peak value, (iii) a yield plateau stage in which the bearing capacity is maintained at the same or at a slightly lower level, and then (iv) a failure stage, in which the specimen fails. The predicted force–displacement curves have the same overall shape as the experimental curves, even if the experimental curves show a small initial slip stage. This is attributed to a possible gap between the upper flange of the U-shaped steel profile and the L-shaped profile (not considered in models), which can lead to a short delay in the development of the compressive force. Through the figure, it can be also noted that the test specimen exhibits a stiffness lower than the one predicted by the models during the initial loading stage. According to the ECCS procedure, the yielding displacement derived from the numerical force-displacement curves can be estimated to Dy^{-}=1.7 mm whether bolt-hole clearances are considered.

The failure modes of the studied fusible link are assessed by monitoring the strain states of different components constituting the link. For illustrative purpose, Figure 2.35 shows the distribution of the Von mises total mechanical strain predicted in all components of the fusible link from the ANSYS model without bolt-hole clearances at simulation end. Strain values exceeding 2% in steel members and 5% in bolts and rods respectively are highlighted. The strain distribution indicates clearly the yield-line patterns arising in the U-shaped profile, at the junctions between the lower flange and the web and the stiffener respectively, and around the rod holes. It can also be noted that the maximum strain in bolts and rods does not exceed the maximum admissible material elongation at break.

The fusible link behaviour in terms of displacements, deformations and failure modes predicted by the two models are very close. The models predict the same failure modes that those observed during the test, corresponding to the bending failures of the lower flange of the U-shaped steel profile (see Figure 2.19). Steel rods suffer also important bending caused by the deformation of the steel profile. As expected, the aluminium bolts are not damaged, the load-bearing capacity being provided mainly by the steel profiles forming the fusible link.

The load-bearing capacity predicted by the models varies between 518 kN and 583 kN depending on whether bolt clearances are considered in numerical models. These load values are reasonably close to the experimental failure load, which is around 580 kN. As for the first tested detail, the differences are believed to be due partly to uncertainties concerning the actual values of the steel strengths of profiles and bolting, the actual values of bolt-hole clearances and the load-bearing capability of the sandwich panel, which can contribute to the overall load-bearing capacity of the link.

For information, Figure 2.36 summarises the main results obtained at failure time of bolts from modelling developed under Ls-dyna without bolt-hole clearances. The results are in good agreement with the ones reported for the ANSYS model.

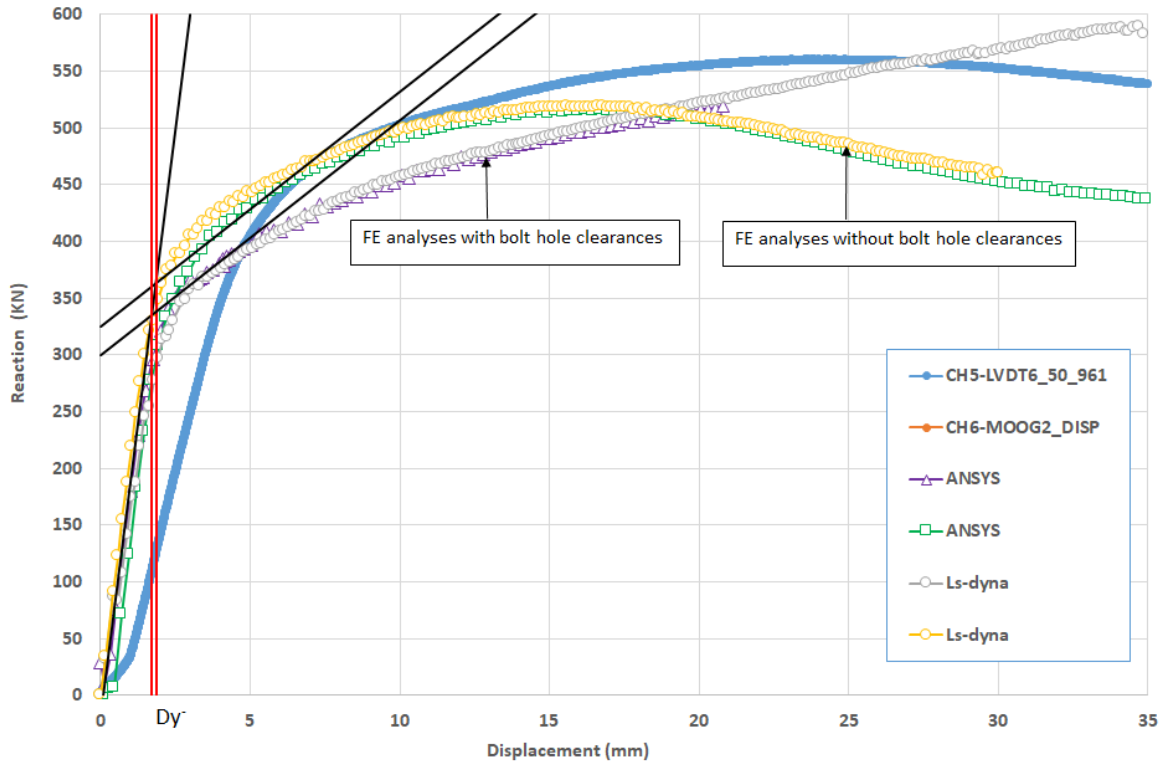

Figure 2.33: Force-displacement curves obtained from FE analyses and experiment for the fusible link configuration n°2 under compressive action

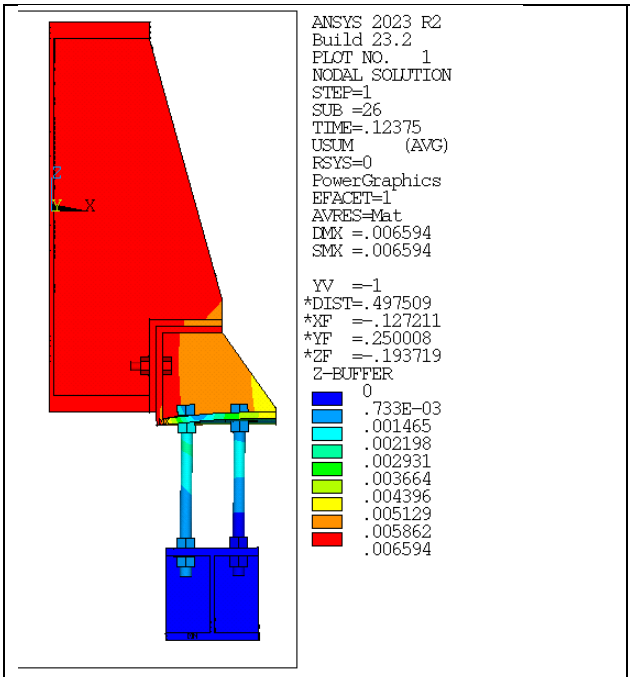

a) U=3.7Dy⁺ (T=451 kN)

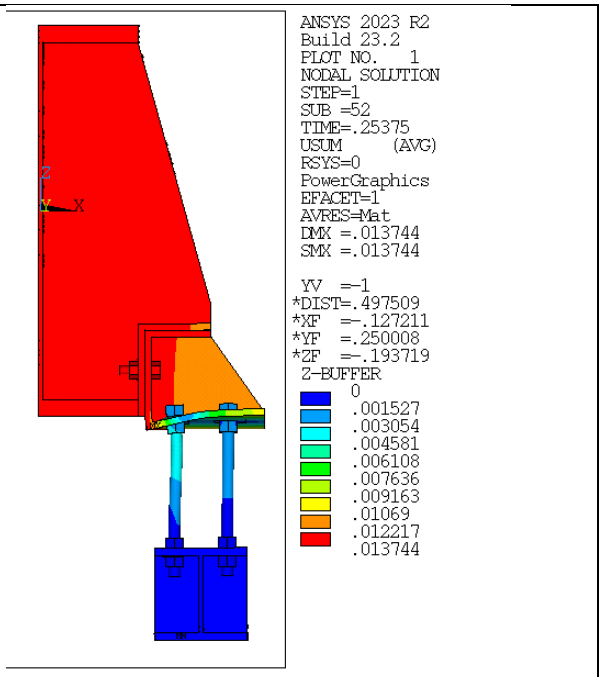

a) U=7.5Dy⁺ (T=507 kN)

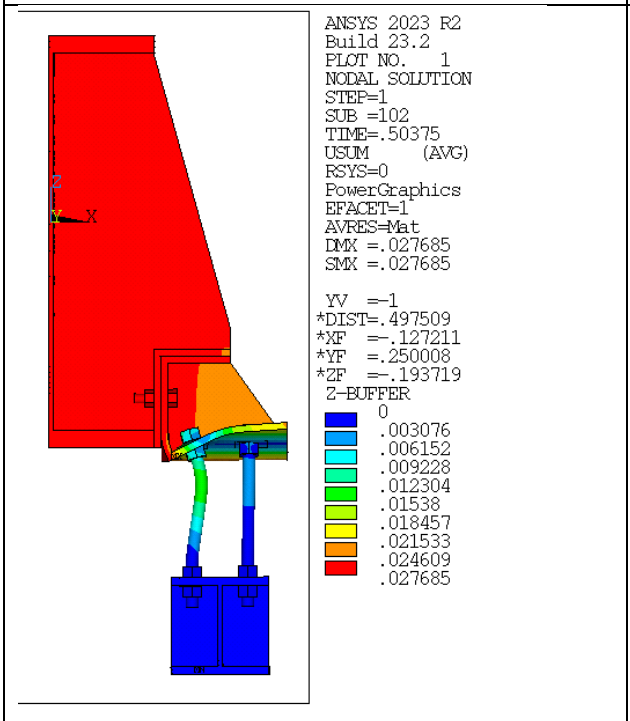

a) U=14Dy⁺ (T=478 kN)

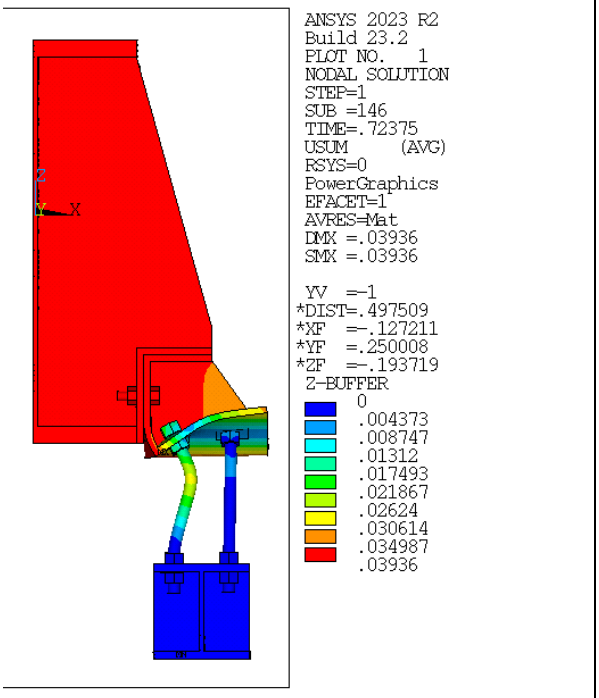

a) U=20Dy⁺ (T=435 kN)

Figure 2.34: Deformed shape of the fusible link configuration n°2 predicted with the ANSYS models without bolt-hole clearances

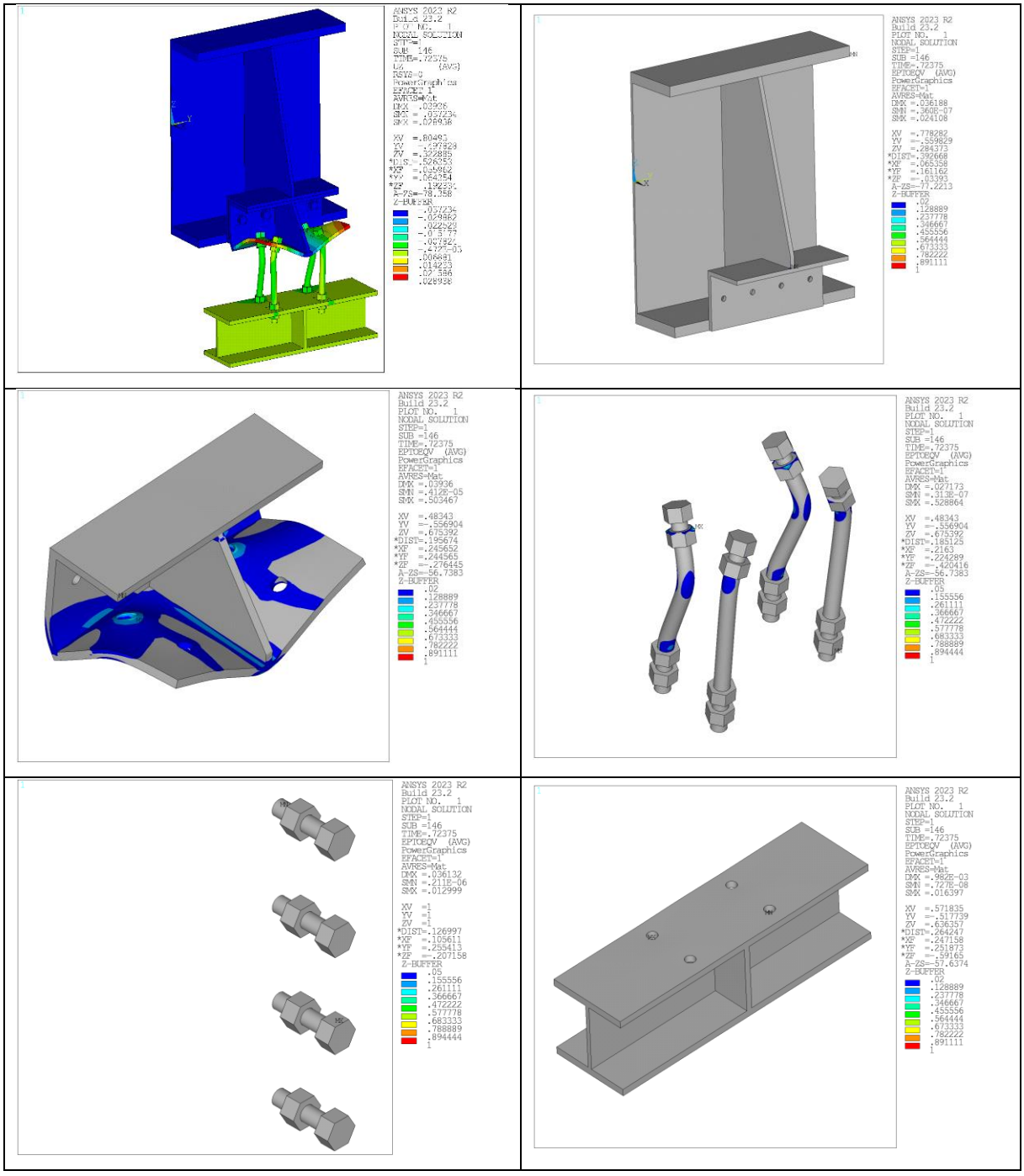

Figure 2.35: Von mises total mechanical strain in components of the fusible link configuration n°2 predicted with the ANSYS model without bolt-hole clearances, at simulation end

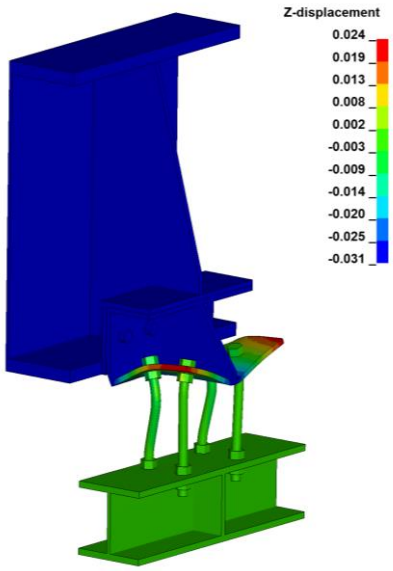

a) Deformed shape

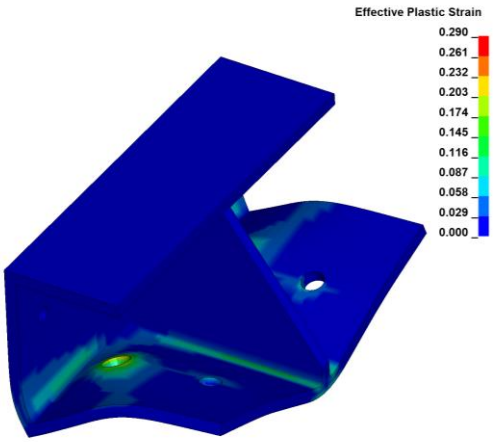

b) Effective plastic strain in the U profile

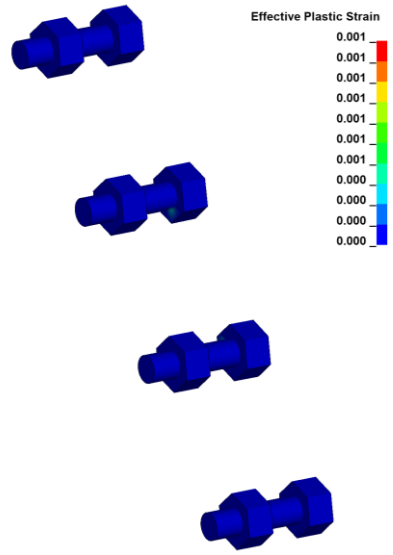

c) Effective plastic strain in aluminium bolts

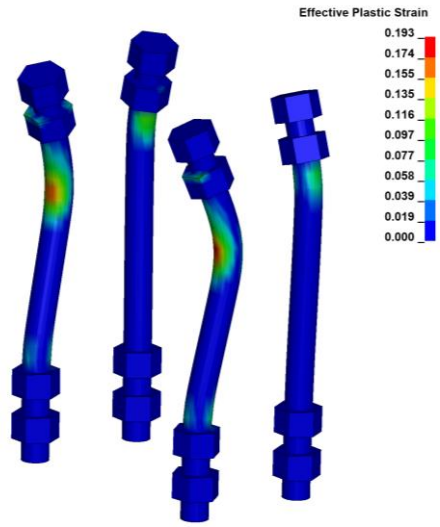

d) Effective plastic strain in the steel rods

Figure 2.36: Main results of the modelling of the fusible link under Ls-dyna without bolt-hole clearances

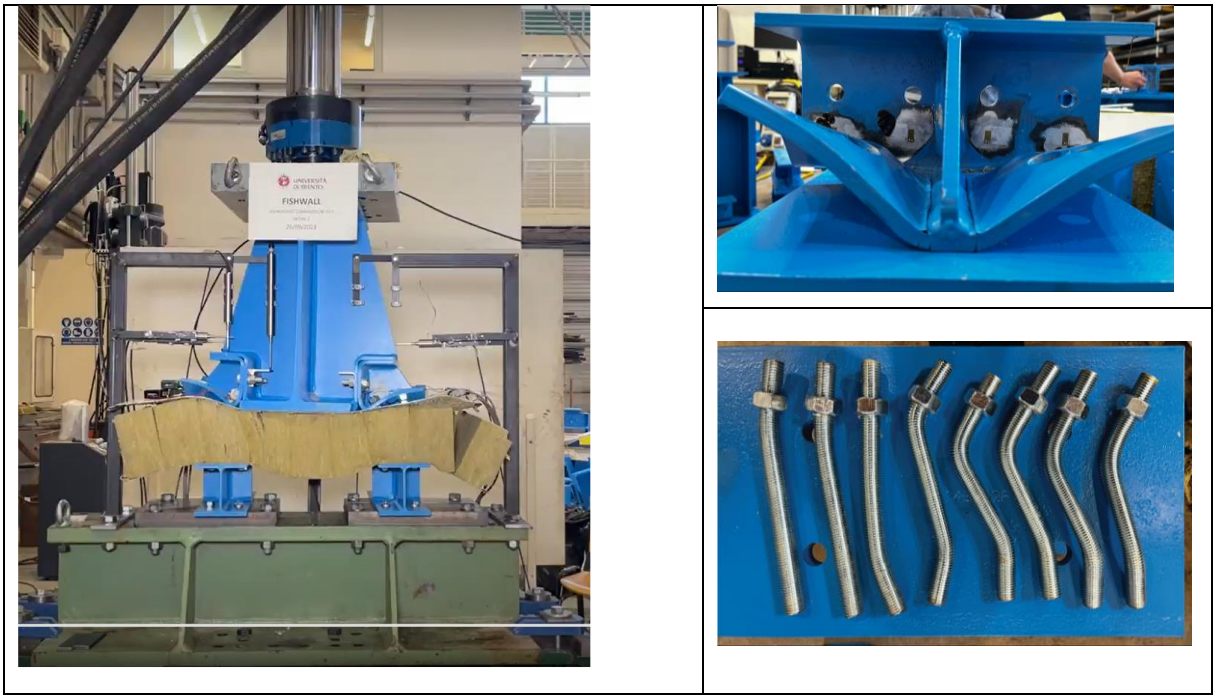

Figure 2.37: Photos of the test specimen after the test.

2.2.2.3 Cyclic loading

The vertical displacement-time curve prescribed in numerical analyses carried out without bolt-hole clearances is given in Figure 2.38 while the yield displacements obtained from monotonic analyses are reported in Table 3.

Table 3: Yield displacements determined from monotonic analyses of the fusible link detail n°2

	Without bolt-hole clearances	With bolt-hole clearances
Dy^+	2.7 mm	4.6
Dy^-	1.7 mm	1.8

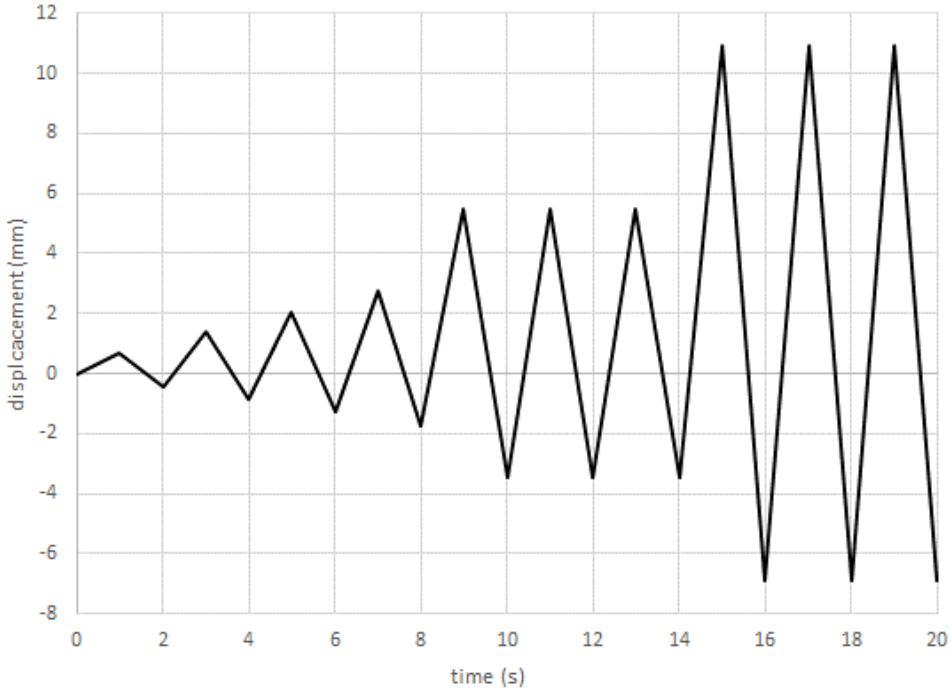

Figure 2.38: Vertical displacement-time curve used in numerical analyses carried out without bolt-hole clearances for the fusible link detail n°2

Figure 2.39 depicts the comparison between the FE predicted hysteresis axial force-displacement responses and the test results. In this figure, the negative values mean that components are under compression, and positive values are for tension. Through the predicted hysteresis curves, it can be noted that in the early stage of loading the specimen remains in the elastic stage and the predicted force–displacement curves are predominantly linear for non-zero forces. The area of the hysteresis loops is very small, and there is no residual deformation. Then, with the increase of loading displacement, the hysteresis loops are still linear in tension, while the hysteresis loops in compression are progressively slightly bow-shaped, indicating that the test specimen enters the yielding stage when approaching the first loading cycle to $2Dy^{+}$. The brittle nature of the detail in tension, highlights a very small hysteretic behaviour of the detail. Accounting for bolt-hole clearance in modelling only leads to a delay in the force increase, which starts when bolts come into bearing within the holes. In this case, the force remains small during the first cycles, until the prescribed displacement peaks exceed the maximum value of displacement that bolts can undergo inside holes. It can be noted that the predicted force-displacement curves display a dissymmetric behaviour in tension and compression, as observed experimentally. The predicted hysteresis curves coincide quite well with each other.

The failure modes of the studied fusible link are assessed by monitoring the strain states of different components constituting the link. The failure of the specimen occurred on the reloading stage at the first cycle to $2Dy^{+}$ because of the shearing of all aluminium bolts. For illustrative purposes, Figure 2.41 shows the distribution of the Von mises total mechanical strain predicted in aluminium bolts from the ANSYS model without bolt-hole clearances. The strain distribution is given here for different levels of imposed displacement, by showing strain values exceeding 5% only. It clearly shows a yielding line progressively propagating in the cross-sectional area of bolts, at the junction between the L and U-shaped steel profiles. Figure 2.42 displays the distribution of the Von mises total mechanical strain predicted in other link components with the ANSYS model without bolt-hole clearances, at the simulation end. Strain values exceeding 2% in steel members and 5% in bolts and rods respectively are highlighted. It can be noted that the strain level exceeds locally the 0.2% yield strain, around the holes of aluminium bolts, highlighting that some bearing occurs in steel plates, with limited holes elongation. Moreover, the strain distribution shows that a yield-line patterns has started to arise in the U-shaped profile, at the junctions between the lower flange and the web and the stiffener, respectively. It can also be noted that the steel bolts and steel rods have only slight deformation, and no damage occurred in these components in analyses.

As the previous case, it should be noted that there is a noticeable discrepancy in the cyclic response of the studied link, between the experiment and the FE modelling. Firstly, like monotonic loading cases, there is a difference in the prediction of the initial stiffness of the specimen, as the experimental stiffness is significantly lower than the numerically predicted one. Secondly, on the

experimental curves, unloading and reloading take place from the first cycle along a different path to that of the first loading stage. When unloaded to a 0 kN load in compression, the residual displacement increases slightly with the repeated unloading-reloading cycles, indicating that the link undergoes plastic stage (or very partially plastic stage), while when unloaded in tension there is a non-zero displacement different to that of numerically predicted, which increases progressively with the repeated unloading-reloading cycles because of the bolt travels within holes. However, the load-bearing capacity predicted for the fusible link is close to the one observed during the tests, namely 310.7 and 321.4 KN, respectively. The differences between the experimental and FE results are believed mainly to be due to clearances and slipping in all hole bolting. Bolt-hole clearances allow some movement in the link and can lead to increased bolt rotation, decreased bolt-hole contact area and then decreased link stiffness. Moreover, the misalignment of bolt and hole, the misalignment of profile or holes of varying sizes can lead to some bolts may remain unstressed from the start of loading.

It should be underlined that the cyclic loading does not affect greatly the load-bearing capacity of the studied fusible link. Indeed, the difference between the monotonic and cyclic maximum resistance does not exceed 5 %.

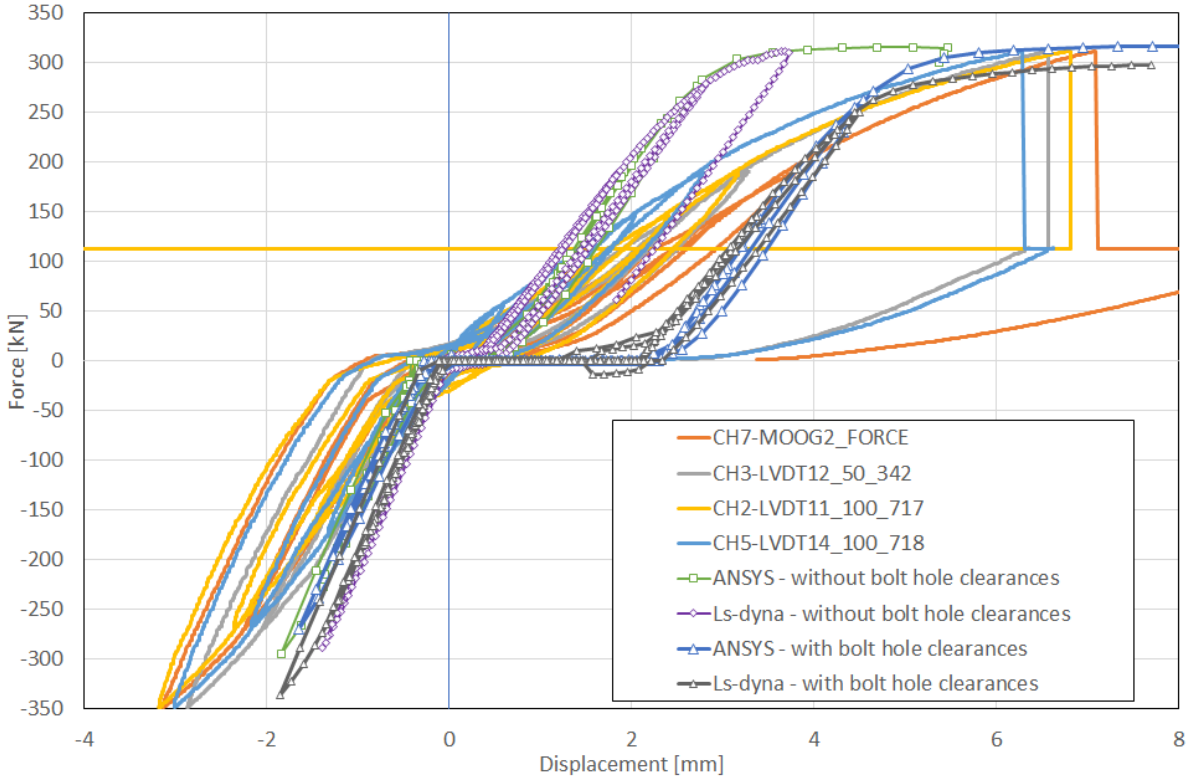

Figure 2.39: Force-displacement curves obtained from FE analyses and experiment (cyclic test n°2) for the fusible link configuration n°2 under cyclic action

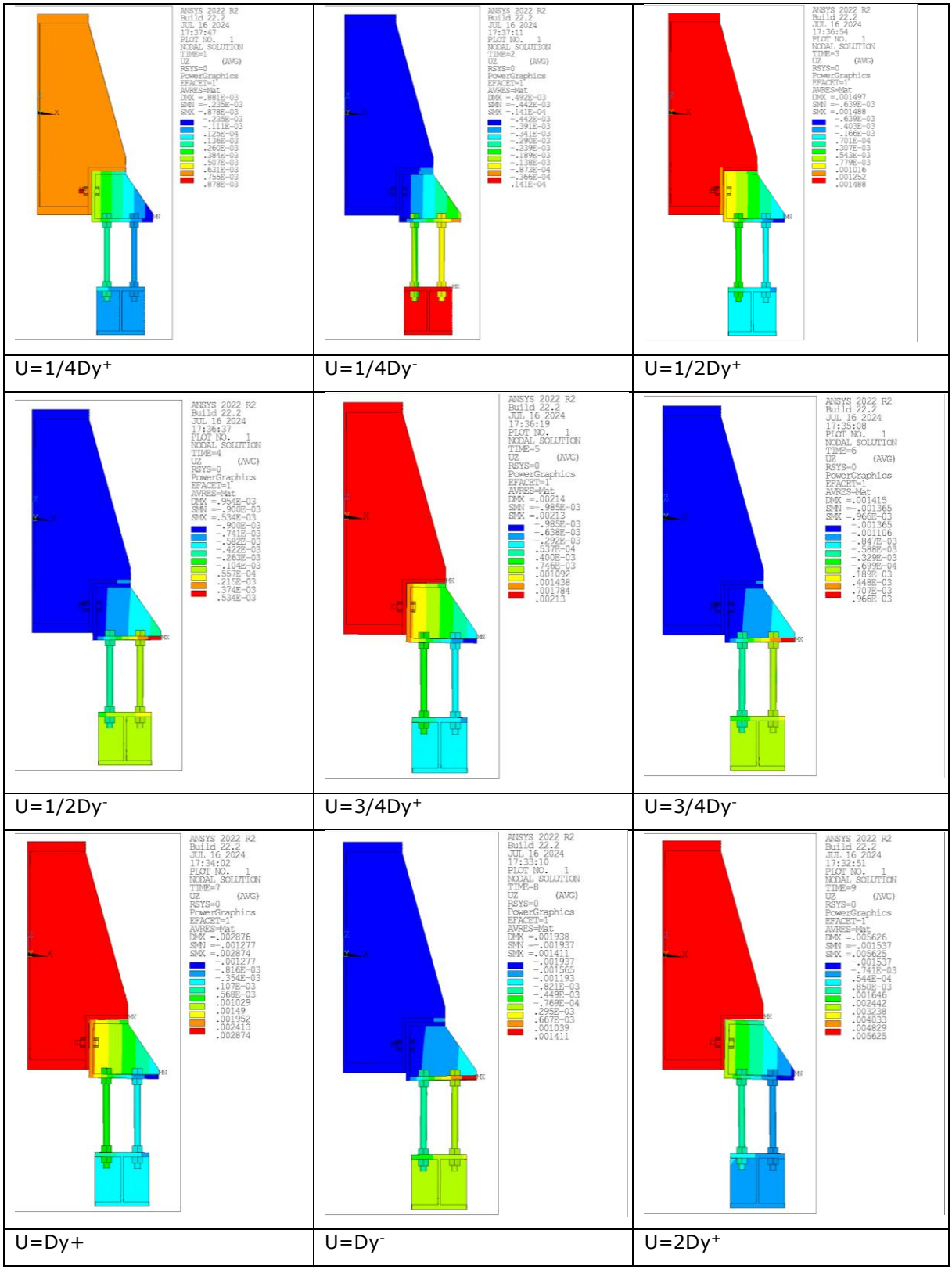

Figure 2.40: Deformed shape of the fusible link configuration n°2 according to imposed displacement values predicted with the ANSYS model without bolt-hole clearances

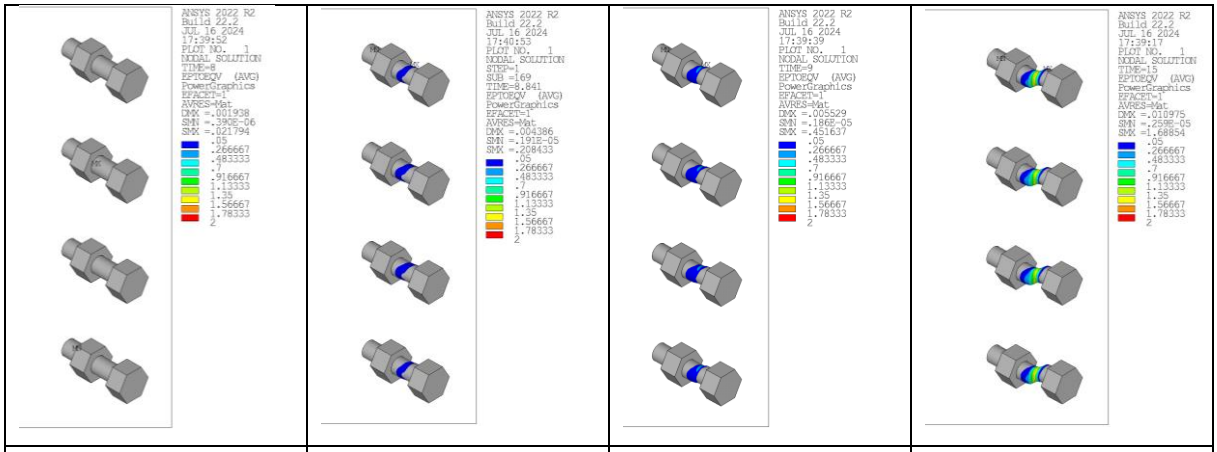

U=Dy⁺	U=1.7Dy⁺	U=2Dy⁺	U=3Dy⁺

Figure 2.41: Von mises total mechanical strain in aluminium bolts of the fusible link configuration n°2 predicted for different values of imposed displacement with the ANSYS model without bolt-hole clearances

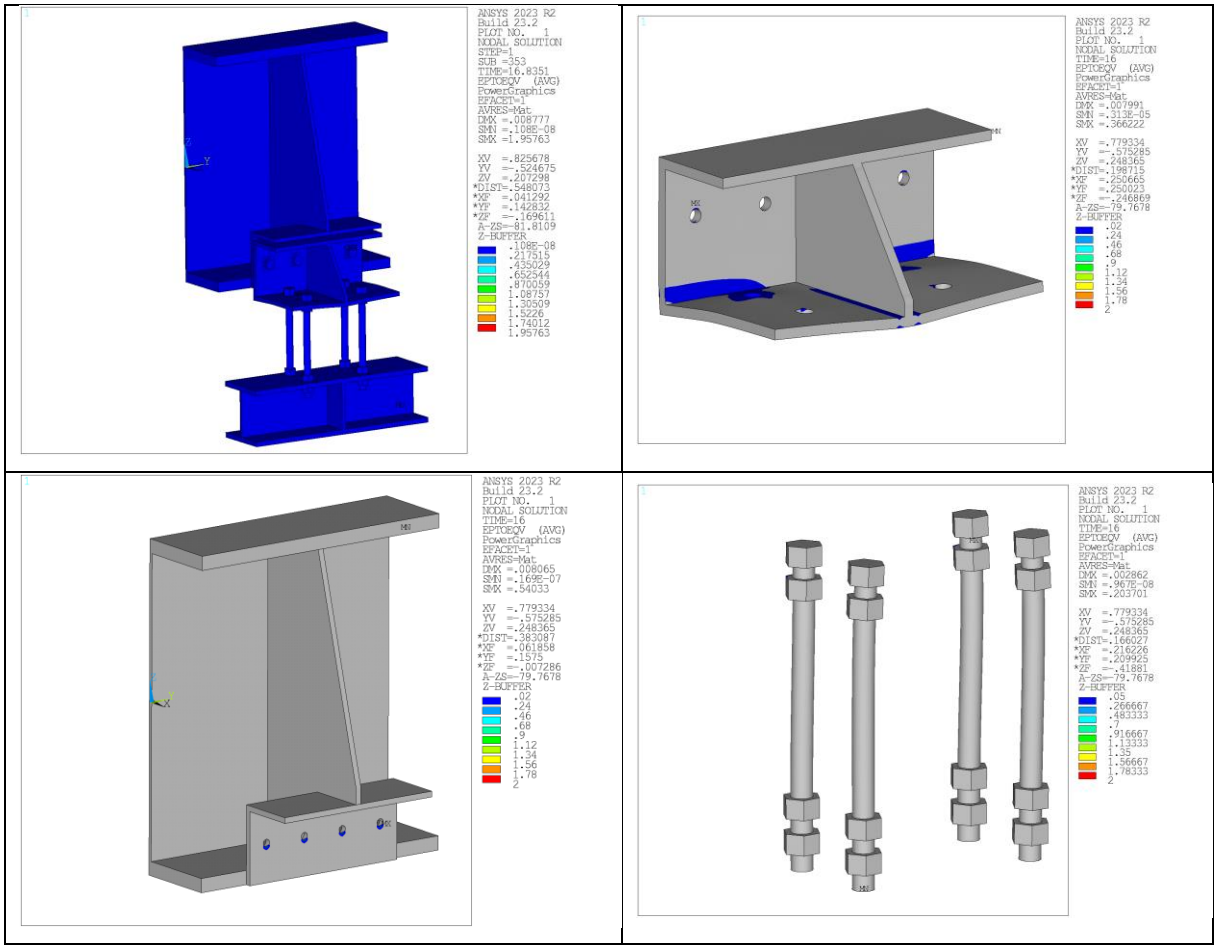

Figure 2.42: Von mises total mechanical strain in components of the fusible link configuration n°2 predicted with the ANSYS model without bolt-hole clearances, at simulation end

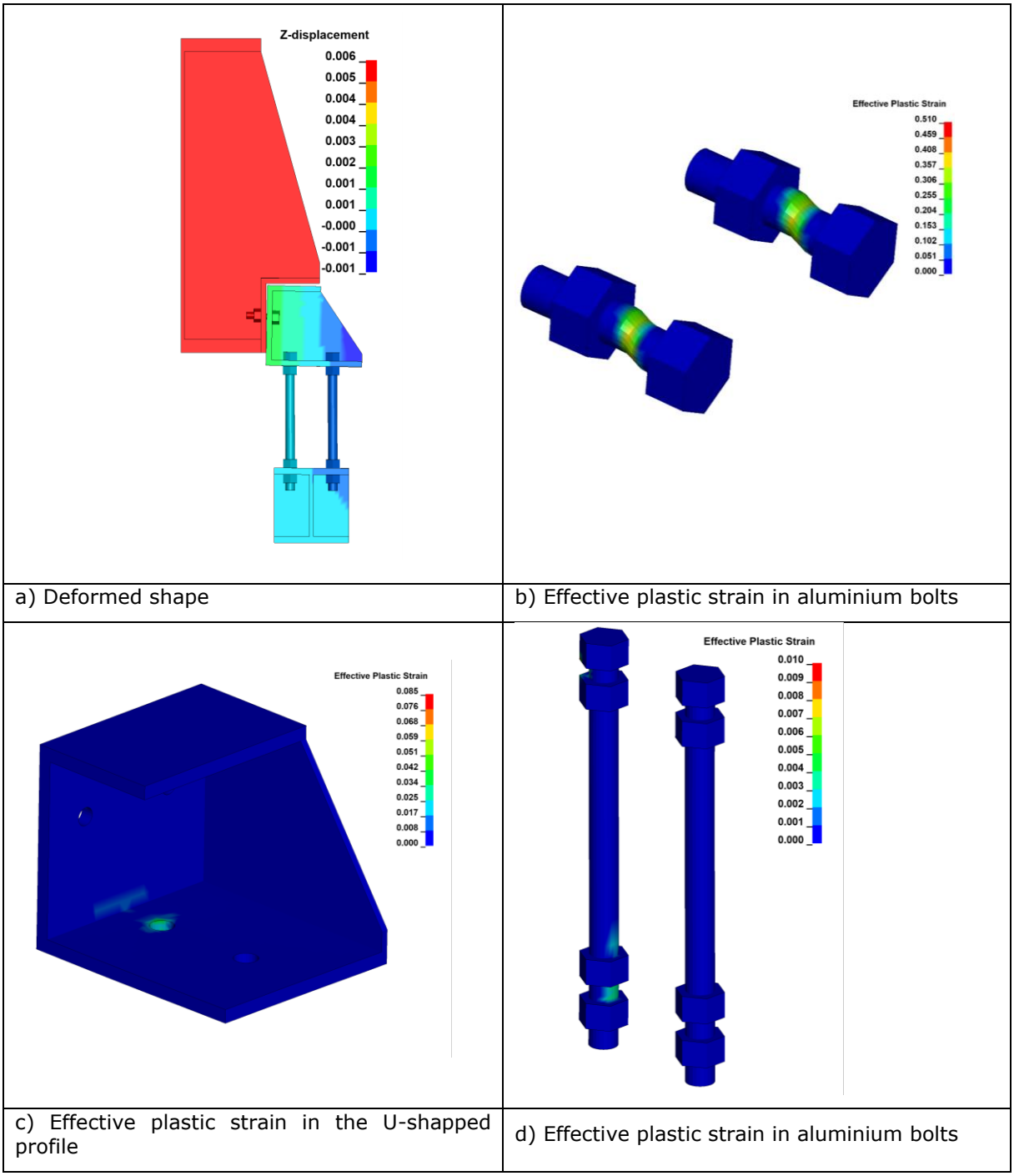

a) Deformed shape

b) Effective plastic strain in aluminium bolts

c) Effective plastic strain in the U-shapped profile

d) Effective plastic strain in aluminium bolts

Figure 2.43: Main results of the modelling of the fusible link n°2 under Ls-dyna without bolt-hole clearances

a) Cyclic test n°1

b) Cyclic test n°2

Figure 2.44: Photos of aluminium bolts after the cyclic tests of the fusible link n°2

2.2.3 Fusible link configuration n°3.1

For the detail 3.1, monotonic analyses were performed with or without bolt-hole clearances.

2.2.3.1 Monotonic tension loading

Figure 2.45 compares the predicted link response in terms of force-displacement to the experimental ones (denoted by "CH0", "CH2" and "CH6" in the figure). Each predicted curve is a resulting plot of the total vertical force calculated by summing the reaction forces of all nodes at the fixed end of the link against the prescribed vertical displacement. Through the figure, it can be noted that the experimental force–displacement curves consist mainly of a bilinear or trilinear (elastic) stage, followed a brittle failure stage. When hole bolt clearances are not considered, the predicted force–displacement curves globally experience a simple linear stage, up to a vertical displacement Dy^{+}=3.6 mm corresponding approximately to a vertical force F=240 kN, followed by a plateau stage corresponding to the shear yielding of the cross-sectional area of all aluminium bolts. Accounting for bolt-hole clearance leads to a delay in the development of the tensile force, which starts when bolts come into bearing within the holes. In addition, the predicted curves exhibit also a lightly stiffness degradation stage after the linear stage. However, there is no significant effect of the failure load value, the peak force value reaching approximately the same value. In this case, the yield displacement Dy^{+} is estimated to 7.6mm. As expected, the models predict the failure of the test specimen by shearing of aluminium bolts. However, the load-bearing capacity predicted for the fusible link is overestimated in comparison to the one observed during the test, namely 190.7 KN (which corresponds to an error of 27% between the predicted and measured values). As highlighted in the seismic tests, the behaviour of Detail 3.1 was, in certain cases, affected by imperfections in the assembly, i.e. not perfect alignment of the holes, slightly different hole dimensions that may have induced higher forces than expected in some aluminium bolts, that collapsed sequentially before reaching the design force. This progressive failure of the aluminium bolts induced a lower degree of symmetry with respect to the other details, except for Detail 3.2 that exhibited similar behaviour. This can be one of the reasons of the capacity overestimation of the numerical models. In addition to resistance, there is some discrepancy between the numerical and experimental curves. Firstly, the experimental curves show what may appear to be a slip stage (from zero to approximately 3 mm of displacement) shorter than the one predicted by models. This is attributed to the clearance values considered in modelling. Secondly, the initial stiffness predicted by the models is significantly higher than that observed experimentally (when compared to the displacement curve "CH6" derived from the displacement transducer associated with the loading device). However, when the experimental curves derived from the displacement transducers placed below one of the steel profiles of the fusible link ('CH0' and 'CH2') are considered once the slipping stage is over, the stiffnesses (defined as the slope of the tangent to the force-displacement curve) appear very close. . The difference between the experimental curves is surprising, indicating that the upper part of the fusible link undergoes greater displacement than the lower part. Lastly, the sudden drop in force observed at the test end is not captured accurately where the bolts fracture is not explicitly considered in the modelling, which leads to over-estimate the deformations that the specimens can really reach, and hence the specimen ductility. On the other hand, a sharply force decreases is obtained if the fracture of bolts is considered in modelling by adding a descending branch in the bolt material law (curve denoted "MLWDB" in Figure 2.45). It can be also that the predicted curves coincide quite well with each other, highlighting the satisfactory agreement between the two models developed, even if some discrepancies can be noted which are mainly attributed to the different contact types used in the ANSYS and Ls-dyna models.

The failure modes of the specimen are recognized by checking the strain level reached in the different components constituting the studied fusible link. For illustrative purposes, Figure 2.47 shows the distribution of the Von mises total mechanical strain predicted in aluminium bolts from the ANSYS model without bolt-hole clearances. The strain distribution is given for different levels of imposed displacement (so different force levels), by showing strain values exceeding 5% only. It clearly shows a yielding line progressively propagating in the cross-sectional area of bolts, in the two shear planes at the junction between steel profiles linked by the aluminium bolts. It can be noticed that the failure predicted by the models involved the collapse of the two aluminium bolts row, starting by the row located on the lower part of the specimen, while the test was characterized by a progressive failure of the aluminium bolts (see Figure 2.50). Figure 2.48 shows the distribution of the Von mises total mechanical strain predicted in the other components of the link with the ANSYS model, at the simulation end. It can be noted that the strain level exceeds locally the 0.2% yield strain, around the holes of aluminium bolts only, highlighting that some bearing occurs in steel plates, with limited holes elongation. Steel bolts and steel rods have only slight deformation, and no damage occurred in analyses.

For information, Figure 2.49 summarises the main results obtained at failure time of bolts from modelling developed under Ls-dyna without bolt-hole clearances. The results are in good agreement with the ones reported for the ANSYS model.

As with other links, the dissimilarities between the experimental and FE results are mainly attributed to clearances and slipping between the steel profiles and all bolting. Bolt-hole clearances allow some movement in the link and can lead to increased bolt rotation, decreased bolt-hole contact area and then decreased link stiffness. Moreover, the misalignment of bolt and hole, the misalignment of profile or holes of varying sizes can lead to some bolts may remain unstressed at the start of loading, or throughout loading. All these phenomena are difficult to be considered accurately in models. This could also be due to phenomena which are not accounted in FE models, like possible slipping between the screw and nut thread or progressive crushing of the bearing flank of the thread (that supports shearing forces) of aluminium bolts with the bearing stresses. It should be noted that some predicted curves may be non-smooth in certain loading stages. As in the previous case, the rough shape observed in the numerical curves is attributed to dynamic effects (due to the speed of load application and the resulting inertia forces), which can cause oscillations at the contact surfaces and interpenetration issues.

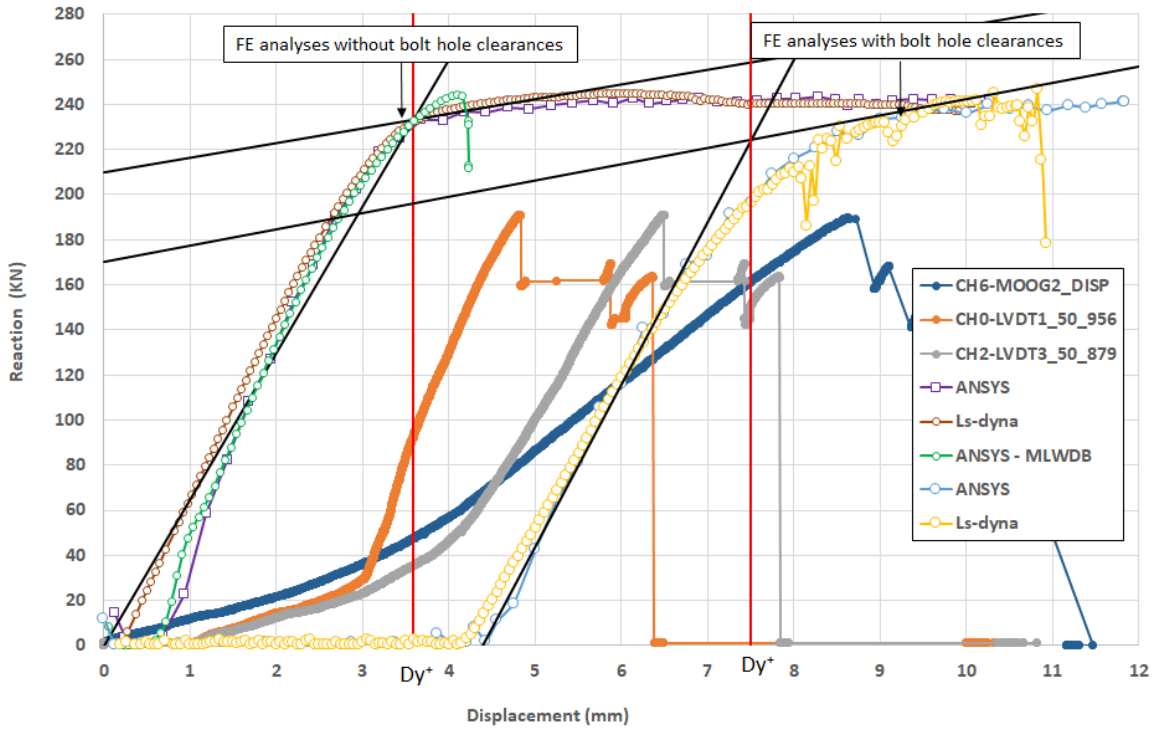

Figure 2.45: Force-displacement curves obtained from FE analyses and experiment for the fusible link configuration n°3.1 under tensile action

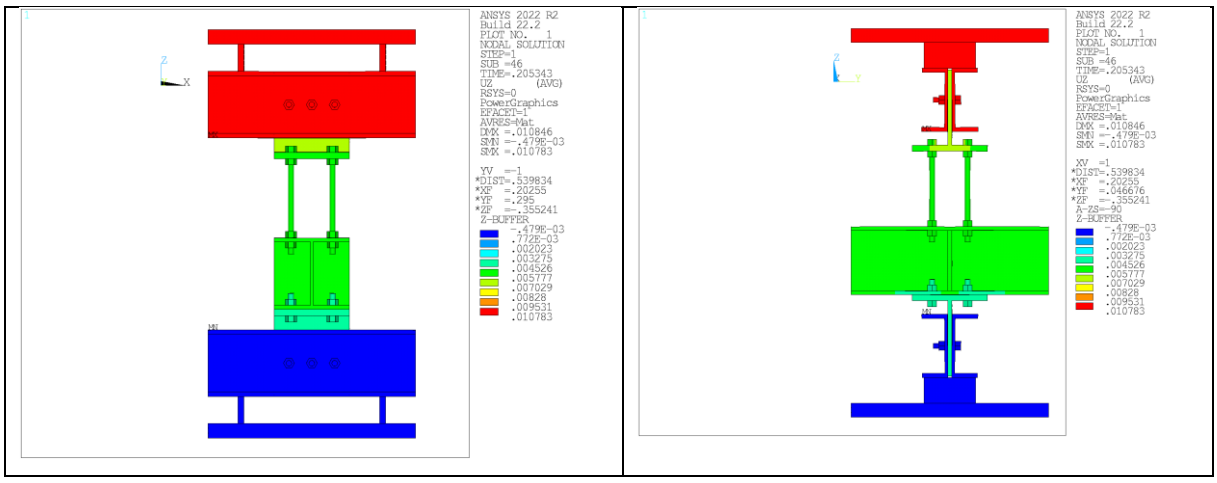

Figure 2.46: Deformed shape of the fusible link configuration n°3.1 predicted with the ANSYS model without bolt-hole clearances

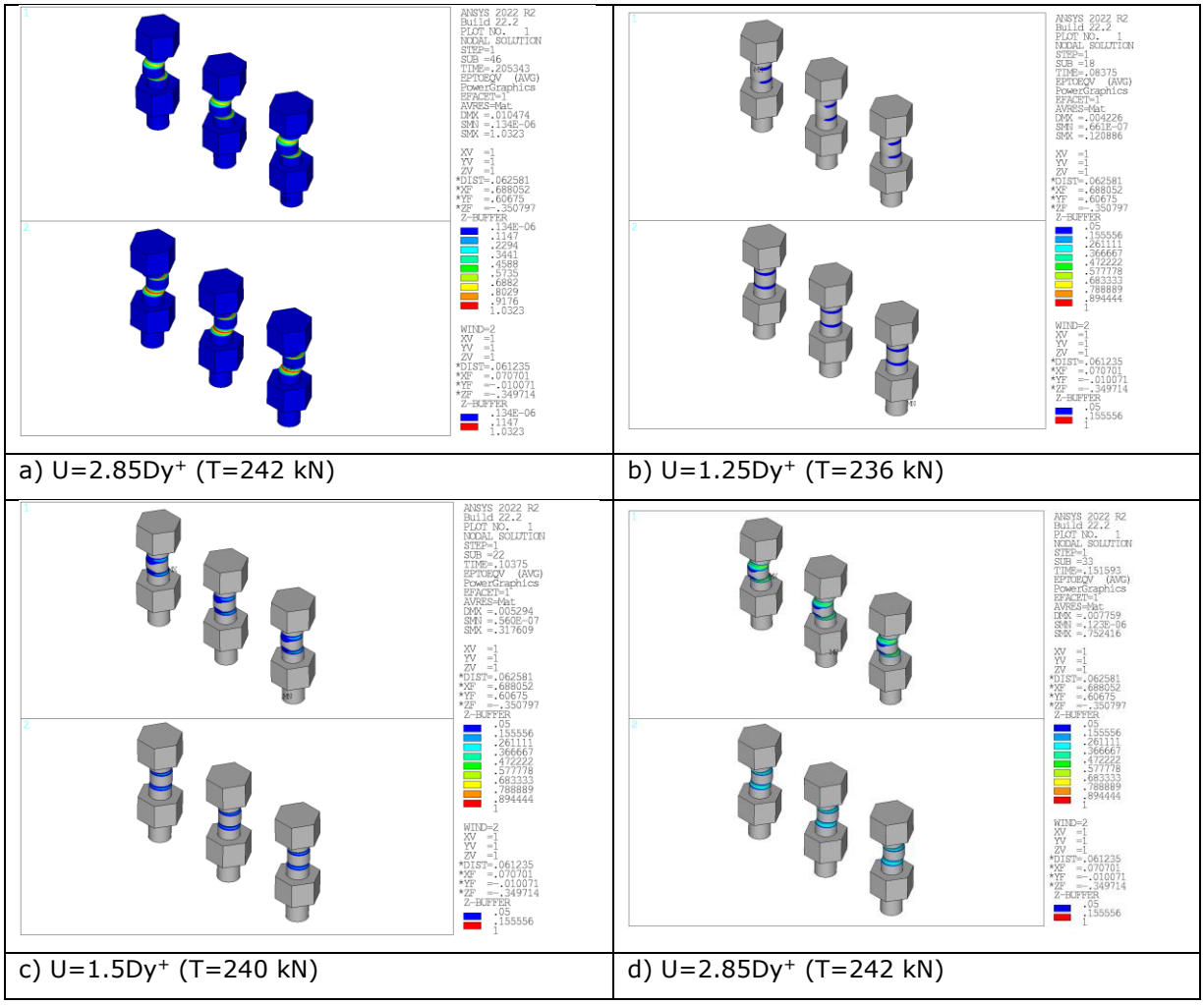

a) U=2.85Dy⁺ (T=242 kN)

b) U=1.25Dy⁺ (T=236 kN)

c) U=1.5Dy⁺ (T=240 kN)

d) U=2.85Dy⁺ (T=242 kN)

Figure 2.47: Von mises total mechanical strain in aluminium bolts of the fusible link configuration n°3.1 predicted for different values of imposed displacement with the ANSYS model without bolt-hole clearances

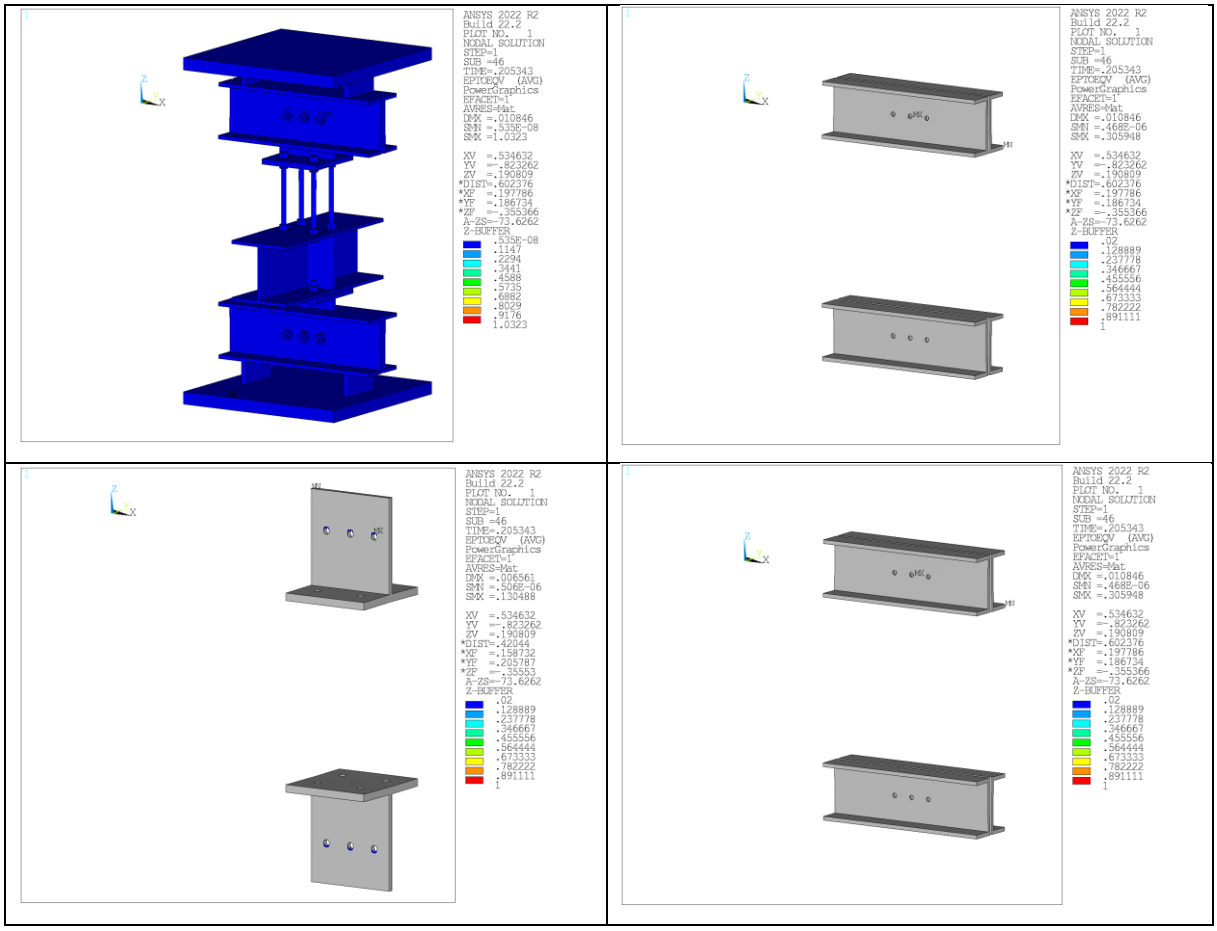

Figure 2.48: Von mises total mechanical strain in components of the fusible link configuration n°3.1 predicted with the ANSYS model without bolt-hole clearances, at simulation end

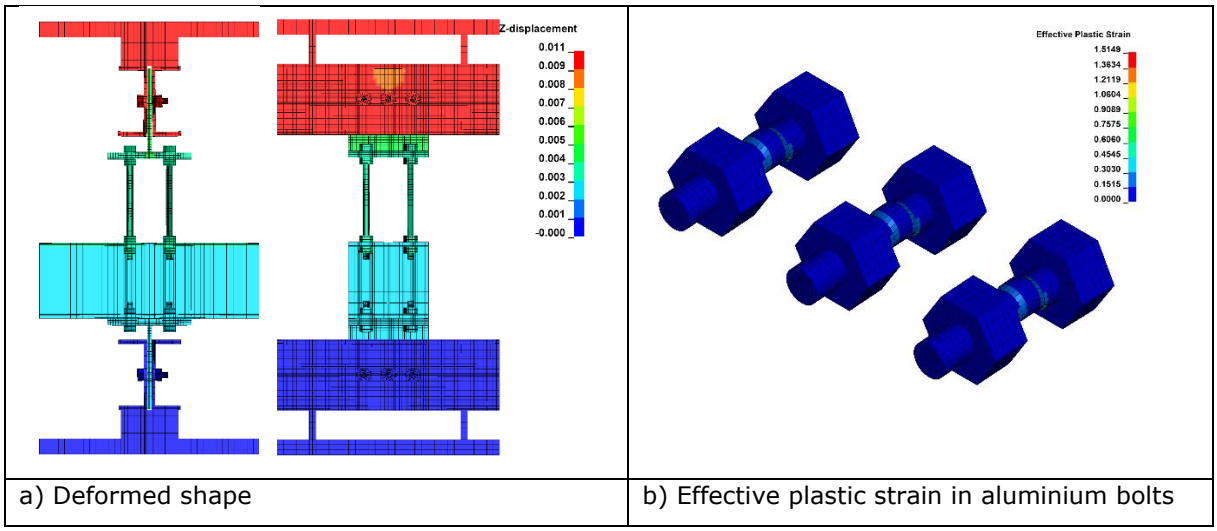

a) Deformed shape

b) Effective plastic strain in aluminium bolts

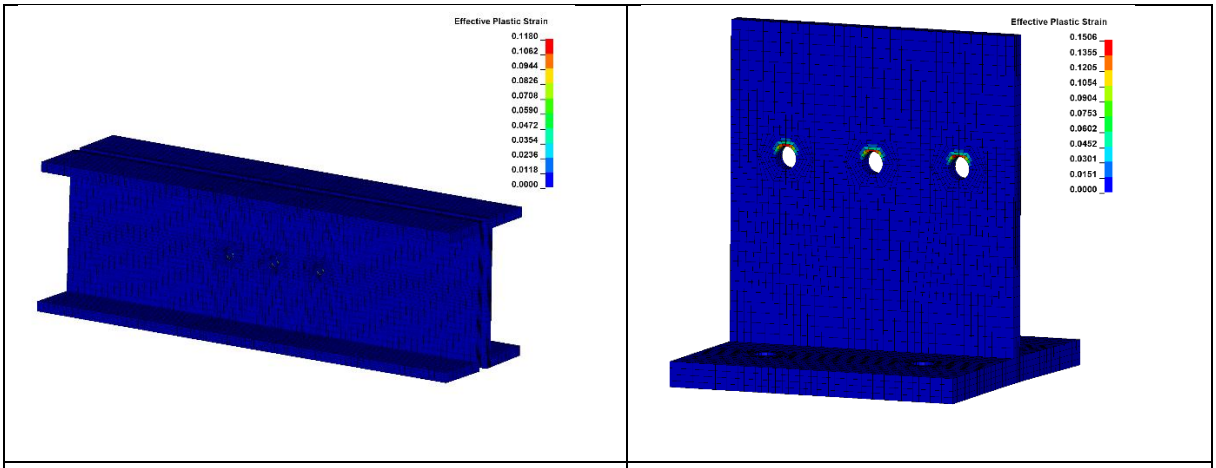

c) Effective plastic strain in the U-profile | d) Effective plastic strain in the T-profile

Figure 2.49: Main results of the modelling under Ls-dyna without bolt-hole clearances at failure time of bolts

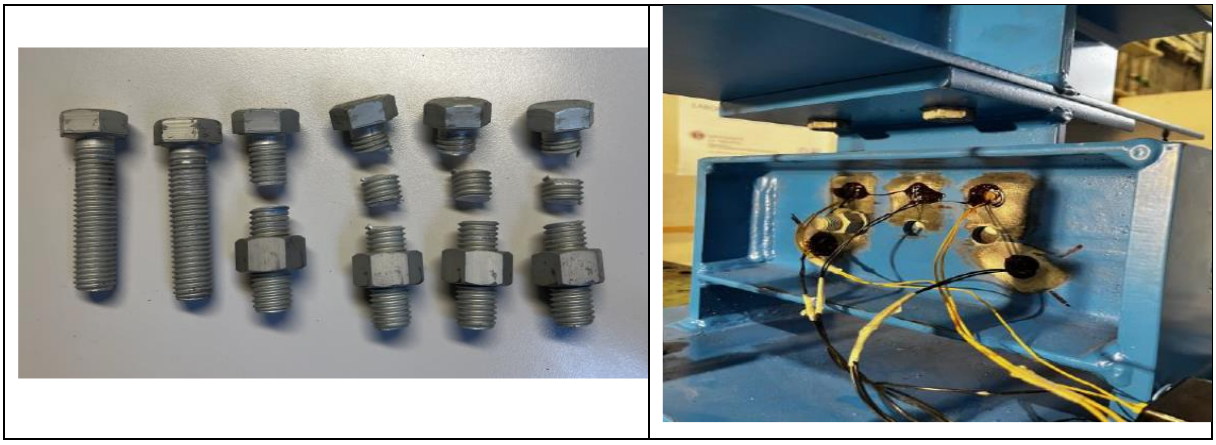

Figure 2.50: Photos of the test specimen after the test.

2.2.3.2 Monotonic compression loading

Figure 2.51 compares the predicted link response in terms of force-displacement to the experimental ones (denoted by "CH3" and "CH6" in the figure). Each predicted curve is a resulting plot of the total vertical force calculated by summing the reaction forces of all nodes at the fixed end of the link against the prescribed vertical displacement. Through the figure, it can be noted that the shape of curves is globally like that observed when the specimen is subjected to a tensile force. So, the same comments can be made about the comparison between experiment and the numerical results. As expected, the models predict the failure of the test specimen by shearing of aluminium bolts. However, the load-bearing capacity predicted by the models is overestimated in comparison to the one observed during the test. the load-bearing capacity predicted is about 250 KN, while the experimental one is 215 KN approximately (which corresponds to an error around 17% between the predicted and measured values). The yield displacement Dy^- estimated from the numerical curves is 2.4 or 6.3mm depending on whether bolt-hole clearances are considered. As for the experiment, it can be noted that the models predict that the load-bearing capacity of the specimen is slightly higher under compression that tension. In addition to the resistance, it can be noted that there is still some discrepancy between the numerical and experimental curves. Firstly, the initial stiffness predicted by the models appears significantly higher than the experimentally observed (when compared to the displacement curve "CH6" derived from the displacement transducer associated with the loading device), even if stiffnesses appear very close by considering the experimental curve derived from the displacement transducer "CH3" placed below one of the steel profiles of the fusible link. The difference between the experimental curves is surprising, indicating that the upper part of the fusible link undergoes greater displacement than the lower part. Lastly, the sudden drop in the force observed at the test end is not captured accurately, since the bolt fracture is not explicitly considered in the given results. It can be also underlined the reasonable agreement between the two models developed under ANSYS and Ls-dyna.

The failure modes of the specimen are recognized by checking the strain level reached in the different components constituting the studied fusible link. For illustrative purposes, Figure 2.53 shows the distribution of the Von mises total mechanical strain predicted in aluminium bolts from the ANSYS model without bolt-hole clearances. The strain distribution is given for different levels of imposed displacement (so different force levels), by showing strain values exceeding 5% only. It clearly shows a yielding line progressively propagating in the cross-sectional area of bolts, in the two shear planes at the junction between steel profiles linked by the aluminium bolts. It can be noted that the failure predicted by the models involved the collapse of the two aluminium bolts row, starting by the row located on the upper part of the specimen.

Figure 2.54 shows the distribution of the Von mises total mechanical strain predicted in other components of the link with the ANSYS model, at the simulation end. It can be noted that the strain level exceeds locally the 0.2% yield strain, around the holes of aluminium bolts, highlighting that some bearing occurs in steel plates, with limited holes elongation. Steel bolts and steel rods have only slight deformation, and no damage occurred in analyses.

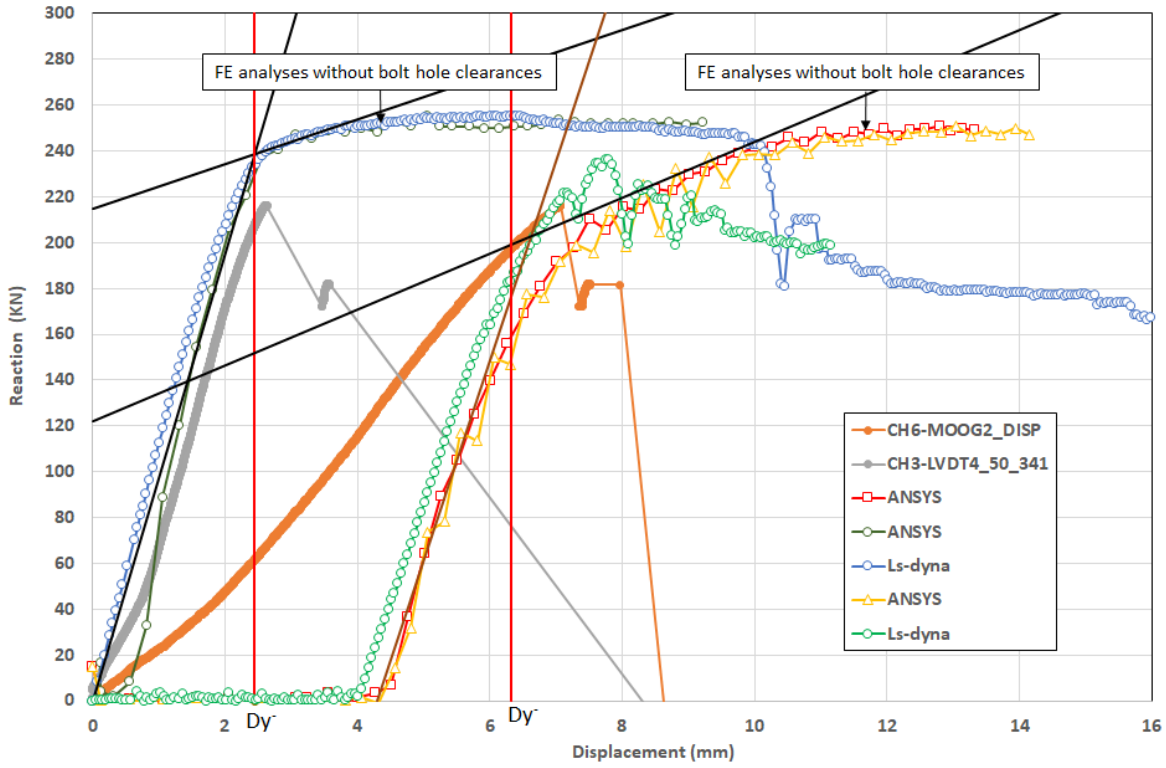

Figure 2.51: Force-displacement curves obtained from FE analyses and experiment for the fusible link configuration n°3.1 under compressive action

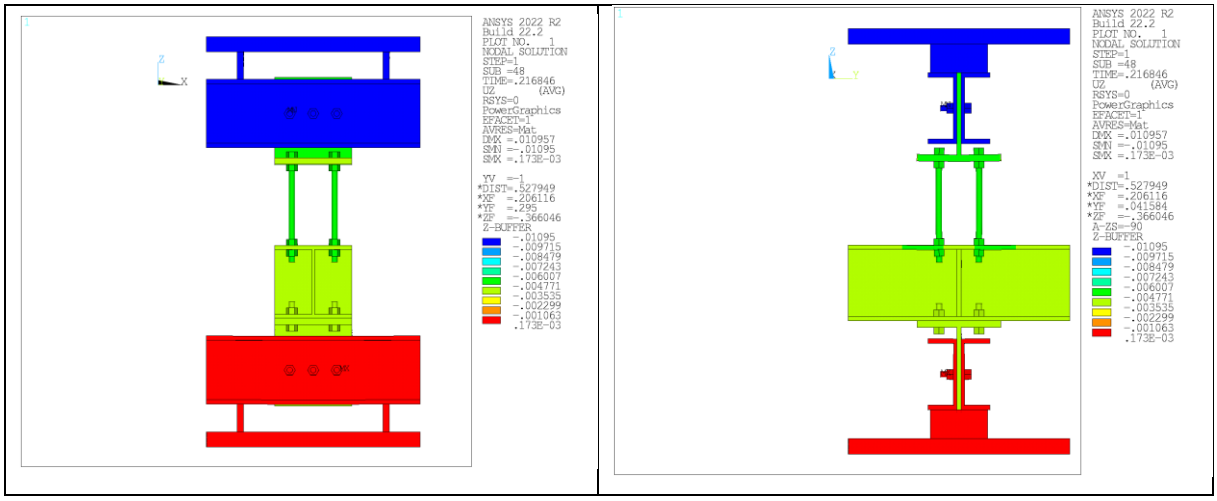

Figure 2.52: Deformed shape of the fusible link configuration n°3.1 predicted with the ANSYS model without bolt-hole clearances

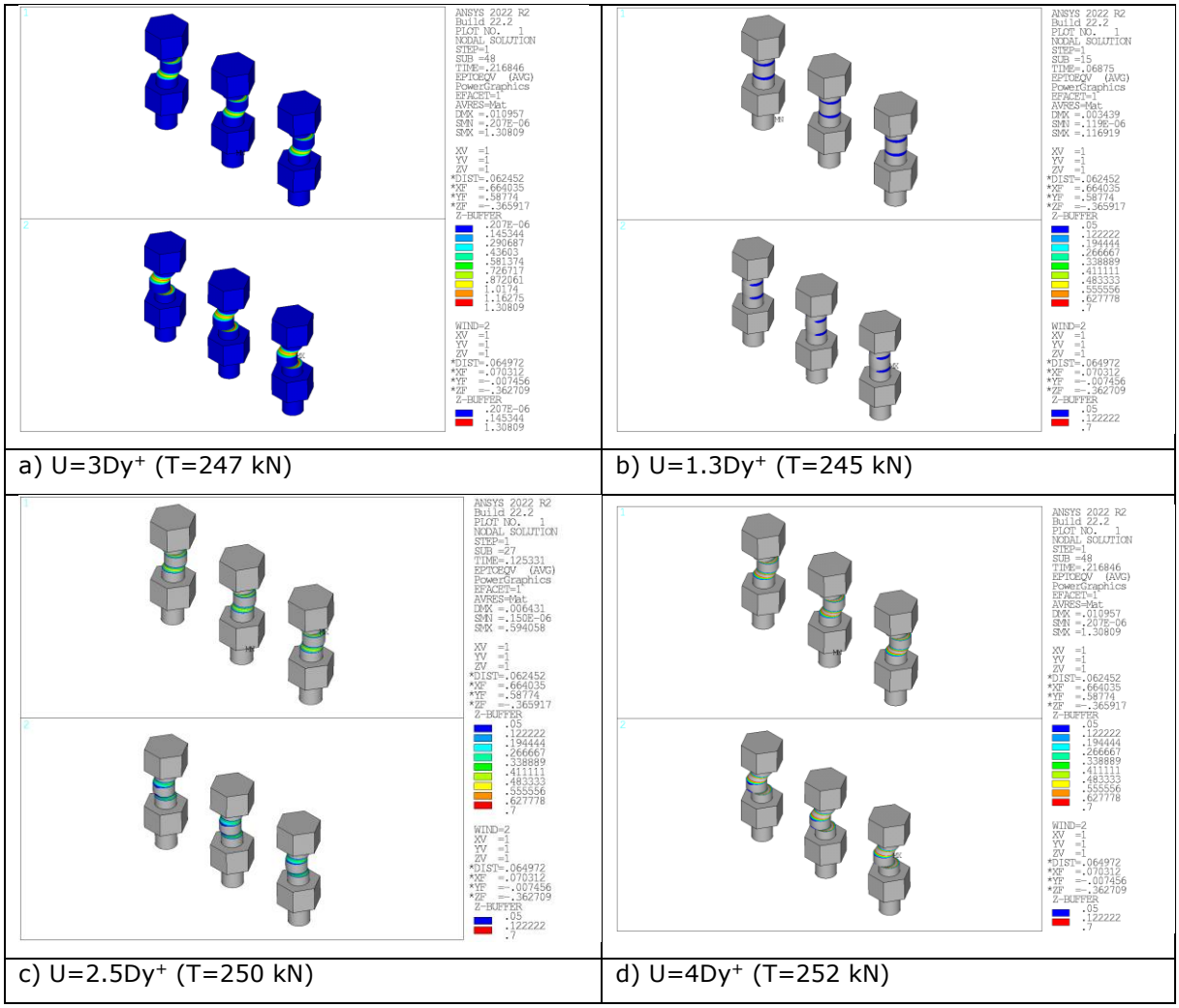

a) U=3Dy⁺ (T=247 kN)

b) U=1.3Dy⁺ (T=245 kN)

c) U=2.5Dy⁺ (T=250 kN)

d) U=4Dy⁺ (T=252 kN)

Figure 2.53: Von mises total mechanical strain in aluminium bolts of the fusible link configuration n°3.1 predicted for different values of imposed displacement with the ANSYS model without bolt-hole clearances

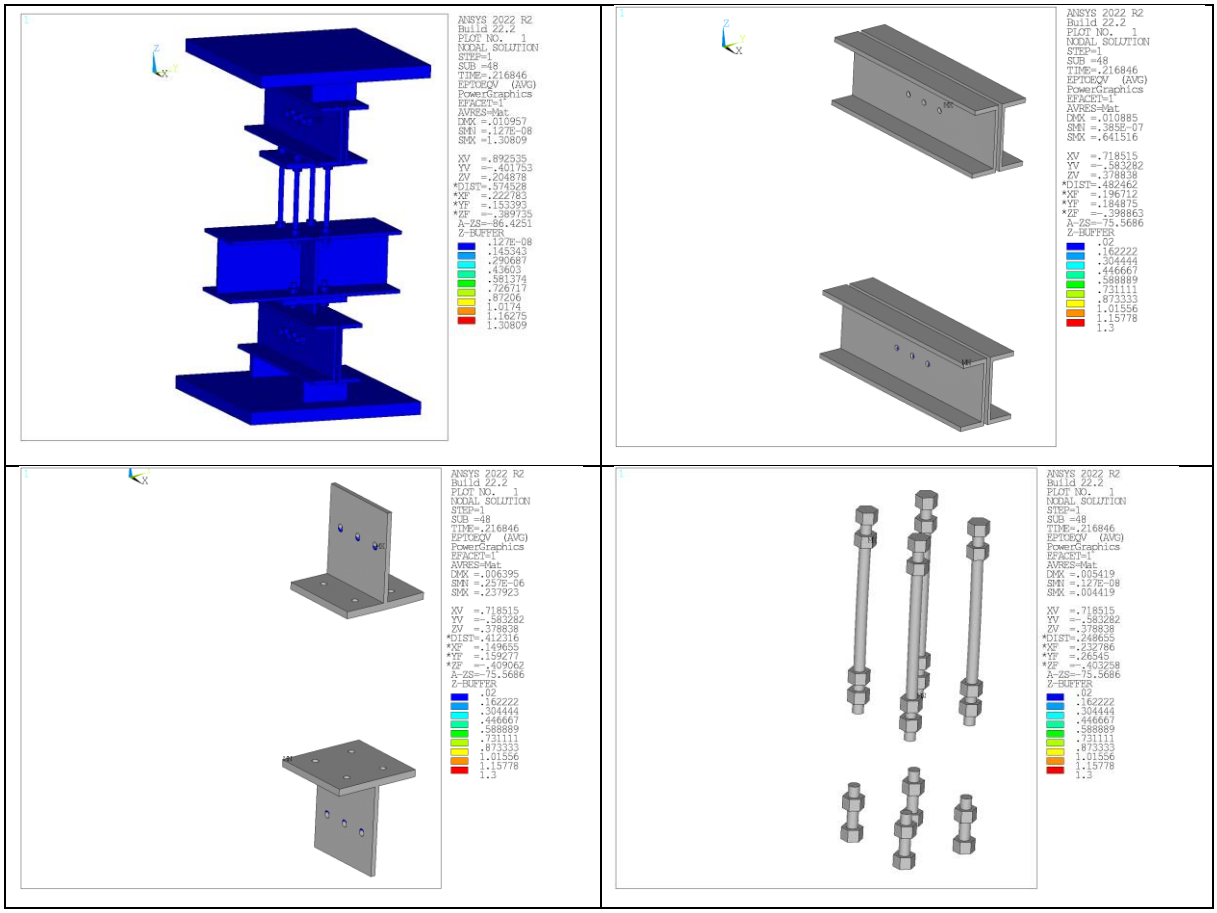

Figure 2.54: Von mises total mechanical strain in components of the fusible link configuration n°3.1 predicted with the ANSYS model without bolt-hole clearances, at simulation end

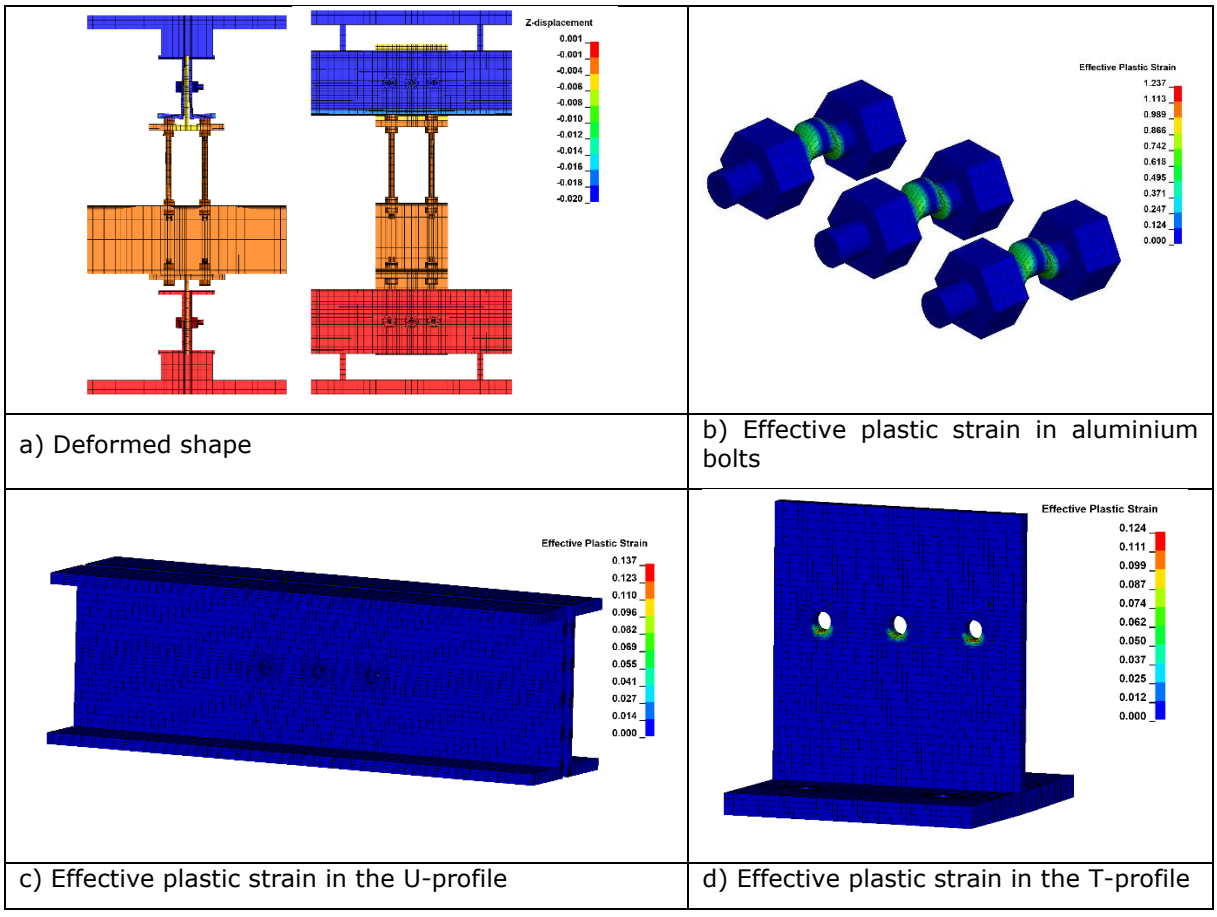

a) Deformed shape

b) Effective plastic strain in aluminium bolts

c) Effective plastic strain in the U-profile

d) Effective plastic strain in the T-profile

Figure 2.55: Main results of the modelling under Ls-dyna without bolt-hole clearances

2.2.3.3 Cyclic loading

The vertical displacement-time curve prescribed in numerical analyses carried out without bolt-hole clearances is showed in Figure 2.56, while the yield displacements obtained from monotonic analyses are reported in Table 4.

Table 4: Yield displacements determined from monotonic analyses of the fusible link detail n°3.1

	Without bolt-hole clearances	With bolt-hole clearances
Dy^+	3.6 mm	7.6
Dy^-	2.4 mm	6.3

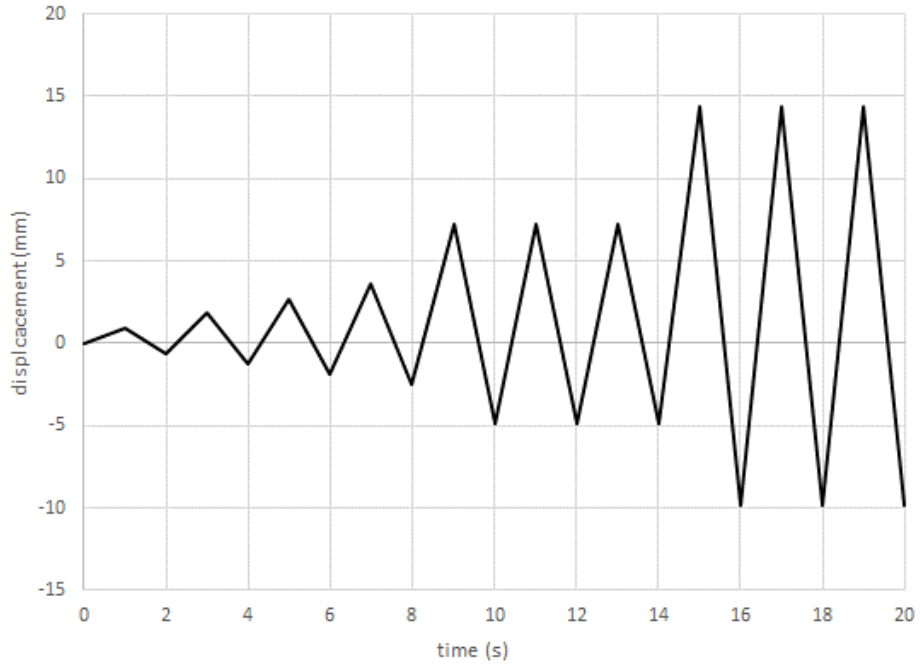

Figure 2.56: Vertical displacement-time curve used in numerical analyses carried out without bolt-hole clearances for the fusible link detail n°3.1

Figure 2.57 and Figure 2.58 depict the comparison between the FE predicted hysteresis axial force-displacement responses and the results from two cyclic tests. In this figure, the negative values mean that components are under compression, and positive values are for tension. Through the hysteresis curves, it can be noted that numerical models predict that the studied link remains in the elastic stage during a major part of the displacement loading. Indeed, the predicted force–displacement curves are predominantly linear, both in tension and compression for non-zero forces. Unloading takes place in the same path than loading, or a closer parallel path to that of the initial stiffness of the link until failure. The brittle nature of the detail in tension and compression highlights a very small hysteretic behaviour of the detail. Accounting for bolt-hole clearance in modelling only leads to a delay in the force increase, which starts when bolts come into bearing within the holes. In this case, the force remains small during the first cycles, until the prescribed displacement peaks exceed the maximum value of displacement that bolts can undergo inside holes. It can be underlined that the predicted force-displacement curves display a similar behaviour in tension and compression, characterized, however, by slightly different initial stiffnesses in accordance with the monotonic analyses. Since no significant plastic deformations occur in steel components, the predicted cyclic response coincides well with the monotonic responses obtained in tension or compression loading. It can be also underlined the satisfactory agreement between the two models developed under ANSYS and Ls-dyna.

The failure modes of the studied fusible link are assessed by monitoring the strain states of different components constituting the link. Figure 2.60 shows the distribution of the Von mises total mechanical strain predicted in some components of the link with the ANSYS model without bolt-hole clearances, at the simulation end. It can be noted that the strain level exceeds locally the 0.2% yield strain around the holes of aluminium bolts only, highlighting that some bearing occurs in steel plates, with limited holes elongation. Steel bolts and steel rods undergo only elastic deformations. The failure of the specimen occurred on the reloading stage at the first cycle to $2Dy^+$ because of the shearing of

all aluminium bolts. For illustrative purposes, Figure 2.61 shows the distribution of the Von mises total mechanical strain predicted in aluminium bolts with the ANSYS model without bolt-hole clearances. The strain distribution is given for different levels of imposed displacement, by showing strain values exceeding 5% only. It clearly shows a yielding line progressively propagating in the cross-sectional area of bolts, in the two shear planes at the junction between steel profiles linked by the aluminium bolts.

It should be noted that there is an important discrepancy in the cyclic response of the studied link, between the experiment and the FE modelling. In addition to different initial stiffnesses, on the experimental curves, unloading takes place from the first cycle in a different path in comparison with the first loading stage. The unloading path includes two parts, an elastic unloading phase along a path that seems parallel to the loading path followed in the force-displacement curves predicted by models and a pinched unloading phase until the loading in the opposite direction happens. When unloaded to a 0 kN force, there is a non-zero residual displacement different from the one numerically predicted, which increases progressively with the repeated unloading-reloading cycles probably due to the bolt travels within holes, even if the link is still in an elastic state. Lastly, as already underlined in the project deliverable related to test results [1], the experimental hysteresis curves display a pronounced pinching phenomenon in the compression part, characterized by the distortion or non-convex shape of the hysteresis loop with an envelope lower than the monotonic curve, which is not captured by the models. It can be also noted that the predicted load-bearing capacity of the link under cyclic loading is of the same order of magnitude than the ones obtained from monotonic analyses. It is approximately 245 kN. In contrast, the peak force value reached in cyclic tests is different and for the studied link, greater than that observed in the monotonic tension test. It varies from 176.6 to 205 KN by considering the force values corresponding to the first failure of some aluminium bolts. It's a little more important by considering the forces corresponding to the failure of all aluminium bolts. It ranges then from 195 to 205 KN.

The differences between experiment and modelling are mainly attributed to clearances and slipping between the steel profiles and all bolting. Bolt-hole clearances allow some movement in the link and can lead to increased bolt rotation, decreased bolt-hole contact area and then decreased link stiffness. Moreover, the misalignment of bolt and hole, the misalignment of profile or holes of varying sizes can determine that some bolts may remain unstressed at the start of loading. All these phenomena are difficult to be considered accurately in models. This could also be due to phenomena which are not accounted in FE models, like possible slipping between the screw and nut thread or progressive crushing of the bearing flank of the thread (that supports shearing forces) of aluminium bolts with the bearing stresses.

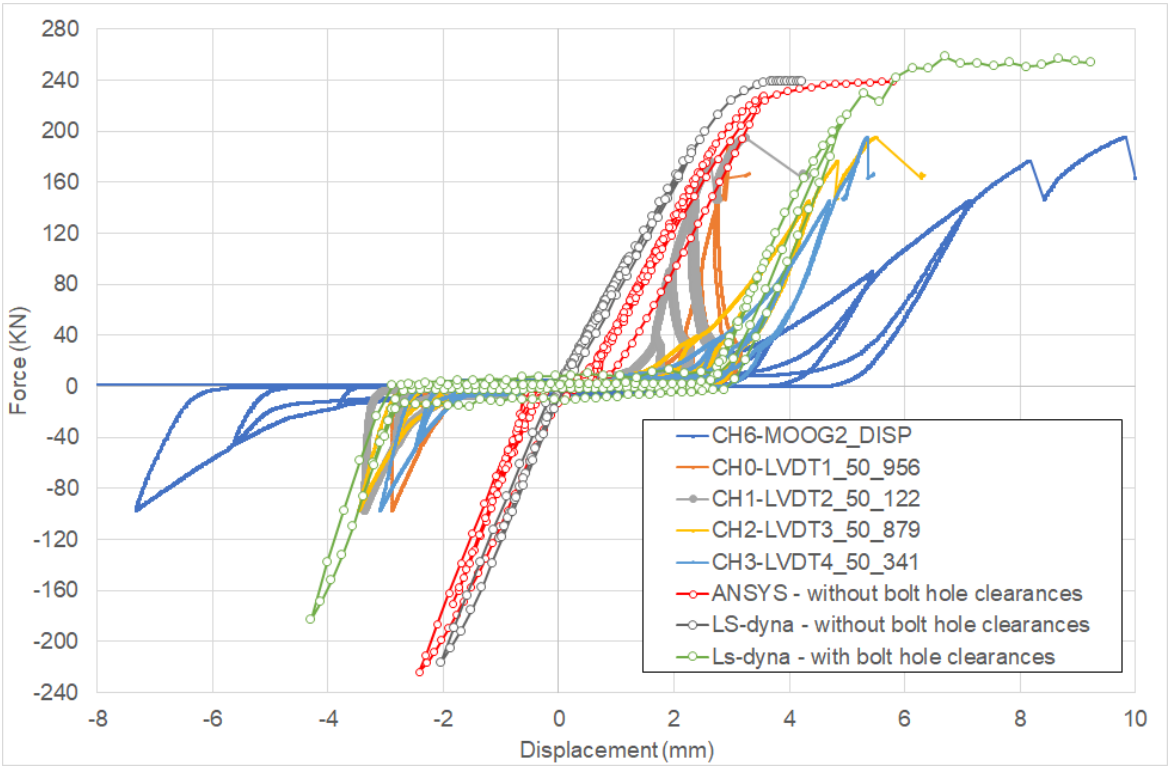

Figure 2.57: Force-displacement curves obtained from FE analyses and experiment (cyclic test n°1) for the fusible link configuration n°3.1 under cyclic action

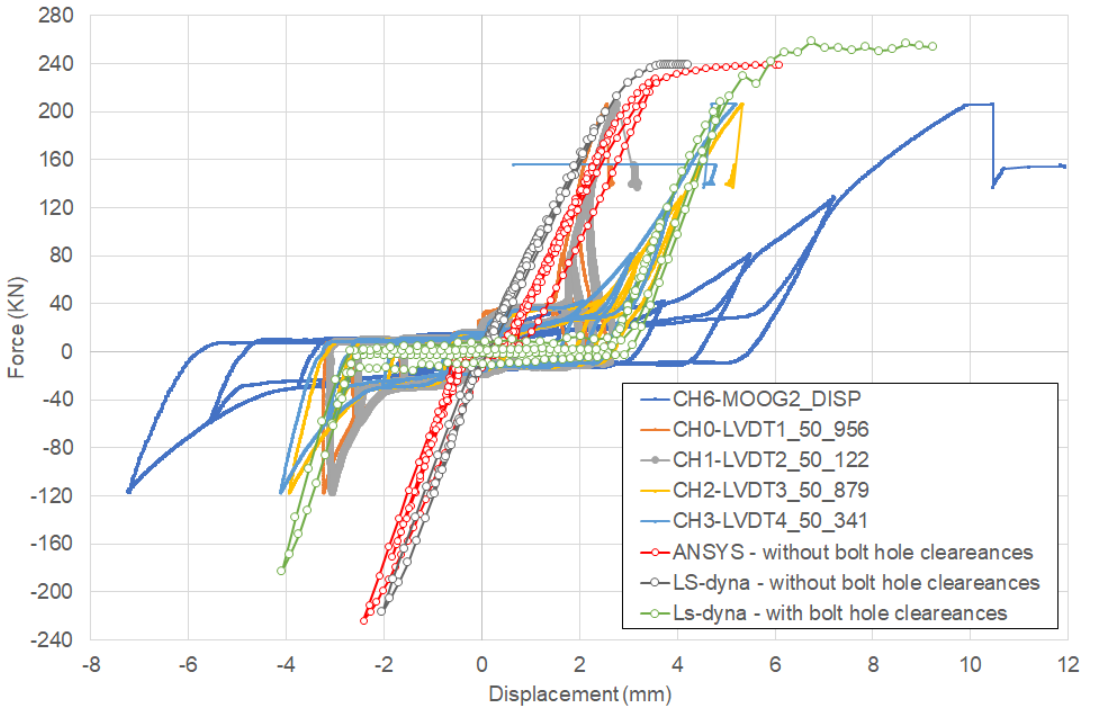

Figure 2.58: Force-displacement curves obtained from FE analyses and experiment (cyclic test n°2) for the fusible link configuration n°3.1 under cyclic action

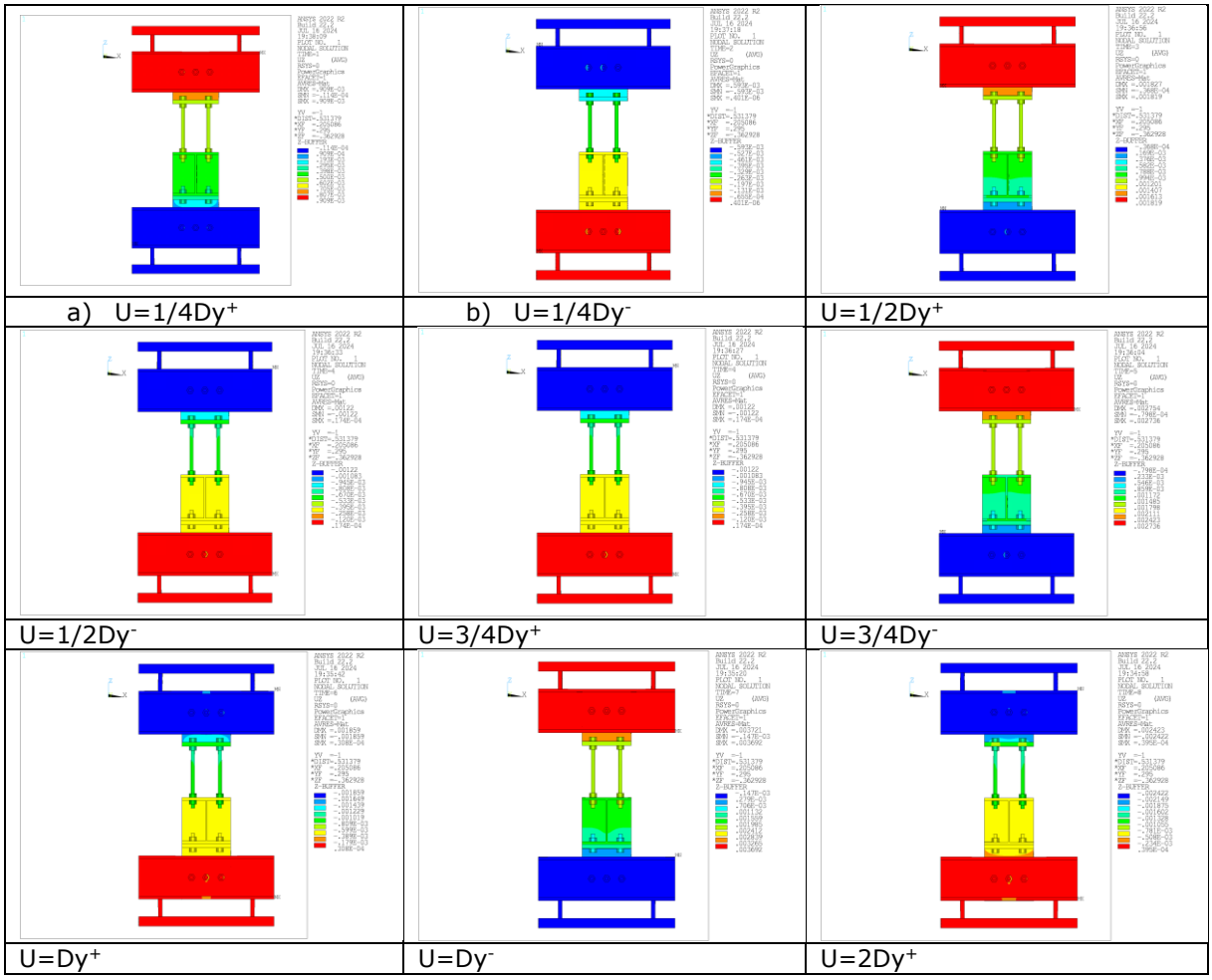

Figure 2.59: Deformed shape of the fusible link configuration n°3.1 according to imposed displacement values predicted with the ANSYS model without bolt-hole clearances

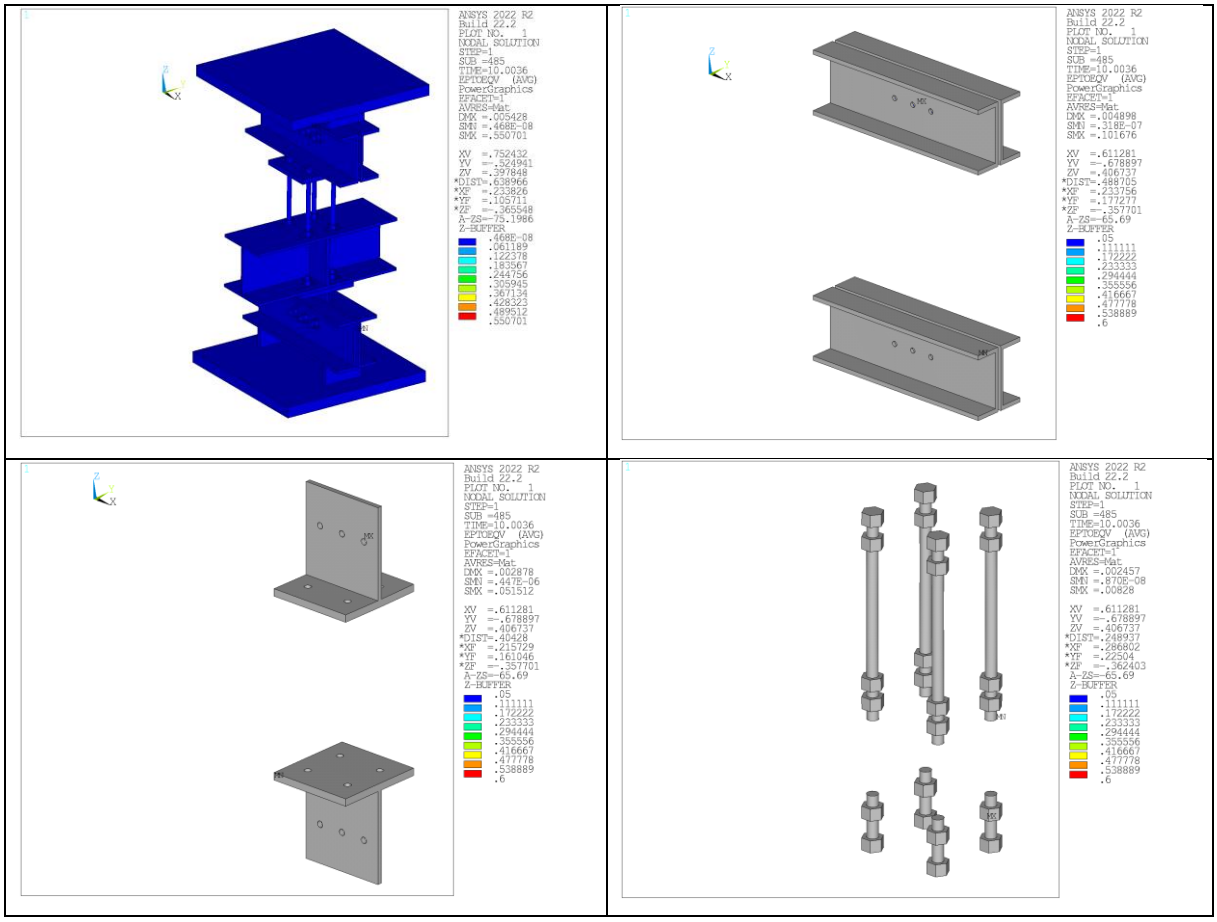

Figure 2.60: Von mises total mechanical strain in components of the fusible link configuration n°3.1 predicted with the ANSYS model without bolt-hole clearances, at simulation end

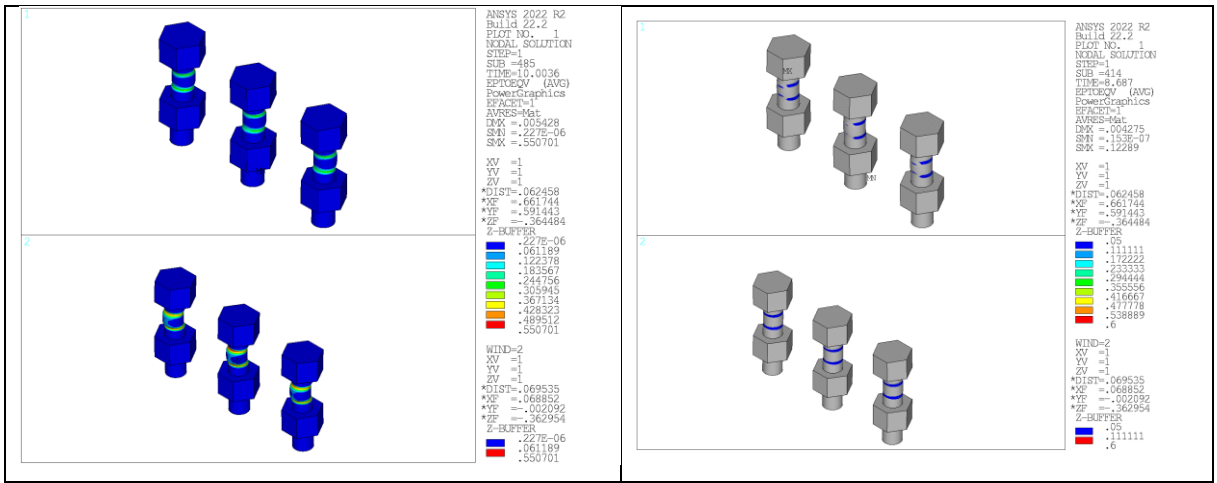

a) At simulation end

b) U=1.1Dy+

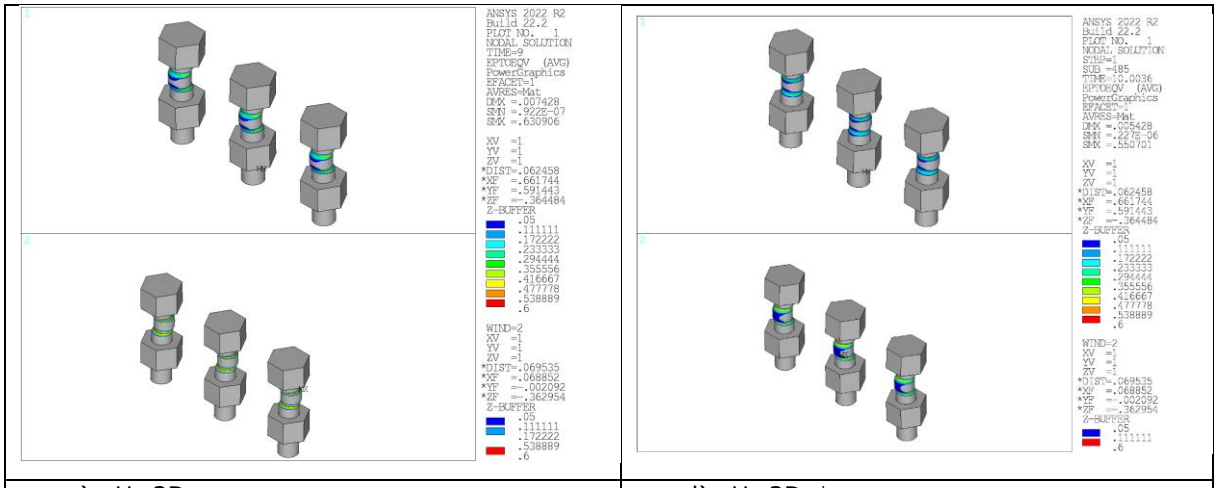

c) $U=2Dy^-$ | d) $U=2Dy^+$

Figure 2.61: Von mises total mechanical strain in aluminium bolts of the fusible link configuration n°3.1 predicted for different values of imposed displacement with the ANSYS model without bolt-hole clearances

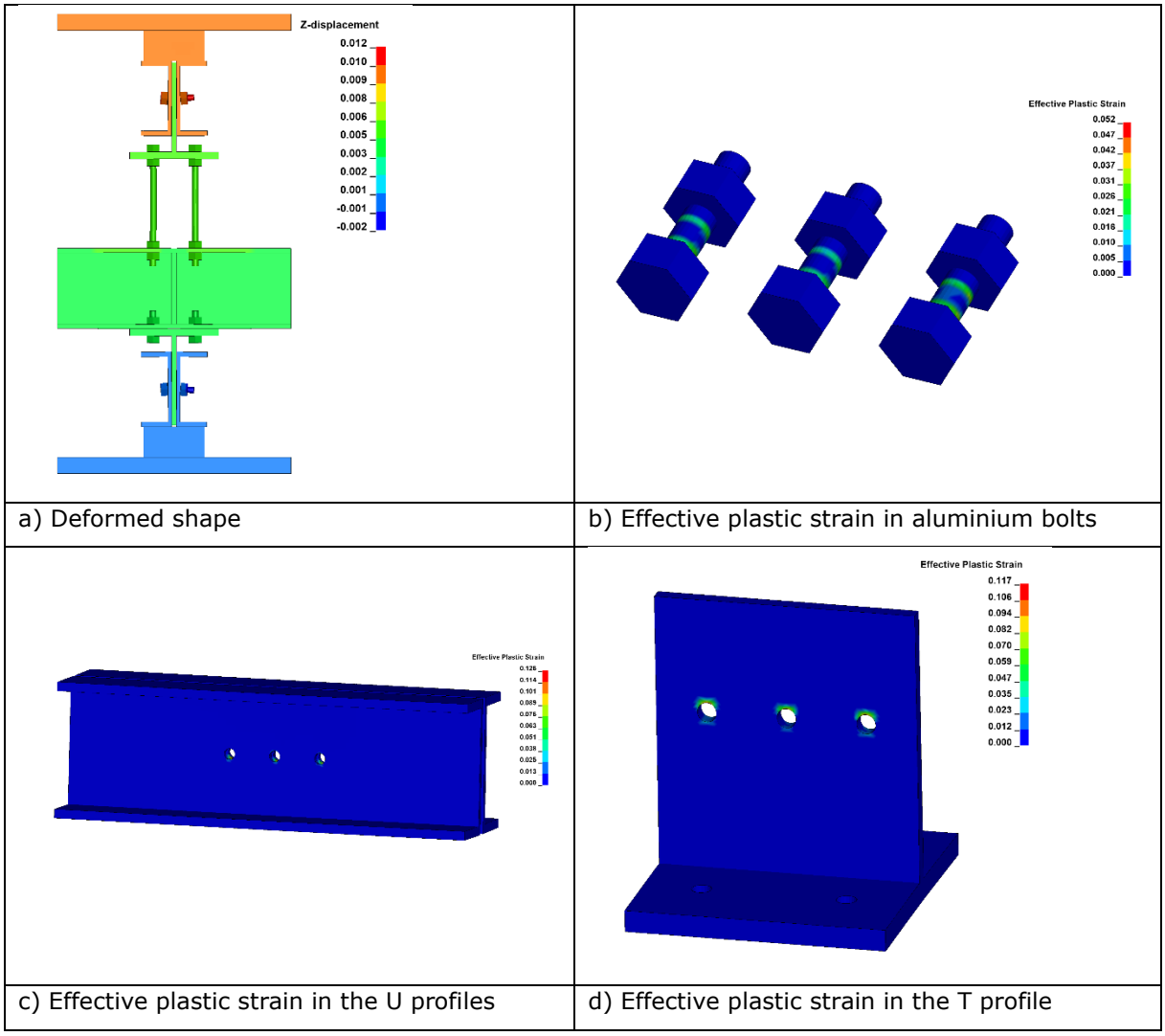

a) Deformed shape | b) Effective plastic strain in aluminium bolts

c) Effective plastic strain in the U profiles | d) Effective plastic strain in the T profile

Figure 2.62: Main results of the modelling under Ls-dyna without bolt-hole clearances at failure time of aluminium bolts

a) Cyclic test n°1 | b) Cyclic test n°2

Figure 2.63: Photos of aluminium bolts after the cyclic tests

2.2.4 Fusible link configuration n°3.2

For the detail 3.2, monotonic analyses were performed with or without bolt-hole clearances.

2.2.4.1 Monotonic tension loading

Figure 2.64 compares the predicted link response in terms of force-displacement to the experimental ones (denoted by "CH0" "CH2" and "CH6"). Each predicted curve is a resulting plot of the total vertical force calculated by summing the reaction forces of all nodes at the fixed end of the link against the prescribed vertical displacement. Through the figure, it can be noted that the experimental force–displacement curves consist mainly of a multilinear (elastic) stage, followed by a failure stage distinguished by sudden force drops. When hole bolt clearances are not considered, the predicted force–displacement curves globally experience a simple linear stage, up to a vertical displacement Dy^+=2.8 mm corresponding approximately to a vertical force F=227 kN, followed by a plateau stage corresponding to the shear yielding of the cross-sectional area of all aluminium bolts. Accounting for bolt-hole clearance leads to a delay in the development of the tensile force, which starts when bolts come into bearing within the holes. In addition, the predicted curves exhibit also a lightly stiffness degradation stage after the linear stage. However, there is no significant effect of the failure load value, the peak force value reaching approximately the same value. In this case, the yield displacement Dy^+ is estimated to 7 mm. As expected, the models predict the failure of the test specimen by shearing of aluminium bolts. However, the load-bearing capacity predicted for the fusible link is overestimated in comparison to the one observed during the test, estimated to 130.2 or 155 kN, whether by considering the force value corresponding to the first failure or the full failure of all aluminium bolts (which corresponds to an error higher than 45% between the predicted and measured values). As highlighted in the seismic tests, the behaviour of Detail 3.2 was, in certain cases, affected by imperfections in the assembly, i.e. not perfect alignment of the holes, slightly different hole dimensions that may have induced higher forces than expected in some aluminium bolts, that collapsed sequentially before reaching the design force. This progressive failure of the aluminium bolts induced a lower degree of symmetry with respect to the other details, except for Detail 3.1 that exhibited similar behaviour, as shown in Section 2.2.3. This can be one of the reasons of the capacity overestimation of the numerical models. Moreover, the larger the number of bolts, the higher the effects of the imperfections. In addition to resistance, there is some discrepancy between the numerical and experimental curves. Firstly, the experimental curves show what may appear to be a slip initial stage (from zero to approximately 2 mm of displacement) shorter than the one predicted by models when a certain level of slippage is taken into account. Secondly, the initial stiffness predicted by the models is significantly higher than that observed experimentally. However, it should be noted that the stiffnesses are closer when considering the final part of the experimental curves derived from the displacement transducers ("CH0" and "CH2") placed beneath one of the steel profiles of the fusible link. . Like the detail 3.1, the difference between the experimental curves is surprising, indicating that the upper part of the fusible link undergoes greater displacement than the lower part. Lastly, the sudden force drops observed at the test end are not captured accurately, since the bolts fracture is not explicitly considered in the modelling, which leads to over-estimate the deformations that the specimens can really reach, and hence the specimen ductility. It can be also underlined the satisfactory agreement between the two models developed under ANSYS and Ls-dyna.

The failure modes of the specimen are recognized by checking the strain level reached in the different components constituting the studied fusible link. For illustrative purposes, Figure 2.67 shows the distribution of the Von mises total mechanical strain predicted in aluminium bolts from the ANSYS model without bolt-hole clearances. The strain distribution is given here for different levels of imposed displacement (so different force levels), by showing strain values exceeding 5% only. It

clearly shows a yielding line progressively propagating in the cross-sectional area of bolts, in the two shear planes at the junction between steel profiles linked by the aluminium bolts. It can be noticed that the failure predicted by the models involved the collapse of the two aluminium bolts row at the same time, while the test was characterized by a progressive failure of the aluminium bolts. Figure 2.66 shows the distribution of the Von mises total mechanical strain predicted in the other components of the link, at the simulation end with the ANSYS model. It can be noted that the strain level exceeds locally the 0.2% yield strain around the holes of aluminium bolts, highlighting that some bearing occurs in steel plates, with limited holes elongation. Steel bolts and steel rods have only slight deformation, and no damage occurs.

For information, Figure 2.68 summarises the main results obtained at failure time of bolts from modelling developed under Ls-dyna without bolt-hole clearances. The results are in good agreement with the ones reported for the ANSYS model.

As with other links, the dissimilarities between the experimental and FE results are mainly attributed to clearances and slipping between the steel profiles and all bolting. Bolt-hole clearances allow some movement in the link and can lead to increased bolt rotation, decreased bolt-hole contact area and then decreased link stiffness. Moreover, the misalignment of bolt and hole, the misalignment of profile or holes of varying sizes can lead to some bolts to remain unstressed at the start of loading, or throughout loading. All these phenomena are difficult to be considered accurately in models. This could also be due to phenomena which are not accounted in FE models, like possible slipping between the screw and nut thread or progressive crushing of the bearing flank of the thread (that supports shearing forces) of aluminium bolts with the bearing stresses. It should be noted that some predicted curves may be non-smooth in certain loading stages. As in the previous case, the rough shape observed in the numerical curves is attributed to dynamic effects (due to the speed of load application and the resulting inertia forces), which can cause oscillations at the contact surfaces and interpenetration issues.

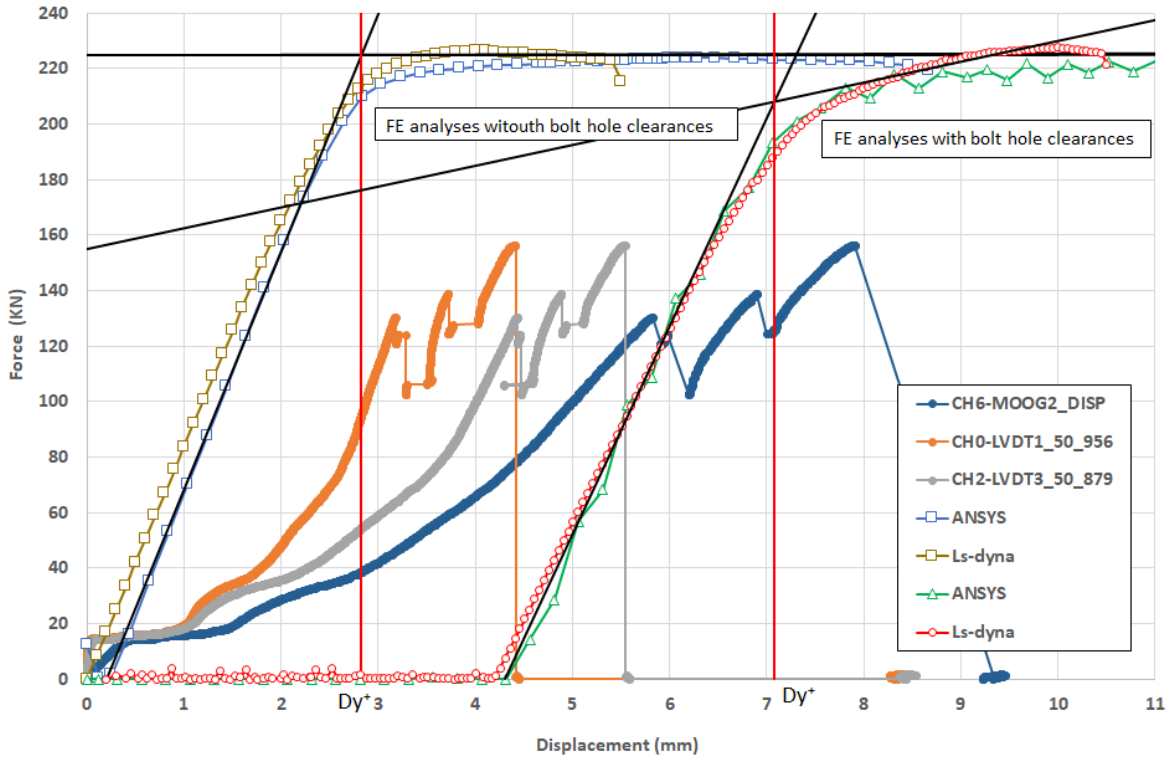

Figure 2.64: Force-displacement curves obtained from FE analyses and experiment for the fusible link configuration n°3.2 under tensile action

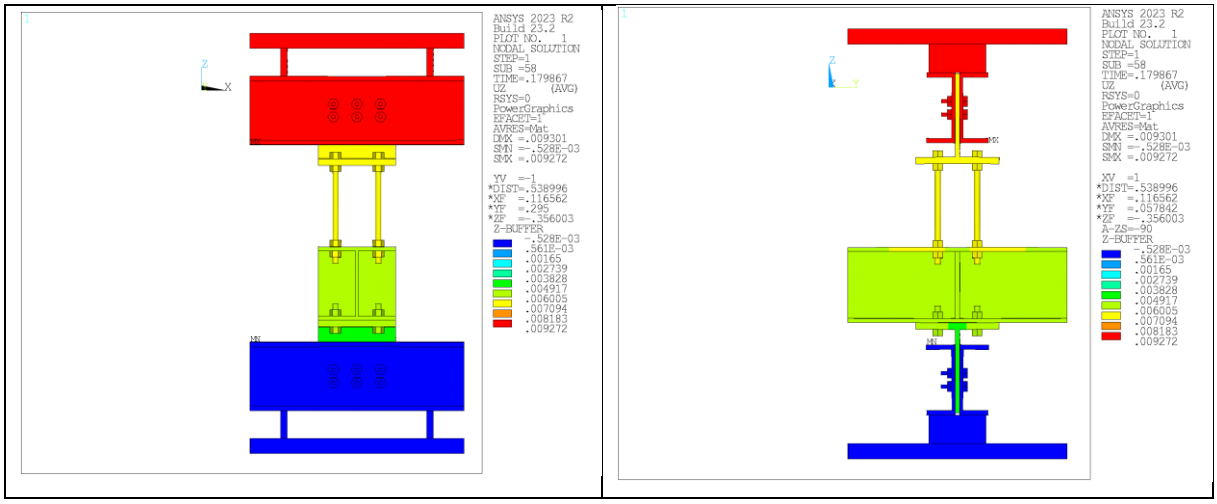

Figure 2.65: Deformed shape of the fusible link configuration n°3.2 predicted with the ANSYS model without bolt-hole clearances

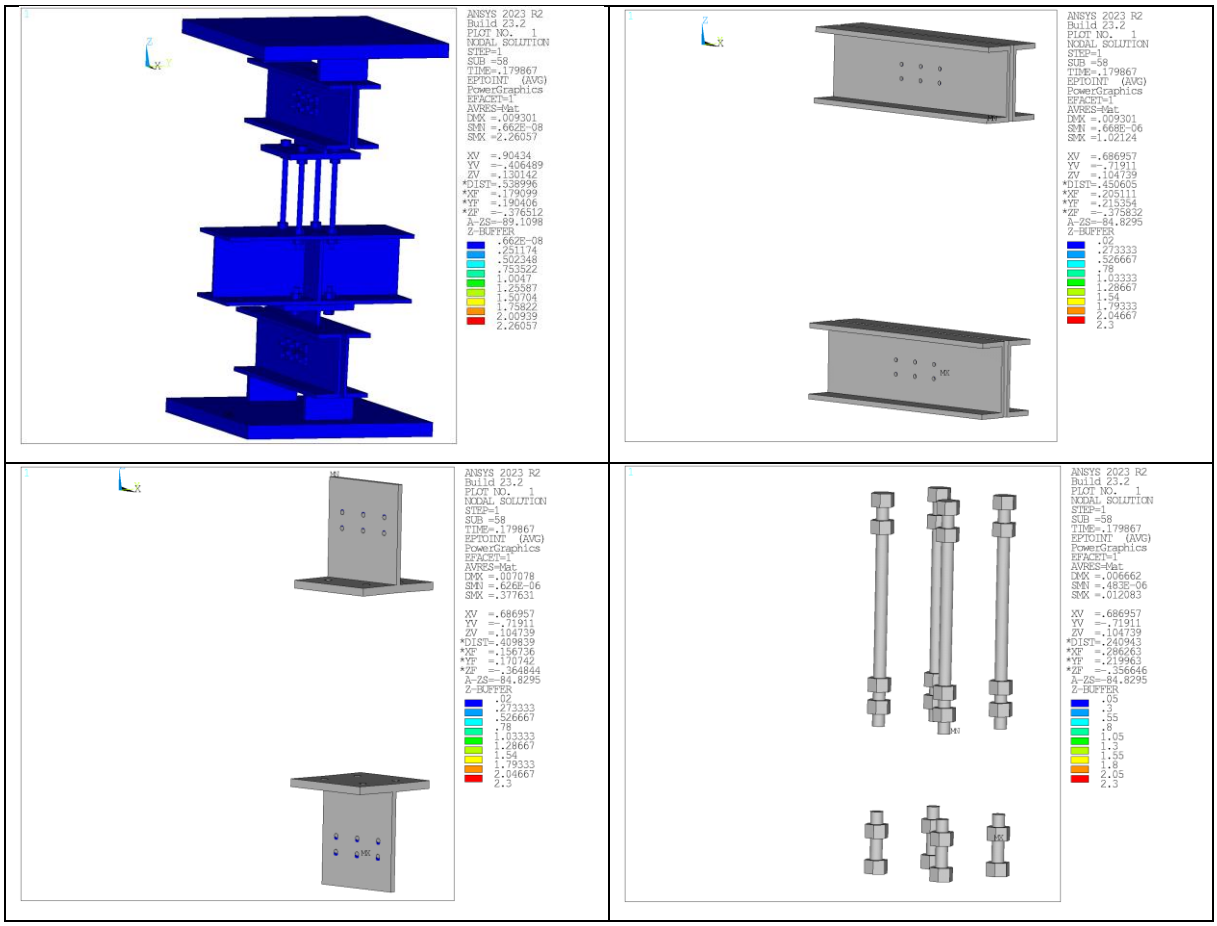

Figure 2.66: Von mises total mechanical strain in components of the fusible link configuration n°3.2 predicted with the ANSYS model without bolt-hole clearances, at simulation end

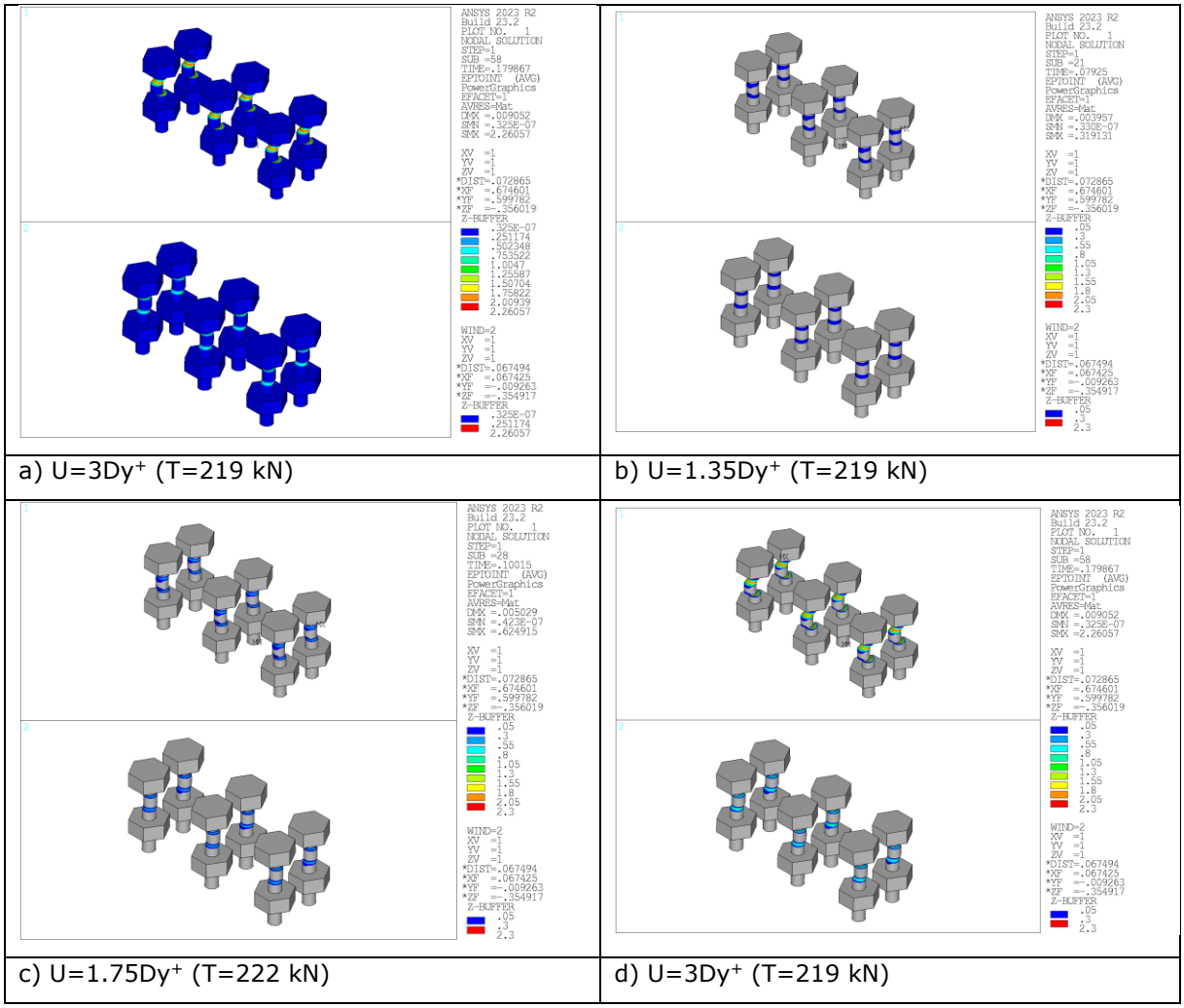

a) U=3Dy⁺ (T=219 kN)

b) U=1.35Dy⁺ (T=219 kN)

c) U=1.75Dy⁺ (T=222 kN)

d) U=3Dy⁺ (T=219 kN)

Figure 2.67: Von mises total mechanical strain in aluminium bolts of the fusible link configuration n°3.2 predicted for different values of imposed displacement with the ANSYS model without bolt-hole clearances

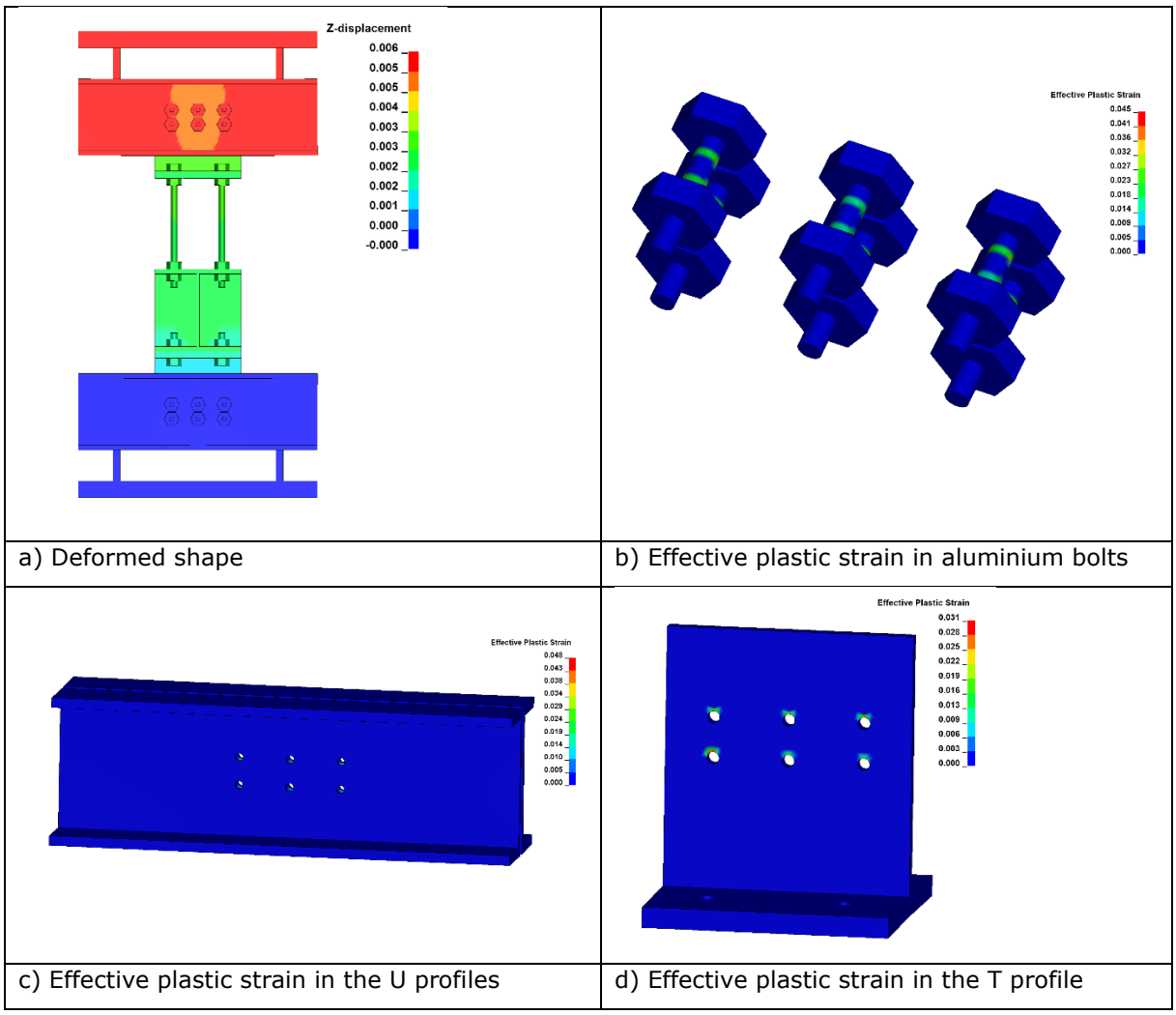

a) Deformed shape | b) Effective plastic strain in aluminium bolts

c) Effective plastic strain in the U profiles | d) Effective plastic strain in the T profile

Figure 2.68: Main results of the modelling under Ls-dyna without bolt-hole clearances at failure time of bolts

2.2.4.2 Monotonic compression loading

Figure 2.69 compares the predicted link response in terms of force-displacement to the experimental ones (denoted by "CH3" and "CH6" in the figure). Each predicted curve is a resulting plot of the total vertical force calculated by summing the reaction forces of all nodes at the fixed end of the link against the prescribed vertical displacement. Through the figure, it can be noted that the experimental force–displacement curves consist of a multi-linear (or elastic) stage, followed a brittle failure stage. When hole bolt clearances are not considered, the predicted force–displacement curves globally experience a simple linear stage, up to a vertical displacement Dy^{+}=2.2 mm corresponding approximately to a vertical force F=239 kN, followed by a plateau stage corresponding to the shear yielding of the cross-sectional area of all aluminium bolts. Accounting for bolt-hole clearance leads to a delay in the development of the force, which starts when bolts come into bearing within the holes. In addition, the predicted curves exhibit a lightly stiffness degradation stage after the linear stage. However, there is no significant effect of the failure load value, the peak force value reaching approximately the same value. In this case, the yield displacement Dy^{-} is estimated to 6.9mm. As expected, the models predict the failure of the test specimen by shearing of aluminium bolts. However, the load-bearing capacity predicted for the fusible link is overestimated in comparison to the one observed during the test, namely 205 KN (which corresponds to an error of 17% between the predicted and measured values). As for experiment, it can be noted that the models predict that the load-bearing capacity of the specimen is slightly higher under compression that tension. In addition to resistance, there is still some discrepancy between the numerical and experimental curves. At the initial loading stage, before what appears to be a slip stage (from 0.5 to 4.5 mm displacement for the CH6 curve), the predicted and experimental stiffnesses are comparable. Next, the stiffness predicted by the models appears significantly higher than the experimentally observed (when compared to the displacement curve "CH6" derived from the displacement transducer

associated with the loading device), even if stiffnesses (defined as the slope of the tangent to the force-displacement curve) appear close by considering the experimental curve derived from the displacement transducer ("CH3") placed beneath one of the steel profiles of the fusible link. The difference between the experimental curves is surprising, suggesting that, at a given load level, the upper part of the fusible link undergoes greater displacement and slipping than the lower part. Lastly, the sudden drop in force observed at the test end is not captured accurately, since not considering bolt fracture overestimates the deformations that the specimen can reach and hence the specimen ductility in compression. It can be also underlined the satisfactory agreement between the two models developed under ANSYS and Ls-dyna.

The failure mode of the specimen is recognized by checking the strain level reached in the different components constituting the studied fusible link. For illustrative purposes, Figure 2.72 shows the distribution of the Von mises total mechanical strain predicted in aluminium bolts from the ANSYS model without bolt-hole clearances. The strain distribution is given here for different levels of imposed displacement (so different force levels), by showing strain values exceeding 5% only. It clearly shows a yielding line progressively propagating in the cross-sectional area of bolts, in the two shear planes at the junction between steel profiles linked by the aluminium bolts. It can be noticed that the failure predicted by the models involved the collapse of the two aluminium bolts rows, while the test was characterized by a failure of all the aluminium bolts of the lower part of the specimen only. Figure 2.71 shows the distribution of the Von mises total mechanical strain predicted in other components of the link with the ANSYS model, at the simulation end. It can be noted that the strain level exceeds locally the 0.2% yield strain around the holes of aluminium bolts, highlighting that some bearing occurs in steel plates, with limited holes elongation. Steel bolts and steel rods have only slight deformation and don't suffer any damage in analyses.

For information, Figure 2.73 summarises the main results obtained at failure time of bolts from modelling developed under Ls-dyna without bolt-hole clearances. The results are in good agreement with the ones reported for the ANSYS model.

As with other links, the differences between the experimental and FE results are mainly attributed to clearances and slipping between the steel profiles and all bolting. Bolt-hole clearances allow some movement in the link and can lead to increased bolt rotation, decreased bolt-hole contact area and then decreased link stiffness. Moreover, the misalignment of bolt and hole, the misalignment of profile or holes of varying sizes can lead to some bolts to remain unstressed at the start of loading, or throughout loading. All these phenomena are difficult to be considered accurately in models. This could also be due to phenomena which are not accounted in FE models, like possible slipping between the screw and nut thread or progressive crushing of the bearing flank of the thread (that supports shearing forces) of aluminium bolts with the bearing stresses.

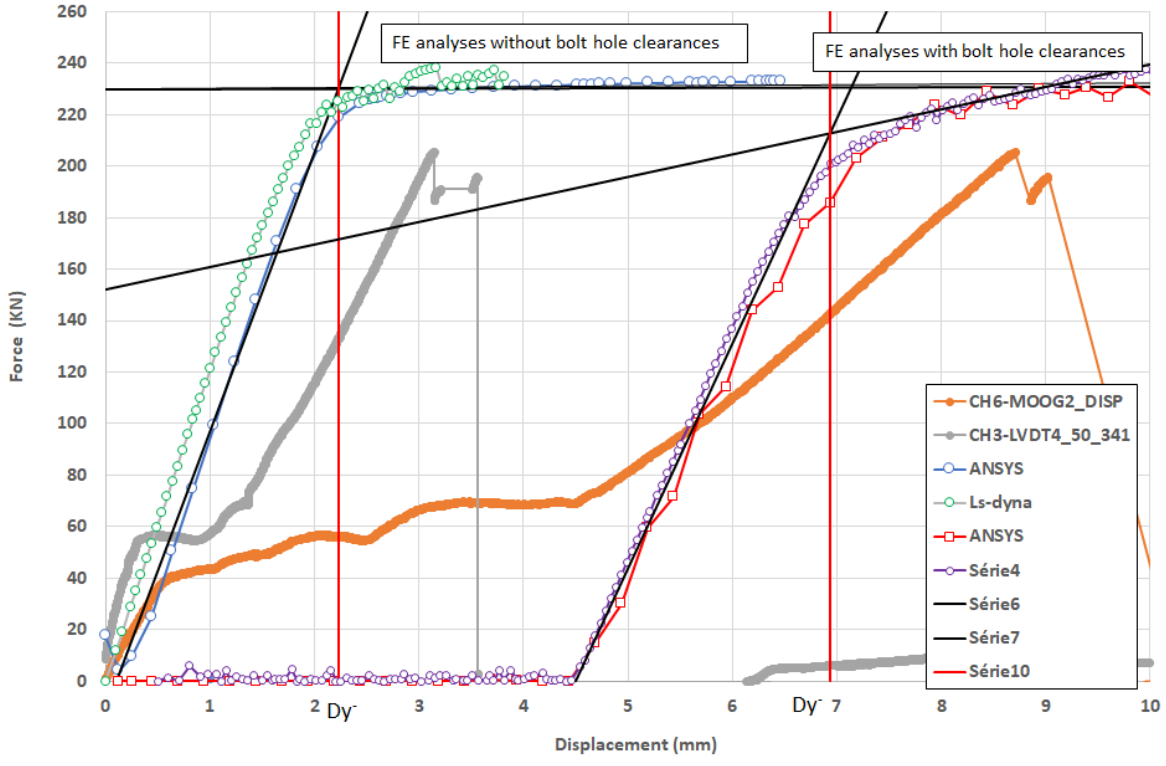

Figure 2.69: Force-displacement curves obtained from FE analyses and experiment for the fusible link configuration n°3.2 under compressive action

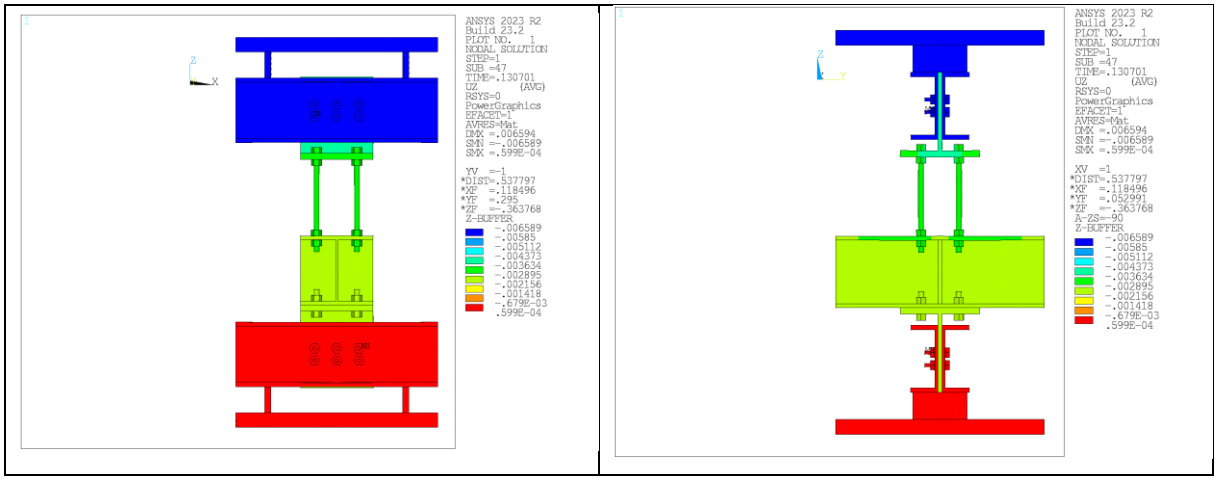

Figure 2.70: Deformed shape of the fusible link configuration n°3.2 predicted with the ANSYS model without bolt-hole clearances

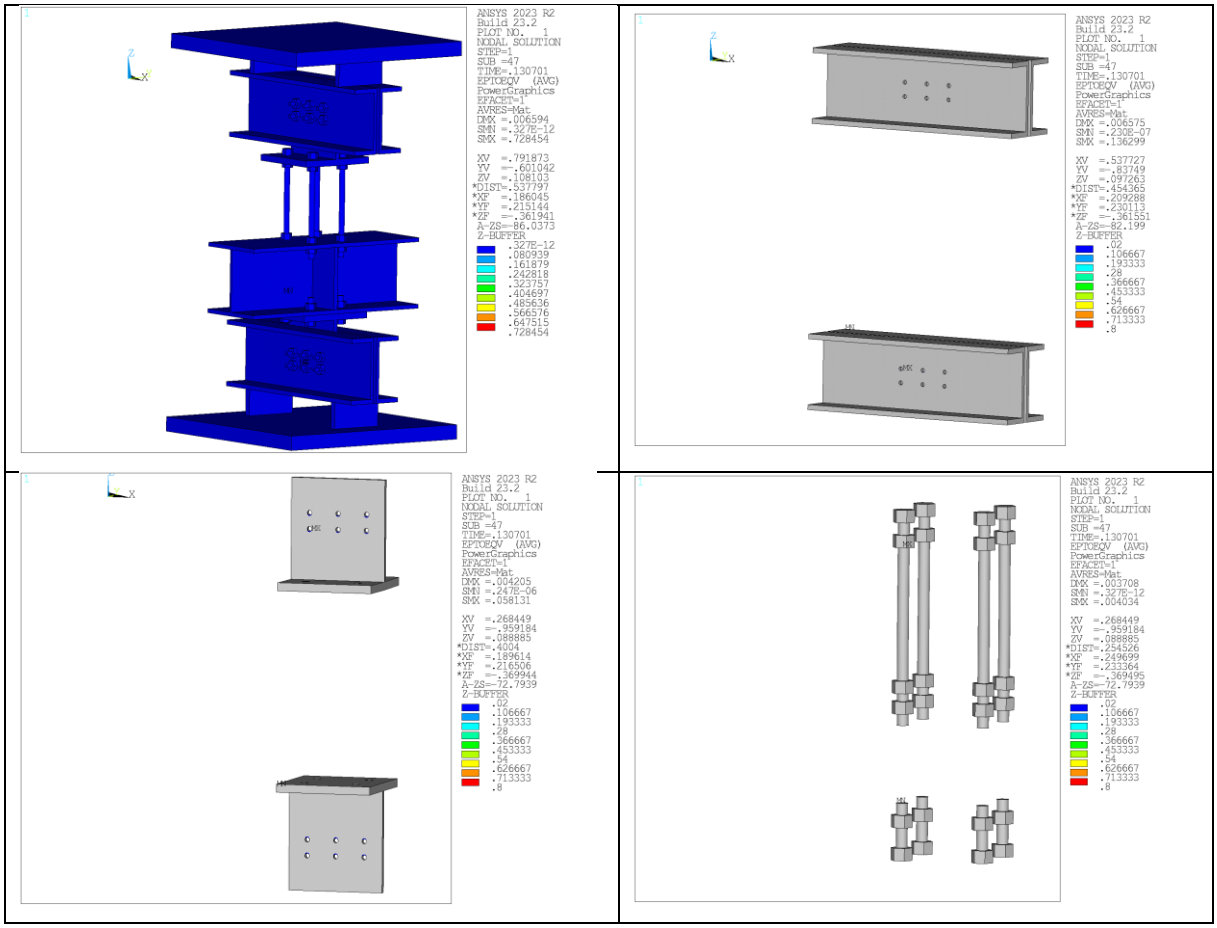

Figure 2.71: Von mises total mechanical strain in components of the fusible link configuration n°3.2 predicted with the ANSYS model without bolt-hole clearances, at simulation end

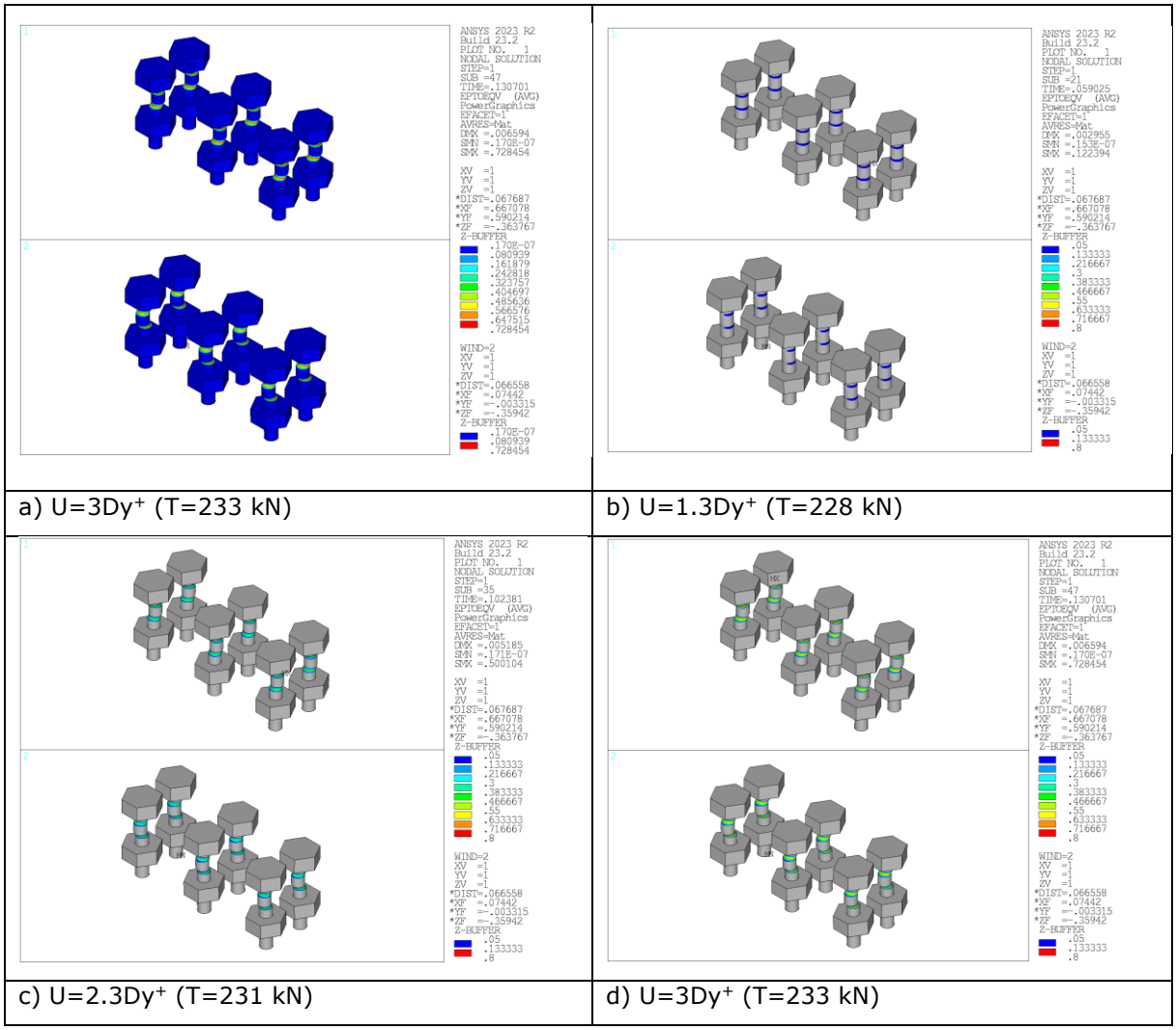

a) U=3Dy⁺ (T=233 kN)

b) U=1.3Dy⁺ (T=228 kN)

c) U=2.3Dy⁺ (T=231 kN)

d) U=3Dy⁺ (T=233 kN)

Figure 2.72: Von mises total mechanical strain in aluminium bolts of the fusible link configuration n°3.2 predicted for different values of imposed displacement with the ANSYS model without bolt-hole clearances

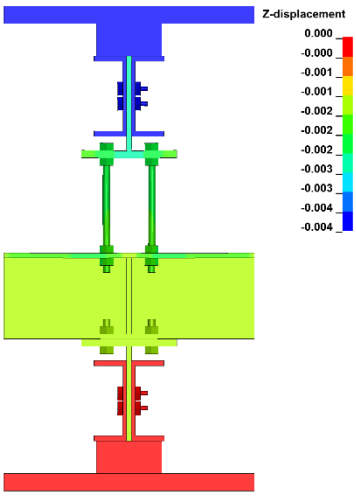

a) Deformed shape

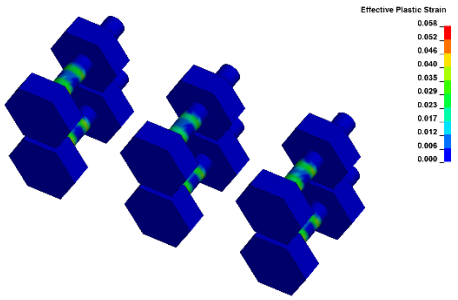

b) Effective plastic strain in aluminium bolts

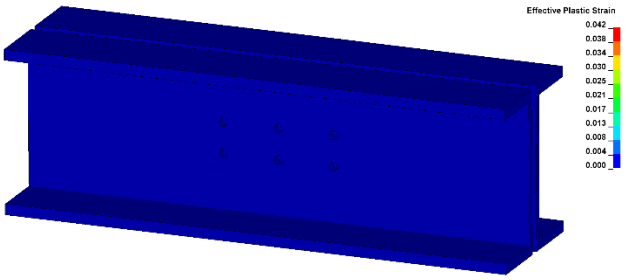

c) Effective plastic strain in the U profiles

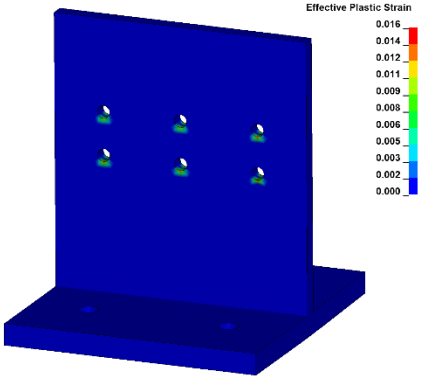

d) Effective plastic strain in the T profile

Figure 2.73: Main results of the modelling under Ls-dyna without bolt-hole clearances at failure time of aluminium bolts

2.2.4.3 Cyclic loading

The vertical displacement-time curve prescribed in numerical analyses carried out without bolt-hole clearances is presented in Figure 2.74, while the yield displacements obtained from monotonic analyses are reported in Table 5.

Table 5: Yield displacements determined from monotonic analyses of the fusible link detail n°3.2

	Without bolt-hole clearances	With Bolt-hole clearances
Dy^+	2.8 mm	7.0 mm
Dy^-	2.2 mm	6.9 mm

Because numerical results indicated that bolt-hole clearances have no significant effect on the failure load of the previous link (link configuration 3.1), only results of simulations carried out without bolt-hole clearances are presented for the link detail n°3.2.

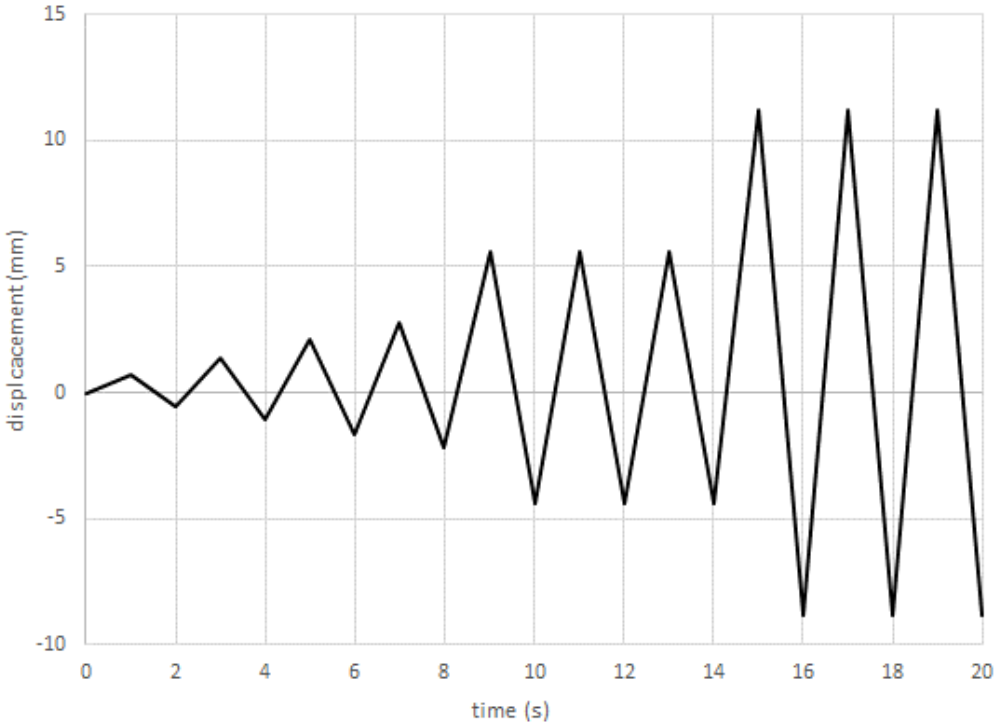

Figure 2.74: Vertical displacement-time curve used in numerical analyses carried out without bolt-hole clearances for the fusible link detail n°3.2

Figure 2.75 to Figure 2.77 depict the comparison between the FE predicted hysteresis axial force-displacement responses and the results from three cyclic tests. In this figure, the negative values means that components are under compression, and positive values are for tension. Through the hysteresis curves, it can be noted that numerical models predict that the studied link remains in the elastic stage during a major part of the displacement loading. Indeed, the predicted force–displacement curves are predominantly linear, both in tension and compression. Unloading takes place in the same path than loading, or a closer parallel path to that of the initial stiffness of the link until failure. The brittle nature of the detail in tension and compression highlights a very small hysteretic behaviour of the detail. It can be underlined that the predicted force-displacement curves display a similar behaviour in tension and compression, characterized, however, by slightly different initial stiffnesses in accordance with the monotonic analyses. Since no significant plastic deformations occur in steel components, the predicted cyclic response coincides well with the monotonic responses obtained in tension or compression loading. It can be also underlined the satisfactory agreement between the two models developed under ANSYS and Ls-dyna.

The failure modes of the studied fusible link are assessed by monitoring the strain states of different components constituting the link. Figure 2.80 shows the distribution of the Von mises total mechanical strain predicted in some components of the link with the ANSYS model, at the simulation end. It can be noted that the strain level exceeds locally the 0.2% yield strain around the holes of aluminium bolts only, highlighting that some bearing occurs in steel plates, with limited holes elongation. Steel bolts and steel rods undergo only elastic deformations. The failure of the specimen predicted by the models occurs on the reloading stage at the first cycle to $2Dy^+$ due to the shearing of aluminium bolts. For illustrative purposes, Figure 2.79 shows the distribution of the Von mises total mechanical strain predicted in aluminium bolts with the ANSYS model. The strain distribution is given here for different levels of imposed displacement, by showing strain values exceeding 5% only. It clearly shows a yielding line progressively propagating in the cross-sectional area of bolts, in the two shear planes at the junction between steel profiles linked by the aluminium bolts.

It should be noted that there is a notable discrepancy in the cyclic response of the studied link, between the experiment and the FE modelling. In addition to different initial stiffnesses, on the experimental curves, unloading takes place from the first cycle in a different path to that of the first loading stage. The unloading path includes two segments, an elastic unloading phase along a path that seems parallel to the loading path followed in the force-displacement curves predicted by models and a pinched unloading phase until the loading in the opposite direction happens. When unloaded to a 0 kN force, there is a non-zero residual vertical displacement which increases progressively with the repeated unloading-reloading cycles, even if the link is still in an elastic state, which is probably due to the bolt travels within holes. As already underlined in the project deliverable related to test

results [1], the experimental hysteresis curves display a pinching phenomenon in the hysteresis loops, which is not captured in the models. Lastly, it is worth noting that the hysteretic loops recorded for the two first cyclic tests (see Figure 2.75 and Figure 2.76) are more pinched in the middle compared to the third test (see Figure 2.77), because of the better bolt alignment operated during the assembly of the corresponding test specimen. It can be noted that the predicted load-bearing capacity of the link under cyclic loading is of the same order of magnitude than the ones obtained from monotonic analyses. It is approximately of 225 kN. In contrast, the peak force values reached in the three cyclic tests are different (from 189 to 228 KN), highlighting the variability of the tested specimen response among the tests, and greater than that observed in the monotonic tension test. In cyclic tests, the failure occurred due to the shearing of all the six aluminium bolts located on the lower part of the specimen, while the tension test was characterized by a progressive failure of aluminium bolts. It can be underlined the good agreement in failure load between experiment and models when bolt alignment was controlled during the specimen assembly.

The dissimilarities between the experimental and FE results are mainly attributed to clearances and slipping between the steel profiles and all bolting. Bolt-hole clearances allow some movement in the link and can lead to increased bolt rotation, decreased bolt-hole contact area and then decreased link stiffness. Moreover, the misalignment of bolt and hole, the misalignment of profile or holes of varying sizes can lead to some bolts to remain unstressed at the start of loading, or throughout loading. All these phenomena are difficult to be considered accurately in models. This could also be due to phenomena which are not accounted in FE models, like possible slipping between the screw and nut thread or progressive crushing of the bearing flank of the thread (that supports shearing forces) of aluminium bolts with the bearing stresses.

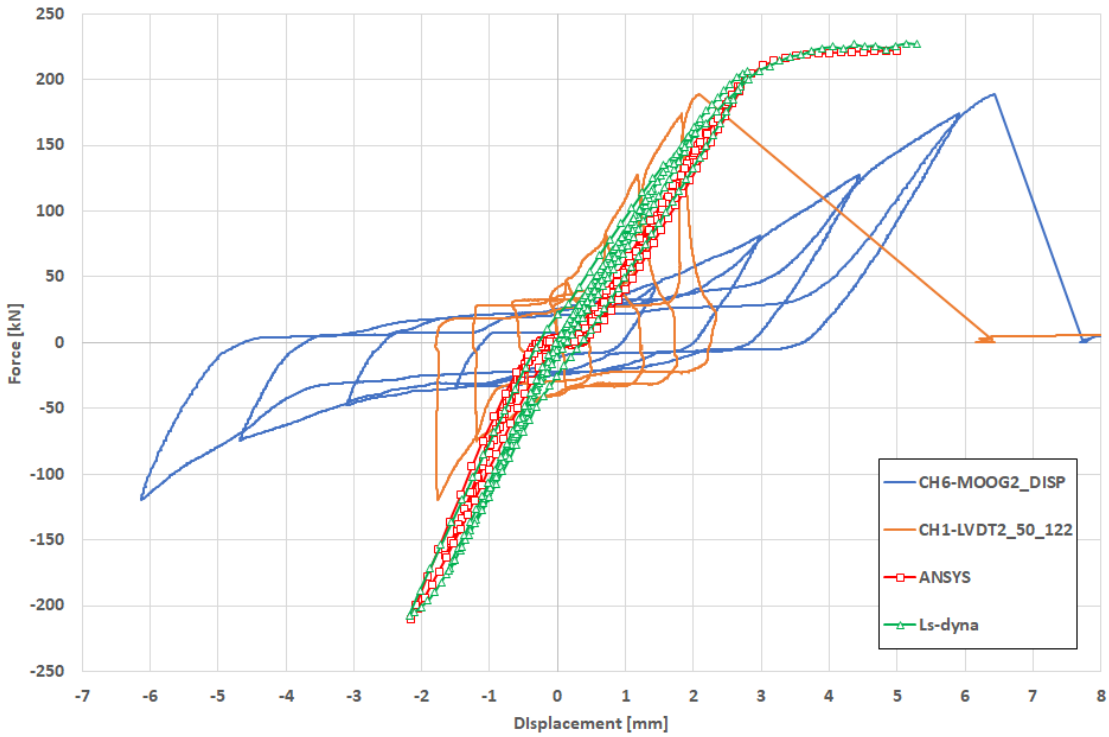

Figure 2.75: Force-displacement curves obtained from FE analyses and experiment (cyclic test n°1) for the fusible link configuration n°3.2 under cyclic action

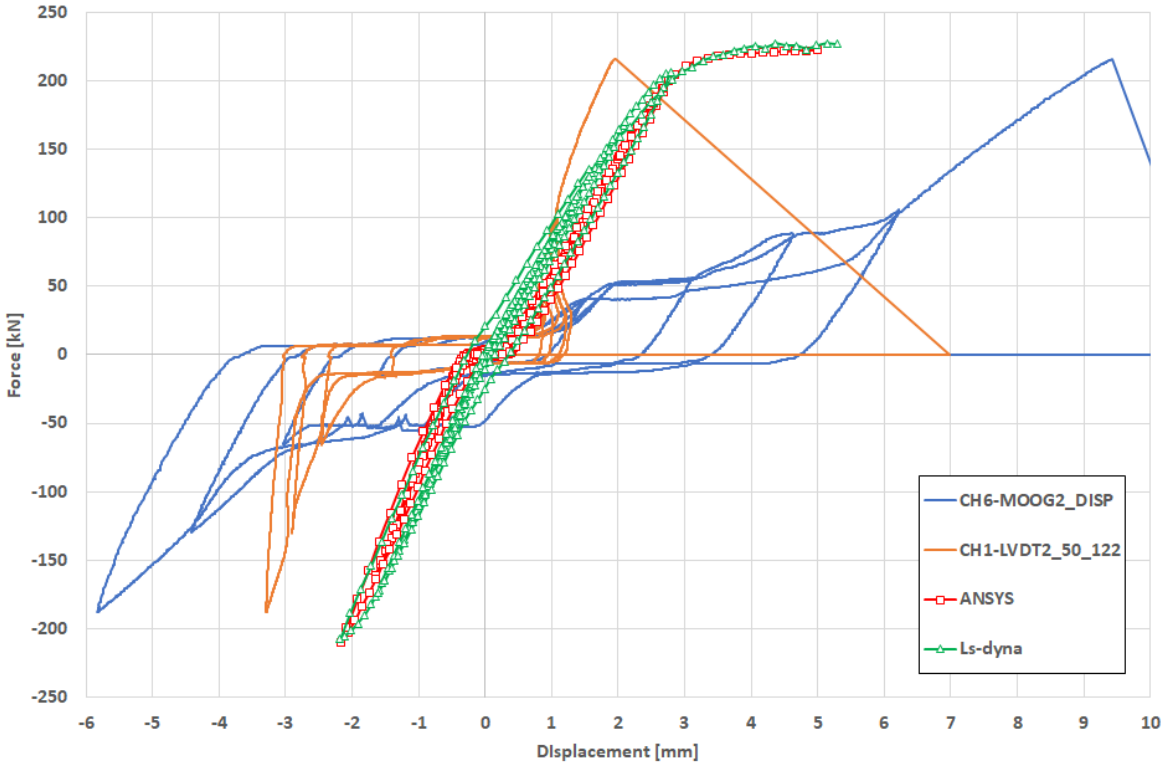

Figure 2.76: Force-displacement curves obtained from FE analyses and experiment (cyclic test n°2) for the fusible link configuration n°3.2 under cyclic action

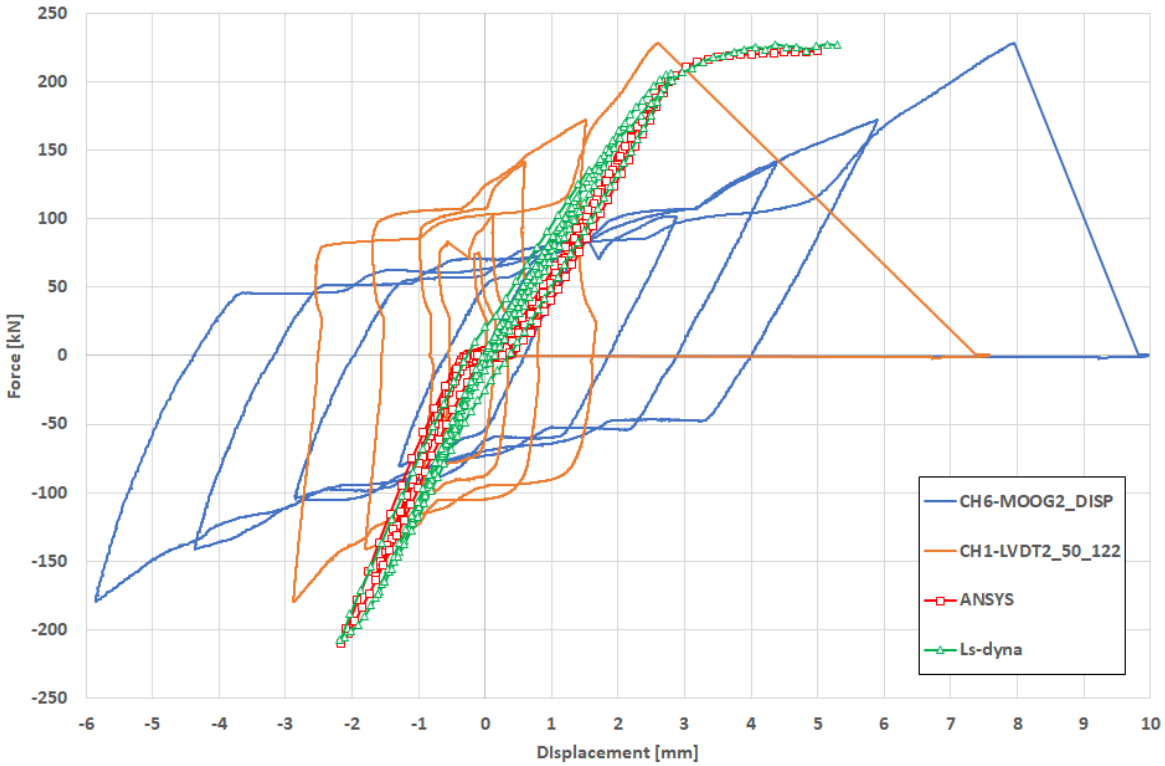

Figure 2.77: Force-displacement curves obtained from FE analyses and experiment (cyclic test n°3) for the fusible link configuration n°3.2 under cyclic action

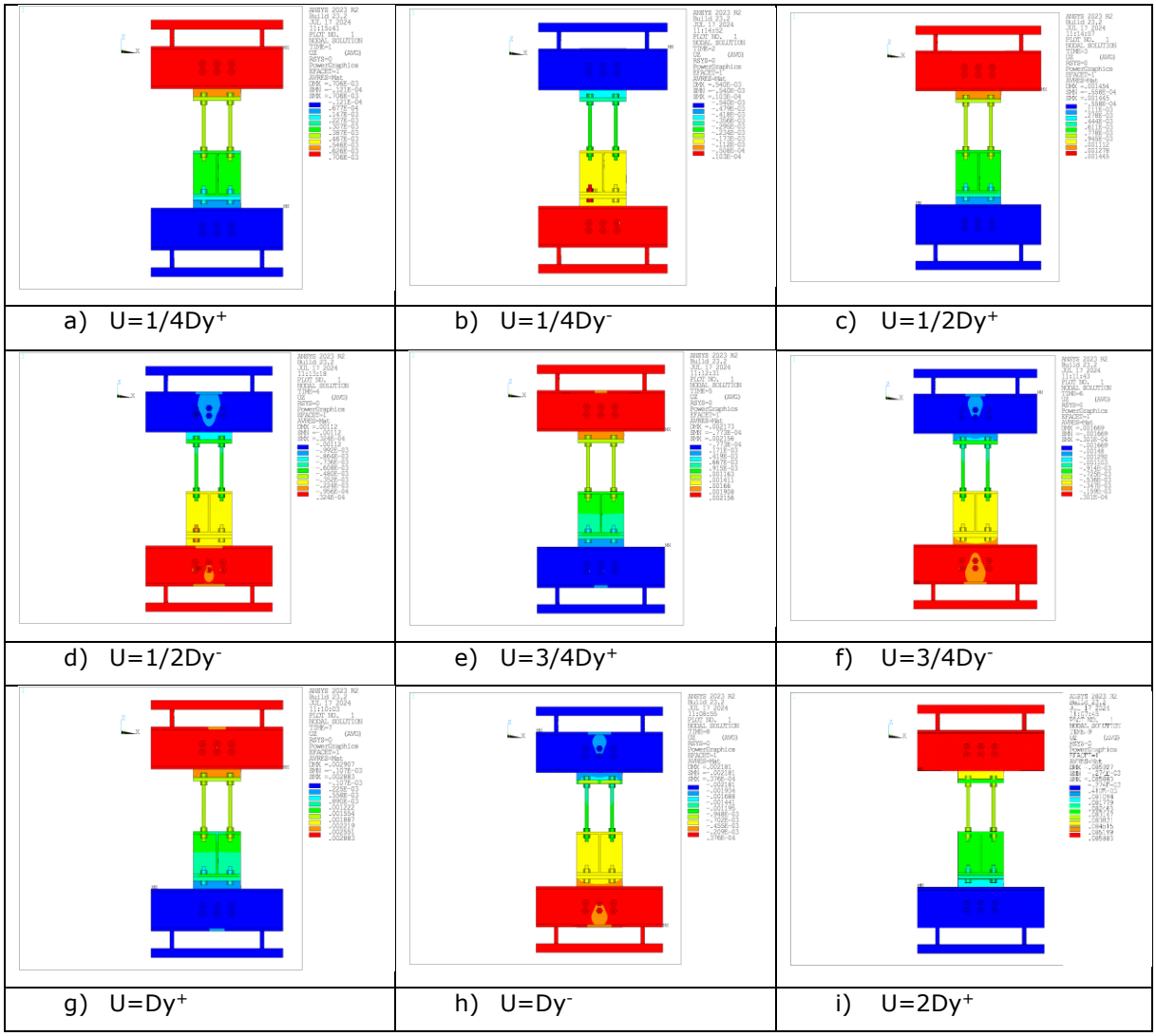

Figure 2.78: Deformed shape of the fusible link configuration n°3.2 according to imposed displacement values predicted with the ANSYS model without bolt-hole clearances

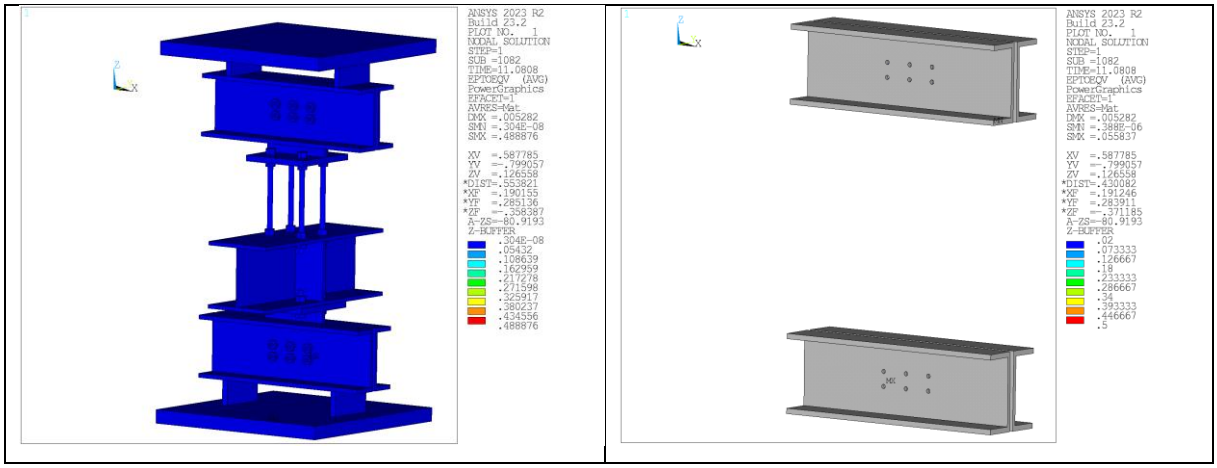

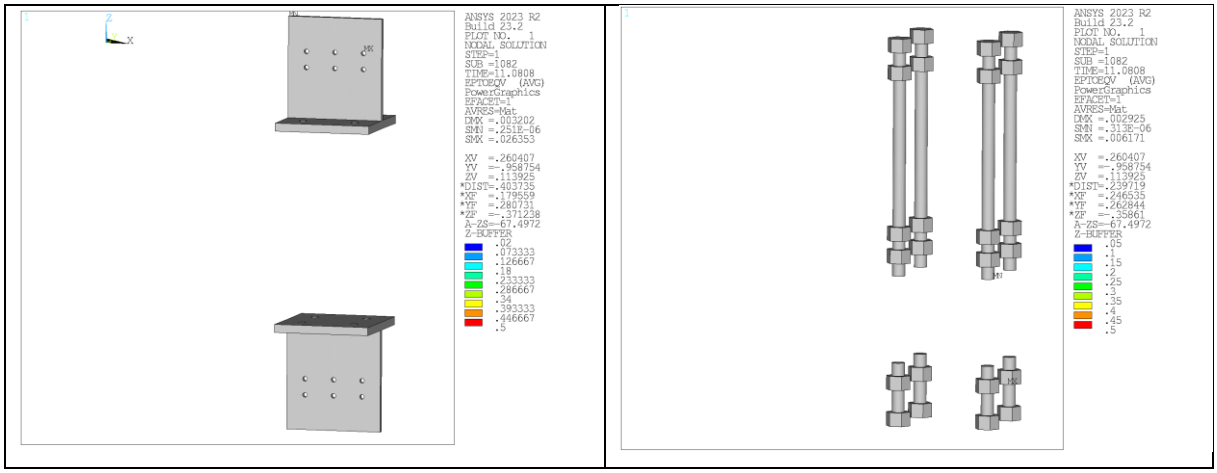

Figure 2.79: Von mises total mechanical strain in components of the fusible link configuration n°3.2 predicted with the ANSYS model without bolt-hole clearances, at simulation end

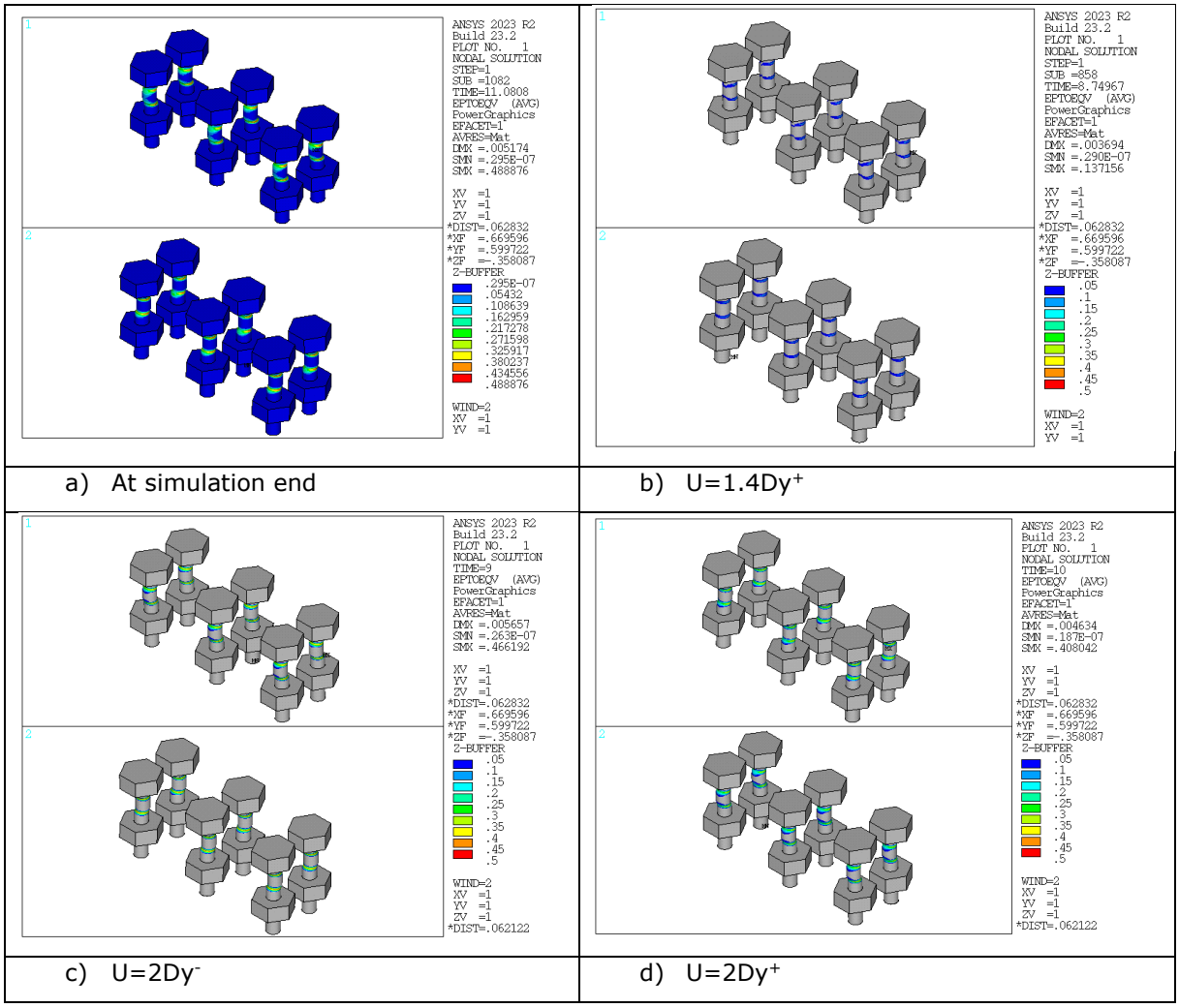

a) At simulation end

b) U=1.4Dy⁺

c) U=2Dy⁻

d) U=2Dy⁺

Figure 2.80: Von mises total mechanical strain in aluminium bolts of the fusible link configuration n°3.2 predicted for different values of imposed displacement with the ANSYS model without bolt-hole clearances

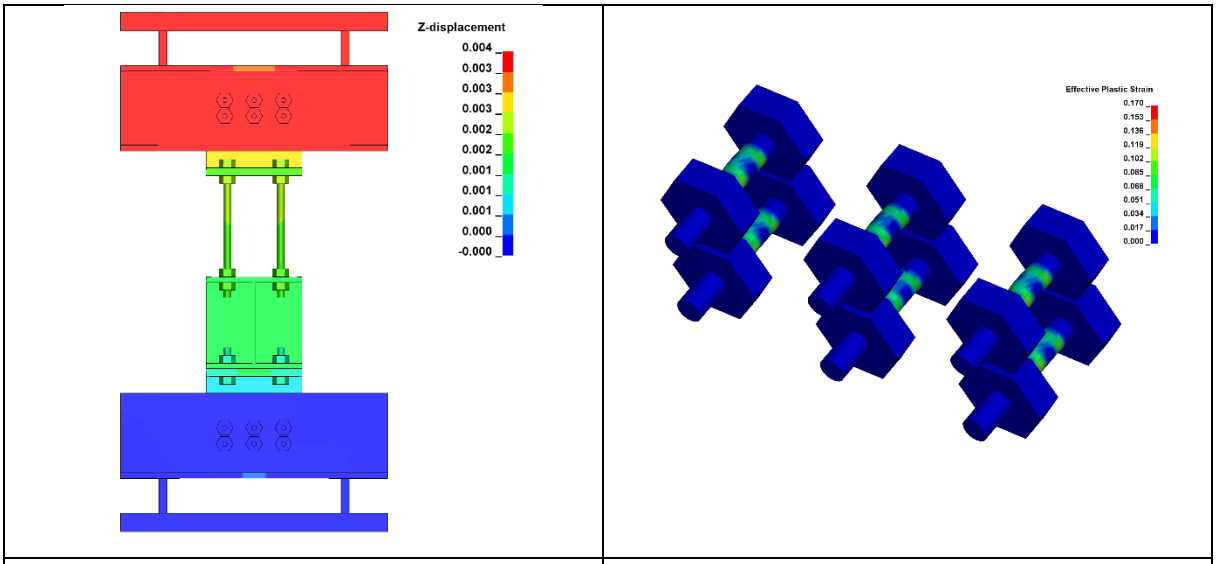

a) Deformed shape	b) Effective plastic strain in aluminium bolts
c) Effective plastic strain in the U profiles	d) Effective plastic strain in the T profile

Figure 2.81: Main results of the modelling under Ls-dyna without bolt-hole clearances at failure time of aluminium bolts

a) Cyclic test n°1	b) Cyclic test n°2	c) Cyclic test n°3

Figure 2.82: Photos of aluminium bolts after the cyclic tests

2.2.5 Fusible link configuration n°4

For the detail 4, monotonic analyses were performed with or without bolt-hole clearances.

2.2.5.1 Monotonic tension loading

Figure 2.83 compares the predicted values in terms of force-displacement to the experimental ones (denoted by "CH6" and "CH2"). Each predicted curve is a resulting plot of the total vertical force calculated by summing the reaction forces of all nodes at the fixed end of the models against the prescribed vertical displacement. Through the figure, it can be noted that the experimental force–displacement curves exhibit a first stage that appears linear (or as such), followed by a brittle failure stage evidenced by sudden drops in force. The predicted force–displacement curves are quite different. For increasing value of imposed displacements, the predicted curves mainly consist of two different stages: a first linear stage at which correspond an initial elastic stiffness and then a stiffness degradation stage highlighting a nonlinear behaviour of the fusible link, until the failure occurs. By neglecting bolt-hole clearances, the yield displacement Dy^+ coming from the numerical curve can be estimated to 10.5mm, which corresponds to the first failure of an aluminium bolt. Accounting for bolt-hole clearance leads to a delay in the force increase, which starts when bolts come into bearing within the holes, as well as an increase of the yield displacement Dy^+, which can be estimated to 16.4mm (by including bolts slipping inside holes). On the other hand, the numerical results indicate here that bolt-hole clearances have a favourable effect on the failure load value. The models predict the link failure by shearing of aluminium bolts, for a force approaching 54 kN or 84 kN whether bolt-hole clearances are considered or not. In comparison, the test failure load was estimated to 57 KN. Thus, the value of the load-bearing capacity predicted without bolt-hole clearances complies well with experiment. In contrast, the load-bearing capacity predicted by the models with bolt-hole clearances is overestimated. Moreover, it can also be seen that there is a discrepancy in the prediction of the initial stiffness of the studied link in comparison to the experimental stiffness, which appears significantly lower than the numerically predicted one. As previously mentioned for the other links, this is believed to be due mainly to clearances and slipping between the steel profiles and all bolting (steel rods, steel bolts and aluminium bolts). This could also be due to some slipping between the screw and nut thread or progressive crushing of the bearing flank of the thread (that supports shearing forces) of aluminium bolts, which is not accounted in FE models. Lastly, it is worth noting that the final part of the experimental curves is not captured accurately where the bolts fracture is not considered, since it leads to over-estimate the deformations that the specimens can really reach, and hence the specimen ductility. On the other hand, two sharply force decreases can been observed, highlighting the progressive failure of aluminium bolts, if the fracture of bolts is considered in modelling by adding a descending branch in the bolt material law (curve denoted "MLWDB" in Figure 2.83). It can be also underlined the satisfactory agreement between the two models developed under ANSYS and Ls-dyna.

The failure modes of the specimen can be recognized by checking/analysing the strain level reached in the different components constituting the studied fusible link. For illustrative purpose, Figure 2.86 shows the distribution of the Von mises total mechanical strain predicted in aluminium bolts from the ANSYS model without bolt-hole clearances. The strain distribution is given here for different levels of imposed displacement (so different force levels), by showing strain values exceeding 5% only. It clearly shows a yielding line progressively propagating in the cross-sectional area of bolts, in the shear plane at the junction between the U and Z shaped steel profiles. Figure 2.85 displays the distribution of the Von mises total mechanical strain predicted in other components of the link with the ANSYS model, at the simulation end. It can be noted that the strain level exceeds locally the 0.2% yield strain around the holes of aluminium bolts only, highlighting that some bearing occurs in steel plates, with limited holes elongation. Steel bolts have only slight deformation, while steel rods have undergone large flexural deformations, but and no damage occurred in simulations.

For information, Figure 2.87 summarises the main results obtained at failure time of bolts from modelling developed under Ls-dyna without bolt-hole clearances. The results are in good agreement with the ones reported for the ANSYS model.

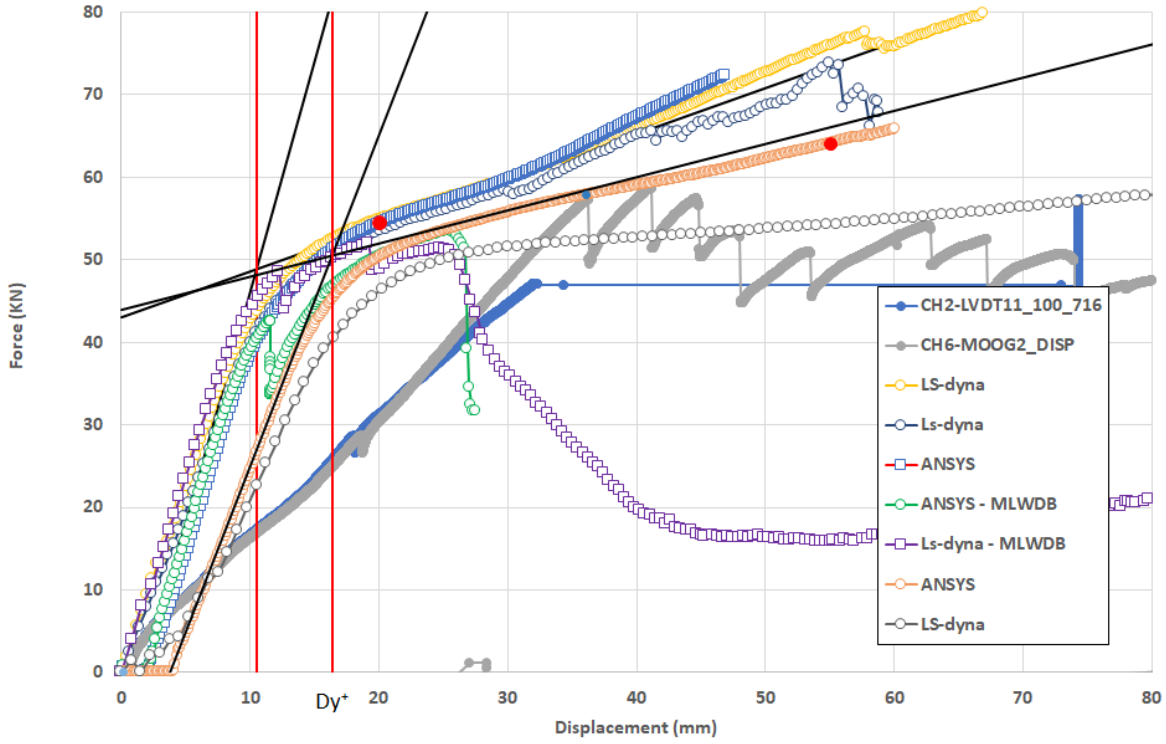

Figure 2.83: Force-displacement curves obtained from FE analyses and experiment for the fusible link configuration n°4 under tensile action

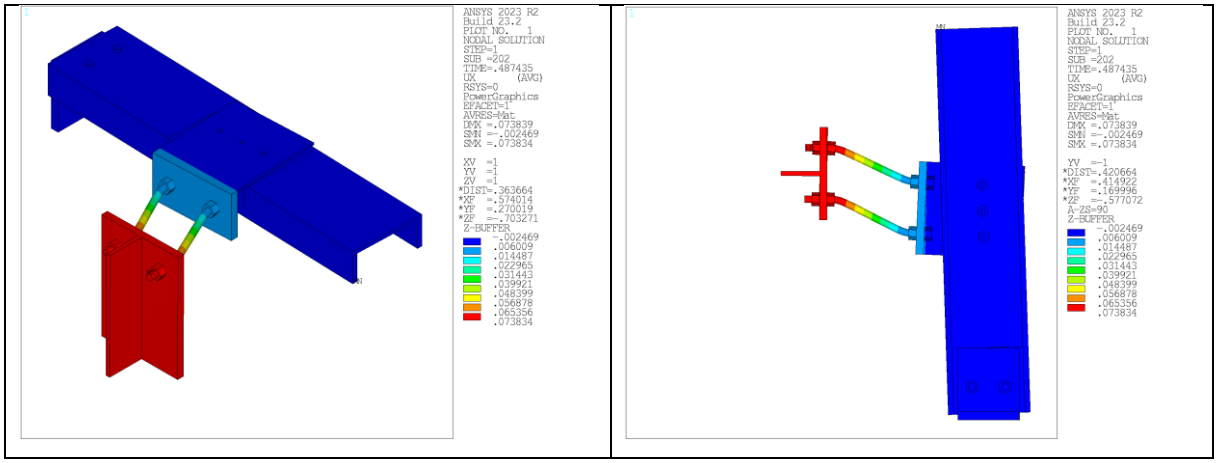

Figure 2.84: Deformed shape of the fusible link configuration n°4 predicted with the ANSYS model without bolt-hole clearances

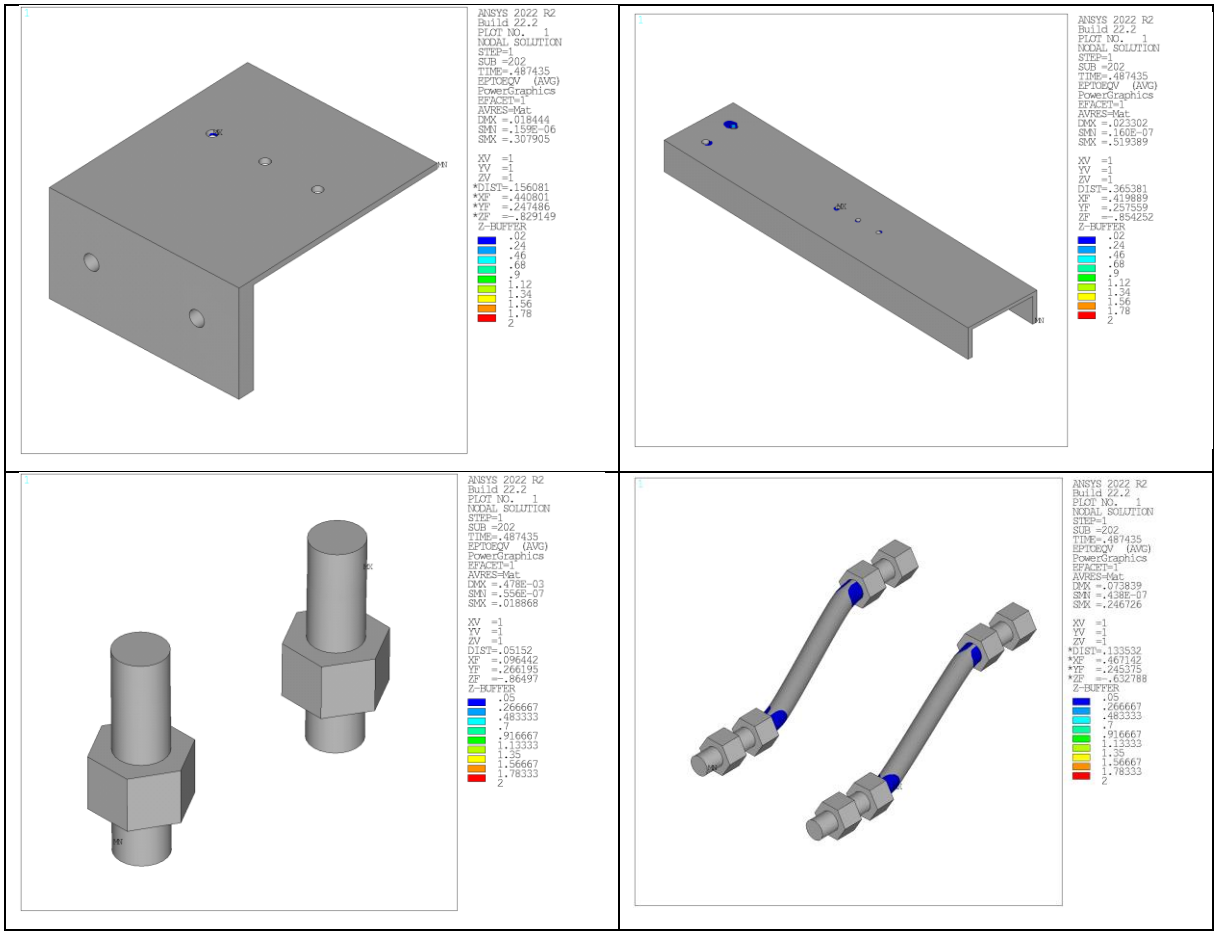

Figure 2.85: Von mises total mechanical strain in components of the fusible link configuration n°4 predicted with the ANSYS model without bolt-hole clearances, at simulation end

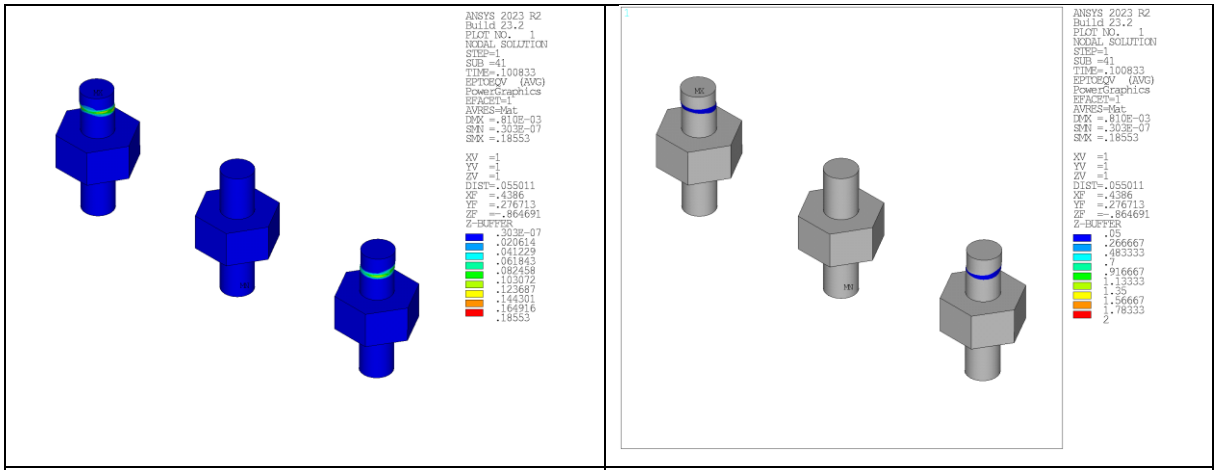

a) U=1.25Dy⁺ (T=126 kN)	b) U=1.25Dy⁺ (T=126 kN)

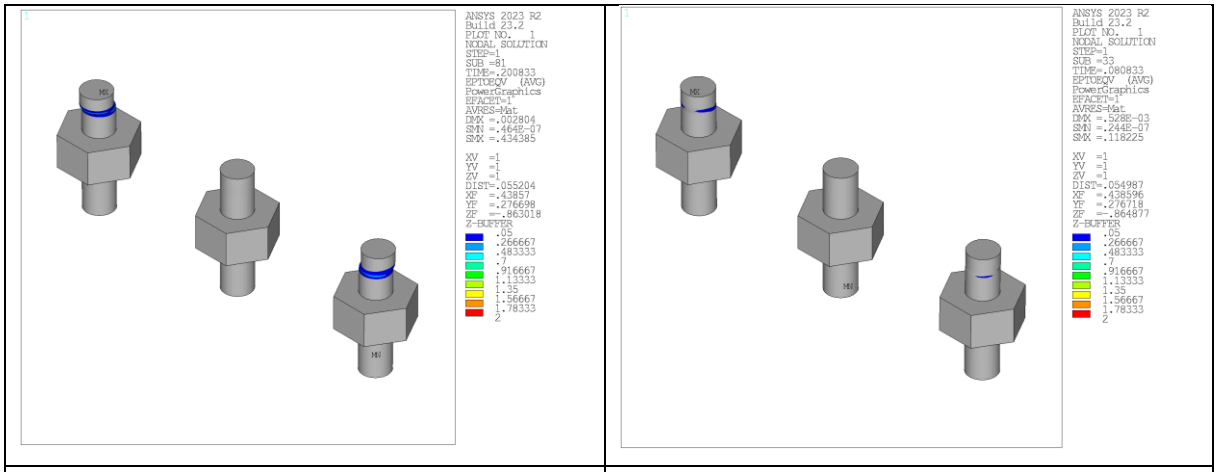

c) U=3Dy⁺ (T=250 kN) | d) U=4.5Dy⁺ (T=375 kN)

Figure 2.86: Von mises total mechanical strain in aluminium bolts of the fusible link configuration n°4 predicted for different values of imposed displacement with the ANSYS model without bolt-hole clearances

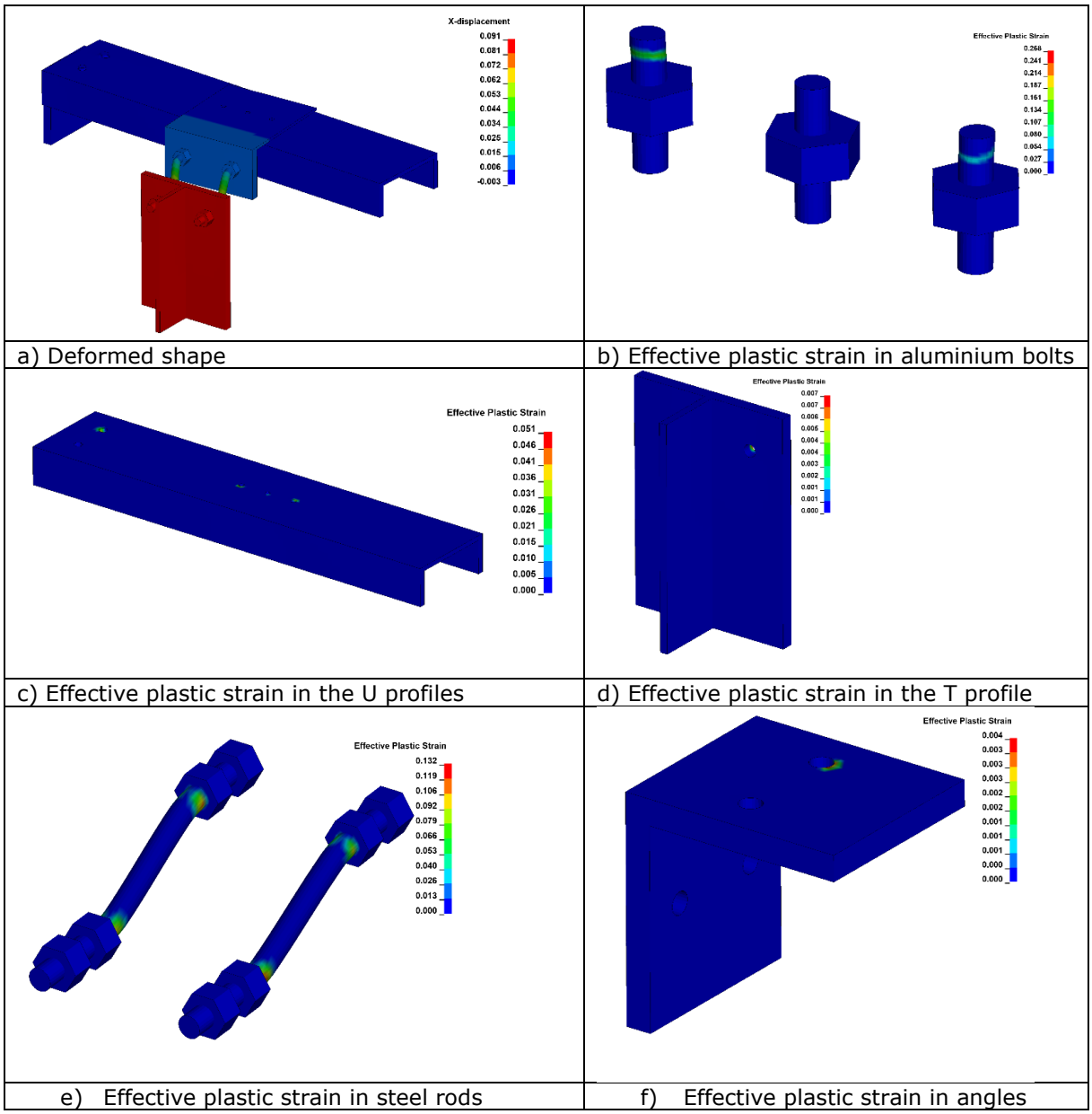

a) Deformed shape | b) Effective plastic strain in aluminium bolts

c) Effective plastic strain in the U profiles | d) Effective plastic strain in the T profile

e) Effective plastic strain in steel rods | f) Effective plastic strain in angles

Figure 2.87: Main results of the modelling under Ls-dyna without bolt-hole clearances at failure time of bolts

2.2.5.2 Monotonic compression loading

Figure 2.88 compares the predicted values in terms of force-displacement to the experimental ones (denoted by "CH3" and "CH6"). Each predicted curve is a resulting plot of the total vertical force calculated by summing the reaction forces of all nodes at the fixed end of the link against the prescribed vertical displacement. The shape of curves is fairly in line with that observed when the specimen is subjected to a tensile force. The experimental force–displacement curves approximately consist of a bilinear stage with many sudden force drops highlighting the progressive failure of aluminium bolts. The predicted force–displacement curves are quite different. For increasing value of imposed displacements, the predicted curves mainly consist of two different stages: a first linear stage at which correspond an initial elastic stiffness and then a stiffness degradation stage highlighting a nonlinear behaviour of the fusible link, until the failure occurs. By neglecting bolt-hole clearances, the yield displacement Dy^- estimated from the numerical curves is 10.6 mm, which corresponds to the first failure of an aluminium bolt. Accounting for bolt-hole clearance leads to a delay in the force increase, which starts when bolts come into bearing within the holes, as well as an increase of the yield displacement Dy^- which can be estimated to 15.8 mm (by including bolts slipping inside holes). On the other hand, the numerical results indicate that bolt-hole clearances have a favourable effect on the failure load value. The models predict the failure of the link by shearing of aluminium bolts, for a force close to 52 kN or 84 kN whether bolt-hole clearances are considered. In comparison, the test failure load was estimated to 52 KN or 72 KN either by considering the force value corresponding to the first failure or the full failure of all aluminium bolts. Thus, the value of the load-bearing capacity predicted without bolt-hole clearances complies well with the load value which led to the first bolt failure observed in experiment. In contrast, the load-bearing capacity predicted by the models with bolt-hole clearances is overestimated. In addition to resistance, there is still a discrepancy in the prediction of the initial stiffness of studied link in comparison to the experimental stiffness, which appears significantly lower than the numerically predicted one. This is believed to be due mainly to clearances and slipping between the steel profiles and all bolting. This could be due also to progressive crushing of the threads of the aluminium bolts, which is not accounted in FE models. Bolt-hole clearances allow some movement in the link and can lead to increased bolt rotation, decreased bolt-hole contact area and then decreased link stiffness. Moreover, the misalignment of bolt and hole, the misalignment of profile or holes of varying sizes can lead to some bolts to remain unstressed at the start of loading, or throughout loading. It can be also underlined the satisfactory agreement between the two models developed under ANSYS and Ls-dyna.

The failure mode of the specimen is recognized by checking the strain level reached in the different components constituting the studied fusible link. Figure 2.91 shows the distribution of the Von mises total mechanical strain predicted in aluminium bolts from the ANSYS model without bolt-hole clearances. The strain distribution is given here for different levels of imposed displacement (so different force levels), by showing strain values exceeding 5% only. It clearly shows a yielding line progressively propagating in the cross-sectional area of bolts, in the two shear planes at the junction between steel profiles linked by the aluminium bolts.

Figure 2.90 shows the distribution of the Von mises total mechanical strain predicted in other components of the link with the ANSYS model, at the simulation end. It can be noted that the strain level exceeds locally the 0.2% yield strain around the holes of aluminium bolts, highlighting that some bearing occurs in steel plates, with limited holes elongation. Steel bolts have only slight deformation while steel rods suffer also important bending.

For information, Figure 2.92 summarises the main results obtained at failure time of bolts from modelling developed under Ls-dyna without bolt-hole clearances. The results are in good agreement with the ones reported for the ANSYS model.

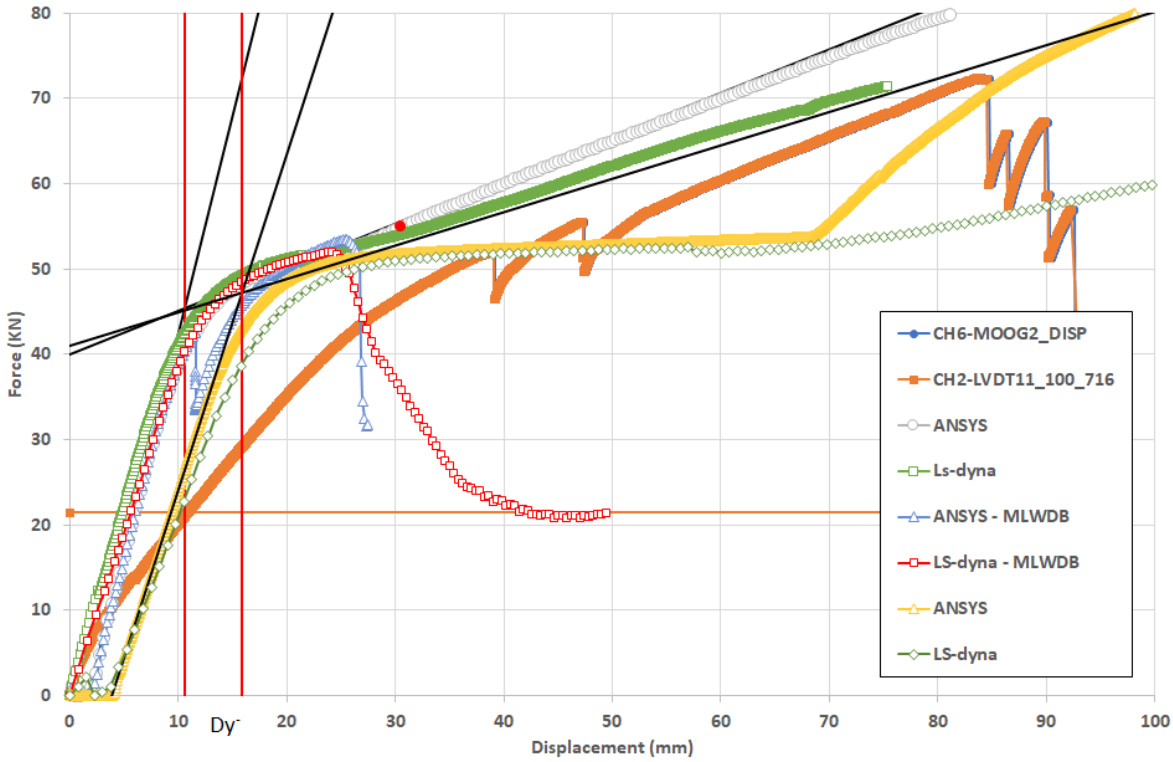

Figure 2.88: Force-displacement curves obtained from FE analyses and experiment for the fusible link configuration n°4 under compression action

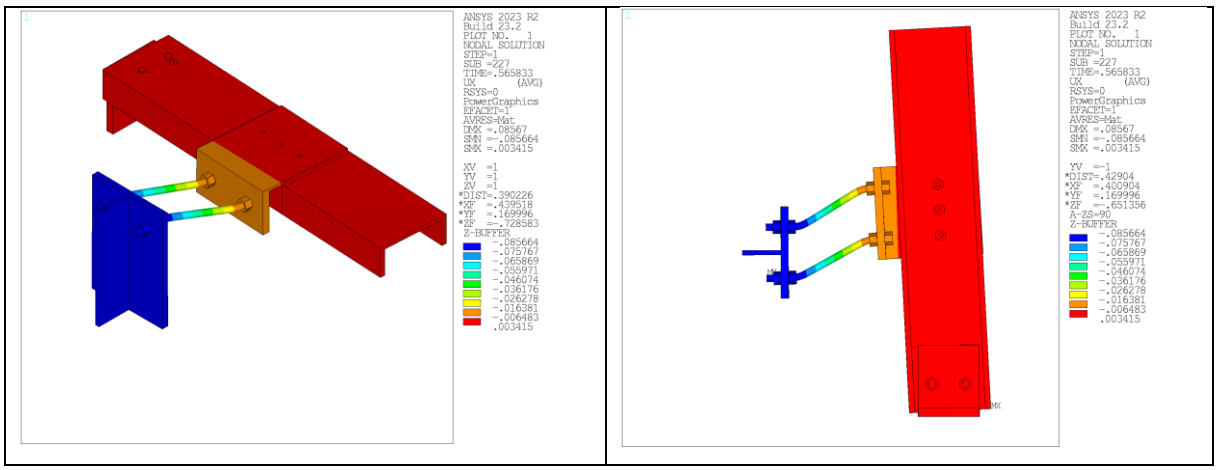

Figure 2.89: Deformed shape of the fusible link configuration n°4 predicted with the ANSYS model without bolt-hole clearances

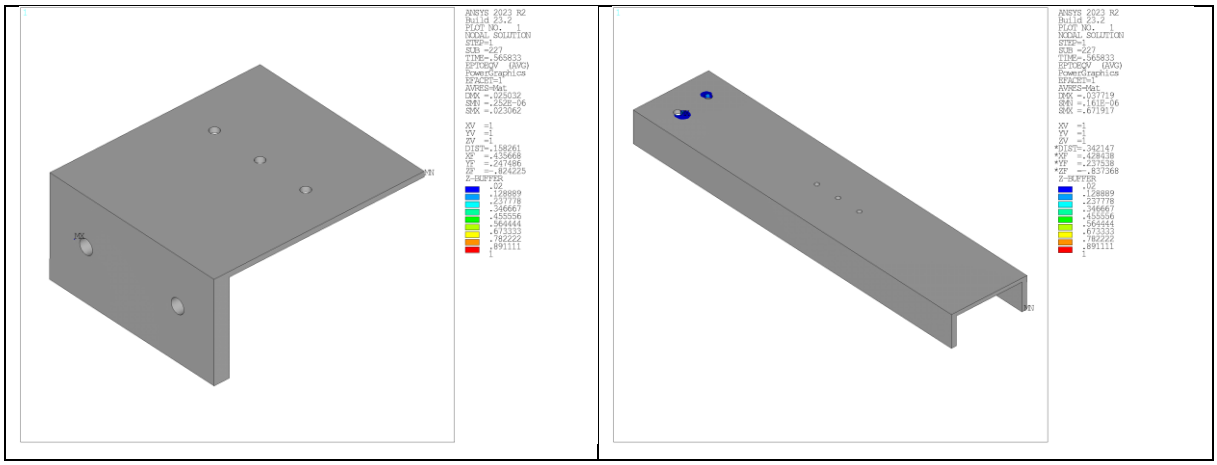

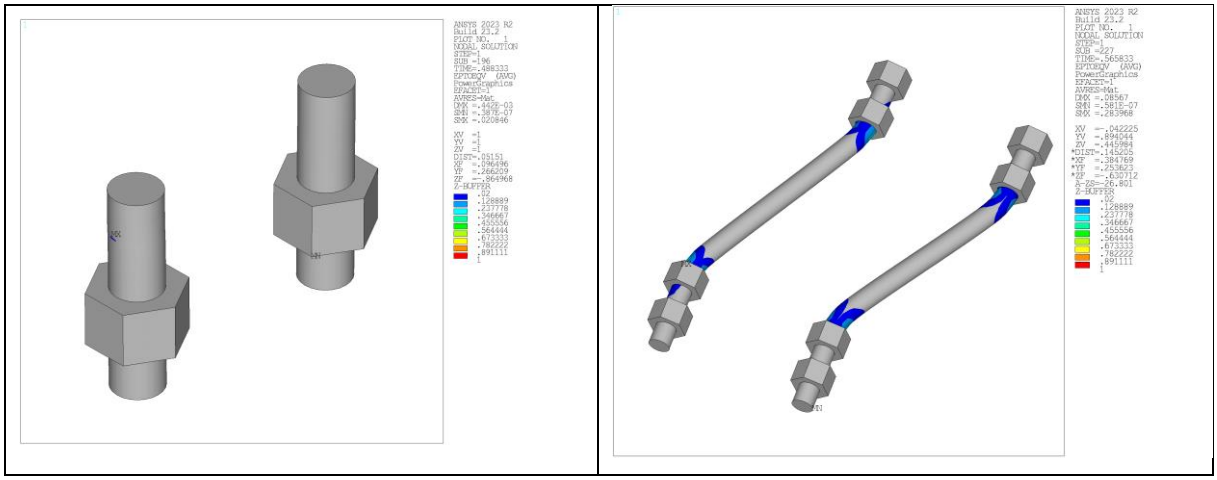

Figure 2.90: Von mises total mechanical strain in components of the fusible link configuration n°4 predicted with the ANSYS model without bolt-hole clearances, at simulation end

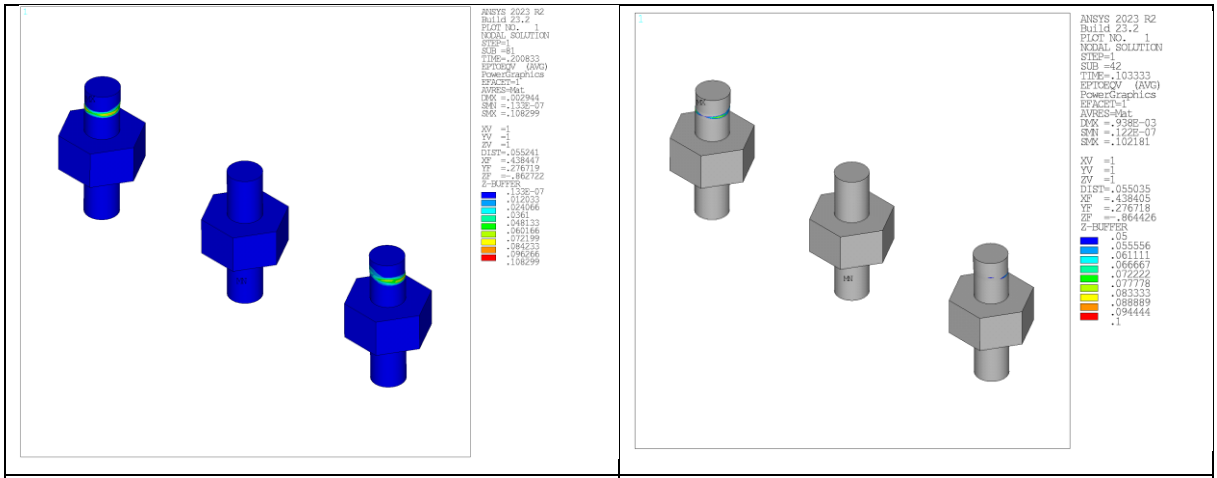

a) U=1.25Dy⁺ (T=126 kN)

b) U=1.4Dy⁺ (T=48 kN)

c) U=2.8Dy⁺ (T=54.7 kN)

d) U=5Dy⁺ (T=66.7 kN)

Figure 2.91: Von mises total mechanical strain in aluminium bolts of the fusible link configuration n°4 predicted for different values of imposed displacement with the ANSYS model without bolt-hole clearances

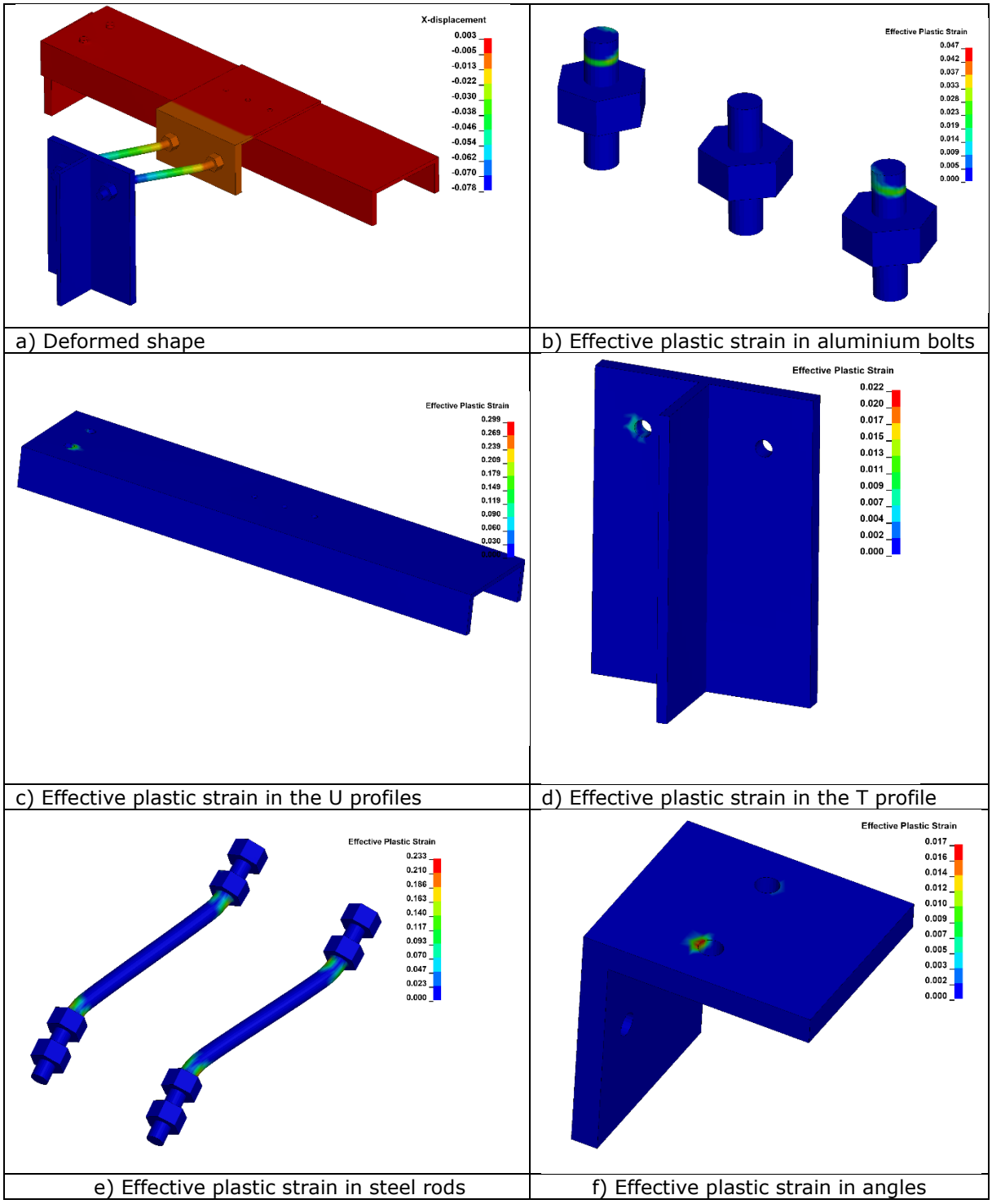

a) Deformed shape | b) Effective plastic strain in aluminium bolts

c) Effective plastic strain in the U profiles | d) Effective plastic strain in the T profile

e) Effective plastic strain in steel rods | f) Effective plastic strain in angles

Figure 2.92: Main results of the modelling under Ls-dyna without bolt-hole clearances at failure time of bolts

2.2.5.3 Cyclic loadings

The vertical displacement-time curve prescribed in numerical analyses is reported in Figure 2.21, while the yield displacements obtained from monotonic analyses are given in Table 2.

Table 6: Yield displacements determined from monotonic analyses of the fusible link detail n°4

	Without bolt-hole clearances	With Both hole clearances
Dy^+	10.5 mm	16.5 mm
Dy^-	10.6 mm	15.8 mm

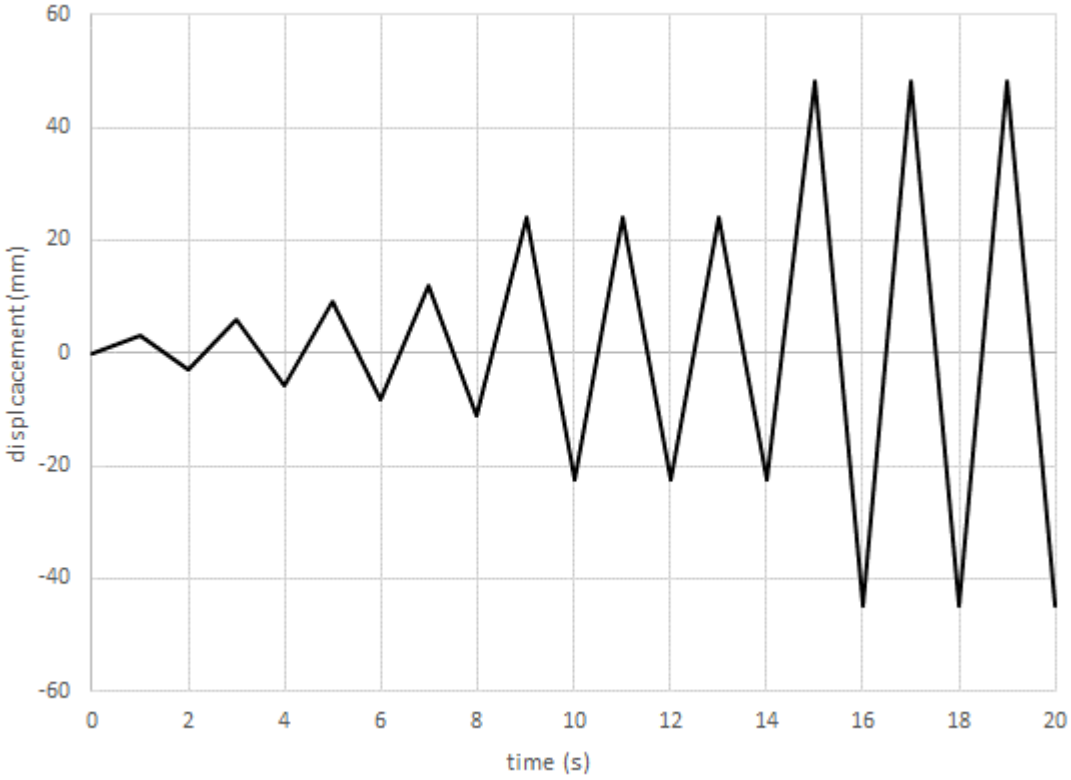

Figure 2.93: Vertical displacement-time curve used in numerical analyses carried out without bolt-hole clearances for the fusible link detail n°4

Figure 2.94 depicts the comparison between the FE predicted hysteresis axial force-displacement responses and the test results. In this figure, the negative values mean that components are under compression, and positive values are for tension. Through the hysteresis curves, it can be noted that numerical models predict that the studied link remains in the elastic stage during a major part of the displacement loading. Indeed, the predicted curves are predominantly linear for non-zero forces, both in tension and compression. Unloading takes place in the same path than loading, or a closer parallel path to that of the initial stiffness of the link until failure. Accounting for bolt-hole clearance in modelling only leads to a delay in the force increase, which starts when bolts come into bearing within the holes. In this case, the force remains small during the first cycles, until the prescribed displacement peaks exceed the maximum value of displacement that bolts can undergo inside holes. It can be also underlined that the predicted force-displacement curves display a similar behaviour in tension and compression, characterized, however, by slightly different initial stiffnesses in accordance with the monotonic analyses. In fact, since no significant plastic deformations occur in steel components, the predicted cyclic response coincides well with the monotonic responses obtained in tension or compression monotonic loading.

The failure modes of the studied fusible link are assessed by monitoring the strain states of different components constituting the link. For example, Figure 2.97 shows the distribution of the Von mises total mechanical strain predicted in some components of the link from the ANSYS model without bolt-hole clearances at the simulation end. It can be noted that the strain level exceeds locally the 0.2% yield strain around the holes of aluminium bolts only, highlighting that some bearing occurs in steel plates, with limited holes elongation. Steel bolts and steel rods undergo only elastic deformations. Figure 2.98 shows the distribution of the Von mises total mechanical strain predicted in aluminium bolts. The strain distribution is given here for different levels of imposed displacement, by showing strain values exceeding 5% only. It clearly shows a yielding line progressively propagating in the cross-sectional area of bolts, in the shear planes at the junction between the steel profiles linked by the aluminium bolts. The failure of the specimen predicted by the models occurs during the reloading at the first cycle to $2Dy^{+}$ due to the shearing of aluminium bolts.

It should be noted that there is a noticeable discrepancy in the cyclic response of the studied link, between the experiment and the FE modelling. Firstly, like monotonic loading cases, there is a difference in the prediction of the initial stiffness of the specimen, as the experimental stiffness is significantly lower than the numerically predicted one. Secondly, on the experimental curves, unloading and reloading take place from the first cycle along a different path to that of the first loading stage. The unloading path includes two parts, an elastic unloading phase along a path that

seems parallel to the loading path followed in the force-displacement curves predicted by models and a pinched unloading phase until the loading in the opposite direction happens. When unloaded to a 0 kN force, there is a larger non-zero residual displacement than numerically predicted, which increases progressively with the repeated unloading-reloading cycles even if the link is still in an elastic state, which is probably due to the bolt travels within holes. Like experiment, it can be noted that the predicted load-bearing capacity of the link under cyclic loading is of the same order of magnitude than the ones obtained from monotonic analyses. The load-bearing capacity predicted from the models is close to the ones recorded during the tests, namely 55 KN against 57 and 50 kN by considering the force values corresponding to the first failure of some aluminium bolts, or against 58.8 and 60 KN if we consider the forces corresponding to the failure of all aluminium bolts.

The dissimilarities between the experimental and FE results are mainly attributed to clearances and slipping between the steel profiles and all bolting. Bolt-hole clearances allow some movement in the link and can lead to increased bolt rotation, decreased bolt-hole contact area and then decreased link stiffness. Moreover, the misalignment of bolt and hole, the misalignment of profile or holes of varying sizes can lead to some bolts to remain unstressed at the start of loading, or throughout loading. All these phenomena are difficult to be considered accurately in models. This could also be due to phenomena which are not accounted in FE models, like possible slipping between the screw and nut thread or progressive crushing of the bearing flank of the thread (that supports shearing forces) of aluminium bolts with the bearing stresses.

It should be underlined that the cyclic loading does not affect greatly the load-bearing capacity predicted for the studied fusible link. Indeed, the difference between the monotonic and cyclic maximum resistance does not exceed 5 %.

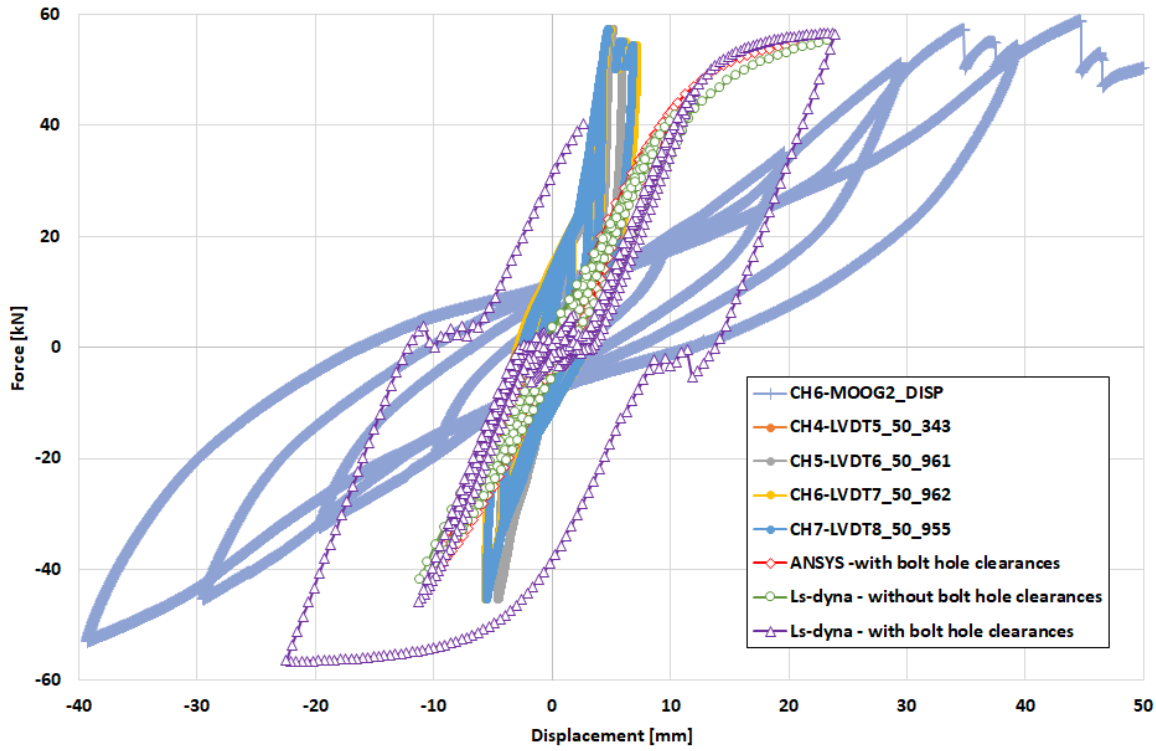

Figure 2.94: Force-displacement curves obtained from FE analyses and experiment (cyclic test n°1) for the fusible link configuration n°4 under cyclic action

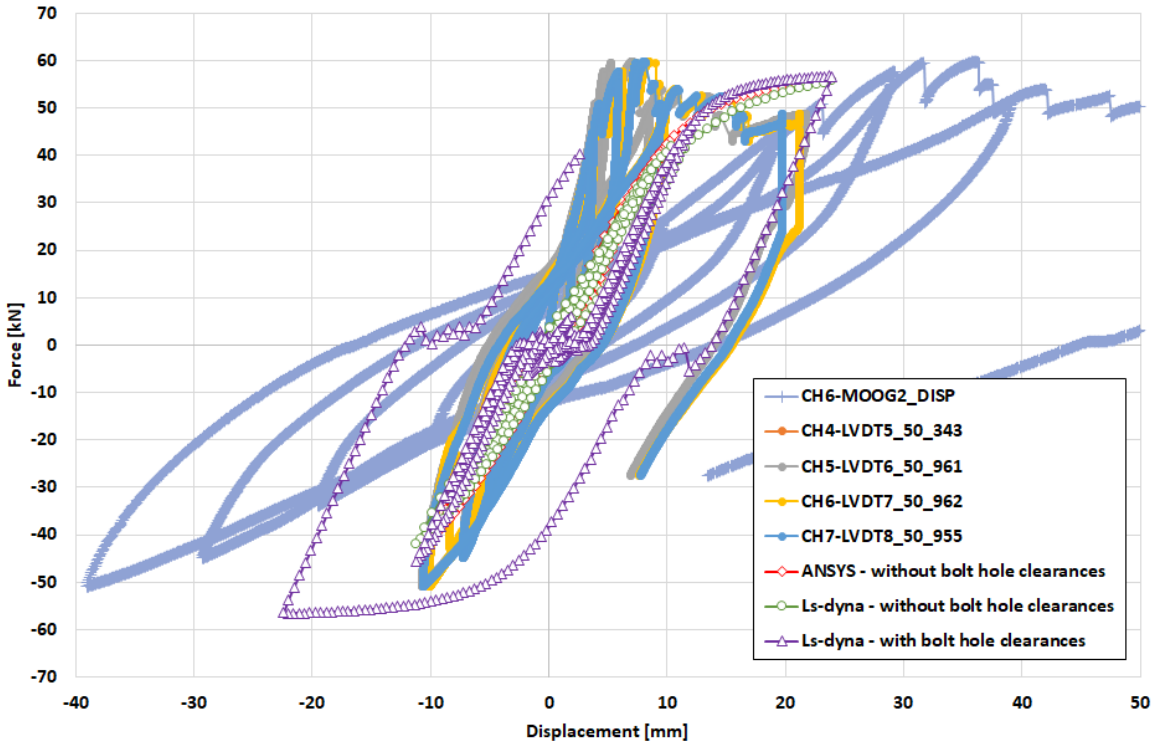

Figure 2.95: Force-displacement curves obtained from FE analyses and experiment (cyclic test n°2) for the fusible link configuration n°4 under cyclic action

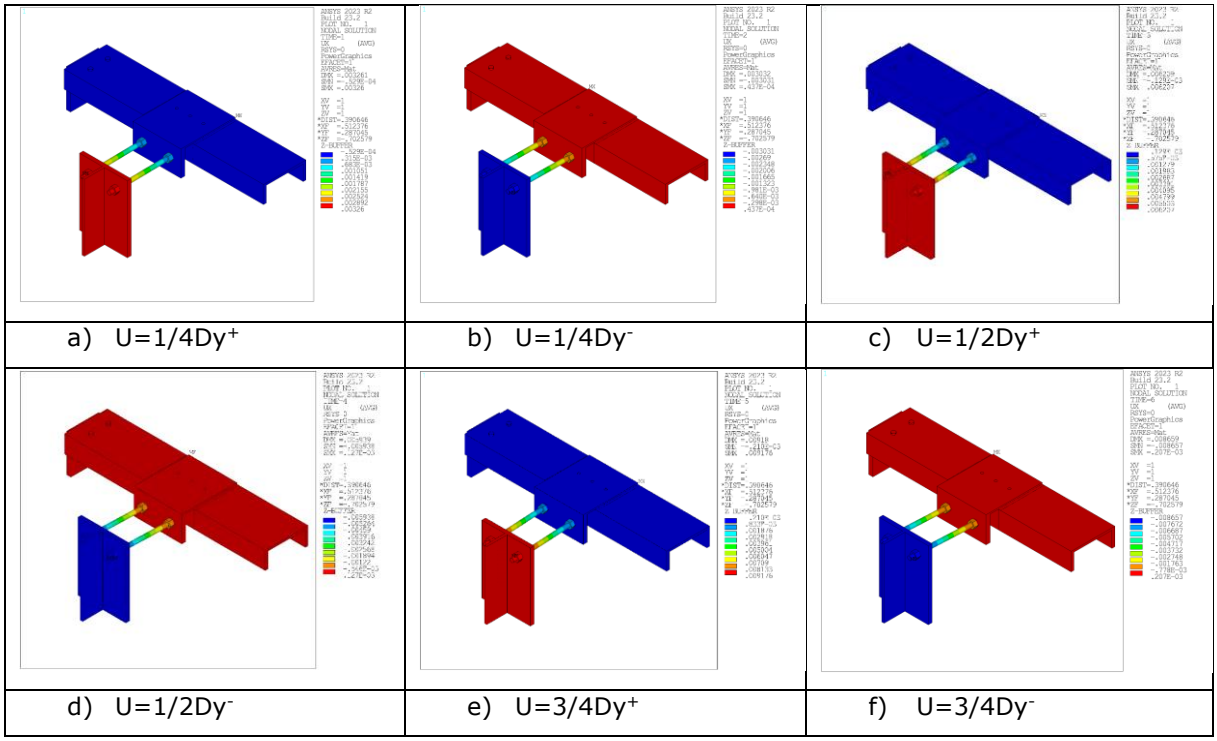

a) U=1/4Dy^{+} b) U=1/4Dy^{-} c) U=1/2Dy^{+}

d) U=1/2Dy^{-} e) U=3/4Dy^{+} f) U=3/4Dy^{-}

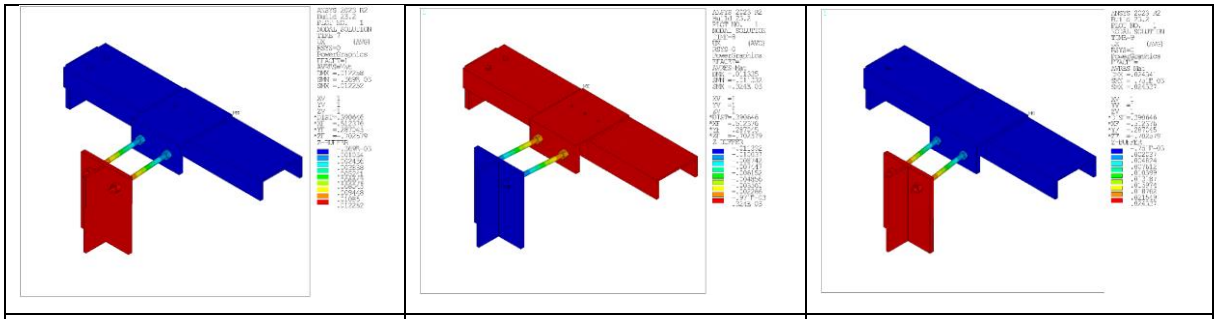

g) $U=Dy^+$	h) $U=Dy^-$	i) $U=2Dy^+$

Figure 2.96: Deformed shape of the fusible link configuration n°4 according to imposed displacement values predicted with the ANSYS model without bolt-hole clearances

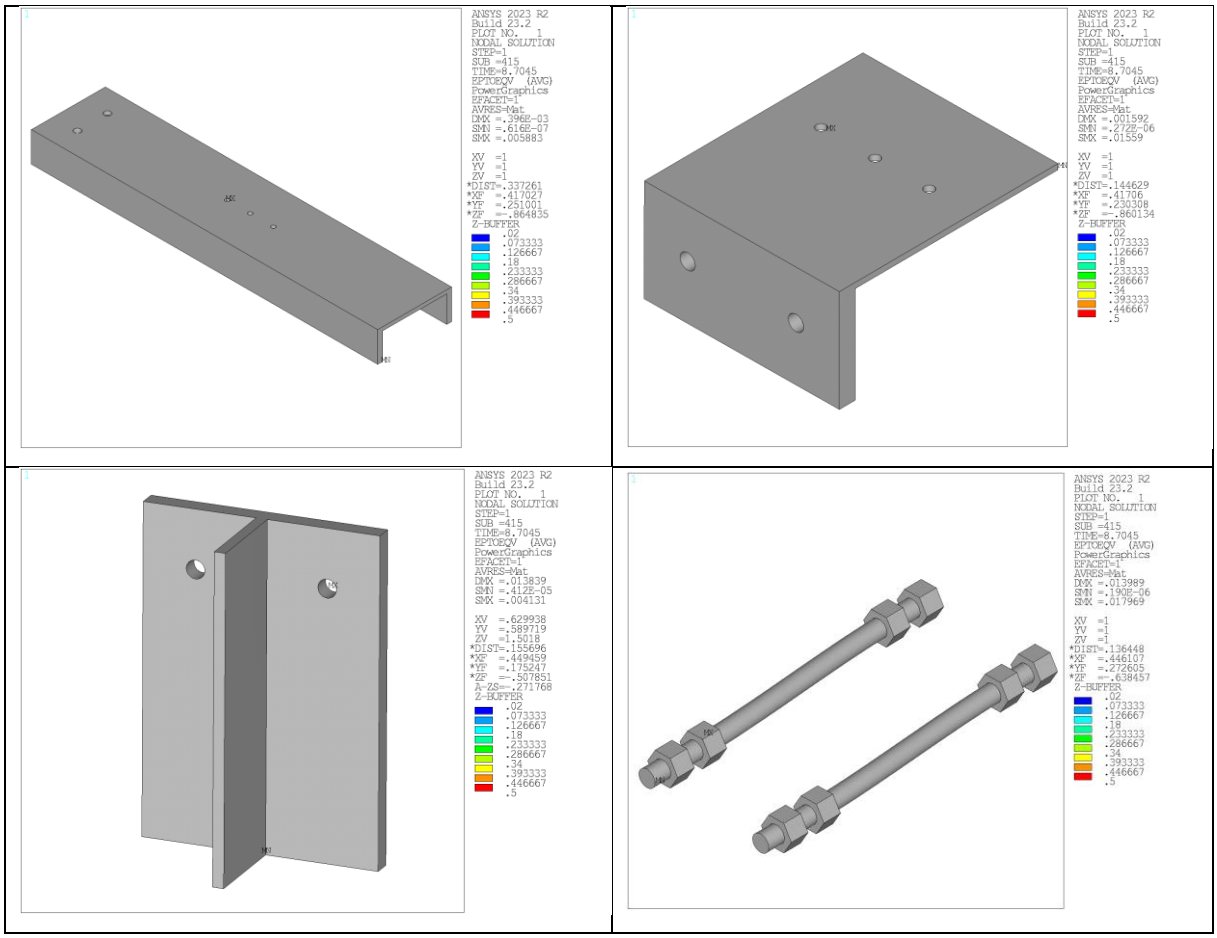

Figure 2.97: Von mises total mechanical strain in components of the fusible link configuration n°4 predicted with the ANSYS model without bolt-hole clearances, at simulation end

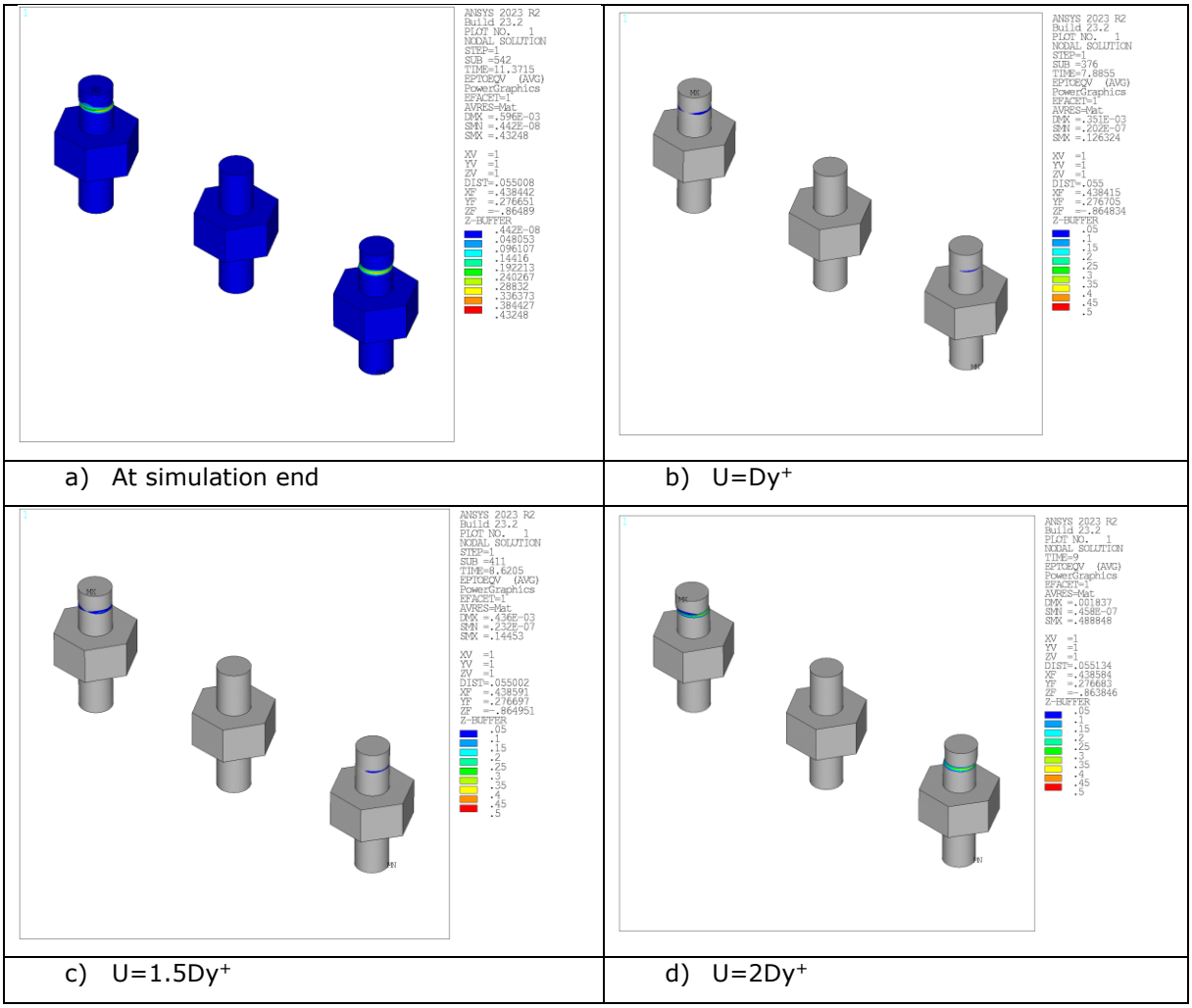

a) At simulation end

b) U=Dy⁺

c) U=1.5Dy⁺

d) U=2Dy⁺

Figure 2.98: Von mises total mechanical strain in aluminium bolts of the fusible link configuration n°4 predicted for different values of imposed displacement with the ANSYS model without bolt-hole clearances

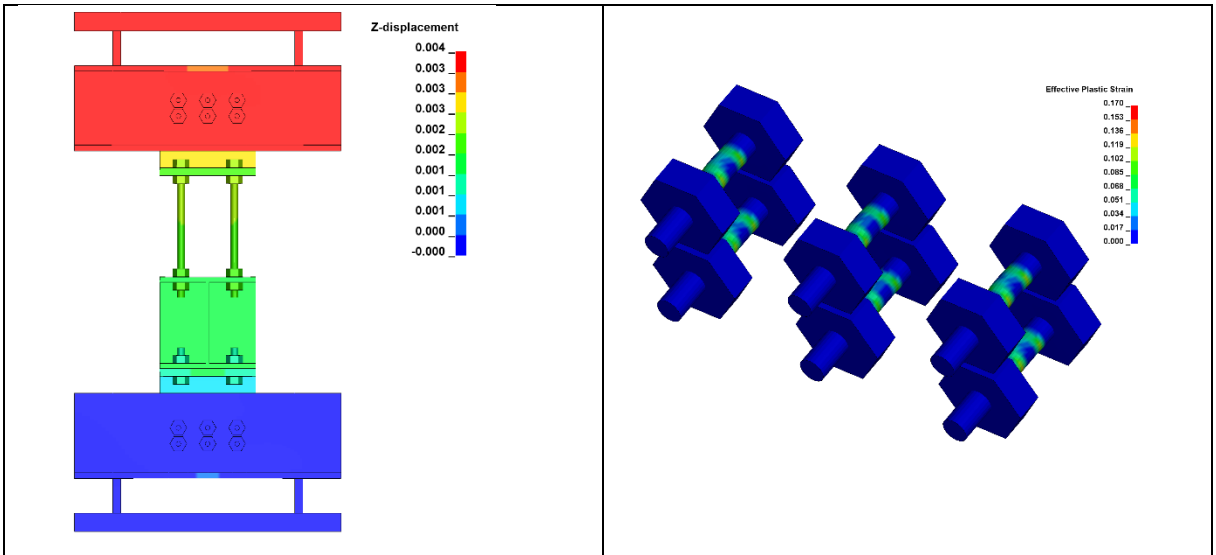

a) Deformed shape

b) Effective plastic strain in aluminium bolts

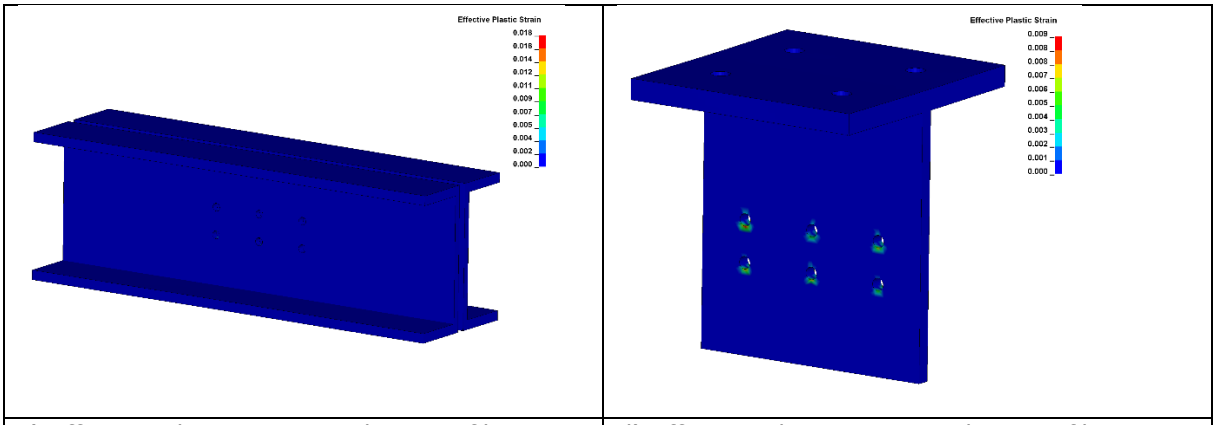

c) Effective plastic strain in the U profiles	d) Effective plastic strain in the T profile

Figure 2.99: Main results of the modelling under Ls-dyna without bolt-hole clearances at failure time of aluminium bolts

a) Cyclic test n°1	b) Cyclic test n°2

Figure 2.100: Photos of aluminium bolts after the cyclic tests

2.2.6 Fusible link configuration n°5

For the detail 5, numerical analyses were performed with or without bolt-hole clearances.

2.2.6.1 Monotonic tension loading

Figure 2.101 compares the predicted values in terms of force-displacement to the experimental ones (denoted by "CH2" and "CH4"). Each predicted curve is a resulting plot of the total vertical force calculated by summing the reaction forces of all nodes at the fixed end of the models against the prescribed vertical displacement. Through the figure, it can be noted that the experimental force–displacement curves consist of several linear parts, with different slopes, followed by a brittle failure stage evidenced by sudden drops in force. The predicted force–displacement curves are quite different. By neglecting bolt-hole clearances, the predicted curves mainly consist of a first linear stage followed by either a stiffness degradation stage highlighting a nonlinear behaviour of the fusible link, or a brittle failure stage symbolised by sudden drops, depending on how the bolt failure is considered in the modelling. In this case, the yield displacement Dy^+ obtained from the numerical curves is equal to 1.5mm approximately, which corresponds to the first failure of an aluminium bolt. Accounting for bolt-hole clearance leads to a delay in the force increase, which starts when bolts come into bearing within the holes, as well as an increase of the yield displacement Dy+, which can be estimated to 5.9mm (by including bolts slipping inside holes). On the other hand, the numerical results indicate here that bolt-hole clearances have a favourable effect on the failure load value. The models predict the failure of the link by shearing of aluminium bolts, for a force approaching 115 kN or 185 kN whether bolt-hole clearances are considered or not. Thus, the load-bearing capacity predicted by the models is either underestimated or overestimated in comparison to the one observed during the test, estimated to 147.6 KN or 155 KN either by considering the force value corresponding to the first failure or the full failure of all aluminium bolts (which corresponds to an error higher than 18% between the predicted and measured values). Lastly, it is worth noting that the final part of the experimental curves is not captured accurately where the bolts fracture is not considered, since it

leads to over-estimate the deformations that the specimens can really reach, and hence the specimen ductility. On the other hand, two sharply force decreases can been observed, highlighting the progressive failure of aluminium bolts, if the fracture of bolts is considered in modelling by adding a descending branch in the bolt material law (curve denoted “MLWDB” in Figure 2.101).

In terms of stiffness in relation to the force-displacement response of the tested detail, it should be noted that the predicted and experimental stiffness values differ significantly, except at the initial loading stage (near to zero force). The stiffness predicted by the models is significantly higher than that observed experimentally when compared to the 'CH6' displacement curve derived from the displacement transducer associated with the loading device.

It can be also noted that the predicted curves coincide quite well with each other, highlighting the satisfactory agreement between the two models developed, even if some discrepancies can be noted which are mainly attributed to the different contact types used in the ANSYS and Ls-dyna models.

As with other links, the dissimilarities between the experimental and FE results are mainly attributed to clearances and slipping between the steel profiles and all bolting, which are difficult to accurately simulate. Bolt-hole clearances allow some movement in the link and can lead to increased bolt rotation, decreased bolt-hole contact area and then decreased link stiffness. Moreover, the misalignment of bolt and hole, the misalignment of profile or holes of varying sizes can lead to some bolts to remain unstressed at the start of loading, or throughout loading. This could also be due to phenomena which are not accounted in FE models, like possible slipping between the screw and nut thread or progressive crushing of the bearing flank of the thread (that supports shearing forces) of aluminium bolts. It should be noted that some predicted curves may be non-smooth in certain loading stages. As in the previous case, the rough shape observed in the numerical curves is attributed to dynamic effects (due to the speed of load application and the resulting inertia forces), which can cause oscillations at the contact surfaces and interpenetration issues.

The failure modes of the studied link can be recognized by checking/analysing the strain level reached in the different components constituting the studied fusible link. For illustrative purpose, Figure 2.104 shows the distribution of the Von mises total mechanical strain predicted in aluminium bolts from the ANSYS model without bolt-hole clearances. The strain distribution is given here for different levels of imposed displacement (so different force levels), by showing strain values exceeding 5% only. Similar results are presented in Figure 2.106 for the modelling considering hole bolt clearances. The figures clearly show a yielding line progressively propagating in the cross-sectional area of bolts, in the shear plane at the junction between the U and Z shaped steel profiles. Figure 2.103 displays the distribution of the Von mises total mechanical strain predicted in other components of the link with the ANSYS model without bolt-hole clearances, at the simulation end. Strain values exceeding 2% in steel members and 5% in steel bolts are highlighted. It can be noted that the strain level exceeds locally the 0.2% yield strain around the holes of aluminium bolts only, highlighting that some bearing occurs in steel plates, with limited holes elongation. Steel bolts have only slight deformation, and no damage occurred in numerical analyses.

For information, Figure 2.105 summarises the main results obtained at failure time of bolts from modelling developed under Ls-dyna without bolt-hole clearances. The results are in good agreement with the ones reported for the ANSYS model.

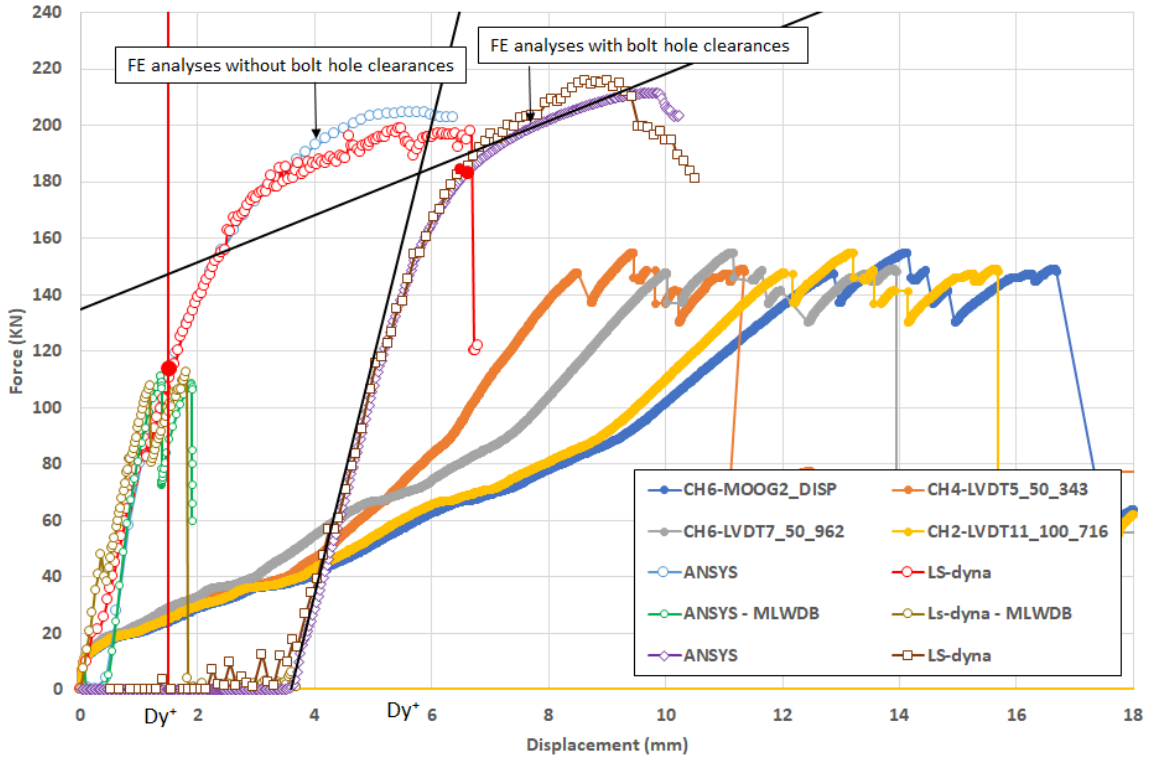

Figure 2.101: Force-displacement curves obtained from FE analyses and experiment for the fusible link configuration n°5 under tensile action

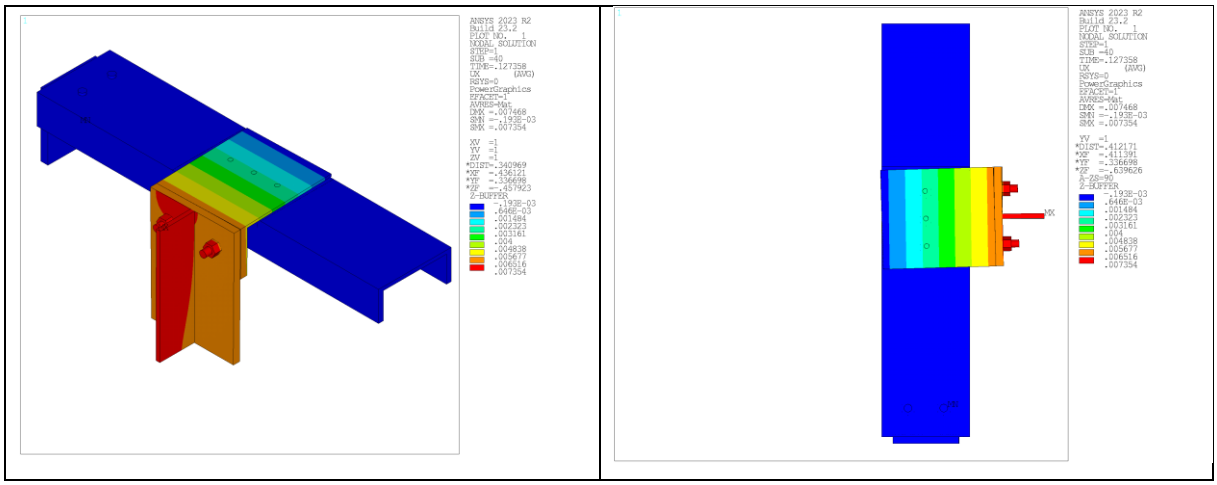

Figure 2.102: Deformed shape of the fusible link configuration n°5 predicted with the ANSYS model without bolt-hole clearances

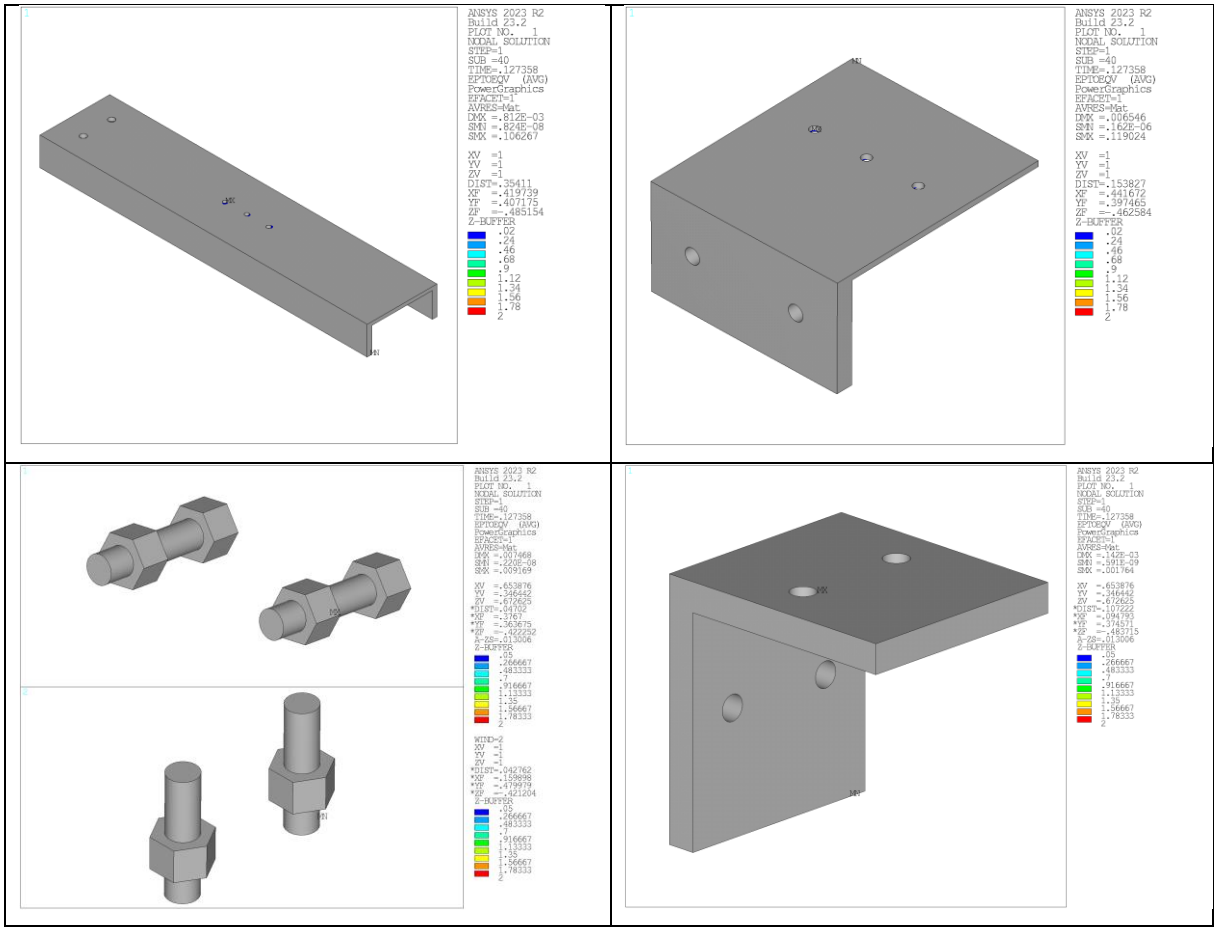

Figure 2.103: Von mises total mechanical strain in components of the fusible link configuration n°5 predicted with the ANSYS model without bolt-hole clearances, at simulation end

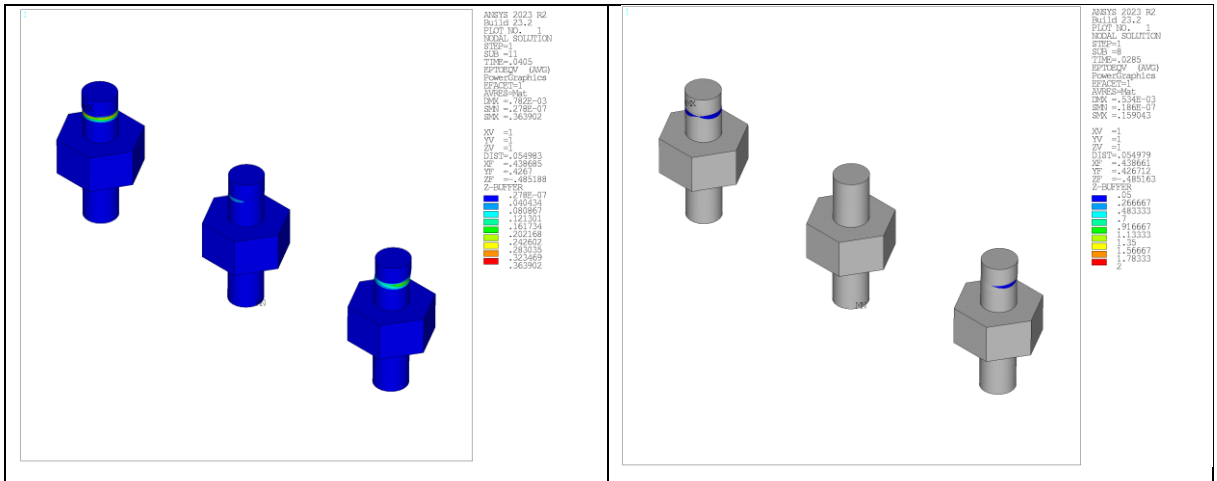

a) U=Dy⁺ (T=113 kN)

b) U=0.95Dy⁺ (T=105 kN)

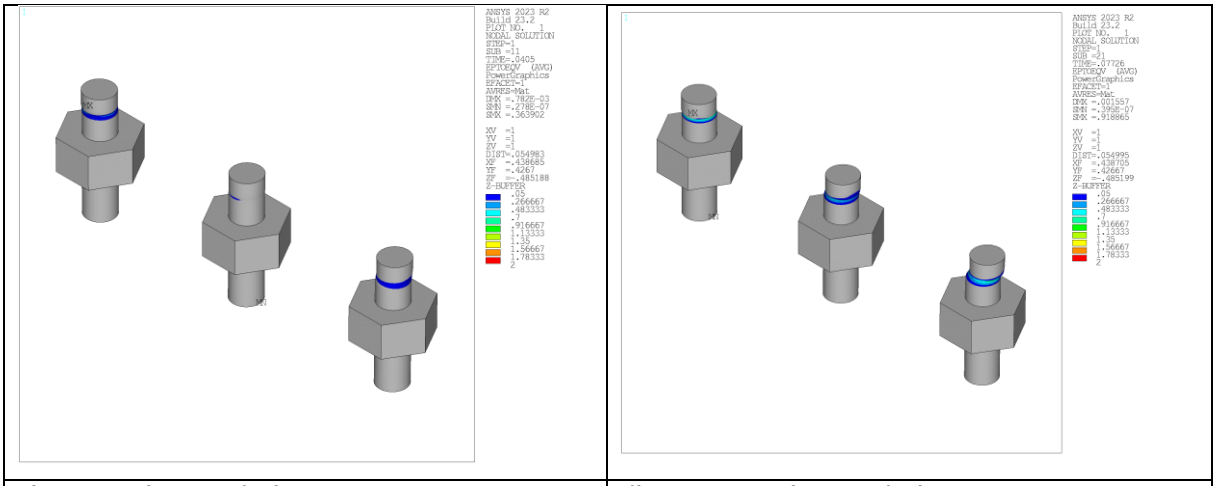

c) U=Dy⁺ (T=113 kN) | d) U=2.5Dy⁺ (T=190 kN)

Figure 2.104: Von mises total mechanical strain in aluminium bolts of the fusible link configuration n°5 predicted for different values of imposed displacement with the ANSYS model without bolt-hole clearances

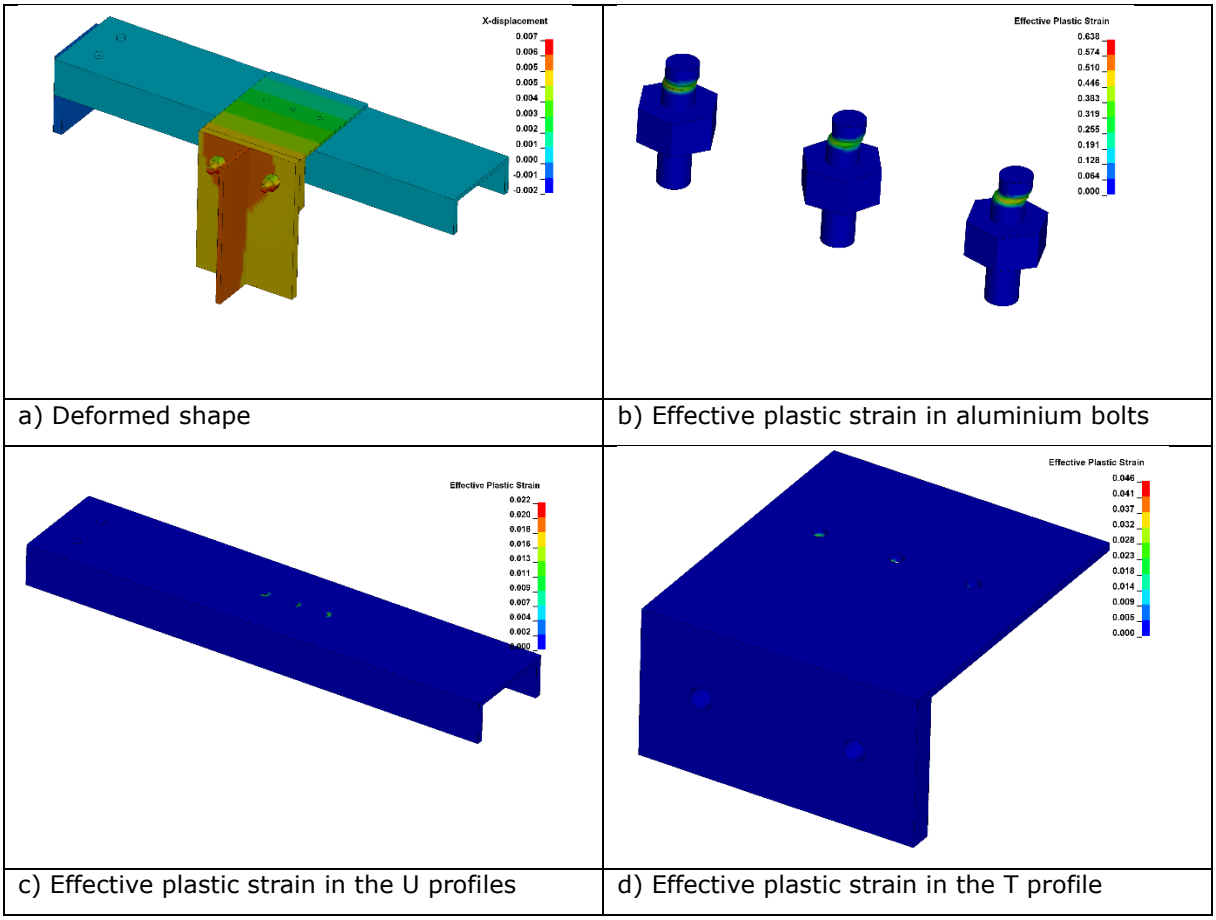

a) Deformed shape | b) Effective plastic strain in aluminium bolts

c) Effective plastic strain in the U profiles | d) Effective plastic strain in the T profile

Figure 2.105: Main results of the modelling under Ls-dyna without bolt-hole clearances at failure time of bolts

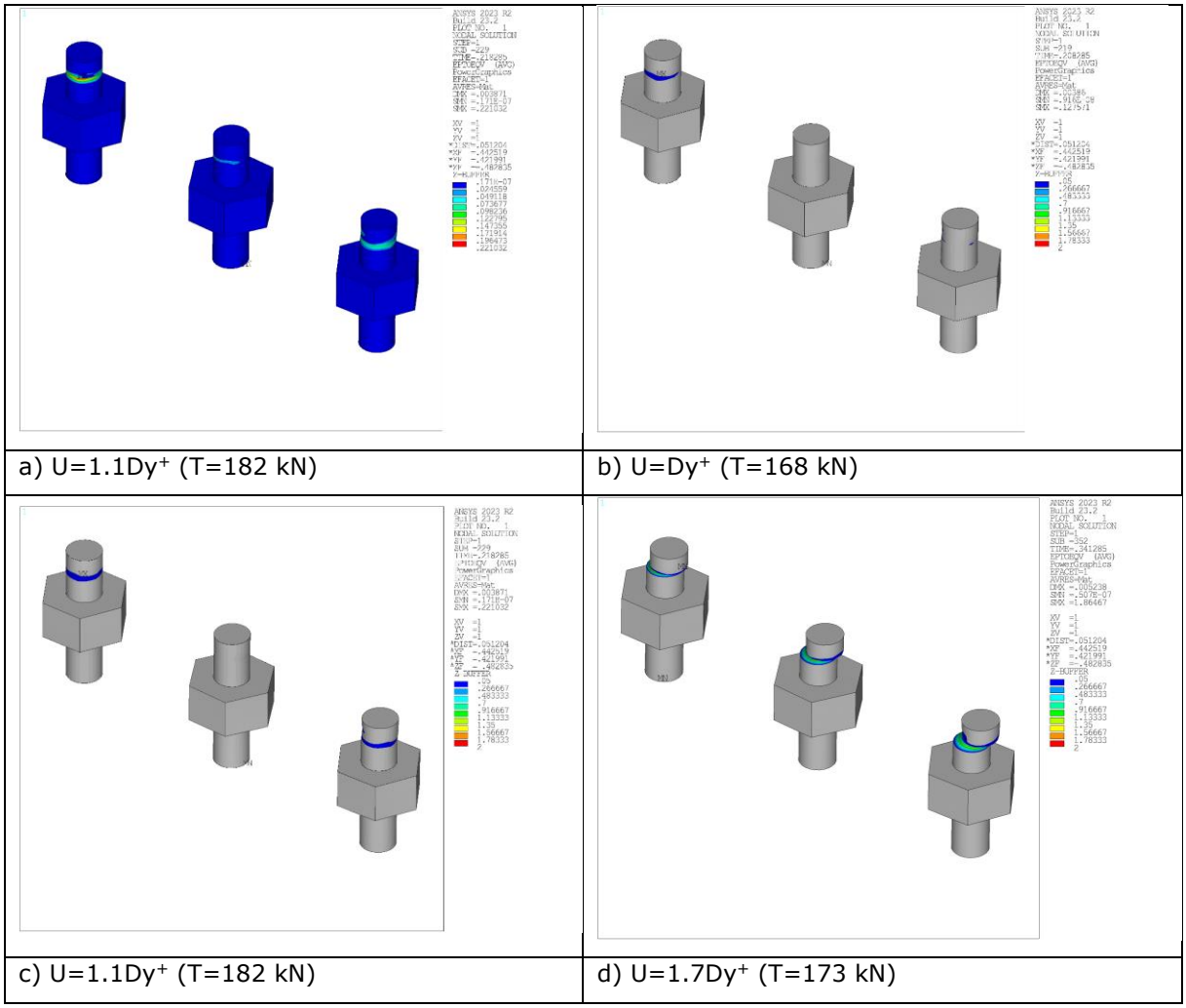

a) U=1.1Dy⁺ (T=182 kN)

b) U=Dy⁺ (T=168 kN)

c) U=1.1Dy⁺ (T=182 kN)

d) U=1.7Dy⁺ (T=173 kN)

Figure 2.106: Von mises total mechanical strain in aluminium bolts of the fusible link configuration n°5 predicted for different values of imposed displacement with the ANSYS model with bolt-hole clearances

2.2.6.2 Monotonic compression loading

Figure 2.107 compares the predicted values in terms of force-displacement to the experimental ones (denoted by "CH2" and "CH4"). Each predicted curve is a resulting plot of the total vertical force calculated by summing the reaction forces of all nodes at the fixed end of the link against the prescribed vertical displacement. The shape of all curves is close to that observed when the studied link is subjected to a tensile force. So, the same comments can be made about the comparison between experiment and the numerical results. As expected, the models predict the failure of the test specimen by shearing of aluminium bolts. However, the load-bearing capacity predicted by the models is more or less underestimated in comparison to the one observed during the test. The predicted resistance ranges from 120 KN to 175 kN whether bolt-hole clearances are considered in modelling or not, while the experimental one is 186 KN approximately. The yield displacements Dy^+ estimated from the numerical curves are 1.4 mm and 5.8 mm respectively. In contrast to experiment, it can be noted that the models predict that the load-bearing capacity of the specimen is similar under compression and tension, with successive bolt failures occurring for similar load levels. In addition to resistance, there is still a discrepancy in the prediction of the initial stiffness of the studied link in comparison to the experimental stiffness, which appears significantly lower than the numerically predicted one. It can be also underlined that the force-displacement response observed experimentally for the tested detail differs significantly between traction and compression tests (in terms of stiffness), whereas the numerical response is similar for both (as expected). It should also be notedthe satisfactory agreement between the two models developed under ANSYS and Ls-dyna.

The dissimilarities between the experimental and FE results are mainly attributed to clearances and slipping between the steel profiles and all bolting. Bolt-hole clearances allow some movement in the link and can lead to increased bolt rotation, decreased bolt-hole contact area and then decreased link stiffness. Moreover, the misalignment of bolt and hole, the misalignment of profile or holes of varying sizes can lead to some bolts may remain unstressed at the start of loading, or throughout loading. This could also be due to phenomena which are not accounted in FE models, like possible slipping between the screw and nut thread or progressive crushing of the bearing flank of the thread (that supports shearing forces) of aluminium bolts. It should be noted that some predicted curves may be non-smooth in certain loading stages. As in the previous case, the rough shape observed in the numerical curves is attributed to dynamic effects (due to the speed of load application and the resulting inertia forces), which can cause oscillations at the contact surfaces and interpenetration issues.

The failure mode of the specimen is recognized by checking the strain level reached in the different components constituting the studied fusible link. For illustrative purpose, Figure 2.110 shows the distribution of the Von mises total mechanical strain predicted in aluminium bolts from the ANSYS model without bolt-hole clearances. The strain distribution is given here for different levels of imposed displacement (so different force levels), by showing strain values exceeding 5% only. Similar results are presented in Figure 2.112 for the modelling considering hole bolt clearances. The figures clearly show a yielding line progressively propagating in the cross-sectional area of bolts, in the two shear planes at the junction between steel profiles linked by the aluminium bolts. Figure 2.109 shows the distribution of the Von mises total mechanical strain predicted in other components of the link with the ANSYS model without bolt-hole clearances, at the simulation end. Strain values exceeding 2% in steel members and 5% in steel bolts are highlighted. It can be noted that the strain level exceeds locally the 0.2% yield strain around the holes of aluminium bolts, highlighting that some bearing occurs in steel plates, with limited holes elongation. Steel bolts and steel rods have only slight deformation, and don't suffer any damage in numerical analyses.

For information, Figure 2.111 summarises the main results obtained at failure time of bolts from modelling developed under Ls-dyna without bolt-hole clearances. The results are in good agreement with the ones reported for the ANSYS model.

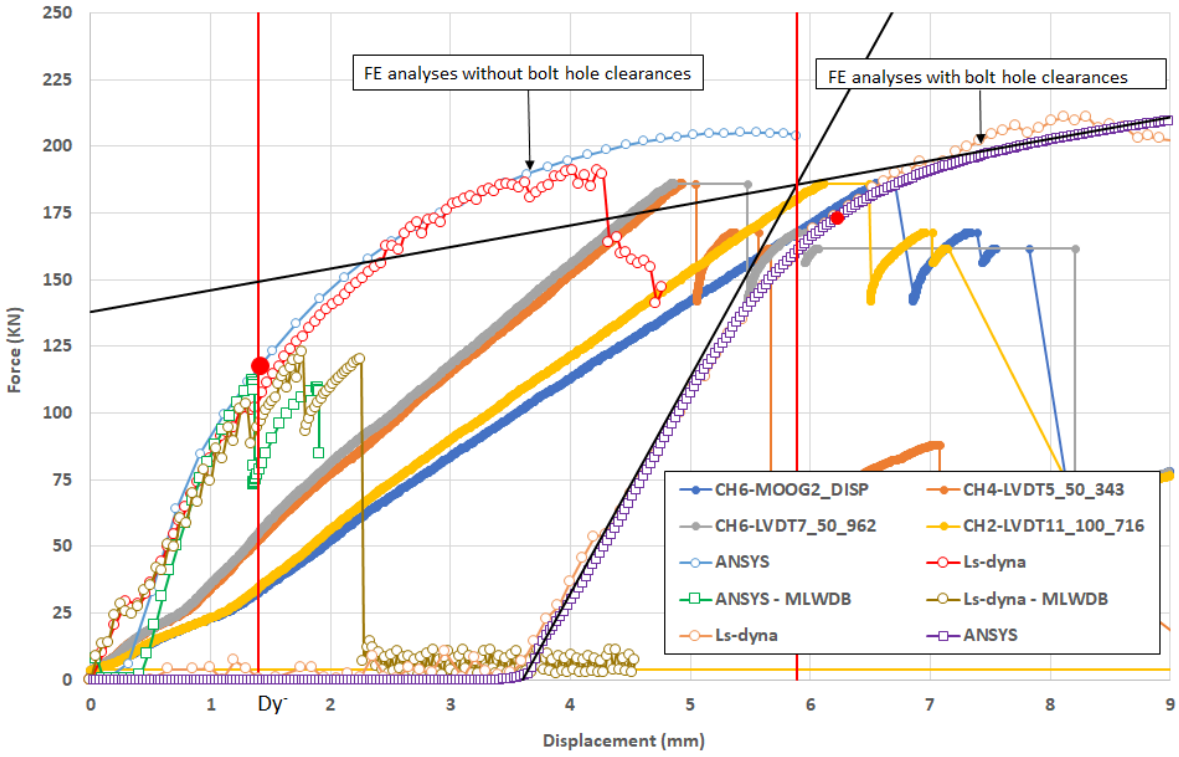

Figure 2.107: Force-displacement curves obtained from FE analyses and experiment for the fusible link configuration n°5 under compression action

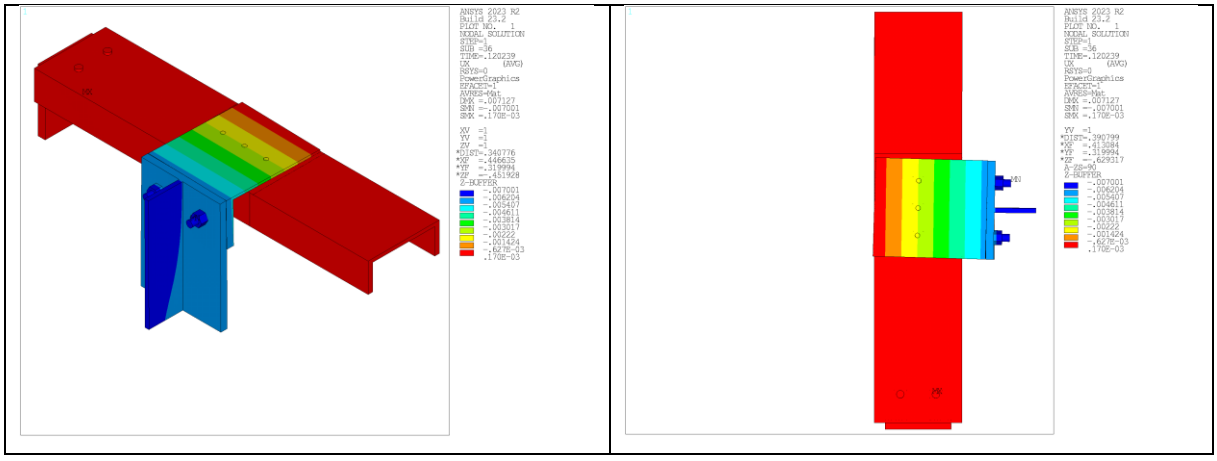

Figure 2.108: Deformed shape of the fusible link configuration n°5 predicted with the ANSYS model without bolt-hole clearances

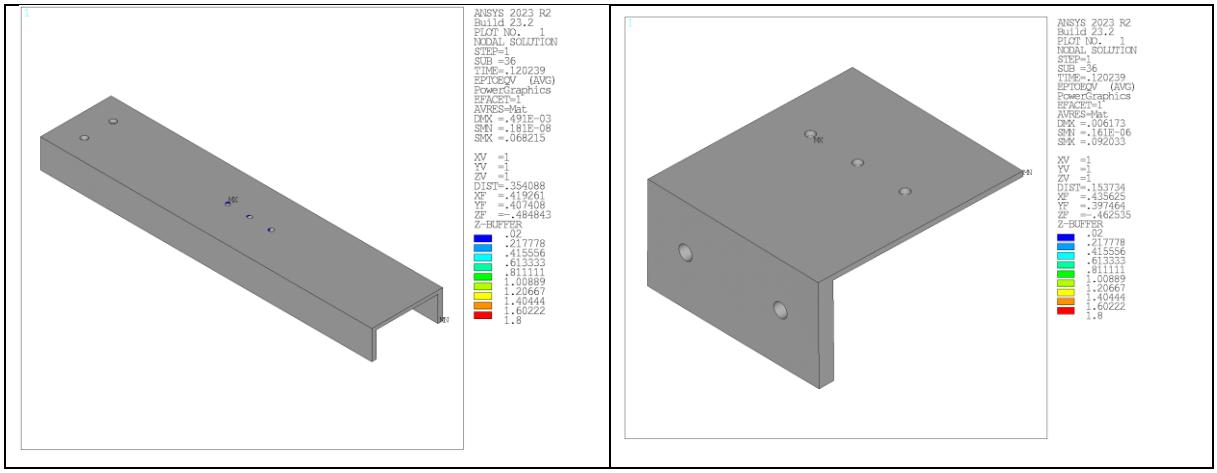

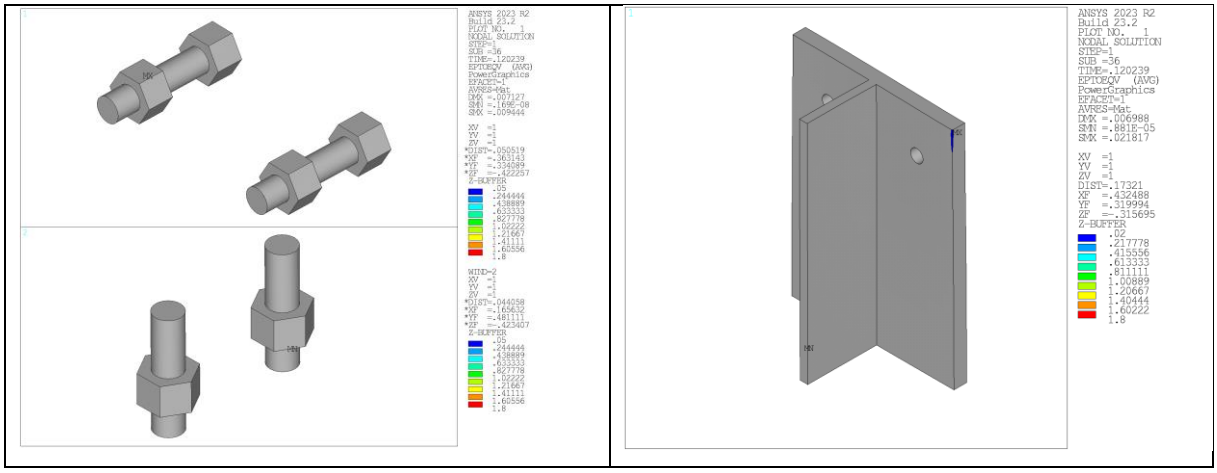

Figure 2.109: Von mises total mechanical strain in components of the fusible link configuration n°5 predicted with the ANSYS model without bolt-hole clearances, at simulation end

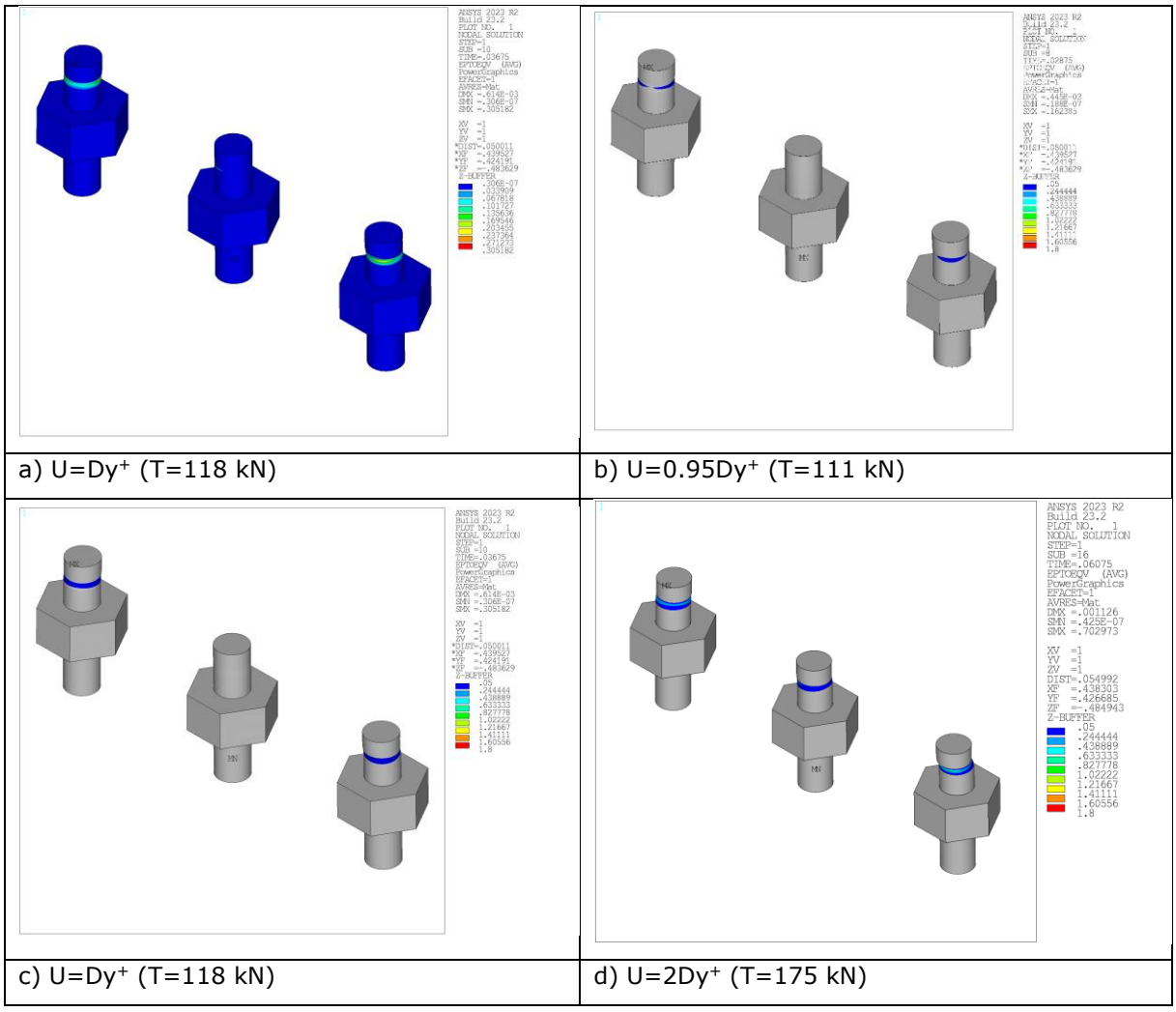

a) U=Dy⁺ (T=118 kN)

b) U=0.95Dy⁺ (T=111 kN)

c) U=Dy⁺ (T=118 kN)

d) U=2Dy⁺ (T=175 kN)

Figure 2.110: Von mises total mechanical strain in aluminium bolts of the fusible link configuration n°5 predicted for different values of imposed displacement with the ANSYS model without bolt-hole clearances

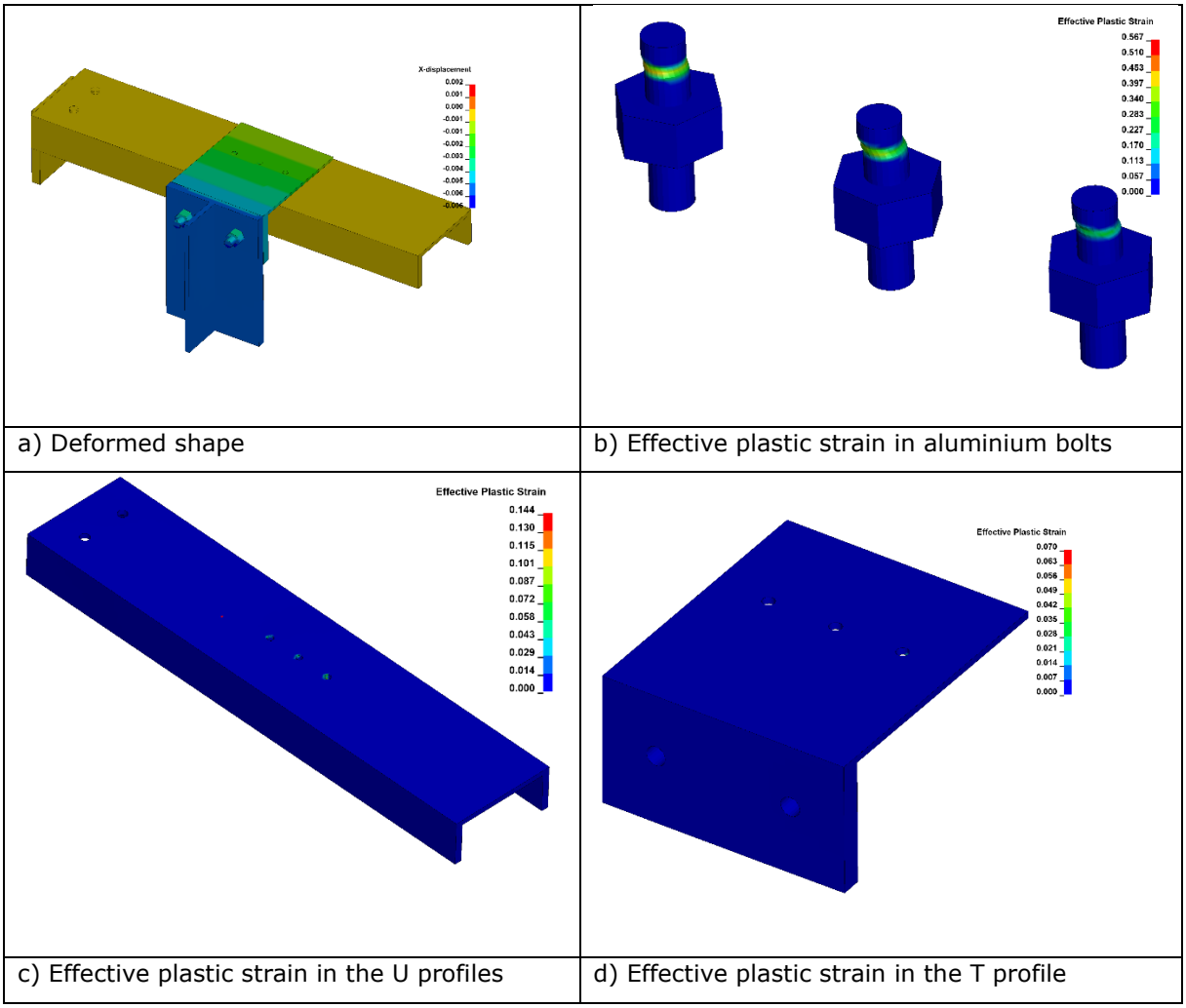

a) Deformed shape

b) Effective plastic strain in aluminium bolts

c) Effective plastic strain in the U profiles

d) Effective plastic strain in the T profile

Figure 2.111: Main results of the modelling under Ls-dyna without bolt-hole clearances at failure time of bolts

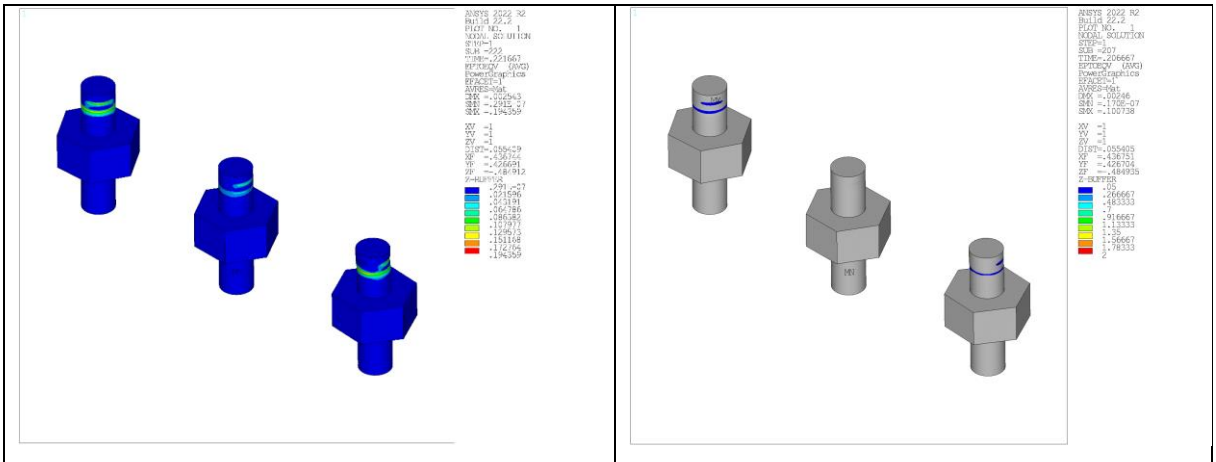

a) U=1.1Dy^{+} (T=184 kN)

b) U=Dy^{+} (T=172 kN)

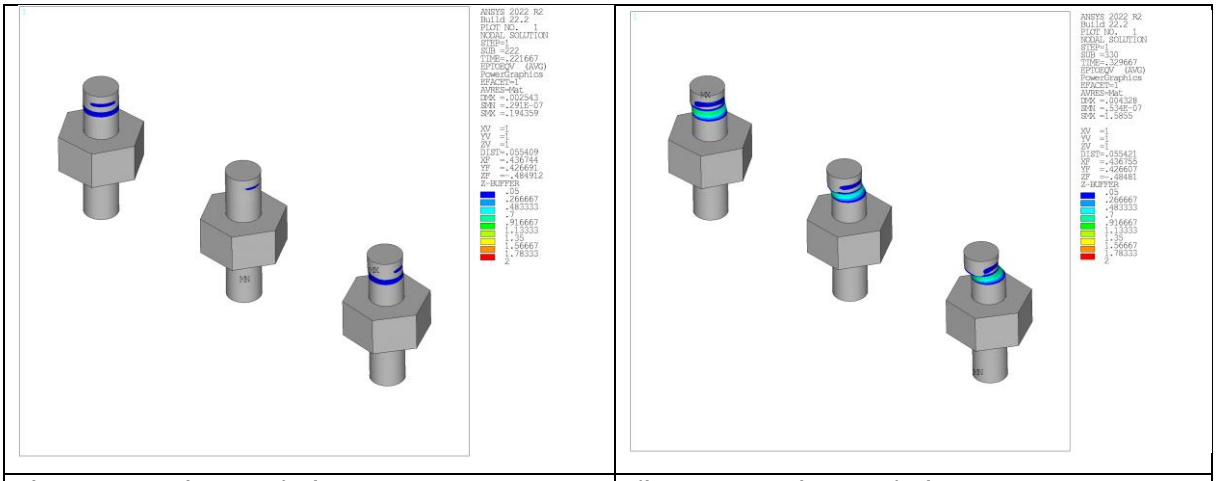

c) U=1.1Dy⁺ (T=184 kN)	d) U=1.7Dy⁺ (T=210 kN)

Figure 2.112: Von mises total mechanical strain in aluminium bolts of the fusible link configuration n°5 predicted for different values of imposed displacement with the ANSYS model with bolt-hole clearances

2.2.6.3 Cyclic loading

The vertical displacement-time curve prescribed in numerical analyses carried out without bolt-hole clearances is reported in Figure 2.21, while the yield displacements obtained from monotonic analyses are given in Table 7.

Table 7: Yield displacements determined from monotonic analyses of the fusible link detail n°5

	Without bolt-hole clearances	With bolt-hole clearances
Dy^+	1.4 mm	5.9 mm
Dy^-	1.5 mm	5.9 mm

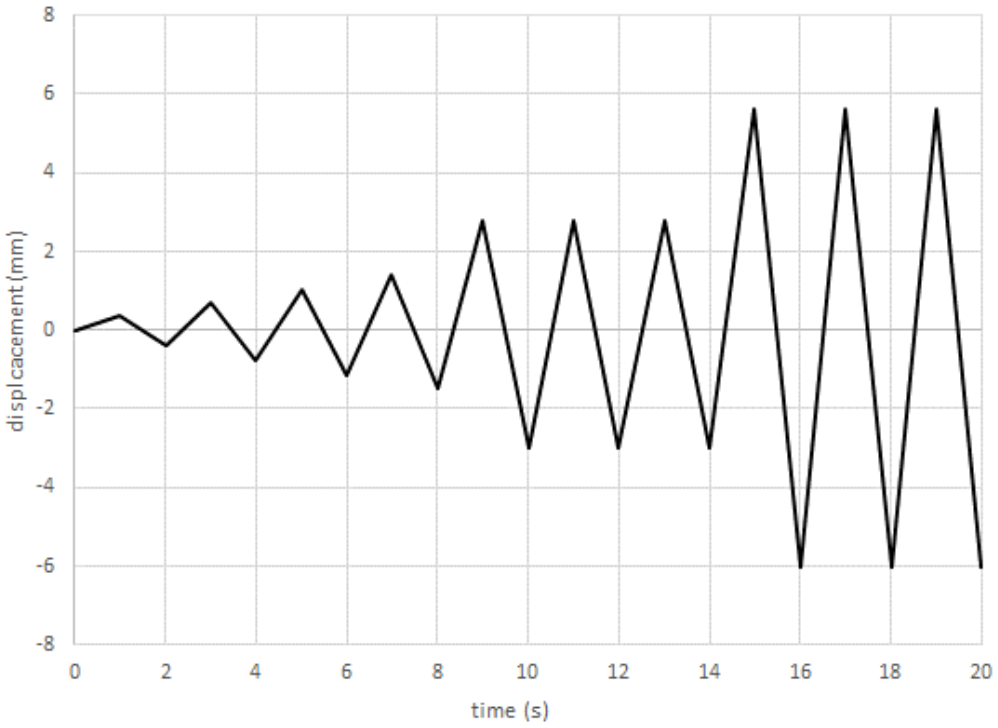

Figure 2.113: Vertical displacement-time curve used in numerical analyses carried out without bolt-hole clearances for the fusible link detail n°5

Figure 2.114 and Figure 2.115 depict the comparison between the FE predicted hysteresis axial force-displacement responses and the test results. In this figure, the negative values mean that components are under compression, and positive values are for tension. Through the hysteresis curves, it can be noted that numerical models predict that the studied link remains in the elastic stage during a major part of the displacement loading. Indeed, the predicted curves are predominantly linear for non-zero forces, both in tension and compression. Unloading takes place in the same path than loading, or a closer parallel path to that of the initial stiffness of the link until failure. Accounting for bolt-hole clearance in modelling only leads to a delay in the force increase, which starts when bolts come into bearing within the holes. In this case, the force remains small during the first cycles, until the prescribed displacement peaks exceed the maximum value of displacement that bolts can undergo inside holes. It can be also underlined that the predicted force-displacement curves display a similar behaviour in tension and compression, characterized, however, by slightly different initial stiffnesses in accordance with the monotonic analyses. In fact, since no significant plastic deformations occur in steel components, the predicted cyclic response coincides well with the monotonic responses obtained in tension or compression monotonic loading.

The failure modes of the studied fusible link are assessed by monitoring the strain states of different components constituting the link. For example, Figure 2.117 shows the distribution of the Von mises total mechanical strain predicted in some components of the link from the ANSYS model without bolt-hole clearances at the simulation end. It can be noted that the strain level exceeds locally the 0.2% yield strain around the holes of aluminium bolts only, highlighting that some bearing occurs in steel plates, with limited holes elongation. Steel bolts undergo only elastic deformations. Figure 2.118 shows the distribution of the Von mises total mechanical strain predicted in aluminium bolts. The strain distribution is given here for different levels of imposed displacement, by showing strain values exceeding 5% only. It clearly shows a yielding line progressively propagating in the cross-sectional area of bolts, in the shear planes at the junction between the steel profiles linked by the aluminium bolts. The failure of the specimen predicted by the models occurs during the reloading at the first cycle to $2Dy^{+}$ due to the shearing of aluminium bolts.

It should be noted that there is a noticeable discrepancy in the cyclic response of the studied link, between the experiment and the FE modelling. Firstly, like monotonic loading cases, there is a difference in the prediction of the initial stiffness of the specimen, as the experimental stiffness is significantly lower than the numerically predicted one. Secondly, on the experimental curves, unloading and reloading take place from the first cycle along a different path to that of the first loading stage. The unloading path includes two parts, an elastic unloading phase along a path that seems parallel to the loading path followed in the force-displacement curves predicted by models and a pinched unloading phase until the loading in the opposite direction happens. When unloaded to a 0 kN force, there is a larger non-zero residual displacement than numerically predicted, which increases progressively with the repeated unloading-reloading cycles even if the link is still in an elastic state, which is probably due to the bolt travels within holes. Like experiment, it can be noted that the predicted load-bearing capacity of the link under cyclic loading is of the same order of magnitude than the ones obtained from monotonic analyses. The load-bearing capacity predicted from the models without bolt-hole clearances is somewhat underestimated in comparison to the ones recorded during the tests, 110 kN against 114.7 and 126.1 kN by considering the force values corresponding to the first failure of some aluminium bolts, or against 135 and 158 kN if we consider the forces corresponding to the failure of all aluminium bolts. In contrast, the load-bearing capacity is slightly overestimated when hole bolt clearances are considered, the latter reaching 175 kN.

The dissimilarities between the experimental and FE results are mainly attributed to clearances and slipping between the steel profiles and all bolting. Bolt-hole clearances allow some movement in the link and can lead to increased bolt rotation, decreased bolt-hole contact area and then decreased link stiffness. Moreover, the misalignment of bolt and hole, the misalignment of profile or holes of varying sizes can lead to some bolts to remain unstressed at the start of loading, or throughout loading. All these phenomena are difficult to be considered accurately in models. This could also be due to phenomena which are not accounted in FE models, like possible slipping between the screw and nut thread or progressive crushing of the bearing flank of the thread (that supports shearing forces) of aluminium bolts with the bearing stresses.

It should be underlined that the cyclic loading does not affect greatly the load-bearing capacity predicted for the studied fusible link. Indeed, the difference between the monotonic and cyclic maximum resistance does not exceed 5 %.

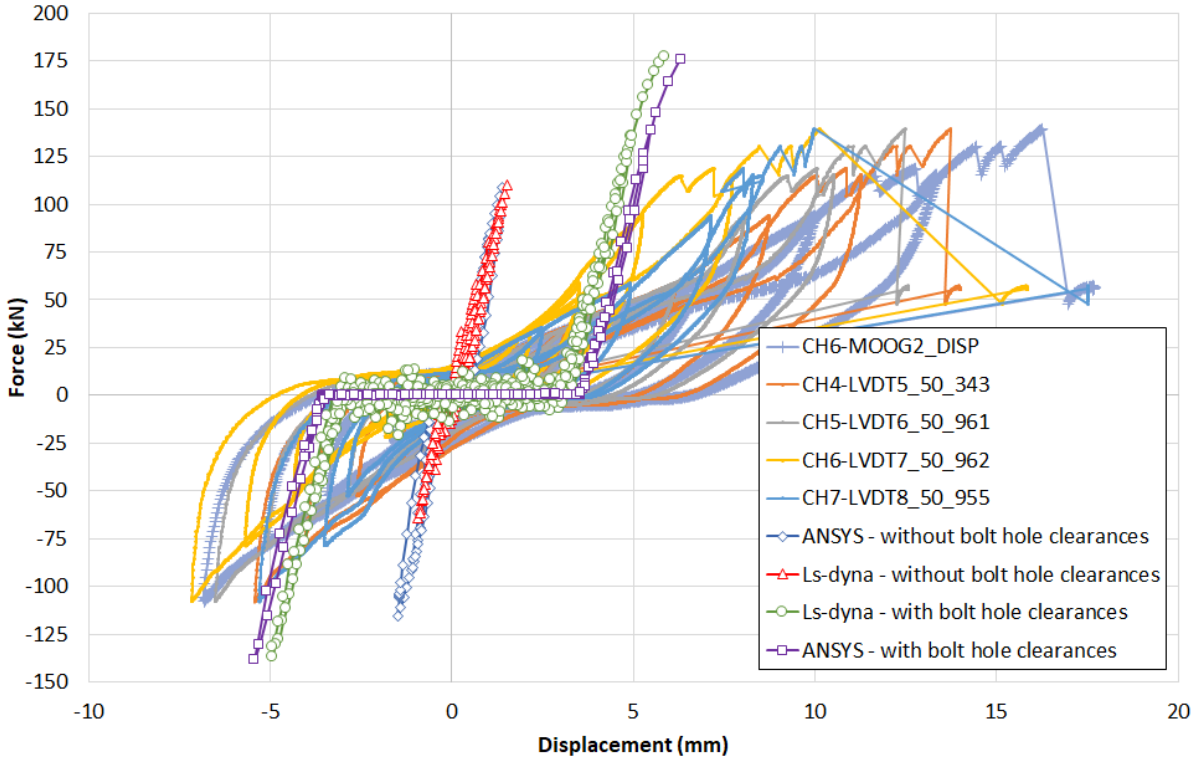

Figure 2.114: Force-displacement curves obtained from FE analyses and experiment (cyclic test n°1) for the fusible link configuration n°5 under cyclic action

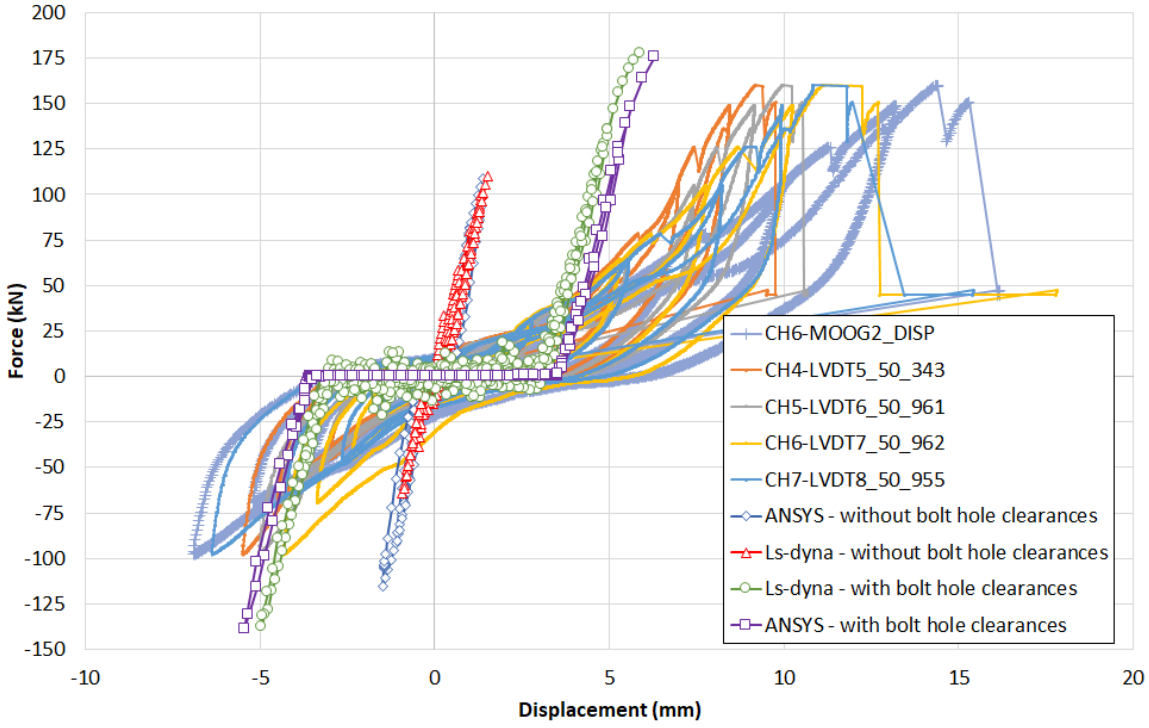

Figure 2.115: Force-displacement curves obtained from FE analyses and experiment (cyclic test n°2) for the fusible link configuration n°5 under cyclic action

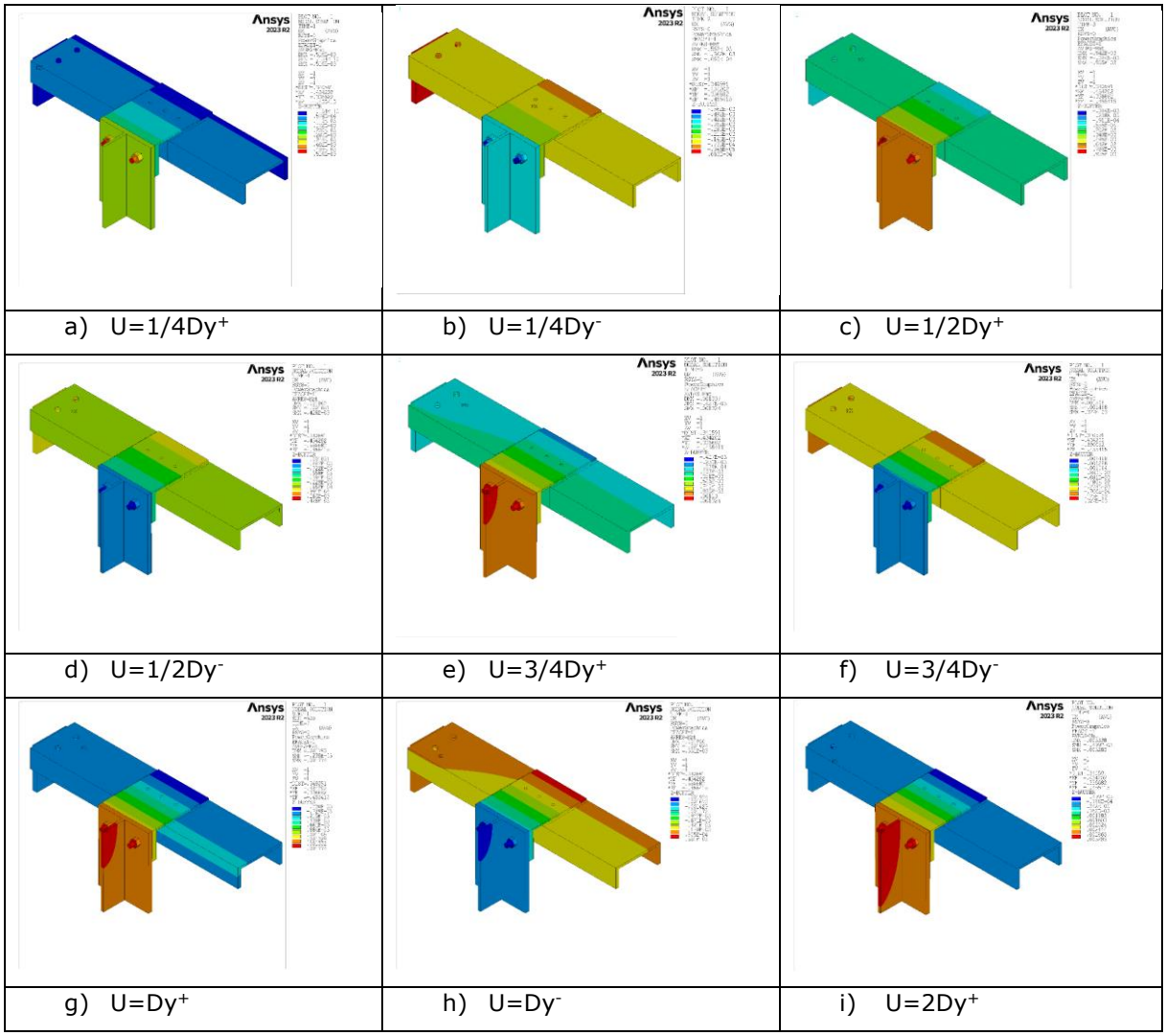

Figure 2.116: Deformed shape of the fusible link configuration n°5 according to imposed displacement values predicted with the ANSYS model without bolt-hole clearances

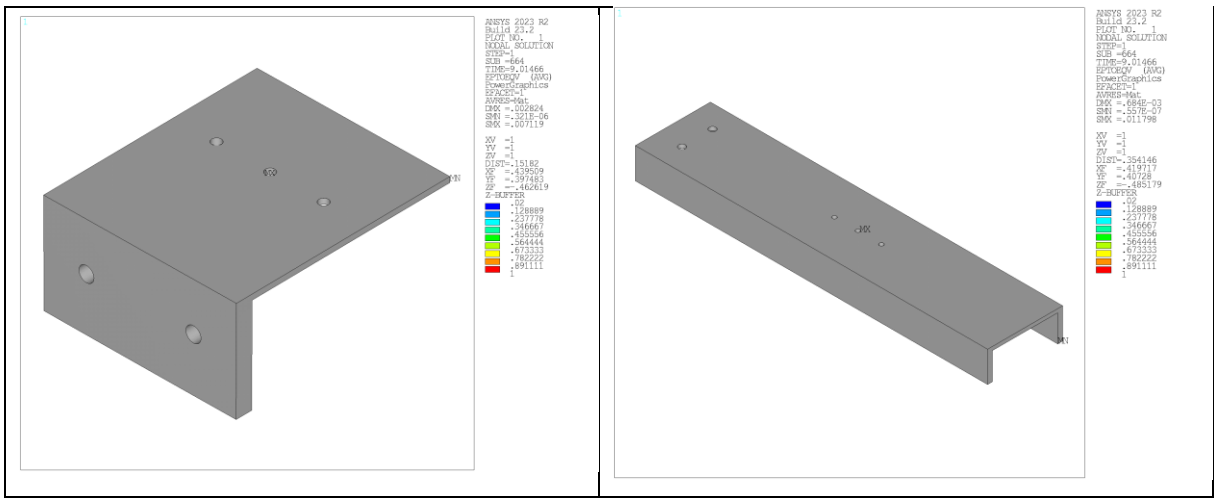

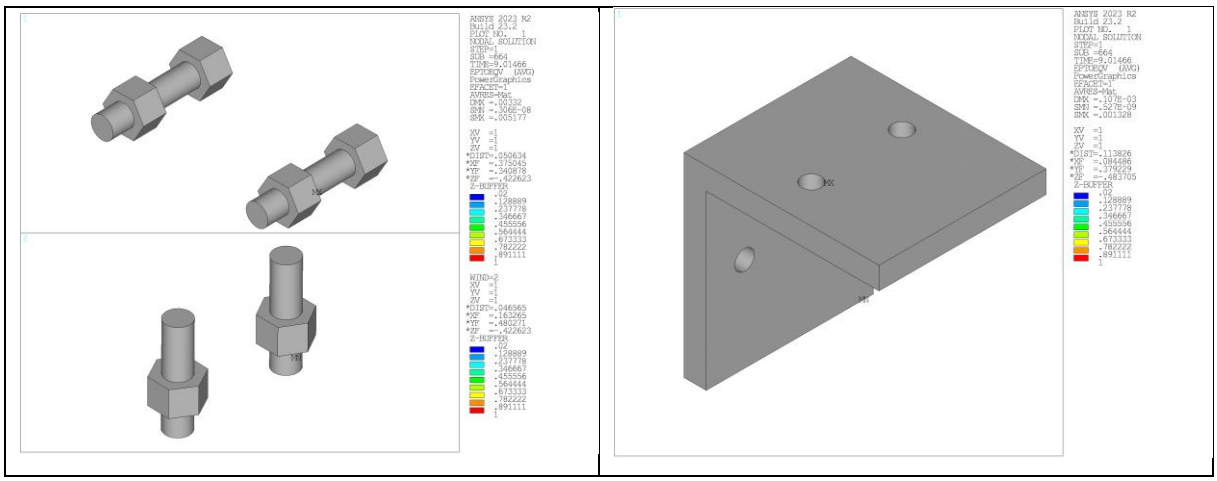

Figure 2.117: Von mises total mechanical strain in components of the fusible link configuration n°5 predicted with the ANSYS model without bolt-hole clearances, at simulation end

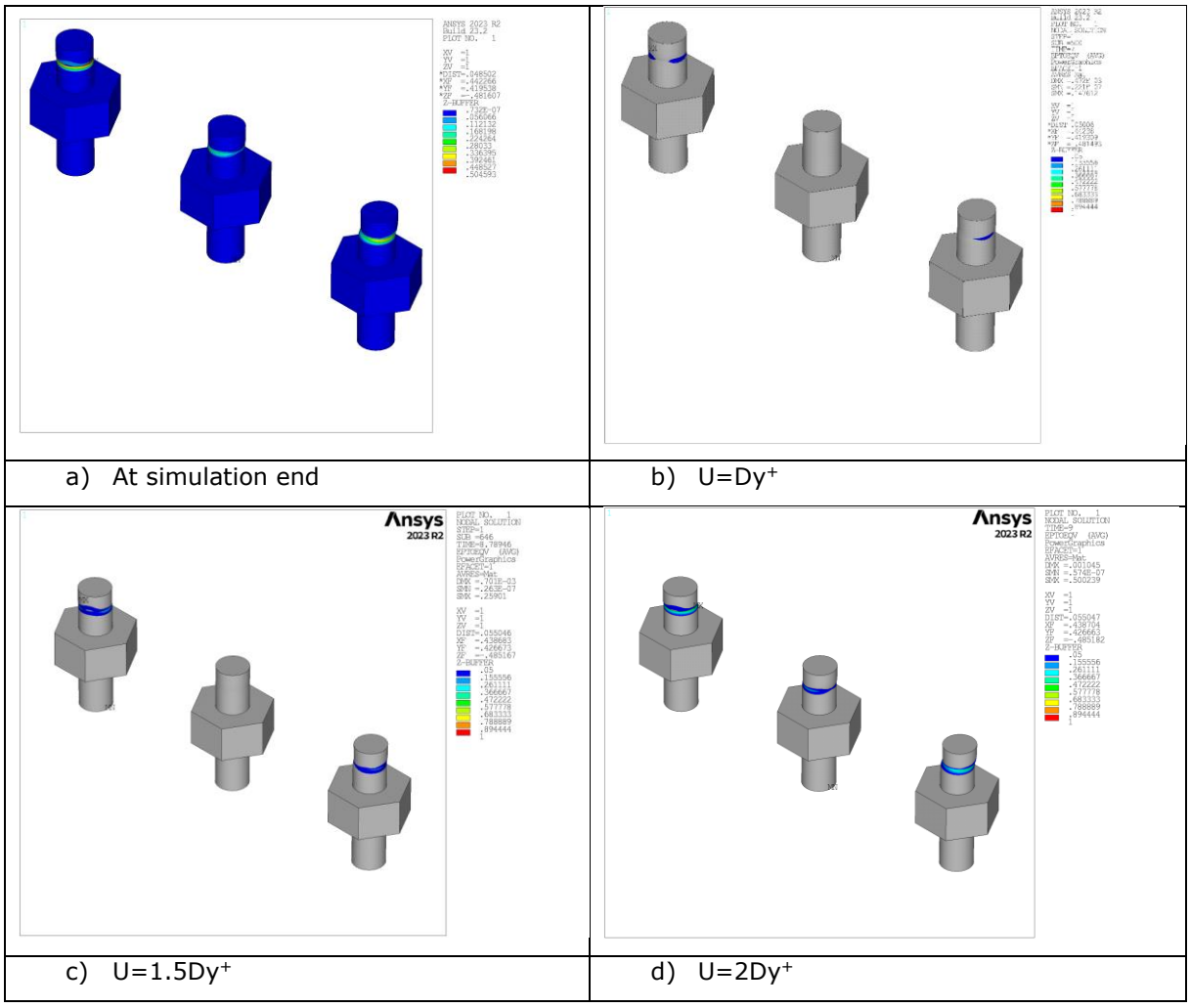

a) At simulation end

b) $U=Dy^{+}$

c) $U=1.5Dy^{+}$

d) $U=2Dy^{+}$

Figure 2.118: Von mises total mechanical strain in aluminium bolts of the fusible link configuration n°5 predicted for different values of imposed displacement with the ANSYS model without bolt-hole clearances

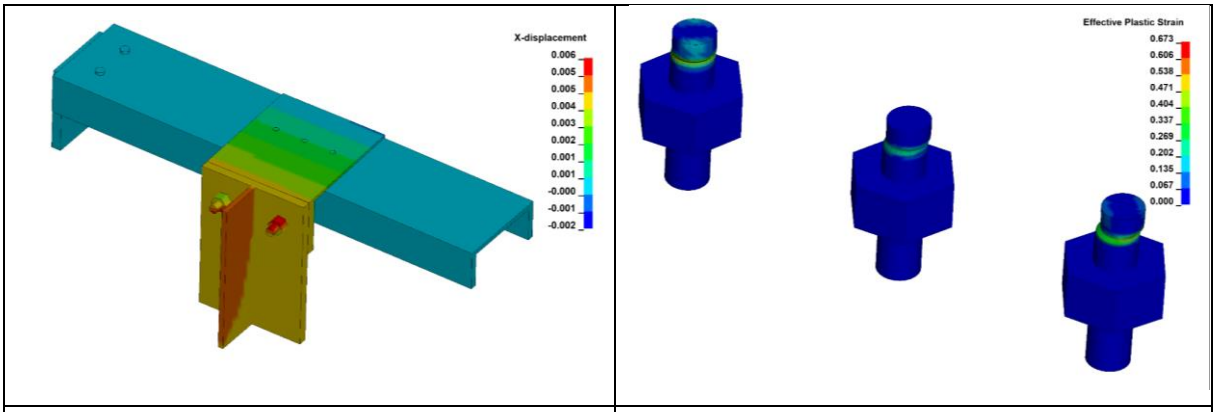

a) Deformed shape

b) Effective plastic strain in aluminium bolts

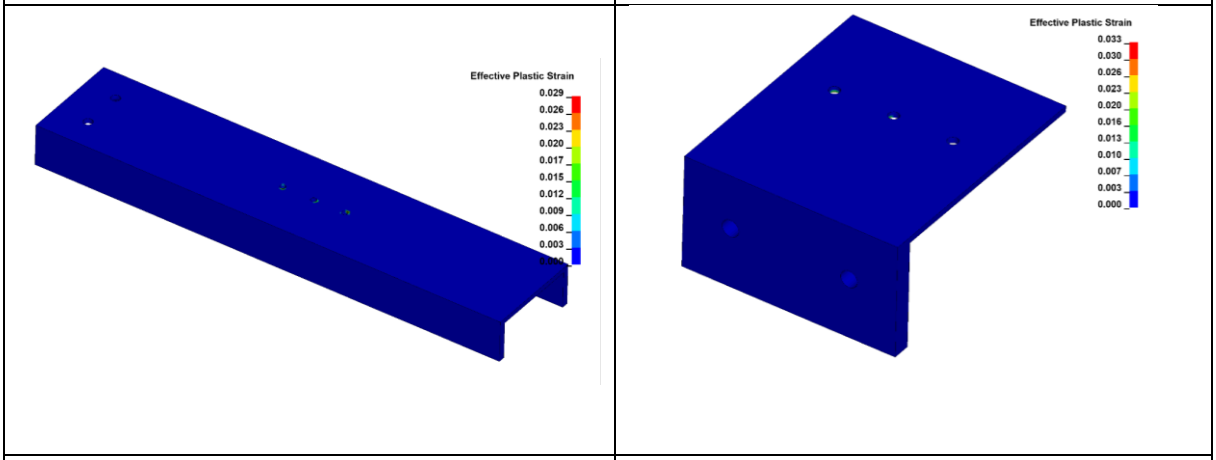

c) Effective plastic strain in the U profiles

d) Effective plastic strain in the T profile

Figure 2.119: Main results of the modelling under Ls-dyna without bolt-hole clearances at failure time of aluminium bolts

a) Cyclic test n°1

b) Cyclic test n°2

Figure 2.120: Photos of aluminium bolts after the cyclic tests

3 CALIBRATION OF LUMPED PLASTICITY MODELS

For each fusible link configuration tested during the experimental campaign carried out at University of Trento, a specific nonlinear numerical model was developed in OpenSees [5]. For the reader's benefit, a brief description of the tests is systemically presented before each proposed model. For a comprehensive description see Deliverable 4.1 [1].

3.1 Pinching4 Material

The pinching4 material was selected to represent the nonlinear behaviour of the investigated fusible link configurations. It is a piecewise uniaxial material model that represents a 'pinched' load-deformation response and exhibits both stiffness and strength degradation under cyclic loading. It is defined by means of damages indices δj_i, whose general formulation is proposed in Lowes *et al*. [6]:

$$\delta j_i = gj1\left(\max\left\{\frac{d_{max,i}}{def_{max}};\frac{d_{min}}{def_{min}}\right\}^{gj3}\right) + gj2\left(\frac{\int_{load\ history} dE_i}{E_{monotonic}}\right)^{gj4}$$

where *j = k, d and f*. In particular, damage models are expressed in terms of damage indices as stiffness degradation δk_i, deformation demand δd_i and strength degradation δf_i, as hereafter defined:

$$k_i = k_0(1-\delta ki)$$

$$d_{max,i} = d_{max,0}(1-\delta di)$$

$$f_{max,j} = f_{max,0}(1-\delta fi)$$

where *gj*1, *gj*2, *gj*3 and *gj*4 are degradation model parameters; $E_{monotonic}$ defines the energy required to achieve failure under monotonic loading; k_i is the unloading stiffness at time t_i; k_0 is the initial unloading stiffness for the case of no damage; def_{max} and def_{min} are the positive and negative deformations respectively that define failure; $d_{max,i}$ and $d_{min,i}$ are the maximum historic and minimum historic deformation demands; $f_{max,i}$ is the current envelope maximum strength at time t_i; and $f_{max,0}$ is the initial envelope maximum strength for the case of no damage.

Under a practical point of view, the material setting in the OpenSees software required the definition of each parameter reported in Figure 3.1, that were precisely defined for each fusible link configuration in consideration by means of an iterative process.

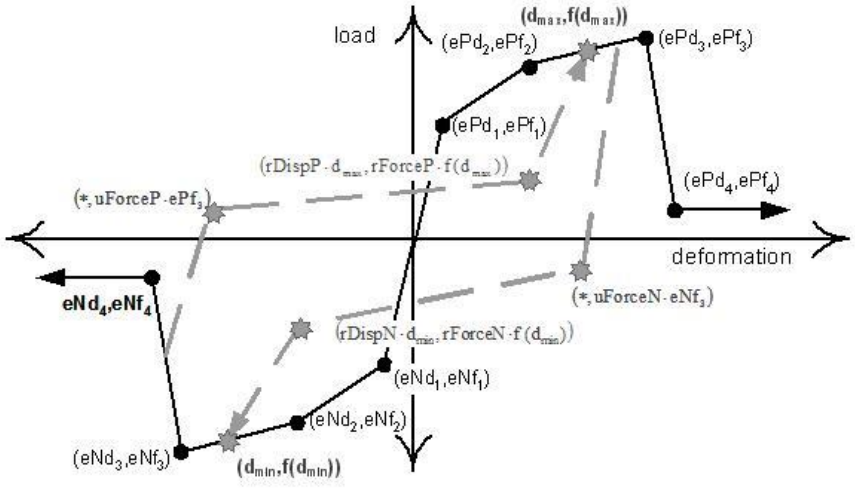

Figure 3.1: Pinching material description

3.2 Fusible link configuration n°1

The test setup and the main components of the fusible link configuration n°1 are shown in Figure 3.2:

a) test setup

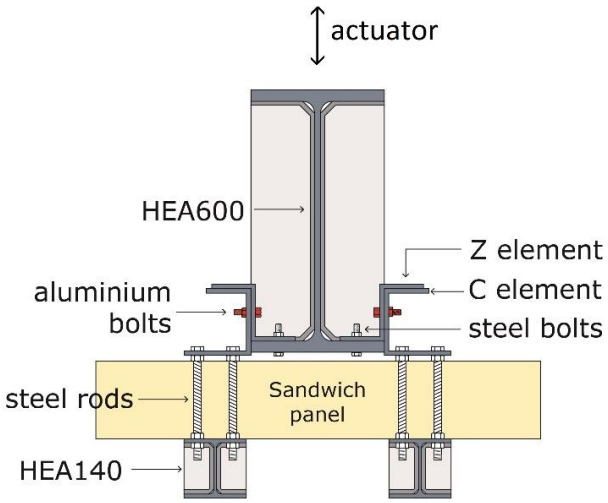

b) main components

Figure 3.2: fusible link configuration n°1

The fusible link detail was designed for a shear value of 80 kN. Four tests were performed on this detail, two monotonic tests and, consequently, two cyclic tests. The cyclic tests results are reported in Figure 3.3, in terms of force-displacement curves.

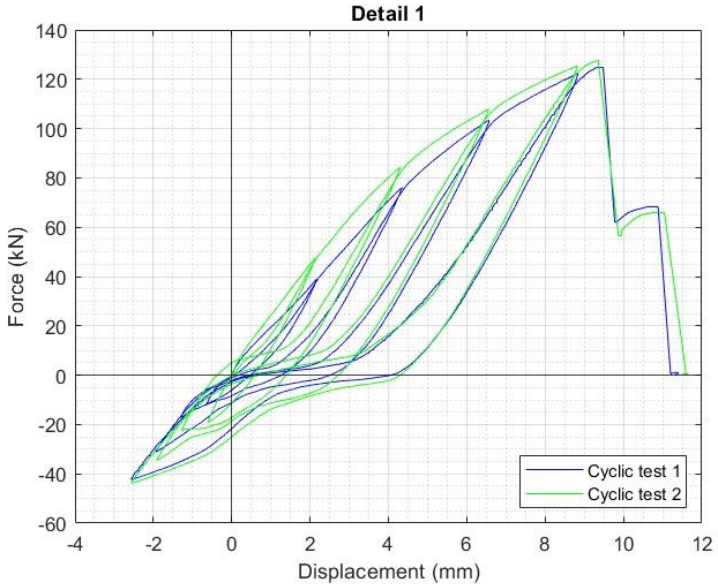

Figure 3.3: Fusible link configuration n°1: cyclic tests results.

Considering the actual configuration of the tested fusible solution link with the aluminum bolts located on both sides of the specimen, two *ZeroLength elements* (ZL) were created to reproduce their nonlinear behaviour. They are indicated by means of two red dots in Figure 3.4 and were defined between three nodes with the same coordinates.

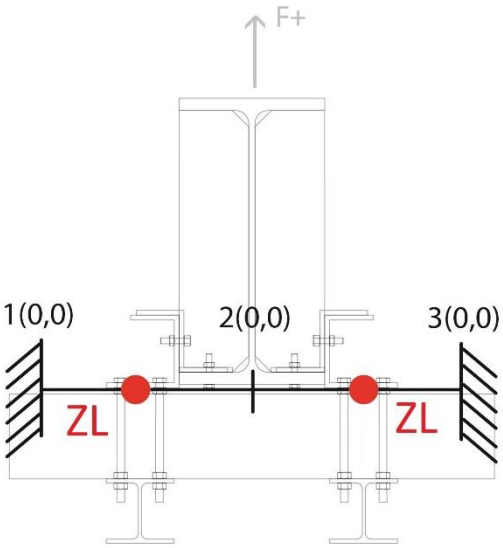

Figure 3.4: Fusible link configuration n°1: numerical model representation

In Table 8 and in Table 9 the *Pinching4 material* parameters defined to describe the experimental behaviour and assigned to the two *ZeroLength elements* are reported.

Table 8: Detail 1, pinching parameters of envelope and target points

Parameter	Value	Parameter	Value	Parameter	Value
ePf1 (N)	19e3	eNPf1 (N)	-5.5e3	rDispP (-)	0.45
ePd1 (mm)	2.12	eNd1 (mm)	-0.64	rForceP (-)	0.12
ePf2 (N)	39.5e3	eNf2 (N)	-8e3	uForceP (-)	-0.05
ePd2 (mm)	4.25	eNd2 (mm)	-0.94	rDispN (-)	0.1
ePf3 (N)	63.75e3	eNf3 (N)	-15.5e3	rForceN (-)	0.7
ePd3 (mm)	9.4	eNd3 (mm)	-1.82	uForceN (-)	-0.1
ePf4 (N)	28.3e3	eNf4 (N)	-21e3		
ePd4 (mm)	10	eNd4 (mm)	-2.47		

Table 9: Detail 1: pinching parameter of damage index

Parameter	Value	Parameter	Value	Parameter	Value
gK (1,2,3,4)	0.0	gD (1,2,3,4)	0.0	gF (1,2,3,4)	0.0
gKLim	-0.9	gDLim	-0.02	gFLim	0.0

Eventually, Figure 3.5 shows the comparison between the numerical results of the calibrated model and the experimental results of the cyclic tests. The numerical curve was obtained from an analysis in displacement control with a displacement history in accordance with the ECCS loading protocol procedure applied in the experimental test.

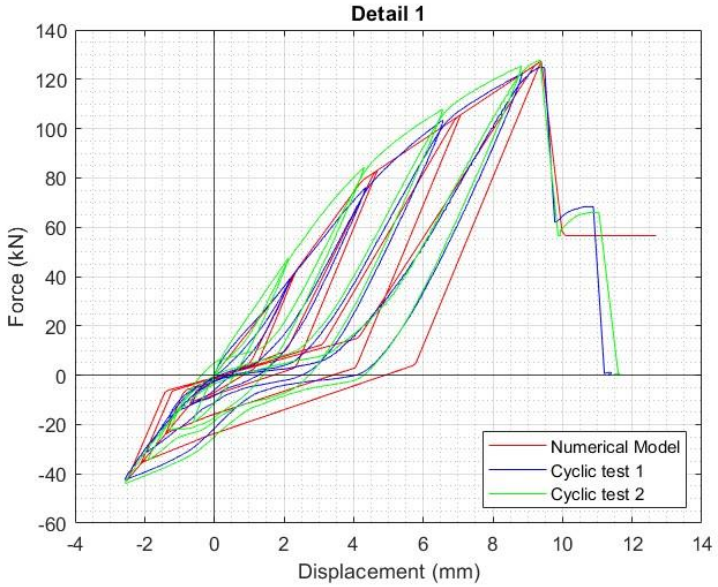

Figure 3.5: Fusible link configuration n°1: numerical and experimental results

As already mentioned, the main objective was to calibrate the numerical model based on the maximum forces observed during the tests. Consequently, as can be observed from Figure 3.5, the maximum forces were captured with a high level of accuracy, despite some inaccuracy in reproducing the unloading stiffness. Table 10 shows the comparison between the numerical and the experimental maximum forces along with the error that resulted less than 5%.

Table 10: Fusible link configuration n° 1: comparison between experimental and numerical maximum forces results

	Max force Cyclic Test 1 (kN)	Max force Cyclic Test 2 (kN)	Max force Numerical model (kN)	Average Error (%)	Max Error (%)
Positive direction	124.7	127.8	127.5	1.00	2.2
Negative direction	-42.3	-43.8	-44.1	2.35	4.1

3.3 Fusible link configuration n°2

The test setup and the main components of the fusible link configuration n°2 are shown in Figure 3.6.

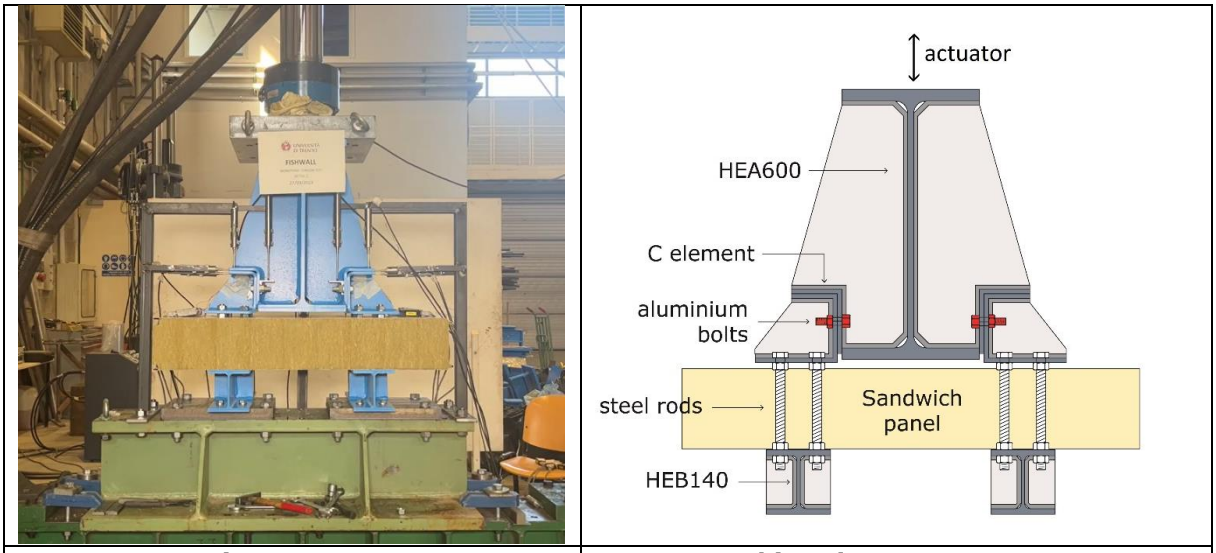

a) test setup **b) main components**

Figure 3.6: Fusible link configuration n° 2

The fusible link configuration n°2 was designed for a shear value of 180 kN. Four tests were performed on this detail, two monotonic tests and two cyclic tests. The cyclic test results are reported in Figure 3.7 in terms of force-displacement curves.

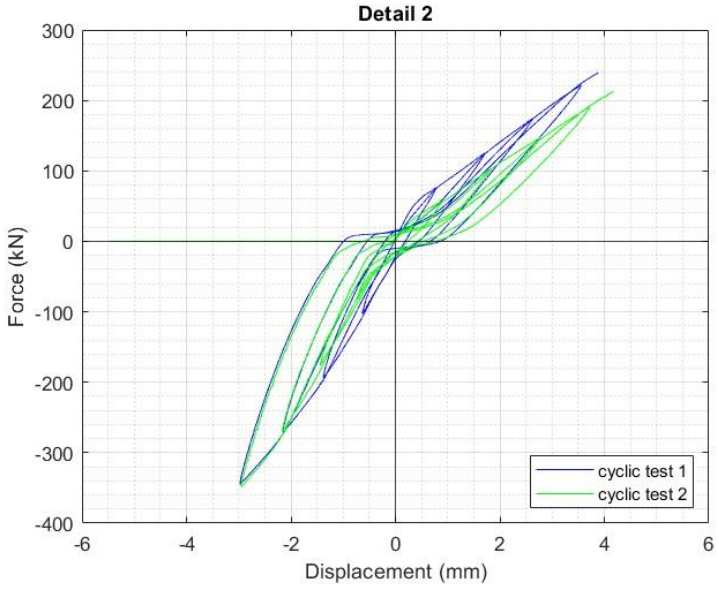

Figure 3.7: Fusible link configuration n°2: cyclic tests results

Considering the actual configuration of the investigated fusible link with the aluminum bolts located on both sides of the specimen, as for the first tested fusible link, two *ZeroLength elements* (ZL) were created to reproduce their nonlinear behaviour. They are indicated by means of two red dots in Figure 3.8 and defined between three nodes with the same coordinates.

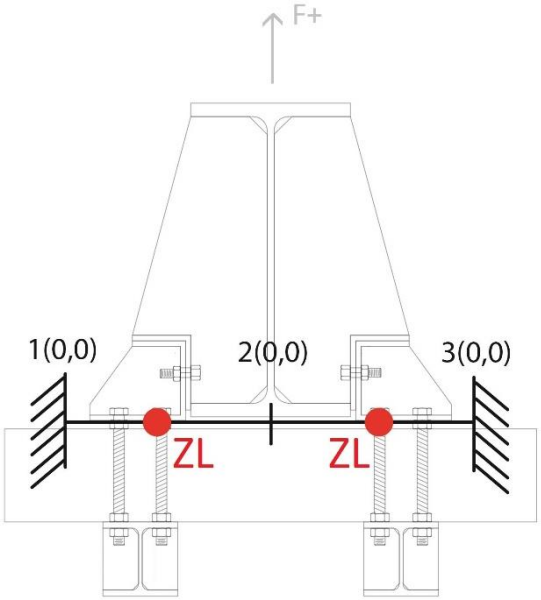

Figure 3.8: Fusible link configuration n°2: numerical model representation

In Table 11 and in Table 12 the *Pinching4 material* parameters defined to describe the experimental behaviour and assigned to the two *ZeroLength elements* are reported.

Table 11: Fusible link configuration n°2: pinching parameters of envelope and target points

Parameter	Value	Parameter	Value	Parameter	Value
ePf1 (N)	36.95e3	eNPf1 (N)	-51.4e3	rDispP (-)	0.14
ePd1 (mm)	0.77	eNd1 (mm)	-0.59	rForceP (-)	0.12
ePf2 (N)	62.85e3	eNf2 (N)	-96.5e3	uForceP (-)	0.05
ePd2 (mm)	1.54	eNd2 (mm)	-1.37	rDispN (-)	0.1
ePf3 (N)	86.75e3	eNf3 (N)	-133.5e3	rForceN (-)	0.1
ePd3 (mm)	2.31	eNd3 (mm)	-2.16	uForceN (-)	0.02
ePf4 (N)	122.5e3	eNf4 (N)	-174e3		
ePd4 (mm)	4.08	eNd4 (mm)	-3.24		

Table 12: Fusible link configuration n°2: pinching parameter of damage index

Parameter	Value	Parameter	Value	Parameter	Value
gK (1,2,3,4)	0.0	gD (1,2,3,4)	0.0	gF (1,2,3,4)	0.0
gKLim	-0.2	gDLim	0.0	gFLim	0.0

Eventually, Figure 3.9 shows the comparison between numerical results of the calibrated model and experimental results of the cyclic tests. The numerical curve was obtained from an analysis in displacement control with a displacement history in accordance with the ECCS loading protocol applied in the experimental test.

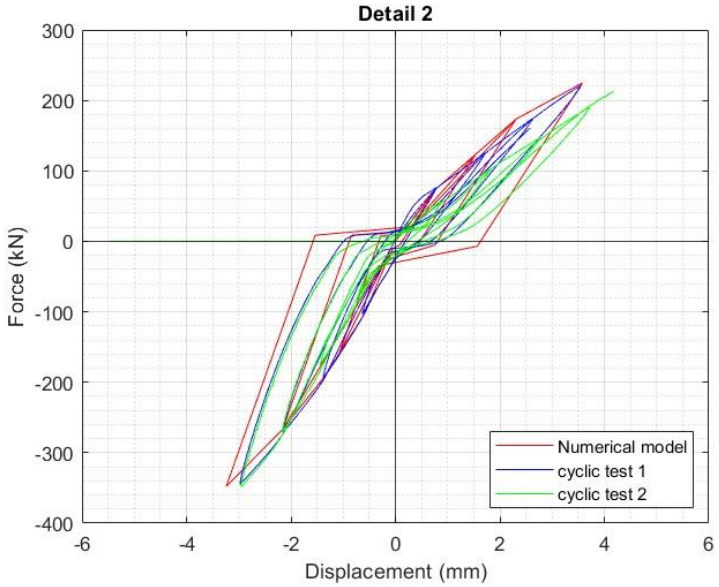

Figure 3.9: Fusible link configuration n°2: numerical and experimental results

From Figure 3.9 it is possible to observe that the numerical outcomes well agree with the experimental data. In particular, on the compression branch both the forces and the stiffness in unloading and reloading were captured. Considering the tension branch, where the two cyclic tests recorded a slightly different stiffness, it was chosen the first branch of the cyclic test to calibrate the numerical model because it reached a higher maximum force. Table 13 shows the comparison between the numerical and the experimental maximum forces along with the error that resulted less than 1%.

Table 13: Fusible link configuration n°2: comparison between experimental and numerical results.

	Max force Cyclic Test 1 (kN)	Max force Cyclic Test 2 (kN)	Max force Numerical model (kN)	Average Error (%)	Max Error (%)
Positive direction	221.2	212.6	220.0	1.5	3.5
Negative direction	-348.6	-348.5	-44.1	0.2	0.2

3.4 Fusible link configuration n°3.1

The test setup and the main components of the fusible link configuration n°3.1 are shown in Figure 3.10.

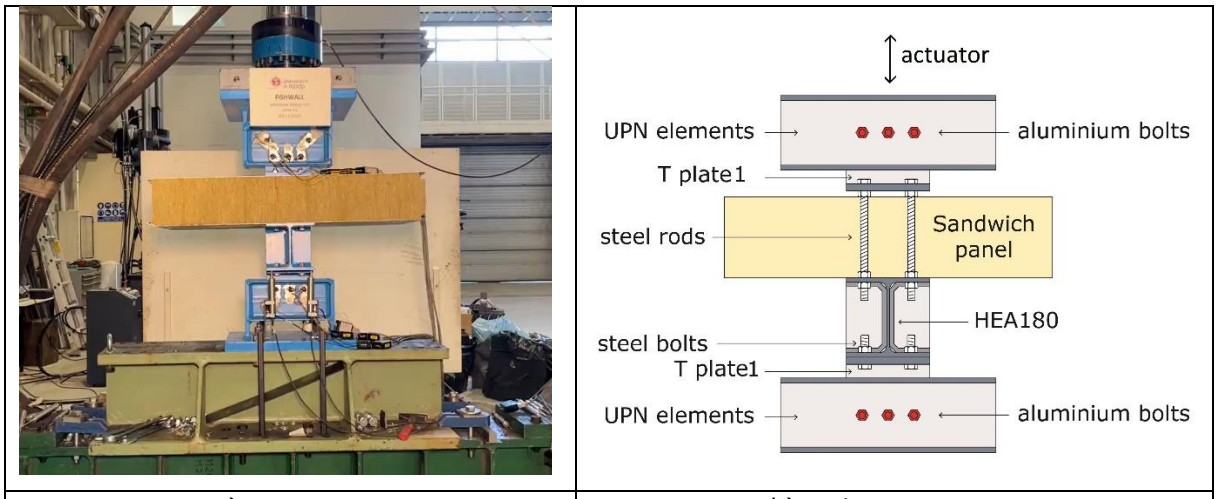

a) test setup | b) main components

Figure 3.10: Fusible link configuration n° 3.1

The fusible link configuration n°3.1 was designed for a shear value of 180 kN. Four tests were performed on this detail, two monotonic tests and two cyclic tests. The cyclic tests results are reported in Figure 3.11 in terms of force-displacement curves.

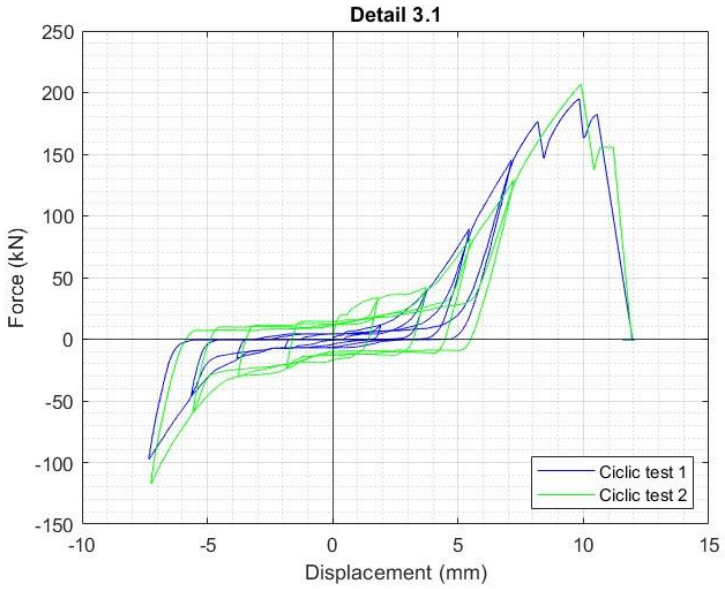

Figure 3.11: Fusible link configuration n°3.1: cyclic tests results

Considering the actual configuration of the investigated fusible link, the aluminum bolts that were designed to withstand the shear force are either on the top part or on the bottom of the specimen. Therefore, one *ZeroLength element* (ZL) was used to represent their behaviour. It is indicated by means of one red dot in Figure 3.12 and defined between two nodes with the same coordinates.

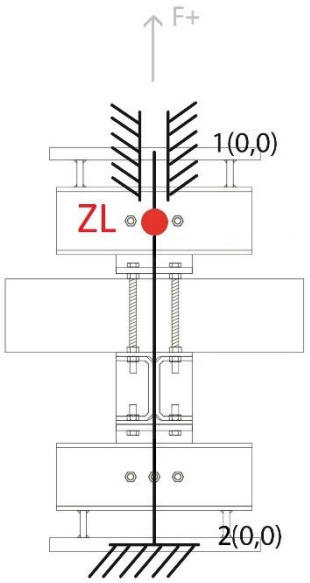

Figure 3.12: Fusible link configuration n°3.1, numerical model representation

In Table 14 and in Table 15 the *Pinching4 material* parameters defined to describe the experimental behaviour and assigned to the one *ZeroLength element* are reported.

Table 14: Fusible link configuration n°3.1: pinching parameters of envelope and target points

Parameter	Value	Parameter	Value	Parameter	Value
ePf1 (N)	20.57e3	eNPf1 (N)	-40.7e3	rDispP (-)	0.3
ePd1 (mm)	1.77	eNd1 (mm)	-3.54	rForceP (-)	0.2
ePf2 (N)	28.23e3	eNf2 (N)	-145e3	uForceP (-)	0.02
ePd2 (mm)	3.54	eNd2 (mm)	-7.07	rDispN (-)	0.3
ePf3 (N)	57.70e3	eNf3 (N)	-206e3	rForceN (-)	0.2
ePd3 (mm)	5.30	eNd3 (mm)	-9	uForceN (-)	0.02
ePf4 (N)	115.6e3	eNf4 (N)	-1e3		
ePd4 (mm)	7.07	eNd4 (mm)	-10		

Table 15: Fusible link configuration n°3.1: pinching parameter of damage index

Parameter	Value	Parameter	Value	Parameter	Value
gK (1,2,3,4)	0.0	gD (1,2,3,4)	0.0	gF (1,2,3,4)	0.0
gKLim	-5	gDLim	0.0	gFLim	0.0

Eventually, Figure 3.13 shows the comparison between the numerical results of the calibrated model and the experimental results of the cyclic tests. The numerical curve was obtained from an analysis in displacement control with a displacement history in accordance with the ECCS procedure applied in the experimental test.

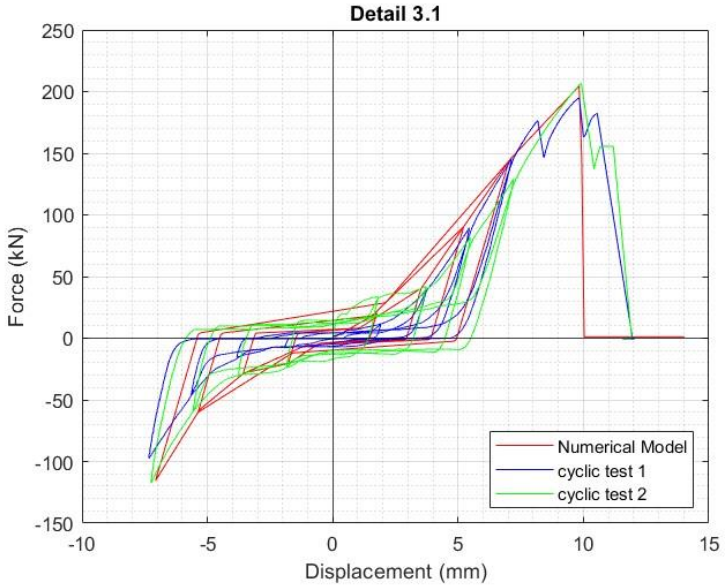

Figure 3.13: Fusible link configuration n°3.1: numerical and experimental results

From Figure 3.13 it is possible to observe that the numerical outcomes well agree with the experimental data in terms of maximum forces in both directions. Table 16 shows the comparison between the numerical and the experimental maximum forces along with the average error that resulted about 8% and maximum error in the order of 18%.

Table 16: Fusible link configuration n°3.1: comparison between experimental and numerical results

	Max force Cyclic Test 1 (kN)	Max force Cyclic Test 2 (kN)	Max force Numerical model (kN)	Average Error (%)	Max Error (%)
Positive direction	194.9	206.5	204.5	1.95	4.9
Negative direction	-97.0	-117.6	-115.0	8	18.2

3.5 Fusible link configuration n°3.2

The test setup and the main components of the fusible link configuration n°3.2 are shown in Figure 3.14.

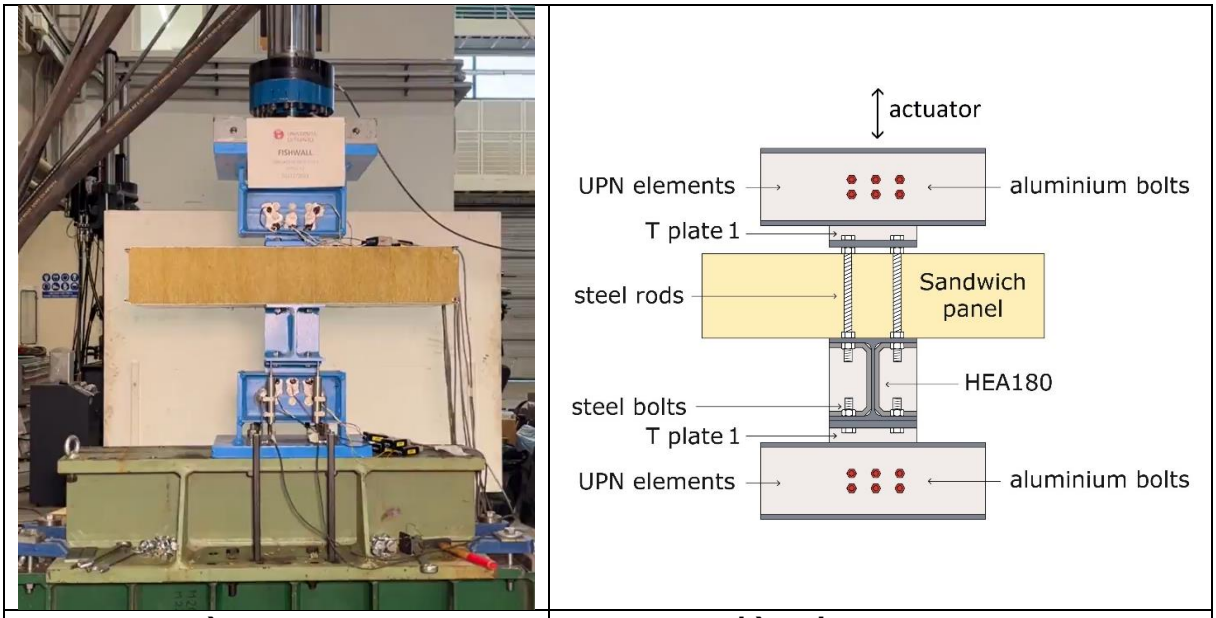

a) test setup | **b) main components.**

Figure 3.14: Fusible link configuration n°.2

The fusible link configuration n°3.2 was designed for a shear value of 180 kN. In this case, five tests were performed, two monotonic tests and three cyclic tests, because the first two cyclic tests exhibited different behaviours due to the high number of aluminium bolts and to the assembling process and imperfections. The cyclic tests results are reported in Figure 3.15 in terms of force-displacement curves.

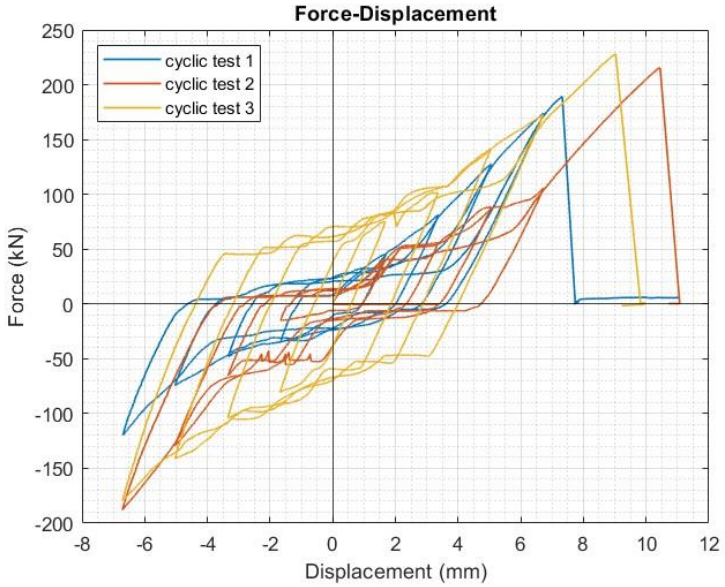

Figure 3.15: Fusible link configuration n°3.2: cyclic tests results

Considering the detail configuration, identical to Detail 3.1, the aluminum bolts that were designed to withstand the shear force are either on the top part or on the bottom part of the specimen. Therefore, one *ZeroLength element* was used to reproduce the experimental behaviour. It is indicated by means of one red dot in Figure 3.16 and defined between two nodes with the same coordinates.

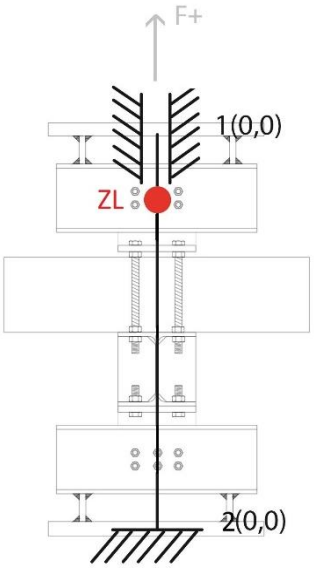

Figure 3.16: Fusible link configuration n°3.2: numerical model representation

In Table 17 and in Table 18 the *Pinching4 material* parameters defined to describe the experimental behaviour and assigned to the one *ZeroLength element* are reported.

Table 17: Fusible link configuration n°3.2: pinching parameters of envelope and target points

Parameter	Value	Parameter	Value	Parameter	Value
ePf1 (N)	30e3	eNPf1 (N)	-43e3	rDispP (-)	0.5
ePd1 (mm)	1.46	eNd1 (mm)	-1.46	rForceP (-)	0.2
ePf2 (N)	64e3	eNf2 (N)	-173e3	uForceP (-)	0.1
ePd2 (mm)	2.91	eNd2 (mm)	-5.82	rDispN (-)	0.4
ePf3 (N)	128e3	eNf3 (N)	-250e3	rForceN (-)	0.4
ePd3 (mm)	4.37	eNd3 (mm)	-7.9	uForceN (-)	0.05
ePf4 (N)	190e3	eNf4 (N)	-1e3		
ePd4 (mm)	5.82	eNd4 (mm)	-9		

Table 18: Fusible link configuration n°3.2: pinching parameter of damage index

Parameter	Value	Parameter	Value	Parameter	Value
gK (1,2,3,4)	0.0	gD (1,2,3,4)	0.0	gF (1,2,3,4)	0.0
gKLim	-6	gDLim	-0.1	gFLim	0.1

Eventually, in Figure 3.17, the calibration results can be observed in comparison with only the first two cyclic test results of the experimental campaign. Indeed, the third cyclic test exhibited an intermediate behaviour between the first two tests with maximum forces reached in both tests. Therefore, by calibrating on the first two tests, the maximum forces were also captured. The numerical curve was obtained from an analysis in displacement control with a displacement history in accordance with the ECCS procedure applied in the experimental test.

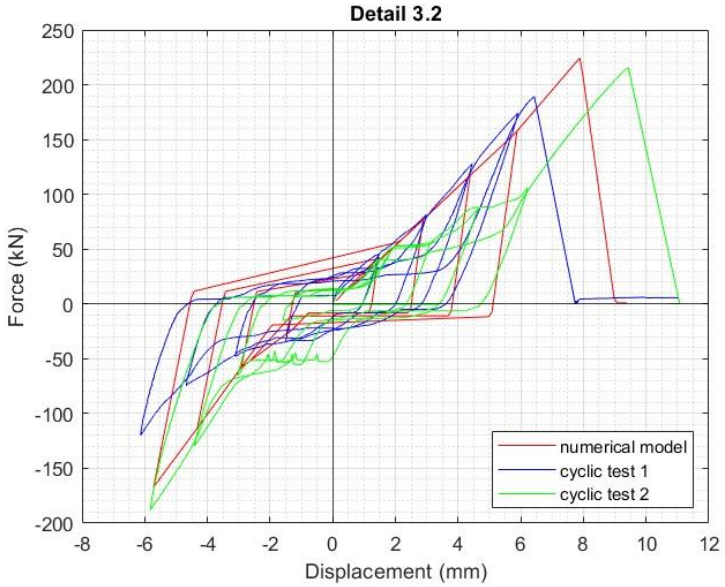

Figure 3.17: Fusible link configuration n°3.2: numerical and experimental results

As can be noticed in Figure 3.17, the positive branch captured with a good level of accuracy the loading and unloading stiffness of the first test, reaching the maximum force of the second one. However, the same could not be observed for the negative direction, where the maximum force is lower than the one observed during Test 2 of 11.4%. Overall, the calibration results are in reasonable agreement with the experimental data. Table 19 shows the comparison between the numerical and the experimental maximum forces along with the average error that resulted about 12 and maximum error in the order of 38%.

Table 19. Fusible link configuration n°3.2: comparison between experimental and numerical results

	Max force Cyclic Test 1 (kN)	Max force Cyclic Test 2 (kN)	Max force Numerical model (kN)	Average Error (%)	Max Error (%)
Positive direction	189.3	215.4	224.4	11.35	18.5
Negative direction	-119.8	-187.8	-167.0	13.6	38.6

3.6 Fusible link configuration n°4

The test setup and the main components of the fusible link configuration n°4 are shown in Figure 3.18.

a) test setup

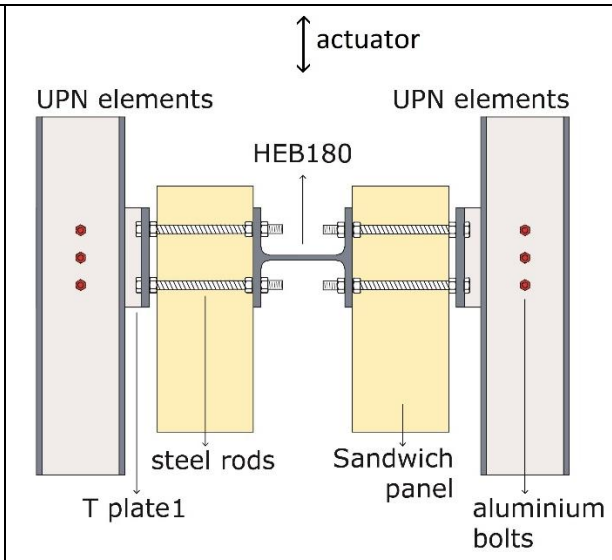

b) main components.

Figure 3.18: Fusible link configuration n°4

The fusible link configuration n°4 was designed for a shear value of 180 kN. Four tests were performed on this detail: two monotonic tests and two cyclic tests. The cyclic tests results are reported in Figure 3.19 in terms of force-displacement curves. The detailed behaviour was described in Deliverable 4.1 [1], where the presence of the sandwich panel induced large deformation and, therefore, additional horizontal forces in the fusible links, that could not withstand the design force

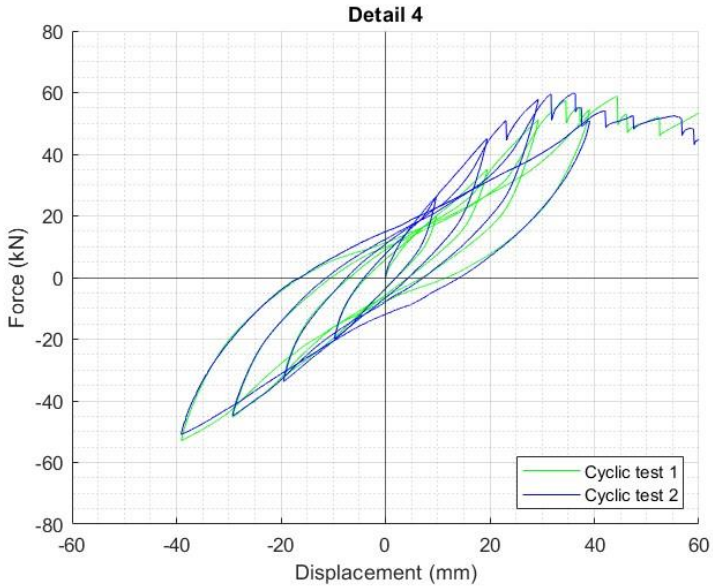

Figure 3.19: Fusible link configuration n°4: cyclic tests results

Considering the detail configuration, where the aluminum bolts are located on both sides of the specimen, two *ZeroLength elements* (ZL) were used to reproduce the experimental behaviour. They are indicated by means of two red dots in Figure 3.20 and defined between three nodes with the same coordinates.

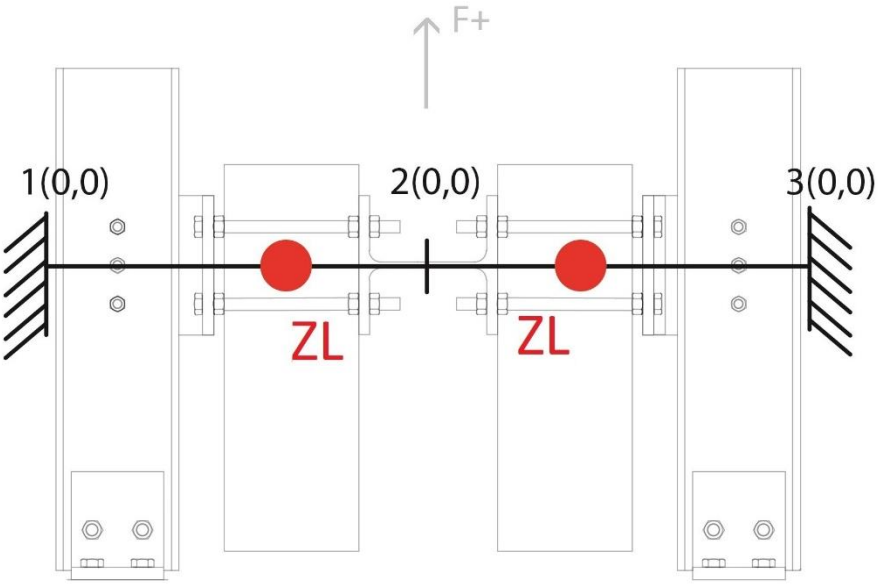

Figure 3.20: Fusible link configuration n°4: numerical model representation

In Table 20 and in

Table 21 are reported the *Pinching4 material* parameters defined to describe the experimental behaviour and assigned to the two *ZeroLength elements* introduced.

Table 20: Fusible link configuration n°4: pinching parameters of envelope and target points

Parameter	Value	Parameter	Value	Parameter	Value
ePf1 (N)	13e3	eNPf1 (N)	-9e3	rDispP (-)	0.55
ePd1 (mm)	9.75	eNd1 (mm)	-9.75	rForceP (-)	0.5
ePf2 (N)	22e3	eNf2 (N)	-16.5e3	uForceP (-)	-0.1
ePd2 (mm)	19.5	eNd2 (mm)	-19.5	rDispN (-)	0.1
ePf3 (N)	30e3	eNf3 (N)	-22e3	rForceN (-)	0.2
ePd3 (mm)	39	eNd3 (mm)	-29.5	uForceN (-)	-0.25
ePf4 (N)	27e3	eNf4 (N)	-26e3		
ePd4 (mm)	42	eNd4 (mm)	-39		

Table 21: Fusible link configuration n°4: pinching parameter of damage index

Parameter	Value	Parameter	Value	Parameter	Value
gK (1,2,3,4)	0.0	gD (1,2,3,4)	0.0	gF (1,2,3,4)	0.0
gKLim	-0.4	gDLim	0.2	gFLim	0.02

Eventually, the Figure 3.21 shows the comparison between numerical results of the calibrated model and experimental results of the two cyclic tests. The numerical curve was obtained from an analysis in displacement control with a displacement history in accordance with the ECCS loading protocol applied in the experimental test. The agreement between the experimental and the numerical results is good with low errors, as shown in Table 22.

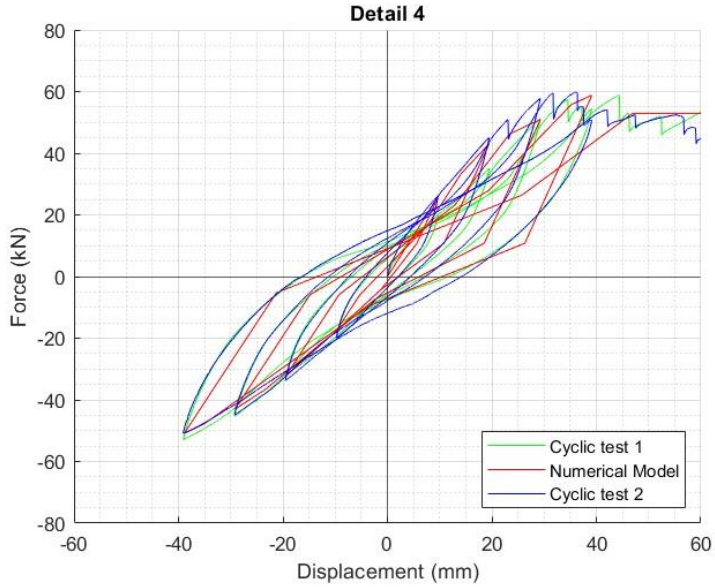

Figure 3.21: Fusible link configuration n°4: numerical and experimental results

Table 22: Fusible link configuration n°4: comparison between experimental and numerical results

	Max force Cyclic Test 1 (kN)	Max force Cyclic Test 2 (kN)	Max force Numerical model (kN)	Average Error (%)	Max Error (%)
Positive direction	50.8	57.4	59.9	9.75	16.4
Negative direction	-50.9	-52.9	-52.6	2.05	3.5

For this detail, the steel rods may undergo non-negligible plastic deformations. Therefore, they were also modelled by means of nonlinear displacement-based beam-column elements [5]. In Figure 3.22 the representation of the abovementioned OpenSees model is shown, with the fusible links behaviour represented by means of *ZeroLength* elements.

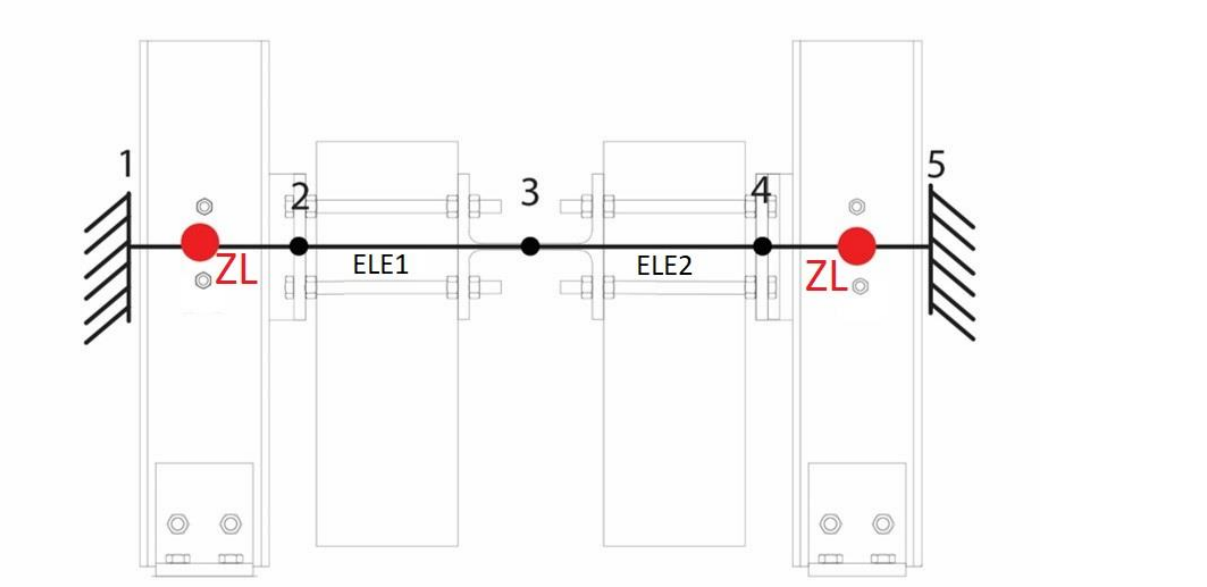

Figure 3.22: Fusible link configuration n°4: OpenSees detailed model representation

In Figure 3.22, the red dots elements, named ZL, are representative of the fusible links characterized by the *Pinching material*, while the *ele1* and *ele2* elements are the steel rods modelled as *dispBeamColumn,* to which the *Steel02 material* was assigned [5].

Once the steel parameters were defined, a calibration was carried out to define the pinching material parameters and, therefore, isolate the aluminium bolts behaviour.

In Table 23 and in Table 24 the *Pinching4 material* parameters defined to describe the experimental behaviour and assigned to the two *ZeroLength elements* are reported.

Table 23: Fusible link configuration n°4: pinching parameters of envelope and target points

Parameter	Value	Parameter	Value	Parameter	Value
ePf1 (N)	12.35e3	eNPf1 (N)	-12e3	rDispP (-)	0.55
ePd1 (mm)	9.83	eNd1 (mm)	-9.83	rForceP (-)	0.5
ePf2 (N)	22.1e3	eNf2 (N)	-12.2e3	uForceP (-)	-0.1
ePd2 (mm)	19.66	eNd2 (mm)	-19.66	rDispN (-)	0.1
ePf3 (N)	33.15e3	eNf3 (N)	-27e3	rForceN (-)	0.2
ePd3 (mm)	29.5	eNd3 (mm)	-29.5	uForceN (-)	-0.25
ePf4 (N)	37e3	eNf4 (N)	-31.2e3		
ePd4 (mm)	34	eNd4 (mm)	-39		

Table 24: Fusible link configuration n°4: pinching parameter of damage index

Parameter	Value	Parameter	Value	Parameter	Value
gK (1,2,3,4)	0.0	gD (1,2,3,4)	0.0	gF (1,2,3,4)	0.0
gKLim	-1	gDLim	0.05	gFLim	0.1

Figure 3.23 reports the comparison between the calibration of the whole detail and the one by separating the fusible links and the steel rod behaviour. The main difference is due to the larger flexibility of the model with the steel rods explicitly modelled. However, the maximum forces are well captured.

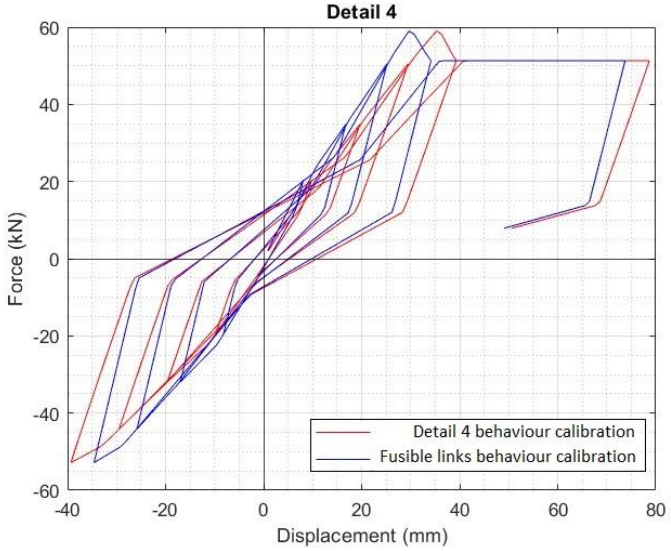

Figure 3.23: Fusible links calibration

3.7 Fusible link configuration n°5

The test setup and the main components of the Fusible link configuration n°5 are shown in Figure 3.24.

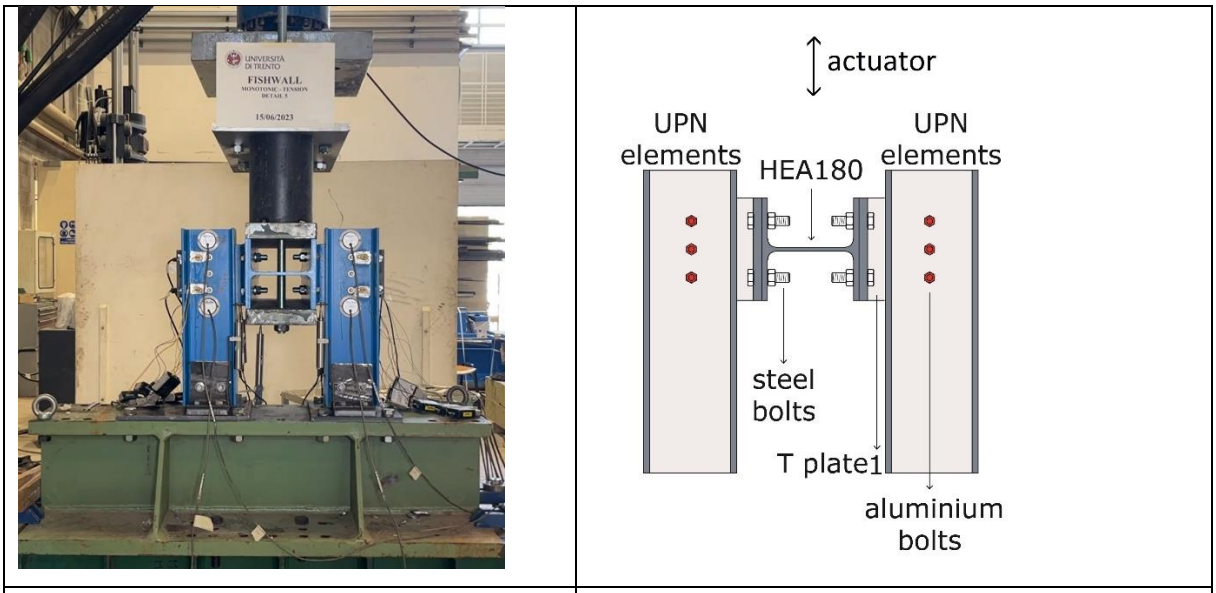

a) test setup | b) main components

Figure 3.24: Fusible link configuration n°5

The fusible link configuration n°5 was designed for a shear value of 180 kN. Four tests were performed on this detail: two monotonic tests and two cyclic tests. The cyclic tests results are reported in Figure 3.25 in terms of force-displacement curves.

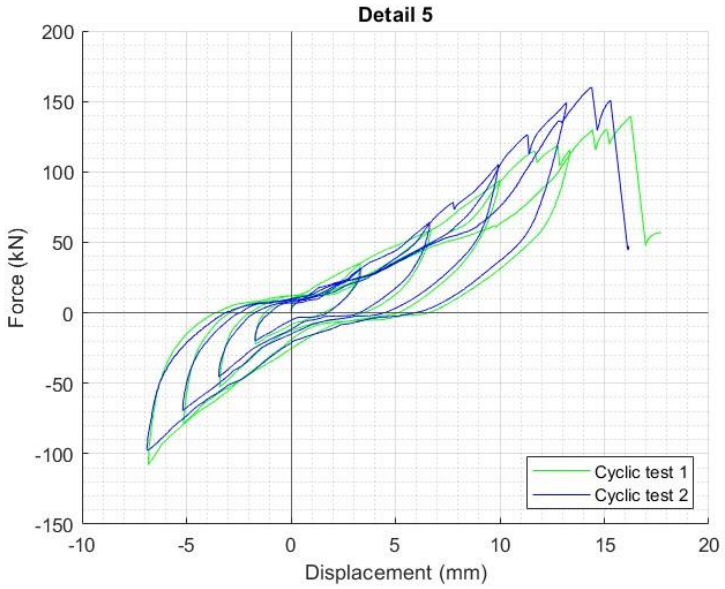

Figure 3.25: Fusible link configuration n°5: cyclic tests results

Considering the detail configuration, where the aluminum bolts are located on both sides of the specimen, two *ZeroLength elements* were used to reproduce the experimental behaviour. They are indicated by means of two red dots in Figure 3.26.

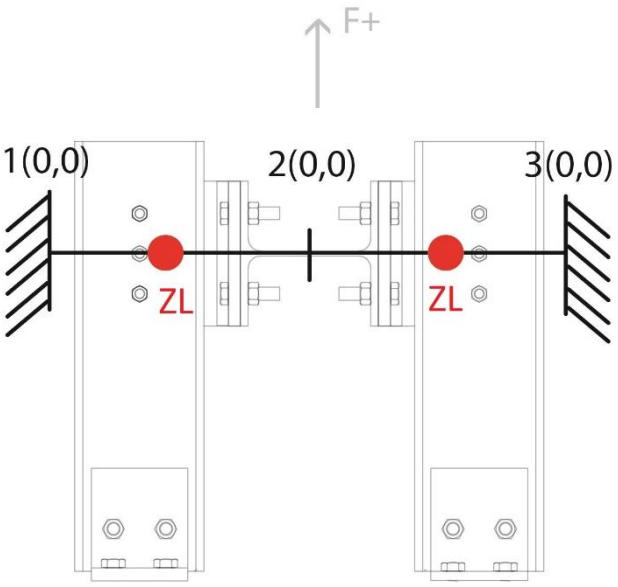

Figure 3.26: Fusible link configuration n°5: numerical model representation

In Table 25 and in Table 26 are reported the *Pinching4 material* parameters defined to describe the experimental behaviour and assigned to the two *ZeroLength elements* (ZL) are reported.

Table 25: Fusible link configuration n°5: pinching parameters of envelope and target points

Parameter	Value	Parameter	Value	Parameter	Value
ePf1 (N)	16.5e3	eNPf1 (N)	-9e3	rDispP (-)	0.25
ePd1 (mm)	3.22	eNd1 (mm)	-1.68	rForceP (-)	0.15
ePf2 (N)	30.5e3	eNf2 (N)	-22e3	uForceP (-)	-0.01
ePd2 (mm)	6.44	eNd2 (mm)	-3.35	rDispN (-)	0.1
ePf3 (N)	80e3	eNf3 (N)	-33.5e3	rForceN (-)	0.2
ePd3 (mm)	14.4	eNd3 (mm)	-5	uForceN (-)	-0.2
ePf4 (N)	1e3	eNf4 (N)	-50e3		
ePd4 (mm)	14.5	eNd4 (mm)	-6.7		

Table 26: Fusible link configuration n°5: pinching parameter of damage index

Parameter	Value	Parameter	Value	Parameter	Value
gK (1,2,3,4)	0.0	gD (1,2,3,4)	0.0	gF (1,2,3,4)	0.0
gKLim	-3	gDLim	0.0	gFLim	0.0

Eventually, Figure 3.27 shows the comparison between the numerical results of the calibrated model and the experimental results of the two cyclic tests. The numerical curve was obtained from an analysis in displacement control with a displacement history in accordance with the ECCS loading protocol applied in the experimental test.

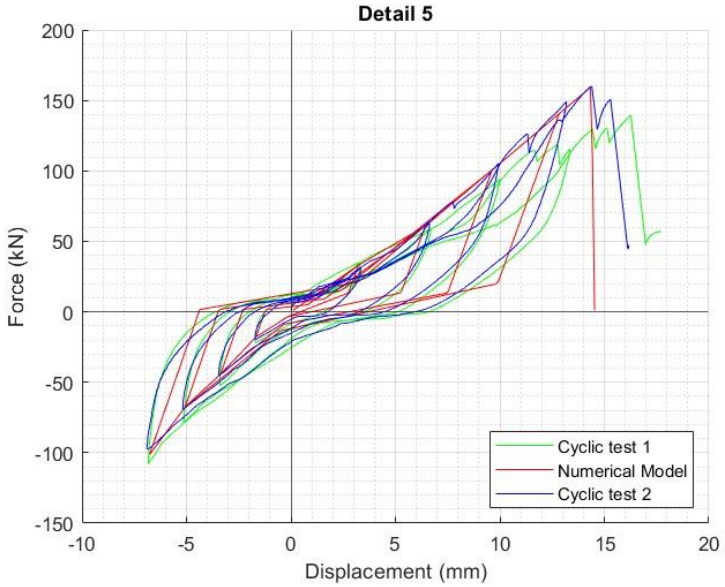

Figure 3.27: Fusible link configuration n°5: numerical and experimental results

In this case, as can be observed, both on the positive and the negative part, the force level and the stiffness are in a good agreement between the experimental and numerical results. Table 27 shows the comparison between the maximum forces along with the average and maximum error that is within 20%.

Table 27: Fusible link configuration n°5: comparison between experimental and numerical results.

	Max force Cyclic Test 1 (kN)	Max force Cyclic Test 2 (kN)	Max force Numerical model (kN)	Average Error (%)	Max Error (%)
Positive direction	126.9	114.6	136.0	13	18.7
Negative direction	-96.6	-107.9	-101.4	10.35	13.2

4 CONCLUSIONS

The present report summarises the results of numerical simulations performed on the set of monotonic and cyclic tests conducted on 6 different fusible link configurations carried out at University of Trento, which are presented in the project report D4.1 [1]. All the simulations were conducted from 3D FE models, allowing to perform detailed analyses and providing a better understanding of the structural behaviour and the failure mechanisms of the investigated fusible links. The main objective of these simulations was to check the capability of the FE models to predict satisfactory the maximum load bearing capacities of the studied fusible links. Two 3D FE models, one with the general-purpose tool ANSYS, the other with the Ls-dyna, were systematically developed for each investigated specimens to make sure of the relevance of numerical results obtained.

Despite the complexity of the cases studied, the results of the numerical simulations of the monotonic tests underlined the satisfactory level of agreement between the two FE models. There was also a satisfactory level of correlation with the experimental results, in terms of load-bearing capacities and failure mechanisms of the tested fusible link configurations (aluminium bolts shearing, components yielding, local flanges bending, etc.).. The ultimate load-bearing capacities of the tested details are reported in Table 28. For most of the tested details, the load-bearing capacity predicted by the models was found to be conservative. However, for links n°3 and n°4, the load-bearing capacity was slightly overestimated. Nevertheless, this is closer to the theoretical shear resistance value (which is also the expected value) calculated for the aluminium bolt groups that make up the tested fusible links, as reported in deliverable D3.1 [7]. These values were estimated to be 237 kN and 222 kN, respectively. On the other hand, there is some discrepancy between the predicted stiffnesses for the analysed fusible links, as determined from their force-displacement responses, and the experimental stiffnesses. Overall, the initial stiffness predicted by the models is significantly higher than that observed experimentally, particularly when compared to the stiffness derived from the displacement curve recorded from the displacement transducer associated with the loading device. However, when disregarding the slip stage, the experimental and predicted 'stiffnesses' (defined as the slope of the tangent to the force-displacement curve) appear similar in some cases (see details 3.1 and 3.2) when considering the experimental curve recorded with displacement transducers placed beneath one of the steel profiles of the fusible link. .

Table 28: Load-bearing capacity (KN) of tested fusible links under monotonic loading

Fusible link configuration	Tension load		Compression load	
	FE models	Test	FE models	test
1 (detail 1)	125	128.8	90-105*	116
2 (detail 2)	315	325	518-583*	580
3 (detail 3.1)	240	190.7	250	215.4
4 (detail 3.2)	227	155	239	205
5 (detail 4)	54-84*	57	52-84*	72
6 (detail 5)	115-185*	155	120-175*	186
* Depending on whether bolt clearances are considered in modelling				

The same comments were made about the cyclic tests, but the ultimate load-bearing capacities were more closely correlated overall (see Table 29). In addition, it can be noted that the developed FE models do not reproduce accurately the hysteretic behaviours, like the pinched shape of the hysteretic loops, which was observed for the tested fusible links. While the loading-unloading loops predicted by the models overlap quite well during a major part of the prescribed cycling loading (because the studied link remains in an elastic stage), unloading and reloading on the experimental curves take place along different paths from that of the first loading stage. Therefore, the developed FE models underestimate the energy dissipation capacity of the studied links (characterised by the areas enclosed by the hysteresis loops), which nevertheless remains quite low due to the brittle behaviour of links. This was expected, because, as mentioned in the introduction, the fusible link details are not designed to dissipate the energy introduced by a seismic event.

Table 29: Load-bearing capacity (KN) of tested fusible links under cyclic loading

Fusible link configuration	FE models	Test
1 (detail 1)	122	124.7/127.8
2 (detail 2)	315	310.7/321.4
3 (detail 3.1)	245	176.6/205
4 (detail 3.2)	225	189/228
5 (detail 4)	55	58.8/60
6 (detail 5)	110	135/158

As no preload force (or only a minimal amount) was applied to the aluminium bolts during installation, the dissimilarities between the experimental and FE numerical results are believed to mainly be due to real conditions of clearances and slipping between the steel profiles and all bolting. Bolt-hole clearances allow some movement in the link and can lead to increased bolt rotation, decreased bolt-hole contact area and then decreased link stiffness. Moreover, the misalignment of bolt and hole, the misalignment of profile or holes of varying sizes can lead to some bolts to remain unstressed at the start of loading, or throughout loading. The discrepancies could also be due to phenomena which are not accounted in FE models, like the possible slipping between the screw and nut thread or the progressive crushing of the bearing flank of the thread (that supports shearing forces) of aluminium bolts.

Further numerical work would be required to address the influence of bolt misalignment and the aforementioned factors on the response of the tested fusible links in more detail. This was not possible due to the time-consuming nature of the dynamic finite element (FE) simulations. These simulations were very expensive, as various sources of nonlinearity were taken into account, including material, geometry and contact nonlinearities (such as sliding).

Despite the imprecise characterisation of the tested fusible links in terms of stiffness, the developed finite element (FE) models can be used to calculate the load-bearing capacity of fusible links with configurations that differ slightly from those tested under cyclic loading.

This report described also the process of numerical calibration of the behaviour of the six fusible link configurations tested. For each configuration, a simplified OpenSees model was developed by means of *ZeroLength* elements, depending on the detail configuration. It is worth pointing out that the calibration was performed on the whole detail based on the maximum force capacity. It may be observed that each numerical result was compared with both cyclic test results performed on the considered test specimen, that did not always have the same outcome. However, for each fusible link configuration, the comparison between numerical and experimental results is generally satisfactory. Only one comparison differed more than 20%, i.e. 38%. As a future development of the project, global numerical analyses of existing building will be carried out integrating the calibrated model presented in this deliverable, so as to evaluate their performance under the seismic action.

5 REFERENCES

[1] S. Pasquali, N. Tondini, G. Zanon, FISHWALL project, RFSC-2020, GAN 101034083, Work Package 4, Deliverable 4.1, Full seismic test report including all detailed experimental data gathered during the seismic tests, 2024.

[2] ANSYS, ANSYS User's Manual for Revision 8.0 – Volume IV – Theory, Swanson Analysis LINK, INC., Houston USA, 1992.

[3] ANSYS, Ls-dyna User's Manual for R13 – Vol I, Vol II and Vol III, 2021

[4] McKenna, F., Fenves, G. L, and Scott, M. H. (2000) Open System for Earthquake Engineering Simulation. University of California, Berkeley, http://opensees.berkeley.edu.

[5] Mazzoni, S., McKenna, F., Scott, M. H., and Fenves, G. L. (2006) OpenSees Command Language Manual. University of California, Berkeley, http://opensees.berkeley.edu/manuals/usermanual.

[6] Lowes LN, Mitra N, Altoontash A. A beam-column joint model for simulating the earthquake response of reinforced concrete frames, Pacific Earthquake Engineering Research Center, PEER. Report n. 2003/10.

[7] Vijayakumar M., Kozich M. and Wald F. FISHWALL project, RFSC-2020, GAN 101034083, Work Package 3, Deliverable 3.1, Experimental analysis of mechanical behaviour of aluminium bolts at ambient and elevated temperature, 2022.

[8] EN 1991-1-2: Eurocode 1: Actions on structures - Part 1-2: General actions - Actions on structures exposed to fire, Brussels, Belgium, CEN, 2002.

[9] EN 1993-1-1: Eurocode 3: Design of steel structures. Part 1-1: General rules and rules for buildings, CEN, 2005.

[10] EN 1993-1-2: Eurocode 3: Design of steel structures – Part 1-2: General rules – Structural fire design, Brussels, Belgium, CEN, 2005.

[11] EN 1999-1-2, Eurocode 9: Design of aluminium structures - Part 1-2: Calculation of fire behaviour, Brussels, Belgium, CEN, 2007.

[12] ANSYS, ANSYS User's Manual for Revision 8.0 – Volume IV – Theory, Swanson Analysis LINK, INC., Houston USA, 1992.